



IntechOpen

Metal-Organic Frameworks

Edited by Fahmina Zafar and Eram Sharmin



METAL-ORGANIC FRAMEWORKS

Edited by **Fahmina Zafar** and **Eram Sharmin**

Metal-Organic Frameworks

<http://dx.doi.org/10.5772/61907>

Edited by Fahmina Zafar and Eram Sharmin

Contributors

Yves Chabal, Kui Tan, Seda Keskin, Xiao Zhang, Xiaobo He, Hao Wang, FengXiang Yin, Yu Liu, Honglai Liu, Gregor Mali, Silvia Quaresma, Vania Andre, Eram Sharmin, Fahmina Zafar

© The Editor(s) and the Author(s) 2016

The moral rights of the and the author(s) have been asserted.

All rights to the book as a whole are reserved by INTECH. The book as a whole (compilation) cannot be reproduced, distributed or used for commercial or non-commercial purposes without INTECH's written permission.

Enquiries concerning the use of the book should be directed to INTECH rights and permissions department (permissions@intechopen.com).

Violations are liable to prosecution under the governing Copyright Law.



Individual chapters of this publication are distributed under the terms of the Creative Commons Attribution 3.0 Unported License which permits commercial use, distribution and reproduction of the individual chapters, provided the original author(s) and source publication are appropriately acknowledged. If so indicated, certain images may not be included under the Creative Commons license. In such cases users will need to obtain permission from the license holder to reproduce the material. More details and guidelines concerning content reuse and adaptation can be found at <http://www.intechopen.com/copyright-policy.html>.

Notice

Statements and opinions expressed in the chapters are these of the individual contributors and not necessarily those of the editors or publisher. No responsibility is accepted for the accuracy of information contained in the published chapters. The publisher assumes no responsibility for any damage or injury to persons or property arising out of the use of any materials, instructions, methods or ideas contained in the book.

First published in Croatia, 2016 by INTECH d.o.o.

eBook (PDF) Published by IN TECH d.o.o.

Place and year of publication of eBook (PDF): Rijeka, 2019.

IntechOpen is the global imprint of IN TECH d.o.o.

Printed in Croatia

Legal deposit, Croatia: National and University Library in Zagreb

Additional hard and PDF copies can be obtained from orders@intechopen.com

Metal-Organic Frameworks

Edited by Fahmina Zafar and Eram Sharmin

p. cm.

Print ISBN 978-953-51-2662-1

Online ISBN 978-953-51-2663-8

eBook (PDF) ISBN 978-953-51-6680-1

We are IntechOpen, the world's leading publisher of Open Access books Built by scientists, for scientists

3,750+

Open access books available

115,000+

International authors and editors

119M+

Downloads

151

Countries delivered to

Our authors are among the
Top 1%

most cited scientists

12.2%

Contributors from top 500 universities



WEB OF SCIENCE™

Selection of our books indexed in the Book Citation Index
in Web of Science™ Core Collection (BKCI)

Interested in publishing with us?
Contact book.department@intechopen.com

Numbers displayed above are based on latest data collected.
For more information visit www.intechopen.com



Meet the editors



Dr Eram Sharmin is an Assistant Professor in Department of Pharmaceutical Chemistry, College of Pharmacy, Umm Al-Qura University, Makkah, Saudi Arabia. She has pursued her PhD [Jamia Millia Islamia (JMI) – A Central University, New Delhi, India, in the year 2007], MSc [Aligarh Muslim University (AMU), Aligarh, UP, India, in 2000], and BSc (AMU in 1998) degree in Chemistry. She has previously worked as Senior Research Fellow, Research Associate, and Senior Research Associate/Scientist Pool (Council of Scientific and Industrial Research, New Delhi, India) at the Department of Chemistry, JMI, New Delhi, India. She has about 80 publications in conference proceedings, refereed journals and books. Her research interests include “green” organic-inorganic hybrid and composite materials as antimicrobial and corrosion-resistant films and coatings.



Dr. Fahmina Zafar is working as Postdoctoral Fellow under the D. S. Kothari Postdoctoral Fellowship (U.G.C, Delhi, India) at Inorganic Materials Research Laboratory, Department of Chemistry, Jamia Millia Islamia (J.M.I.) – A Central University, New Delhi, India. Dr. Zafar has received her Ph.D. in Chemistry from the same University in 2006. She was a Senior Research Associate/Scientist Pool, Research Associate and Senior Research Fellow (C.S.I.R., India) at the Department of Chemistry, J.M.I. She holds M.Sc. in Organic Chemistry from J.M.I. in 1999 and B.Sc. in Chemistry and Textile Clothing from Mahila Vidyalaya Degree College, Lucknow University, Uttar Pradesh, in 1995. She has more than 100 publications in conference proceedings, refereed journals and books. Her pioneer work is in the development of bio-based polymers, metallopolymer, organic-inorganic hybrid, and nanocomposites for Green Environment in different fields of applications. Dr. Zafar is expert in synthesis and characterization of renewable resource-based polymeric materials such as polyurethanes, poly(ester amides), poly(urethane amides), and coordination polymers for antimicrobial and corrosion-protective applications.

Contents

Preface XI

Section 1 Introduction 1

- Chapter 1 **Introductory Chapter: Metal Organic Frameworks (MOFs) 3**
Eram Sharmin and Fahmina Zafar

Section 2 Characterization 17

- Chapter 2 **Interaction of Small Molecules within Metal Organic Frameworks Studied by In Situ Vibrational Spectroscopy 19**
Kui Tan and Yves Jean Chabal

- Chapter 3 **Looking into Metal-Organic Frameworks with Solid-State NMR Spectroscopy 37**
Gregor Mali

- Chapter 4 **Molecular Simulations for Adsorption-Based CO₂ Separation Using Metal Organic Frameworks 61**
Seda Keskin

- Chapter 5 **Classical Density Functional Theory for Fluids Adsorption in MOFs 87**
Yu Liu and Honglai Liu

Section 3 Applications 113

- Chapter 6 **Metal-Organic Frameworks and their Applications in Hydrogen and Oxygen Evolution Reactions 115**
Fengxiang Yin, Xiao Zhang, Xiaobo He and Hao Wang

Chapter 7	Bio-Inspired Metal-Organic Frameworks in the Pharmaceutical World: A Brief Review	137
	Vânia André and Sílvia Quaresma	

Preface

Over the past few decades, Metal organic frameworks (MOFs) have witnessed extensive interest in their preparation, characterization, and applications. MOFs are synthesized from metal ions or clusters coordinated by organic linkers or bridging-ligands, with permanent porosity. Based on the type of inorganic metal unit or cluster and organic linker or bridging ligand, the properties and applications of MOFs can be readily tuned. MOFs comprising biomolecules are environmentally and biologically compatible as well, which makes them amenable for versatile applications such as storage and separation, catalysis, sensors, gas adsorption, drug delivery, and other therapeutic applications. The emerging and interesting field of MOF encouraged us to bring forth the book titled “Metal Organic Frameworks”.

The book briefly introduces the reader to the world of MOFs and also highlights some important applications of MOFs with characterization techniques. The book is divided into three sections. Section 1 consists of introduction, with an introductory chapter briefly discussing about MOFs and examples of metal containing units and bridging ligands. The chapter also discusses biomolecules based MOFs, acquainting the reader to the significant researches and recent advancements on the same. Section 2 is dedicated to the synthesis and characterization techniques with chapters on spectral techniques. Section 3 comprises applications of MOFs describing applications such as radioactive nuclides capture, storage, separation, gas evolution, and adsorption, pharmaceutical applications of MOFs.

This book should be useful for scientists and researchers or students interested in the field of MOFs. The book “Metal Organic Frameworks: finally sees the light of the day due to mutual understanding, cooperation, and tremendous efforts of the authors, contributors, and the technical staff of InTech Open Access Publisher. Ms. Andrea Koric and Ms. Ana Pantar, Publishing Process Managers, deserve special thanks for their noteworthy efforts and cordial coordination with editors and contributors. The funding agency University Grants Commission, New Delhi, India, is also being acknowledged for D. S. Kothari Postdoctoral Fellowship to the Editor Dr. Fahmina Zafar. It is a great pleasure to thank all who endeavored to bring forward this book. Lastly, as editors working with Intech Open Access Publishers this for us was altogether a valuable learning experience. We feel honored to be a part of the InTech team.

Dr. Fahmina Zafar Ph.D.

Inorganic Materials Research Laboratory,
Department of Chemistry, Jamia Millia Islamia,
New Delhi, India

Dr. Eram Sharmin

Department of Pharmaceutical Chemistry,
College of Pharmacy, Umm Al-Qura University,
Makkah Al-Mukarramah, Saudi Arabia

Introduction

Introductory Chapter: Metal Organic Frameworks (MOFs)

Eram Sharmin and Fahmina Zafar

Additional information is available at the end of the chapter

<http://dx.doi.org/10.5772/64797>

1. Introduction

Over the past 50 decades, porous materials, from zeolites, coordination polymers to metal organic frameworks (MOFs), have gained considerable attention. The interesting feature is their porosity that allows the diffusion of guest molecules into the bulk structure. The shape and size of pores govern the shape and size selectivity of the guests to be incorporated. MOFs as defined by Yaghi et al. are porous structures constructed from the coordinative bonding between metal ions and organic linkers or bridging ligands (**Figure 1**) [1]. MOFs are formed by anchoring metal-containing units or secondary-building units (SBUs) with organic linkers, by coordination, yielding open frameworks that show exceptional feature of permanent porosity, stable framework, enormous surface area, and pore volume. The porosity is a consequence of long organic linkers that confer large storage space and numerous adsorption sites within MOFs. They also bear the ability to systematically vary and functionalize their pore structure [2, 3]. In the history of MOFs, a benchmark was represented by the synthesis of MOF-5 ($Zn_4O(bdc)_3$, bdc = terephthalate) and HKUST-1 ($Cu_3(btc)_2$, btc = 1,3,5-benzenetricarboxylate) with high porosity and low pressure gas sorption, followed by the development of chromium(III) terephthalate (MIL-101) with high chemical stability, MOF-74 ($Zn_2(dhbdc)$, dhbdc = 2,5-dihydroxy-1,4-benzenedicarboxylate) with low pressure adsorption of CO_2 , and several isostructural analogs of Mg-MOF-74 termed as IRMOF-74-I to IRMOF-74-XI, with large pore apertures to accommodate protein, NU-110E with acetylene-expanded hexatopic linker, having material highest experimental Brunauer-Emmett-Teller (BET) surface area of any porous material reported to date ($7140\text{ m}^2\text{ g}^{-1}$) Some examples of MOFs and their applications are given in **Table 1** [1–15].

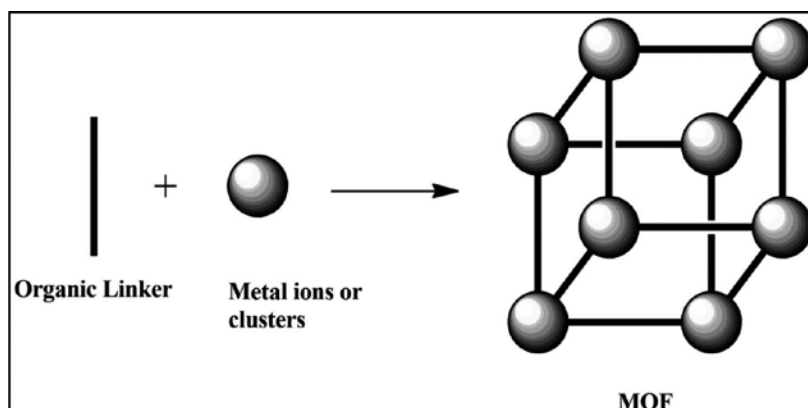


Figure 1. Structure of MOF.

Application	MOF	Metal	Ligand	Year	Author ^{Rf}
Drug delivery	MIL-101 [Cr ₃ O(OH,F,H ₂ O) ₃ (1,4-bdc) ₃ and MIL-100	Cr	1,4-benzenedicarboxylate moieties (bdc) or H ₃ btc: Benzene-1,3,5-tricarboxylate	2006	Patricia Horcajada et al. [4]
Methane Storage	MOF-5 Zn ₄ (1,4-bdc) ₃	Zn	bdc	2002	Li and Eddaoudi, et al. [5, 6]
Adsorption and storage	HKUST (Hong Kong University of Science and Technology)-1 Cu ₂ (H ₂ O) ₂ (CO ₂) ₄	Cu	H ₃ btc	2006	Rowsell and Yaghi [7]
Adsorption and storage	IRMOF-9 Zn ₄ O(bpdc) ₃	Zn	4,4'-biphenyldicarboxylate (bpdc)	2006	Rowsell and Yaghi [7]
Adsorption and storage	MOF-74, Zn ₂ (C ₈ H ₂ O ₆)	Zn	2,5-dihydroxybenzene-1,4-dicarboxylic acid	2006	Rowsell and Yaghi [7]
-	(In) MIL-68-NH ₂ or IHM-2	In	bdc-NH ₂ : 2-aminoterephthalates	2011	Savonnet and Farrusseng [8]
Drug delivery	metal-organic Zn(bix) spheres with encapsulated DOX [DOX/Zn(bix)], SN-38 [SN-38/Zn(bix)], CPT [CPT/Zn(bix)] and DAU [DAU/Zn(bix)] Doxorubicin (DOX), SN-38, camptothecin (CPT) and daunomycin (DAU)	Zn	Bix: 1,4-bis(imidazol-1-ylmethyl)benzene	2010	Inhar Imaz et al. [9]

Application	MOF	Metal	Ligand	Year	Author ^{Rf}
Soft coupling–deprotection sequence	(In) MIL-68-NH-ProFmoc and (In) MIL-68-NH-Ala-FmocIn *fluorenylmethyloxycarbonyl group (Fmoc), a base-label protecting group for amines	In	Amino acid such as L-proline (Pro-OH) and D-alanine (Ala-OH)	2011	Jerome Canivet et al. [10]
Antibacterial	Cu-BTC(MOF-199)	Cu	H ₃ btc	2014	Rodriguez et al. [11]
Highly potent bacteriocidal activity	Co-TDM	Co	H ₈ tdm: tetrakis [(3,5-dicarboxyphenyl)-oxamethyl] methane	2012	Wenjuan Zhuang et al. [12]
Delivery of nitric oxide	MIL-100(Fe or Cr) and MIL-127(Fe)	Fe, Cr or Fe	tricarboxylate or tetracarboxylate	2014	Eubank et al. [13]
Antibacterial	Ag ₂ (O-IPA)(H ₂ O)·(H ₃ O) and Ag ₅ (PYDC) ₂ (OH)	Ag	HO-H ₂ ipa = 5-hydroxyisophthalic acid and H ₂ pydc = pyridine-3, 5-dicarboxylic acid	2014	Xinyi Lu et al. [14]
Adsorption of CO ₂ over N ₂	Mn ₃ (HCOO) ₆ ·DMF	Mn	3-nitrophthalic acid (H ₂ npta) and 4,4'-bipyridine (4,4'-bipy)	2014	Ying-Ping Zhao et al. [15]

Table 1. Some examples of MOFs and their applications.

2. Chemistry

MOFs consist of both inorganic and organic units. The organic units (linkers/bridging ligands) consist of carboxylates, or anions, such as phosphonate, sulfonate, and heterocyclic compounds (**Figures 2** and **3**). The inorganic units are the metal ions or clusters termed as SBUs. Its geometry is determined by the coordination number, coordination geometry of the metal ions, and the nature of the functional groups. A variety of SBU geometries with different number of points of extension such as octahedron (six points), trigonal prism (six points), square paddle-wheel (four points), and triangle (three points) have been observed in MOF structures (**Figure 4**). In principle, a bridging ligand (ditopic, tritopic, tetratopic, or multitopic linkers) reacts with a metal ion with more than one vacant or labile site. The final framework topology of MOF is governed by both SBU connectors and organic ligand linkers. Depending upon the nature of the system used, infinite-extended polymeric or discrete-closed oligomeric structures can arise (**Figure 4**). Metal-containing units and organic linkers can be varied resulting in a variety of MOFs, tailored for different applications [3]. MOFs with large spaces may result in the formation of interpenetrating structures. Thus, it is very important to inhibit interpenetration by carefully choosing the organic linkers. The pore size is allowed to be tuned and spatial cavity arrangement be controlled, by judicious selection of metal centers

and organic ligands and also by adjusting their conditions of synthesis. The large porosity allows their applications in adsorption and separation of gaseous molecules, catalysis, microelectronics, optics, sensing applications, bioreactors, drug delivery, and others. MOFs have pore openings up to 2-nm size, which can accommodate small molecules. However, the pore openings rarely allow the inclusion of large molecules (e.g., proteins and enzymes). Attempts have been taken to increase the pore size to mesopore regime (pore size of 2–50 nm) and to decrease the crystal size to the nanometer scale. The large pore aperture benefits surface modification with a number of functionalities, without sacrificing the porosity of MOFs, also allowing the encapsulation of large molecule MOFs. The synthesis of MOFs involves reaction conditions and simple methods such as solvothermal, ionothermal, diffusion, microwave methods, ultrasound-assisted, template-directed syntheses, and others [2, 3].

An interesting and significant advancement in the field is to combine MOFs with functional nanoparticles, yielding new nanocomposite materials with unparalleled properties and performance. Nano-MOFs are advantageous over conventional nanomedicines owing to their structural and chemical diversity, high loading capacity, and biodegradability. The final properties are dependent on the particle composition, size, and morphology. These can be obtained as either crystalline or amorphous materials. As soft porous crystals, framework flexibility (triggered by an external stimulus, e.g., mechanical stress, temperature, light interactions) may be shown by MOFs, also in the absence of guests or with no involvement of adsorption and desorption [1–3, 16].

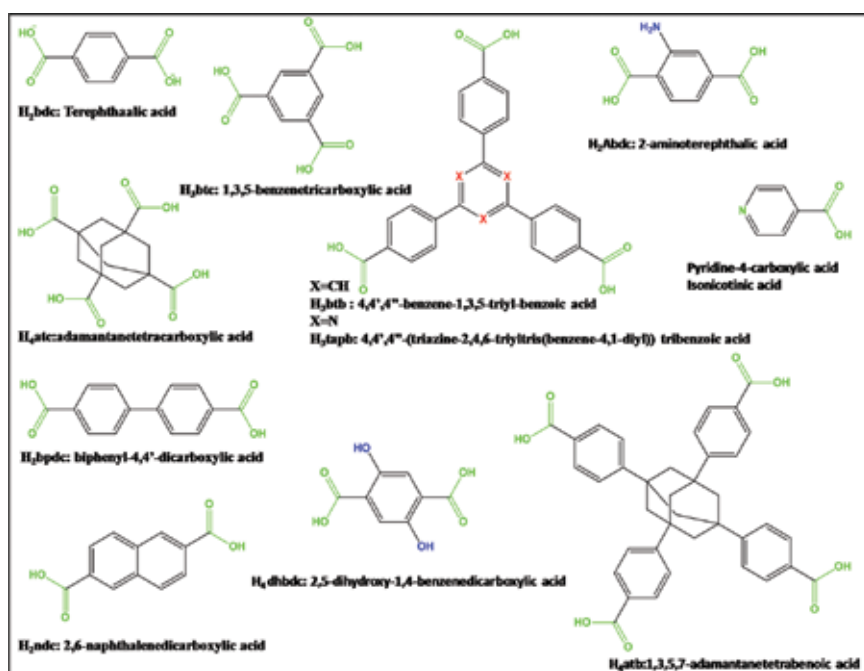


Figure 2. Some examples of organic ligands with carboxylic functionality used for the preparation of MOFs.

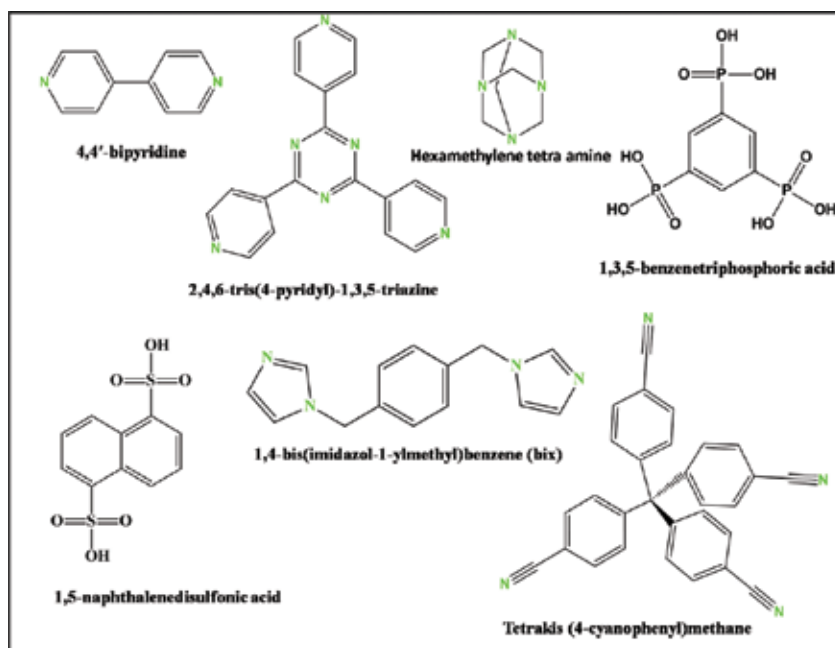


Figure 3. Some examples of ligands containing nitrogen, sulfur, phosphorous and heterocycles used for the preparation of MOFs.

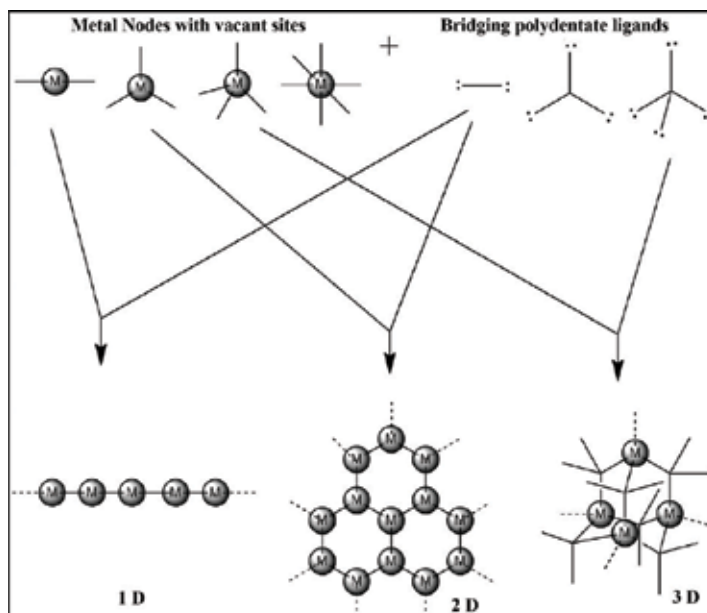


Figure 4. MOFs resulting from different metal nodes and bridging ligands.

3. Metal biomolecule frameworks (BioMOFs)

Biomolecules are naturally and abundantly available. They are cost-effective, rigid, and flexible with different coordination sites, rendering structurally diverse, biologically compatible MOFs. MOFs have also been synthesized from nontoxic endogenous cations (such as Ca, Mg, Fe, and Zn) and ligands consisting of naturally occurring derivatives or biomolecules [17]. These BioMOFs are usually biocompatible and suitable for biomedical applications [17–47]. Such combinations of natural ligands with endogenous cations are also associated with several therapeutic effects (anti-allergic, anti-inflammatory, antimicrobial, anticarcinogenic activities). **Table 2** shows some examples of BioMOFs and their applications [18–47]. Such biologically and environmentally compatible MOFs are designed and constructed based on specific composition criteria governed by judiciously selecting metal ions and organic linkers as building blocks, which are nontoxic and biologically and environmentally compatible. Biomolecules such as amino acids, peptides, proteins, nucleobases, carbohydrates, and other natural products such as cyclodextrins, porphines, and some carboxylic acids (**Figure 5**) serve as emerging building blocks for the design and construction of metal-biomolecule frameworks with novel and interesting properties and applications that cannot be obtained through the use of traditional organic linkers [17, 43, 44, 48, 49].

Application	BioMOF	Metal	Ligand	Year	Author ^{Rf}
Ar and CH ₄ sorption	[Cu(trans-fum)]	Cu	Fum:Fumaric acid	2001	K. Seki et al [18]
Reversible H ₂ O sorption/desorption	[Ni ₂ (suc) ₆ (OH) ₂ (H ₂ O) ₂ ·2H ₂ O	Ni	Suc: Succinic acid	2002	Forster et al. [19]
–	[Ni ₂ (suc) ₄ (OH) ₆ (H ₂ O) ₃]·7H ₂ O	Ni	Suc	2003	Guillou et al. [20]
Sorption of more than 30 kinds of guests (e.g. DMF, benzene, etc.); structural change	[Mn ₃ (HCOO) ₆]·(CH ₃ OH)·(H ₂ O)	Mn	Formic acid	2004	Wang et al. [21]
Selective CO ₂ and H ₂ sorption	Mn(HCOO) ₂ ·1/3(C ₄ H ₈ O ₂)	Mn	Formic acid	2004	Dybtsev et al. [22]
Adsorption	Fe ₃ O(MeOH) ₃ (fum) ₃ (CO ₂ CH ₃)·4.5MeOH	Fe	Fum	2004	Serre et al. [23]
1,3-Butanediol sorption	[Ni ₂ O(L-Asp)H ₂ O]·4H ₂ O	Ni	Amino acid L-Asp: L-aspartic acid	2004	Anokhina et al. [24]
Enantioselective separation and catalytic	Zn ₂ (bdc)(L-lac)(DMF)	Zn	bdc: 1,4-benzendicarboxylic acid and L-lac:Lactic acid	2006	Dybtsev et al. [25]

Application	BioMOF	Metal	Ligand	Year	Author ^{ref}
CO ₂ sorption	[Ni ₂ (L-Asp) ₂ (4,4'-bipy)] ·2H ₂ O	Ni	L-Asp and 4,4'-bipy : 1,2-bis (4-pyridyl)ethane	2006	Vaidhyanathan et al. [26]
H ₂ sorption	Co ₂ (L-Asp) ₂ (4,4'-bipy)]·2H ₂ O	Co	L-Asp and 4,4' -bipy	2008	Zhu et al. [27]
Heterogeneous asymmetric catalysts for the methanolysis of rac-propylene oxide	Ni ₂ (L-Asp) ₂ (4,4'-bipy) ·(HCl)1.8(MeOH)	Ni	L-Asp and 4, 4'-bipy	2008	Ingleson et al. [28]
Heterogeneous asymmetric catalysts for the methanolysis of rac-propylene oxide	Cu ₂ (L-Asp) ₂ (bpe)·(HCl) ₂ · (H ₂ O) ₂	Cu	L-Asp and bpe: 1,2-bis(4- pyridyl)ethane	2008	Ingleson et al. [28]
Cation exchange capabilities, including cationic drugs and lanthanide ions	Zn ₈ (Ade) ₄ (bpdc) ₆ O·2 Me ₂ NH ₂ · 8DMF·11H ₂ O	Zn	Nucleobases Adenine:Ade and bpdc: biphenyldicarboxylate	2009	An et al. [29]
Selective CO ₂ sorption	Co ₂ (Ade) ₂ (CO ₂ CH ₃) ₂ ·2DMF· 0.5H ₂ O	Co	Ade	2010	An et al. [30]
Drug delivery and imaging	Fe ₃ O(MeOH) ₃ (fumarate) ₃ · (CO ₂ CH ₃) ₄ ·5 MeOH and [Fe ₃ O(MeOH) (C ₆ H ₄ O ₈) ₃ Cl]·6MeOH		Fumarate and C ₆ H ₄ O ₈ is galactarate	2010	Horcajada et al. [31]
Therapeutic agent	BioMIL-1	Fe	Nicotinic acid (pyridine-3- carboxylic acid, also called niacin or vitamin B3)	2010	Miller et al. [32]
Reversible flexible structure; CO ₂ , MeOH and H ₂ O sorption	[Zn(GlyAla) ₂] _n ·(solvent)	Zn	Peptide, Glycine-adenine	2010	Rabone et al. [33]
	(γ-CD) (KOH) ₂	K	Saccharides γ-CD: cyclodextrins	2010	Smaldone et al. [35]
Inclusion of several molecules (e.g. Rhodamine B,	(γ-CD) (RbOH) ₂	Rb	γ-CD γ-CD is a (chiral) cyclic oligosaccharide	2010	Smaldone et al. [34]

Application	BioMOF	Metal	Ligand	Year	Author ^{ref}
4-phenylazoplenol,etc.)			composed of eightR-1,4-linkedD-glucopyranosyl (R-1,4-D-Glup)		
Highly selective adsorption of CO ₂	CD-MOF-2	Rb	γ-CD	2011	Jeremiah J. Gassensmith et al. [35]
Photostable O ₂ sensor	Zn ₈ (Ade) ₄ (bpdc) ₆ ·O-2Me ₂ NH ₂] loaded with lanthanide cations(Tb(III), Sm(III), Eu(III) and Yb(III))	Zn and lanthanide	Ade and bpdc	2011	An et al. [36]
–	M(II/III) Gallates	Fe, Mn, Co and Ni	H ₄ gal: gallic acid	2011	Saines et al. [37]
Porous	α-CD-MCF	Rb	α-CD R-cyclodextrin (R-CD), comprised of sixR-1,4-D-Glupresidues portrayed in their stable 4C1 conformations	2012	Gassensmith et al. [38]
Adsorption	CD-MOF-1 and CD-MOF-2 CD-MOF-3	K, Rb and Cs	γ-CD	2012	Forgan et al. [39]
Drug storage and release or for the immobilization and organization of large biomolecules	Bio-MOF-100	Zn	Ade	2012	Jihyun An et al. [40]
–	MIL-151 to -154	Zr	H ₄ gal	2014	Cooper et al. [41]
Antibacterial	BioMIL-5	Zn	AzA: azelaic acid	2014	Tamames-Tabar et al. [42]
Antioxidant carrier	Mg(H ₄ gal)	Mg	H ₄ gal	2015	Cooper et al. [43]
Inclusion and	CD-MOF-1	Na	β-CD:	2015	Lu et al.

Application	BioMOF	Metal	Ligand	Year	Author ^{Ref}
loading the drug molecules			cyclodextrins		[44]
Electrochemical nitrite detection	MOF-525	Zr	H ₄ tcpp: meso-tetra (4-carboxyphenyl) porphine	2015	Kung et al. [45]
Ammonia uptake	Al-PMOF	Al	H ₄ tcpp	2015	Wilcox et al. [46]
Highly active anti-diabetic activity	[Zn(ain)(atz)] _n	Zn	Hatz : 5-aminotetrazole and Hain: 2-amino-4-isonicotinic	2016	David Briones et al. [47]

Table 2. Some examples of BioMOFs and their applications.

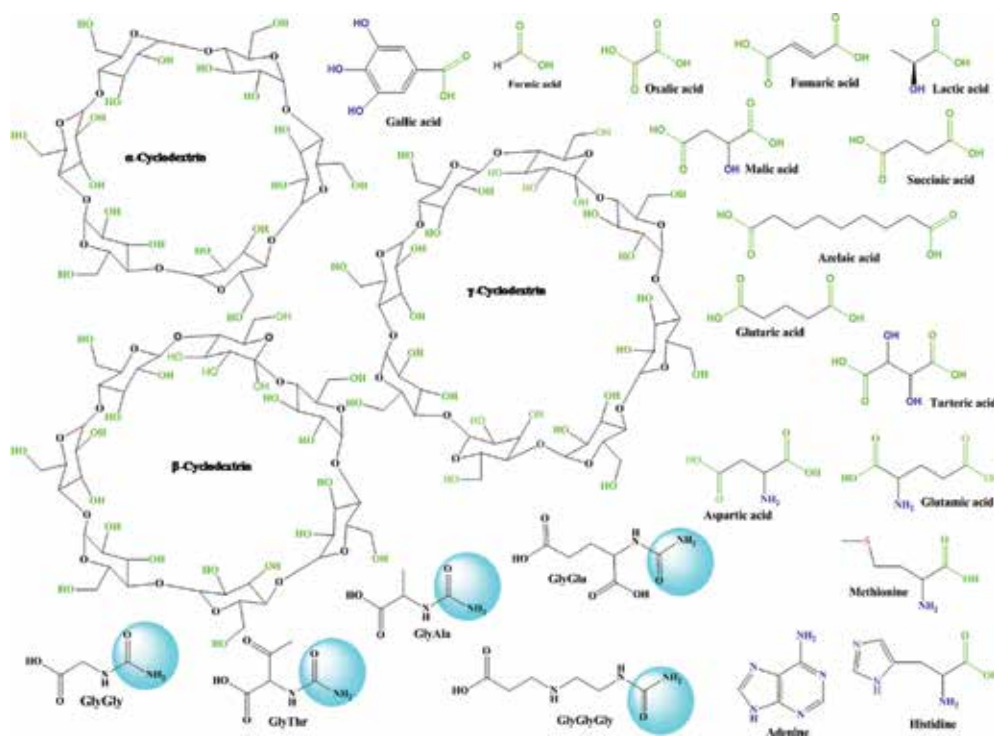


Figure 5. Examples of organic linkers used for the synthesis of BioMOFs.

4. Summary

MOFs find versatile applications as drug-delivery agents, sensors, storage and separation systems, catalysts, and others. Nontoxic nano-MOFs bearing tailored cores and surfaces can be used as nanodrug carriers for antitumor and anti-HIV drugs (biomedicine, nontoxic, drug). MOFs with biomolecules as organic linkers are still in cradle stage in contrast to their counterparts bearing traditional organic linkers. However, biomolecules confer biological compatibility and easy recyclability to MOFs. They also confer unique characteristics such as chirality and specific recognition, self-assembly characteristic, separation, ion exchange, and catalytic properties, also rendering bioinspired structures. In future, a better understanding and control of chemistry and design of MOFs may provide plethora of opportunities towards their structures, properties, and applications in different fields.

Acknowledgements

Dr Fahmina Zafar is thankful to UGC (New Delhi, India) for Dr DS Kothari Postdoctoral Fellowship, Ref. # F.4/2006(BSR)/13-986/2013(BSR). The author is also thankful to Prof. Nahid Nishat (Mentor), Inorganic Materials Research Lab, Department of Chemistry, Jamia Millia Islamia (a Central University) New Delhi, India, for her kind support.

Author details

Eram Sharmin¹ and Fahmina Zafar^{2*}

*Address all correspondence to: fahmzafar@gmail.com

1 Department of Pharmaceutical Chemistry, College of Pharmacy, Umm Al-Qura University, Makkah Al-Mukarramah, Saudi Arabia

2 Inorganic Materials Research Laboratory, Department of Chemistry, Jamia Millia Islamia, New Delhi, India

References

- [1] James SL. Metal-organic frameworks. *Chem. Soc. Rev.* 2003;32:276–288. DOI: 10.1039/b200393g.
- [2] Furukawa H, Cordova KE, O’Keeffe M, Yaghi OM. The chemistry and applications of metal-organic frameworks. *Science* 2013;341:1230444. DOI: 10.1126/science.12304.

- [3] Lu W, Wei Z, Gu Z-Y, Liu T-F, Park J, Park J, Tian J, Zhang M, Zhang Q, Gentle III T, Bosch M, Zhou H-C. Tuning the structure and function of metal-organic frameworks *via* linker design. *Chem. Soc. Rev.* 2014;43:5561–5593. DOI: 10.1039/C4CS00003J.
- [4] Horcajada P, Serre C, Vallet-Reg M, Sebban M, Taulelle F, Frey G. Metal-organic frameworks as efficient materials for drug delivery. *Angew. Chem. Int. Ed.* 2006;45:5974 –5978. DOI: 10.1002/anie.200601878.
- [5] Li H, Eddaoudi M, O’Keeffe M, Yaghi OM. Design and synthesis of an exceptionally stable and highly porous metal-organic framework. *Nature* 1999;402:276–279. doi: 10.1038/46248.
- [6] Eddaoudi M, Kim J, Rosi N, Vodak D, Wachter J, O’Keeffe M, Yaghi OM. Systematic design of pore size and functionality in isorecticular MOFs and their application in methane storage. *Science* 2002;295:469–472. DOI: 10.1126/science.1067208.
- [7] Rowsell JLC, Yaghi OM. Effects of functionalization, catenation, and variation of the metal oxide and organic linking units on the low-pressure hydrogen adsorption properties of metal-organic frameworks. *J. Am. Chem. Soc.* 2006;128:1304–1315. DOI: 10.1021/ja056639q.
- [8] Savonnet M, Farrusseng D. PCT Appl. WO2011048284, 2011.
- [9] Imaz I, Rubio-Martinez M, Garcia-Fernandez L, Garcia F, Ruiz-Molina D, Hernando J, Puentes V, MasPOCH D. Coordination polymer particles as potential drug delivery systems. *Chem. Commun.* 2010;46:4737–4739. DOI: 10.1039/c003084h.
- [10] Canivet J, Aguado S, Bergeret G, Farrusseng D. Amino acid functionalized metal-organic frameworks by a soft coupling-deprotection sequence. *Chem. Commun.* 2011;47:11650–11652. DOI: 10.1039/C1CC15541E.
- [11] Rodriguez HS, Hinestroza JP, Ochoa-Puentes C, Sierra CA, Soto CY. Antibacterial activity against *Escherichia coli* of Cu-BTC (MOF-199) metal-organic framework immobilized onto cellulosic fibers. *J. Appl. Polym. Sci.* 2014. DOI: 10.1002/APP.40815.
- [12] Zhuang W, Yuan D, Li J-R, Luo Z, Zhou H-C, Bashir S, Liu J. Highly potent bactericidal activity of porous metal-organic frameworks. *Adv. Healthcare Mater.* 2012;1:225–238. DOI: 10.1002/adhm.201100043.
- [13] Eubank JF, Wheatley PS, Lebars G, McKinlay AC, Leclerc H, Horcajada P, Daturi M, Vimont A, Morris RE, Serre C. Porous, rigid metal(III)-carboxylate metal-organic frameworks for the delivery of nitric oxide. *Apl. Mater.* 2014;2:124112. DOI: 10.1063/1.4902996.
- [14] Lu X, Ye J, Zhang D, Xie R, Bogale RF, Sun Y, Zhao LZQ, Ning G. Silver carboxylate metal-organic frameworks with highly antibacterial activity and biocompatibility. *J. Inorg. Biochem.* 2014;138:114–121. DOI: 10.1016/j.jinorgbio.2014.05.005.

- [15] Zhao Y-P, Yang H, Wang F, Du Z-Y. A microporous manganese-based metal-organic framework for gas sorption and separation. *J. Mol. Struct.* 2014;1074:19–21. DOI: 10.1016/j.molstruc.2014.05.033.
- [16] Tamames-Tabar C, Cunha D, Imbuluzqueta E, Ragon F, Serre C, Blanco-Prieto M J, Horcajada P. Cytotoxicity of nanoscaled metal–organic frameworks *J. Mater. Chem. B.* 2014;2:262. DOI: 10.1039/c3tb20832j.
- [17] Imaz I, Rubio-Martinez M, An J, Sole-Font I, Rosi NL, Maspoch D. Metal–biomolecule frameworks (MBioFs). *Chem. Commun.* 2011;47:7287–7302. DOI: 10.1039/c1cc11202c.
- [18] Seki K, Takamizawa S, Mori W. Characterization of microporous copper (II) dicarboxylates (fumarate, terephthalate, and trans-1,4-cyclohexanedicarboxylate) by gas adsorption. *Chem. Lett.* 2001;122–123. doi:10.1246/cl.2001.122.
- [19] Forster PM, Cheetham AK. Open-framework nickel succinate, $[\text{Ni}_7(\text{C}_4\text{H}_4\text{O}_4)_6(\text{OH})_2(\text{H}_2\text{O})_2]2\text{H}_2\text{O}$: a new hybrid material with three-dimensional ni–o–ni connectivity. *Angew. Chem., Int. Ed.* 2002;41:457–459N.
- [20] Guillou N, Livage C, van Beek W, Nogues M, Ferey G. A layered nickel succinate with unprecedented hexanickel units: structure elucidation from powder-diffraction data, and magnetic and sorption properties. *Angew. Chem. Int. Ed.* 2003;42:643–647. DOI: 10.1002/anie.200390177.
- [21] Wang ZM, Zhang B, Fujiwara H, Kobayashi H, Kurmoo M. $\text{Mn}_3(\text{HCOO})_6$: a 3D porous magnet of diamond framework with nodes of Mn-centered MnMn_4 tetrahedron and guest-modulated ordering temperature. *Chem. Commun.* 2004;416–417. DOI: 0.1039/b314221c.
- [22] Dybtsev DN, Chun H, Yoon SH, Kim D, Kim K. Microporous manganese formate: a simple metal-organic porous material with high framework stability and highly selective gas sorption properties. *J. Am. Chem. Soc.* 2004;126:32–33. DOI: 10.1021/ja038678c.
- [23] Serre C, Millange F, Surble S, Ferey G. A route to the synthesis of trivalent transition-metal porous carboxylates with trimeric secondary building units. *Angew. Chem. Int. Ed.* 2004;43:6285–6289. DOI: 10.1002/anie.200454250.
- [24] Anokhina EV, Jacobson AJ. $[\text{Ni}_2\text{O}(\text{L-Asp})(\text{H}_2\text{O})_2] \cdot 4\text{H}_2\text{O}$: a homochiral 1D helical chain hybrid compound with extended Ni–O–Ni bonding. *J. Am. Chem. Soc.* 2004;126:3044–3045. DOI: 10.1021/ja031836f.
- [25] Dybtsev DN, Nuzhdin AL, Chun H, Bryliakov KP, Talsi EP, Fedin VP, Kim K. A homochiral metal–organic material with permanent porosity, enantioselective sorption properties, and catalytic activity. *Angew. Chem. Int. Ed.* 2006;45:916–920. DOI: 10.1002/anie.200503023.

- [26] Vaidhyanathan R, Bradshaw D, Rebilly JN, Barrio JP, Gould JA, Berry NG, Rosseinsky MJ. A family of nanoporous materials based on an amino acid backbone. *Angew. Chem., Int. Ed.* 2006;45:6495–6499. DOI: 10.1002/anie.200602242.
- [27] Zhu P, Gu W, Cheng FY, Liu X, Chen J, Yan SP, Liao DZ. Design of two 3D homochiral Co(II) metal–organic open frameworks by layered-pillar strategy: structure and properties. *Cryst. Eng. Commun.* 2008;10: 963–967. DOI: 10.1039/B801177J.
- [28] Ingleson MJ, Barrio JP, Bacsá J, Dickinson C, Park H, Rosseinsky MJ. Generation of a solid Brønsted acid site in a chiral framework. *Chem. Commun.* 2008;11:1287–1289. DOI: 10.1039/B718443C.
- [29] An J, Geib SJ, Rosi NL. Cation-triggered drug release from a porous zinc-adeninate metal-organic framework. *J. Am. Chem. Soc.* 2009;131:8376–8377. doi: 10.1021/ja902972w.
- [30] An J, Geib SJ, Rosi NL. High and selective CO₂ uptake in a cobalt adeninate metal–organic framework exhibiting pyrimidine and amino-decorated pores. *J. Am. Chem. Soc.* 2010;132:38–39. DOI: 10.1021/ja909169x.
- [31] Horcajada P, Chalati T, Serre C, Gillet B, Sebrie C, Baati T, Eubank JF, Heurtaux D, Clayette P, Kreuz C, Chang JS, Hwang YK, Marsaud V, Bories PN, Cynober L, Gil S, Ferey G, Couvreur P, Gref R. Porous metal–organic-framework nanoscale carriers as a potential platform for drug delivery and imaging. *Nat. Mater.* 2010;9:172–178. doi: 10.1038/nmat2608.
- [32] Miller SR, Hertaux D, Baati T, Horcajada P, Greneche JM, Serre C. Biodegradable therapeutic MOFs for the delivery of bioactive molecules. *Chem. Commun.* 2010;46:4526–4528. DOI: 10.1039/C001181A.
- [33] Rabone J, Yue YF, Chong SY, Stylianou KC, Bacsá J, Bradshaw D, Darling GR, Berry NG, Khimyak YZ, Ganin AY, Wiper P, Claridge JB, Rosseinsky MJ. *Science* 2010;329:1053–1057. doi: 10.1126/science.1190672.
- [34] Smaldone RA, Forgan RS, Furukawa H, Gassensmith JJ, Slawin AMZ, Yaghi OM, Stoddart JF. Metal–organic frameworks from edible natural products. *Angew. Chem. Int. Ed.* 2010;49:8630–8634. DOI : 10.1002/anie.201002343.
- [35] Gassensmith JJ, Furukawa H, Smaldone RA, Forgan SS, Botros YY, Yaghi OM, Stoddart JF. *J. Am. Chem. Soc.* 2011;133:15312–15315. DOI: 10.1021/ja206525x.
- [36] An J, Shade CM, Chengelis-Czegán DA, Petoud S, Rosi NL. Strong and reversible binding of carbon dioxide in a green metal organic framework. *J. Am. Chem. Soc.* 2011;133:1220–1223. DOI: 10.1021/ja206525x.
- [37] Saines PJ, Yeung HH-M, Hester JR, Lennie AR, Cheetham AK. Detailed investigations of phase transitions and magnetic structure in Fe(III), Mn(II), Co(II) and Ni(II) 3,4,5-trihydroxybenzoate (gallate) dihydrates by neutron and X-ray diffraction. *Dalton Trans.* 2011;40:6401–6410. DOI: 10.1039/c0dt01687j.

- [38] Gassensmith JJ, Smaldone RA, Forgan RS, Wilmer CE, Cordes DB, Botros YY, Slawin AMZ, Snurr RQ, Stoddart JF. Polyporous metal-coordination frameworks. *Org. Lett.* 2012;14:1460–1463. DOI: 10.1021/ol300199a.
- [39] Forgan RS, Smaldone RA, Gassensmith JJ, Furukawa H, Cordes DB, Li Q, Wilmer CE, Botros YY, Snurr RQ, Slawin AMZ, Stoddart JF. Nanoporous carbohydrate metal-organic frameworks. *J. Am. Chem. Soc.* 2012;134:406–417. DOI: 10.1021/ja208224f.
- [40] An J, Farha OK, Hupp JT, Pohl E, Yeh JI, Rosi NL. Metal-adeninate vertices for the construction of an exceptionally porous metal-organic framework. *Nature Commun.* 2012;3:604–609. DOI: 10.1038/ncomms1618.
- [41] Cooper L, Guillou N, Martineau C, Elkaim E, Taulelle F, Serre C, Devic T. Zr^{IV} coordination polymers based on a naturally occurring phenolic derivative. *Eur. J. Inorg. Chem.* 2014;36:6281–6289. DOI:10.1002/ejic.201402891.
- [42] Tamames-Tabar C, Imbuluzqueta E, Guillou N, Serre C, Miller SR, Elkaim E, Horcajada P, Blanco-Prieto M. J. A Zn azelate MOF: combining antibacterial effect. *Cryst. Eng. Commun.* 2015;17:456–462 DOI:10.1039/c4ce00885e.
- [43] Cooper L, Hidalgo T, Gorman M, Lozano-Fernandez T, Simon-Vazquez R, Olivier C, Guillou N, Serre C, Martineau C, Taulelle F, Damasceno-Borges D, Maurin G, Gonzalez-Fernandez A, Horcajada P, Devic T. A biocompatible porous Mg-gallate metal-organic framework as an antioxidant carrier. *Chem. Commun.* 2015;51:5848–5851. DOI: 10.1039/c5cc00745c.
- [44] Lu H, Yang X, Li S, Zhang Y, Sha J, Li C, Sun J. Study on a new cyclodextrin based metal-organic framework with chiral helices. *Inorg. Chem. Commun.* 2015;61:48–52. DOI: 10.1016/j.inoche.2015.08.015.
- [45] Kung C-W, Chang T-H, Chou L-Y, Hupp JT, Farha OK, Ho K-C. Porphyrin-based metal-organic framework thin films for electrochemical nitrite detection. *Electrochem. Commun.* 2015;58:51–56. DOI: 10.1016/j.elecom.2015.06.003.
- [46] Wilcox OT, Fateeva A, Katsoulidis AP, Smith MW, Stone CA, Rosseinsky MJ. Acid loaded porphyrin-based metal-organic framework for ammonia uptake. *Chem. Commun.* 2015;51:14989–14991. DOI: 10.1039/C5CC06209H.
- [47] Briones D, Fernández B, Calahorra AJ, Fairen-Jimenez D, Sanz R, Martínez F, Orcajo G, Sebastián ES, Seco JM, González CS, Llopis J, Rodríguez-Diéguez A. Highly active anti-diabetic metal-organic framework. *Cryst. Growth Des.* 2016;16:537–540. DOI: 10.1021/acs.cgd.5b01274.
- [48] Keskin S, Kızılel S. Biomedical applications of metal organic frameworks. *Ind. Eng. Chem. Res.* 2011;50:1799–1812. DOI: 10.1021/ie101312k.
- [49] Imaz I, Rubio-Martinez M, Garcia-Fernandez L, Garcia F, Ruiz-Molina D, Hernando J, Puntosa V, MasPOCH D. Coordination polymer particles as potential drug delivery systems. *Chem. Commun.* 2010;46:4737–4739. DOI: 10.1039/C003084H.

Characterization

Interaction of Small Molecules within Metal Organic Frameworks Studied by *In Situ* Vibrational Spectroscopy

Kui Tan and Yves Jean Chabal

Additional information is available at the end of the chapter

<http://dx.doi.org/10.5772/64906>

Abstract

Molecular-level characterization of interaction between small gases and metal organic frameworks (MOFs) is crucial to elucidate the adsorption mechanism and establish the relationship between the structure and chemical features of MOFs with observed adsorptive properties, which ultimately guide the new structure design and synthesis for enhanced functional performance. Among different techniques, vibrational spectroscopy (infrared and Raman), which provides fingerprint of chemical bonds by their vibrational spectra, is one of the most powerful tools to study adsorbate-adsorbent interaction and give rich detailed information for molecular behaviors inside MOFs pores. This chapter reviews a number of exemplary works utilizing vibrational spectroscopy to study the interaction of small molecules with metal organic frameworks.

Keywords: interaction, small molecules, metal organic frameworks (MOFs), infrared (IR), Raman spectroscopy, vdW-DF calculation

1. Introduction

In the past decade, metal organic frameworks (MOFs) have become one of the fastest growing new fields in chemistry. Tremendous advances has been made in synthesis for new structures (>20,000 reported), structure determination or postmodification, and exploration of potential application in different fields such as gas storage and separation (H_2 , CO_2 , N_2 , and CO_2), drug delivery, sensing, luminescence, and catalysis based on adsorption. The mechanistic understanding of the interaction of the molecules with MOFs is critical for the rational design of new MOFs with desired properties and accurate assessment of functional perform-

ance in practical applications. Traditional characterization methods for MOFs materials have relied mainly on physical measurements, such as X-ray diffraction, thermogravimetric, gas adsorption isotherm, and breakthrough analysis. These techniques are powerful in deriving some critical parameters, such as crystal structures, chemical composition, thermal stability, adsorptive uptake, enthalpy, and selectivity, for assessing adsorption properties; however, mechanistic information about the local bonding sites, adsorption geometry, and guest-host, guest-guest cooperative, or competitive interaction is particularly difficult to derive. Experimental methods currently employed by the community to analyze how the molecules interact with a framework include infrared and Raman spectroscopy, X-ray (neutron) diffraction, and inelastic neutron scattering. While all these techniques have been shown to be useful to identify the binding sites of the MOFs toward the small molecules, vibration spectroscopy, i.e., infrared and Raman spectroscopy is particularly sensitive to probe the local interaction between guest molecules and the surface of metal organic frameworks. These two spectroscopic techniques provide complementary information about the nature of interaction, bonding configurations, intermolecular attraction, or repulsion through their vibrational spectra. Furthermore, they require lower capital cost and have greater accessibility of the instrumentation, which is easily modified for *in situ* measurements in a wide range of temperatures and pressures.

In this chapter, the recent progress of infrared and Raman spectroscopy studies on the underlying interactions that govern adsorption behaviors of small molecules, i.e., H_2 , CO_2 , H_2O , O_2 , CO , NO , H_2S , SO_2 , in different MOFs materials is discussed and summarized. In most cases for nonreactive molecules, such as H_2 and CO_2 , van der Waals forces dominate the interaction between the guest molecules and the building units of the MOFs. In some cases, chemical reaction involving electron transfer occurs upon adsorption of reactive molecules, e.g., H_2O , leading to a significant modification of MOFs crystalline structure. Combined with calculation, especially the recent successful effort to include van der Waals forces, self-consistently in DFT(Density functional theory) in the form of a van der Waals density functional, molecular weak physical interactions within MOFs materials are accurately described and experimental data can be well interpreted and rationalized.

2. Interaction of small molecules with MOFs

2.1. Energy carrier H_2

H_2 molecule is IR inactive as other homonuclear diatomic molecules due to their lack of dipole moment; however, once the molecule interacts with the MOF, it undergoes a perturbation that polarizes the originally symmetric molecule and makes it weakly IR active. This perturbation is usually accompanied by red shift of the H—H stretching modes, located at 4161 and 4155 cm^{-1} for para and ortho H_2 , respectively. Nijem's measurement on different type of prototypical MOFs suggest that magnitudes of the H_2 stretching frequency shifts, intensities, and line widths contains important information about the nature of the H_2 interaction in the pores and depend on the structure and chemical nature of the MOF hosts [1].

By examining several prototypes of metal organic framework materials such as $M(\text{bdc})(\text{ted})_{0.5}$ (bdc = 1, 4-benzenedicarboxylate; ted = triethylenediamine), $M(\text{bodc})(\text{ted})_{0.5}$ ($M = \text{Ni}, \text{Co}$; bodc = bicyclo[2. 2. 2]octane-1, 4-dicarboxylate), $M_3(\text{HCOO})_6$ ($M = \text{Ni}, \text{Mn}, \text{Co}$, HCOO = formate), and $\text{Zn}_2(\text{bpdc})_2(\text{bpee})$, where bpdc = 4,4'-biphenyl dicarboxylate and bpee = 1,2-bis(4-pyridyl)ethylene [1], it is concluded (see **Table 1**) that IR shifts are dominated by the environment (organic ligand, metal center, and structure) rather than the strength of the interaction. For instance, the organic ligands with π = electrons such as benzene rings cause the frequency of H_2 shift more than the ligand without π = electrons, e.g., H_2 bands are more shifted ($\sim -3 \text{ cm}^{-1}$) for $\text{Ni}(\text{bdc})(\text{ted})_{0.5}$ than $\text{Ni}(\text{bodc})(\text{ted})_{0.5}$ even though $\text{Ni}(\text{bodc})(\text{ted})_{0.5}$ has a higher binding energy. The same observation was also found by comparing the IR shift (-38 cm^{-1}) of hydrogen molecules in $\text{Zn}(\text{bdc})(\text{ted})_{0.5}$ with that (-30 cm^{-1}) in MOF-74 (also called $M_2(\text{dobdc})$, $M = \text{metal ions}$; $\text{dobdc}^{4-} = 2,5\text{-dioxidobenzene-1,4-dicarboxylate}$), a structure containing unsaturated metal center Zn^{2+} with a higher binding energy (10 kJ/mol).

MOF	Ligand type	$\Delta\nu(\text{H—H})$ (cm^{-1})	Fwhm (cm^{-1})	Pore structure/size (\AA)	Binding energy (kJ/mol)
$\text{Zn}(\text{bdc})(\text{ted})_{0.5}$	Aromatic, aliphatic	-38	20	3D/ ~ 7.8	5-5.3
$\text{Ni}(\text{bdc})(\text{ted})_{0.5}$	Aromatic, aliphatic	-37	20	3D/7.8	NA
$\text{Cu}(\text{bdc})(\text{ted})_{0.5}$	Aromatic, aliphatic	-38	20	NA	4.9-6.1
$\text{Ni}(\text{bodc})(\text{ted})_{0.5}$	Aliphatic	-34	32	1D/ $\sim 7-7.3$	5.7-6.5
$\text{Ni}_3(\text{COOH})_6$	Short aliphatic	-30	13	1D/ $\sim 5-6$	8.3-6.5
$\text{Mn}_3(\text{COOH})_6$	Short aliphatic	-28	13	1D/ $\sim 5-6$	NA
$\text{Co}_3(\text{COOH})_6$	Short aliphatic	-28	12	NA	NA
$\text{Zn}_2(\text{bpdc})_2(\text{bpee})$	Sromatic	-38	16	1D/ $\sim 5 \times 7$	9.5 _{viral} /8.8 _{poly}

Reprinted with permission from [1]. Copyright (2010) American Chemical Society.

Table 1. Comparison between the different properties of the different MOFs.

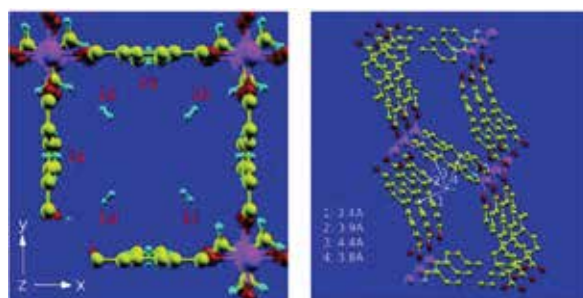


Figure 1. Hydrogen adsorption sites in $\text{Zn}(\text{bdc})(\text{ted})_{0.5}$ (left) and $\text{Zn}_2(\text{bpdc})_2(\text{bpee})$ (right). The interaction lines between one of the H atoms and carbon atoms in four different ligands are illustrated. Reprinted with permission from [1]. Copyright (2010) American Chemical Society.

Integrated intensity of the H_2 stretching modes is a sensitive measure of the number and symmetry of the sites and local interaction between H_2 and organic ligand. Asymmetric site with multiple interaction points produced larger induced dipole moment and the corresponding IR cross-section is higher [1]. The symmetric sites lead to reduced dynamic dipole moment and lower the IR band intensity. **Figure 1** compares the adsorption site of H_2 in $M(bdc)(ted)_{0.5}$ and $Zn_2(bpdc)_2(bpee)$: H_2 interacts with several benzene rings in $Zn_2(bpdc)_2(bpee)$ and the adsorption site is very asymmetric. Furthermore, the delocalized electrons in the double benzene rings in $Zn_2(bpdc)_2(bpee)$ is more easily polarized by adsorbed H_2 than that in the single benzene ring in $M(bdc)(ted)_{0.5}$. All these factors cause IR intensity of H_2 adsorbed in $Zn_2(bpdc)_2(bpee)$ almost a magnitude higher than that of H_2 adsorbed in $M(bdc)(ted)_{0.5}$.

It is worth to note that IR is not only sensitive to host-guest interaction but also capable to detect molecular interactions within confined nanopores. In MOF-74 with unsaturated metal center, a small shift (-30 cm^{-1} with respect to the unperturbed molecules) is observed in the low loading regime when H_2 is dominantly adsorbed on the metal site [2]. Additional $\sim -32\text{ cm}^{-1}$ IR shift and a large variation in dipole moment are observed once the neighboring oxygen site was occupied with H_2 molecule to form a “pair” with H_2 molecules on the metal site. Since large variation of dynamic dipole moment take place as a function of loading, due to the interaction among the adsorbed molecules and therefore the integrated areas of IR bands do not always correlate with the amount of molecules adsorbed. Cautions must be taken when using variable temperature IR to measure the absorbance of molecular hydrogen bands and estimate the adsorption energy [3].

2.2. Greenhouse emission CO_2

CO_2 is a linear molecule and has large quadrupole moment and high polarizability. The symmetric stretching mode (ν_1 , 1342 cm^{-1}) is Raman active but not IR active, whereas the antisymmetric modes (β , 667 cm^{-1} and ν_3 , 2349 cm^{-1}) are IR active. By interaction with adsorbent surface, the frequency position is perturbed and the adsorption band is affected.

Upon adsorption of CO_2 onto the active binding site of open metal ions within M-MOF-74 systems ($M = Mg^{2+}$, Zn^{2+} , Ni^{2+} , Co^{2+} , Mn^{2+}), the induced frequency shift of antisymmetric mode ν_3 is highly dependent on the nature of metal ions: it undergoes a blue shift in Mg^{2+} MOF while red shifts in Zn^{2+} MOF and other transitional metal analogs as shown in **Figure 2** [4, 5]. *Ab initio* calculations were performed in Mg^{2+} and Zn^{2+} MOFs utilizing vdW-DF, finding three factors contributing to this shift, i.e., namely, (i) the change in the molecule length, CO_2 molecules in Zn-MOF-74 experiences a larger elongation (0.0009 \AA) than in Mg-MOF-74 (0.0009 \AA), (ii) the asymmetric distortion of the CO_2 molecule, the asymmetric distortion in Mg-MOF-74 is stronger than that in Zn-MOF-74, which is consistent with a larger blue shift effect in the CO_2 ν_3 frequency, and (iii) the direct influence of the metal center. Specifically, the presence of the d orbitals in Zn^{2+} prevents the charge density transfer within the adsorbed CO_2 molecules, leading to small charge transfer compared to Mg^{2+} case [4].

Splitting of bending mode $\beta(CO_2)$ due to the removal of degeneracy of the in-plane and out-of-plane bending is commonly observed in the case of electron-donor-acceptor (EDA) com-

plexes of CO₂ with basic functional groups in polymer such as —NH₂, —OH via carbon of CO₂ as an electron acceptor [7]. The earliest spectroscopic evidences for the formation of an electron-donor-acceptor complex between CO₂ and functional groups of MOFs was reported in a MOF of type MIL-53 (MIL stands for Materials Institute Lavoisier) and amino-based MOF Zn₄O(NH₂-BDC)₃ (IR-MOF-3) and (NH₂-MIL-53(Al)) [6, 8]. Two bands at 669 and 653 cm⁻¹ in **Figure 3**, corresponding bending mode of CO₂ was observed, indicating a lowering of symmetry upon adsorption. Moreover, ν(OH) and δ(OH) modes are red shifted by -19 and -30 cm⁻¹, respectively, suggesting that oxygen atoms of hydroxyl group act as the electron donor.

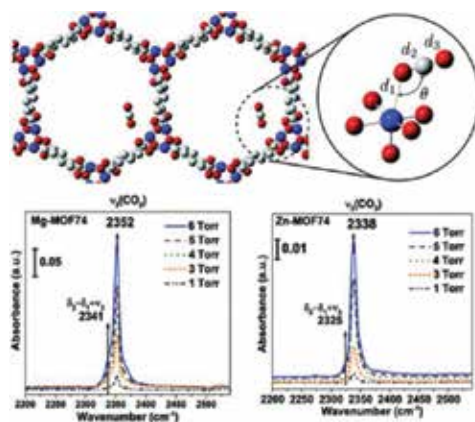


Figure 2. (Top) Illustration of CO₂ adsorbed in Zn, Mg-MOF-74. (Bottom) IR absorption spectra of CO₂ adsorbed into Mg-MOF-74 (bottom left) and Zn-MOF-74 (bottom right) at changing CO₂ pressure (1–6 Torr). Adapted with permission from [4]. Copyrighted by the American Physical Society.

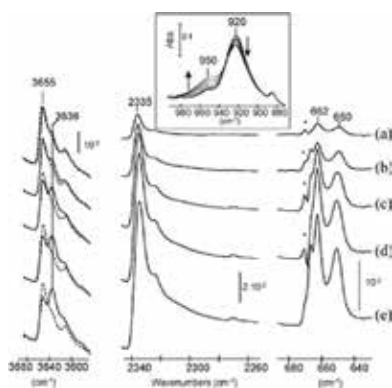


Figure 3. CO₂ introduction on MIL-53 (Cr) activated at 473 K. Spectra of activated MIL-53(Cr) deposited on silicon wafer (dotted lines) in three regions and then after introduction of increasing CO₂ equilibrium pressures into the cell (full lines): (a) 1066 Pa, (b) 2400 Pa, (c) 3850 Pa, (d) 5000 Pa, (e) 5850 Pa. Inset: perturbation of the δ(OH) mode upon CO₂ adsorption. Reproduced from [6] with permission of The Royal Society of Chemistry.

MOF $H_3[(Cu_4Cl)_3(BTtri)_8](H_3BTtri = 1,3,5\text{-tri}(1H\text{-}1,2,3\text{-triazol-4-yl)benzene)$ functionalized with N, N' -dimethylethylenediamine (mmen) shows significantly enhanced CO_2 adsorption with exceptional large isosteric heat of CO_2 around 96 kJ/mol [9]. The strong interaction of amine group of mmen with CO_2 molecules was directly proved by diffuse reflectance infrared Fourier-transform spectroscopy (DRIFTS) measurements. Upon dosing CO_2 to the sample with increasing pressure, the intensity of $\nu(N-H)$ band at 3283 cm^{-1} is significantly weakened and a new band at 1669 cm^{-1} appears, suggesting the formation of zwitterionic carbamates. $N-H$ stretching band returns to back by regeneration of the solid under vacuum and heating to 60°C .

A very recent work shows that diamine-appended metal-organic frameworks $M_2(\text{dobpdc})$ ($\text{dobpdc}^{4-} = 4,4'\text{-dioxidobiphenyl-3,3'\text{-dicarboxylate}}$), an expanded variant of the well-studied metal-organic framework MOF-74, with N, N' -dimethylethylenediamine (mmen) can behave as “phase change” adsorbents, with unusual step-shaped CO_2 adsorption isotherms that shift markedly with temperature [10]. In the unprecedented cooperative process it was found that, above a metal-dependent threshold pressure, CO_2 molecules insert into metal-amine bonds, inducing the reorganization of ammine into well-ordered chains of ammonium carbamate. **Figure 4** shows the insertion mechanism for CO_2 adsorption and spectral evolution upon cooling process. The formation of ammonium carbamate was confirmed by detecting the $\nu(C=O)$ mode at 1690 cm^{-1} , $\nu(C-N)$ at 1334 cm^{-1} , and broadening of $\nu(N-H)$ band, characteristic features of ammonium.

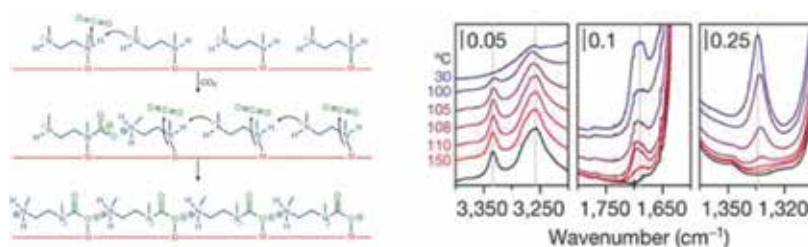


Figure 4. (Left) A cooperative insertion mechanism for CO_2 adsorption. (Right) Infrared spectra on dosing an activated sample of mmen- $Mg_2(\text{dobpdc})$ (black) with CO_2 and cooling from 150°C to 30°C (red to blue) under 5% CO_2 in N_2 . The three different regions show bands corresponding to $N-H$ (left), $C=O$ (middle), and $C-N$ (right) stretching vibrations. Reprinted by permission from Macmillan Publishers Ltd: [Nature] [10], copyright (2015).

CO_2 molecules are also stimuli to induce the structural transformation of some flexible MOFs. One of the earliest reports was CO_2 adsorption in chromium terephthalate MIL-53 [11]. CO_2 isotherm exhibits two-step adsorption and combined study of *in situ* diffraction and IR measurement provides clear explanation to this observation: after the first portion of CO_2 is absorbed into degassed solid, the host-guest interactions force the framework to close and cell to shrink. A further adsorption of CO_2 between 5 and 10 bar, reopens the framework while accepting additional CO_2 molecules into a newly formed channel. The strong interaction of CO_2 with the frameworks involves the formation of electron-donor-acceptor complexes between C atom of molecules and electron-donor center OH group of the framework, which was deduced from bending mode $\beta(CO_2)$ splitting and $\nu(OH)$ mode red shift by *in situ* IR

spectroscopy. The pore opening phenomenon was also observed in CO₂ adsorption in Zn₂(bpdc)₂(bpee) [12]. Raman and IR spectroscopy are combined together to investigate the CO₂ molecules interaction with Zn₂(bpdc)₂(bpee) and found that interaction of CO₂ with the framework weakens the C—C inter-ring of the bpdc ligand, allowing it to rotate slightly around the monodentate connectivity C—O—Zn node. This rotation causes a series of changes resulting in pore opening, which is responsible for the preferential adsorption of CO₂ over N₂. Raman spectra in **Figure 5** shows the spectroscopic evidences for these changes: that the C—C inter-ring stretching in the bpdc ligand at 1296 cm⁻¹ undergoes a red shift of ~-3 cm⁻¹ and coordinated C—O symmetric stretching at 1355 cm⁻¹ blue shift by ~+10 cm⁻¹. A ~+4 cm⁻¹ blue shift of the band at 1644 cm⁻¹ corresponding to the C=C stretching in the ethylene of the bpee ligand, is also observed. DFT calculations provide the support for the qualitative picture derived from the experimental analysis that more energetically favorable positions for the CO₂ molecules are closer to the C—C bond of the bpee and the C—C bond of the bpdc instead of their benzene and pyridine rings.

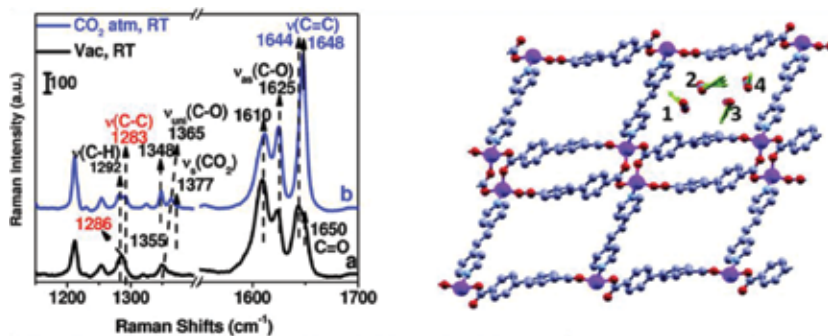


Figure 5. (Left) Raman spectra of activated Zn₂(bpdc)₂(bpee) in a vacuum and after introduction of 1 atm of CO₂ at room temperature; (right) adsorption sites of CO₂ in complete occupation in Zn₂(bpdc)₂(bpee) determined by vdW-DFT, where each pore within a unit cell is occupied by four CO₂ molecules. Reprinted with permission from [12]. Copyright (2011) American Chemical Society.

2.3. Reactive gas molecules

Water stability is a main concern for any potential applications of MOFs in industrial settings because moisture is ubiquitous in the environment, i.e., complete removal of H₂O from gas sources is difficult. Many widely investigated MOFs, particularly built by carboxylate acid ligand such as MOF-5 [13], MOF-177 [14], HKUST-1 [15], and MOF-74 [16] are susceptible to reaction with moisture. Understanding the degradation mechanism is a complex problem because there are a variety of independent factors that play a critical role in the stability of MOFs. However, the metal-ligand bond is regarded as the weakest point of a MOF structure. To decouple the effects of metal-ligand bond from other factors such as topology, porosity, and surface areas on the structural stability of MOFs, two types of prototypical and representative isostructure MOFs with different metal centers: (1) MOFs M(bdc)(ted)_{0.5} [M = Cu²⁺, Zn²⁺, Ni²⁺, Co²⁺] with saturated metal centers and (2) MOF-74 [M₂(dobdc), M = Mg²⁺, Zn²⁺, Ni²⁺, Co²⁺]

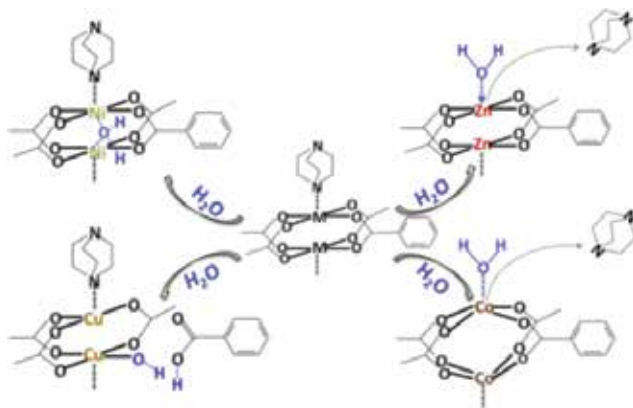


Figure 6. Schematic illustration of decomposition pathway of $M(\text{bdc})(\text{ted})_{0.5}$ [$M = \text{Cu}, \text{Zn}, \text{Ni}, \text{Co}$] reaction with D_2O molecules. Reprinted with permission from [17]. Copyright (2012) American Chemical Society.

with unsaturated metal centers were chosen for study [17, 18]. The former involves a secondary building unit (metal center configuration) that is very common to MOFs. The latter, referred to as MOF-74, is one of the most characterized materials for single gas adsorption as it is one of the best carbon capture materials. Combining spectroscopy methods (*in situ* infrared absorption and Raman) and powder X-ray diffraction, it was found that the stability of MOF in the presence of water vapor critically depends on their structure and the specific metal cation in the building units; and that water condensation inside pores, which is highly dependent on external vapor pressure and temperature, is the critical phenomenon that induces the hydrolysis reaction. In the case of $M(\text{bdc})(\text{ted})_{0.5}$, the metal-bdc bond is the most vulnerable for $\text{Cu}(\text{bdc})(\text{ted})_{0.5}$, while the metal-ted bond is first attacked for the Zn and Co analogs. In contrast, $\text{Ni}(\text{bdc})(\text{ted})_{0.5}$ remains stable under conditions where all other $M(\text{bdc})(\text{ted})_{0.5}$ materials are chemically attacked as shown in **Figure 6**. In the case of $M_2(\text{dobdc})$, or MOF-74, the weak link is the phenolate-metal bond. At room temperature, water is molecularly adsorbed inside the MOF channel. Above 150°C , the water molecule is dissociatively adsorbed at the metal-oxygen group with OH adsorption directly on the metal center and H adsorption on the bridging O of the phenolate group. Interestingly, the latter O—H bond is only detected when D_2O is used due to the strong vibrational coupling of the O—H bending vibration to the *dobdc* linker vibrations (see **Figure 7**). In contrast, the O—D bending vibration is fully decoupled from the linker vibrations (i.e., behaves as a local vibrational mode) leading to a strong, sharp, and detectable absorption band. Due to the passivation of open metal sites by hydroxyl group, the MOFs compounds lose a substantial fraction of their original gas uptake capacity.

NO adsorption has been studied before in Ni, Co-MOF-74 by isotherm, X-ray diffraction infrared and Raman spectroscopy, showing that NO interacts strongly with metal centers, forming NO coordination adduct with a binding energy of 90–92 kJ/mol [19, 20]. Infrared spectra shows that the stretching band $\nu(\text{NO})$ of adsorbed NO molecules appears at a frequency between 1845 and 1838 cm^{-1} as coverage increases (see **Figure 8**). The red shift from the gas phase value at 1876 cm^{-1} indicates the interaction between NO and Ni-MOF-74 involves

back donation of d electrons from the metal to the antibonding orbital of nitrosyl group, therefore weakening N—O bond. The coverage dependent of $\nu(\text{NO})$ stretching frequency suggest dipole-dipole interaction of adsorbed NO molecules. By gradually dosing the water vapor on the NO loaded sample, infrared spectra of **Figure 8** shows that NO is gradually removed. This ability of water displacing preadsorbed NO in slow kinetics make this materials a promising candidate for NO delivery in biological tissues.

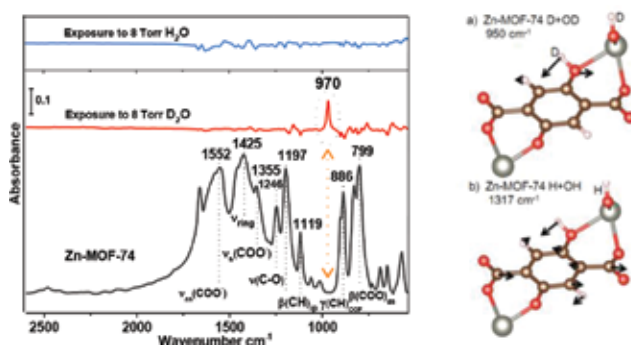


Figure 7. (Left) IR spectra of Zn-MOF-74 exposed to H_2O (blue) and D_2O (red), referenced to the activated MOF spectra, compared with IR absorption spectra of activated MOF-74, referenced to the KBr pellet; (right) calculated vibrational modes of (a) Zn-MOF-74 with dissociated D_2O (D + OD) at 950 cm^{-1} , (b) Zn-MOF-74 with dissociated H_2O (H + OH) at 1317 cm^{-1} . Reprinted with permission from [18]. Copyright (2014) American Chemical Society.

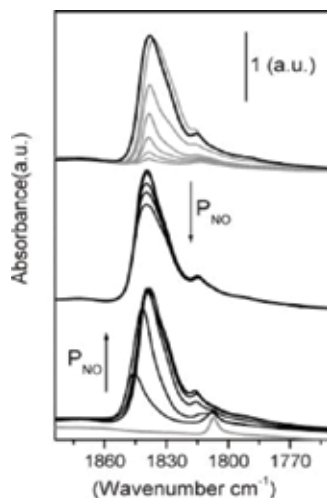


Figure 8. (Bottom) IR spectra of increasing NO equilibrium pressures dosed at RT on Ni-MOF-74 (equilibrium $p_{\text{max}} = 0.1\text{ mbar}$). Bold gray curve, vertically translated for clarity, reports the spectrum collected before NO dosage. (Middle) Spectra obtained upon successive progressive outgassing of loaded NO. (Top) Effect of water dosage on the irreversible NO (last spectrum of the middle part). Black spectra report the effect of 0.1 mbar NO dosage. Gray curves show the further interaction of water, at the vapor pressure as a function of contact times (up to 10 min). Reprinted with permission from [19]. Copyright (2008) American Chemical Society.

CO is demonstrated to be reversibly adsorbed in MOF-74 ($M = \text{Mg, Mn, Fe, Co, Ni, Zn}$) analogies with the binding strength following by the order of $\text{Ni} > \text{Co} > \text{Fe} > \text{Mg} > \text{Mn} > \text{Zn}$ [21]. This sequence is in distinct contrast to that observed for CO_2 adsorption in these materials. The molecular adsorption configurations are shown in **Figure 9**. While CO_2 interaction with metal ions of MOF-74 frameworks is predominately electrostatic, CO coordination also involves σ and π orbital interactions, as being probed by infrared spectroscopy. For instance, CO exhibits a small blue shift in Fe, and Co-MOF-74 compared to Mg and Zn-MOF-74 since π back-donation in Fe and Co weaken the C-O bond, however, Mg^{2+} ions lack d electrons and unable to back-donate into the empty CO orbitals and Zn^{2+} ions has full occupied 3d orbital and are not available to accept σ charge donation from CO.

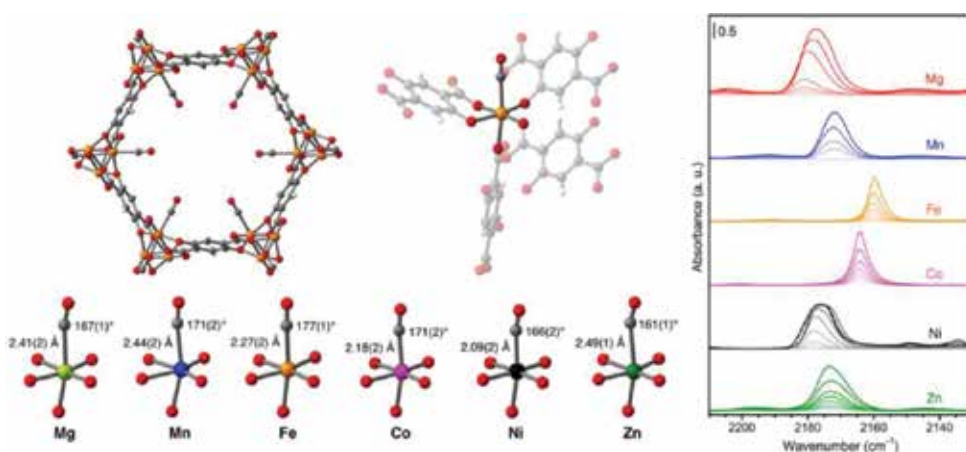


Figure 9. (Upper left) Structures from powder neutron diffraction. A view down a channel (along the c axis) in the structure of $\text{Fe}_2(\text{dobdc})\cdot 1.5\text{CO}$, as determined by Rietveld analysis of powder neutron diffraction data and (upper right) coordination environment for a single Fe^{2+} site in $\text{Fe}_2(\text{dobdc})\cdot 1.5\text{CO}$; (bottom) first coordination sphere for the M^{2+} ions in $\text{M}_2(\text{dobdc})\cdot 1.5\text{CO}$, with M—CO distances and M—C—O angles indicated; (Right) Background subtracted FTIR spectra of $\text{M}_2(\text{dobdc})$ collected at 77 K in the presence of CO. Light to dark lines represent increasing CO coverage on samples. Reprinted with permission from [21]. Copyright (2014) American Chemical Society.

O_2 is IR inactive and nonreactive to many MOFs materials, however, gas adsorption isotherms at 298 K indicate that $\text{Fe}_2(\text{dobdc})$ binds O_2 preferentially over N_2 via electron transfer interaction, with an irreversible capacity of 9.3 wt%, corresponding to the adsorption of one O_2 molecule per two iron centers [22]. Infrared spectra show that upon oxygenation at low temperature. A partially reduced (near superoxo) O_2 species coordinated to FeII/III sites was observed at 1129 cm^{-1} , assigned to $\nu(\text{O—O})$. The formation of iron(III)-peroxide species at 790 cm^{-1} was detected at room temperature. The charge-transfer interaction was also found in adsorption of O_2 in a Zn-MOF containing 7, 7, 8, 8-tetracyano-p-quinodimethane (TCNQ) ligand where organic linker is the active adsorption site. The large red shift of the sharp $\nu(\text{O=O})$ band by 100 cm^{-1} was observed in IR spectra upon loading O_2 at 90 K [23]. This frequency shift is too large to be induced by the confinement effect alone. It suggests that O_2 molecules accommodated in TCNQ MOF have a partial negative charge, donated by electron rich organic linker.

SO₂ adsorption has been studied in MOFs materials such as IR-MOFs (which have the same underlying topology as MOF-5 [24], M(bdc)(ted)_{0.5} [25], FMOF-2 [26], and NOTT-300 [27]). Among all studied structures, the uptake of SO₂ in M(bdc)(ted)_{0.5} at room temperature is highest, 9.97 mol/kg at 1.13 bar [25]. The adsorption mechanism of SO₂ within this class of MOFs is further explored by *in situ* IR spectroscopy, finding that the major adsorbed SO₂ molecules contributing to the isotherm measurements are characterized by stretching bands at 1326 and 1144 cm⁻¹, -36 and -7 cm⁻¹ (see **Figure 10**), red shift respectively from the unperturbed values of 1362 and 1151 cm⁻¹ of gas phase. In addition, the IR spectra reveal the presence of another minor species at 1242 and 1105 cm⁻¹ that is more strongly bound, requiring a higher temperature (~150°C) to remove. SO₂ adsorption also induces significant changes to the frameworks vibrational modes (see **Figure 10**): (1) a blue shift of the ν_{as}(COO) mode (Δν = +56 cm⁻¹) and of the ν_s(COO) mode (Δν = +39 cm⁻¹), and (2) a decrease in intensity of ν_{as}(CH₂), ν_s(CH₂), and ν(CH) modes at 2874, 2938, and 3076 cm⁻¹, respectively. Furthermore, the CH₂ rocking mode and benzene ring deformation mode σ₁₂ are red shifted by -8 and -12 cm⁻¹. Calculations based on vdW-DF codes suggest that two adsorption configurations are possible for these SO₂ molecules. One geometry involves an SO₂ molecule bonded through its sulfur atom to the oxygen atom of the paddlewheel building unit and its two oxygen atoms to the C—H groups of the organic linkers by formation of hydrogen bonds. Such a configuration results in a distortion of the benzene rings, which is consistent with the experimentally observed shift of the ring deformation mode.

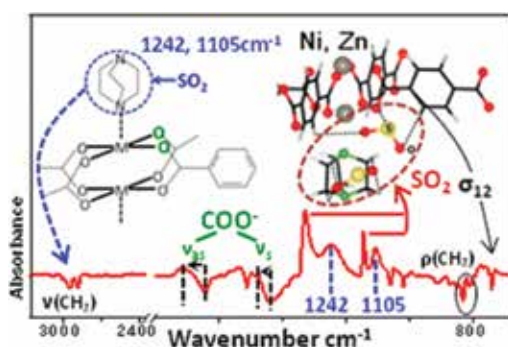


Figure 10. Snapshot of initial adsorption configuration models of SO₂ in Zn(bdc)(ted)_{0.5} and IR absorption spectra after loading SO₂ at 256 Torr, recorded immediately after evacuation of gas phase (within 16 s). Reprinted with permission from [25]. Copyright (2013) American Chemical Society.

MOFs such as MIL-47 (V), MIL-53(Al, Cr) with saturated metal center show weak interaction with H₂S and adsorption/desorption behavior is completely reversible in isotherm measurement. For some MOFs structures MIL-101(Cr), HKUST-1 with unsaturated metal sites [28, 29], the adsorption of H₂S is quite reactive, leading to release of BTC ligand from coordination with copper metal center and the formation of carboxylate C=O group as indicated by the appearing of a band at 1710 cm⁻¹. MOF-74 with nickel center shows a strong binding strength toward H₂S with an adsorption heat ΔH_{ads} of ~57 kJ/mol [30]. The PXRD pattern shows that the structure itself is stable under H₂S exposure, which is consistent with the observation from

IR spectra that most MOFs phonon modes are slightly affected. The molecular state of H_2S in Ni-MOF-74 is characterized by its clear IR features at 2626, 2614, and 1182 cm^{-1} , corresponding to asymmetric, symmetric stretching, and bending mode.

2.4. Coadsorption

Compared to the extensive studies that focus on the single component adsorption, the coadsorption of multicomponents remains scarcely investigated due in part to experimental difficulties, for instance, the isotherm of multicomponent adsorption, the composition of each species adsorbed can only be derived indirectly by measuring variation of gas-phase composition. Methods, such as mass spectrometry, have to be incorporated with isotherm measurements. *In situ* IR spectroscopy in conjunction with *ab initio* modeling can provide information on local bonding sites and exchange mechanisms, as demonstrated by recent work in prototypical structure MOF-74 [31]. Using CO_2 as a probe molecule, competitive coadsorption of CO_2 with a variety of small molecules (H_2O , NH_3 , SO_2 , NO , NO_2 , N_2 , O_2 , and CH_4) in M-MOF-74 ($\text{M} = \text{Mg}$, Co , Ni) was investigated by infrared spectroscopy. Surprisingly, the displacement of CO_2 adsorbed at the metal center by other molecules such as H_2O , NH_3 , SO_2 , NO , NO_2 , N_2 , O_2 , and CH_4 is mainly observed for H_2O and NH_3 , even though SO_2 , NO , and NO_2 have higher binding energies ($\sim 70\text{--}90\text{ kJ/mol}$) to metal sites (Mg^{2+} , Ni^{2+} , Co^{2+}) than that of CO_2 ($\sim 38\text{--}48\text{ kJ/mol}$) and slightly higher than that of water ($\sim 60\text{--}80\text{ kJ/mol}$) as shown in **Figure 11**. The exchange process is differentiated by plotting the intensity of H_2O band $\nu(\text{OH})$ \sim above 2600 cm^{-1} and CO_2 band ν_{as} at 2341 cm^{-1} (see **Figure 12**). The uptake of water is dominated by transport; therefore, taking its complement (red curve in **Figure 12**) for the CO_2 release (gray curve) simulates what is expected if exchange kinetics

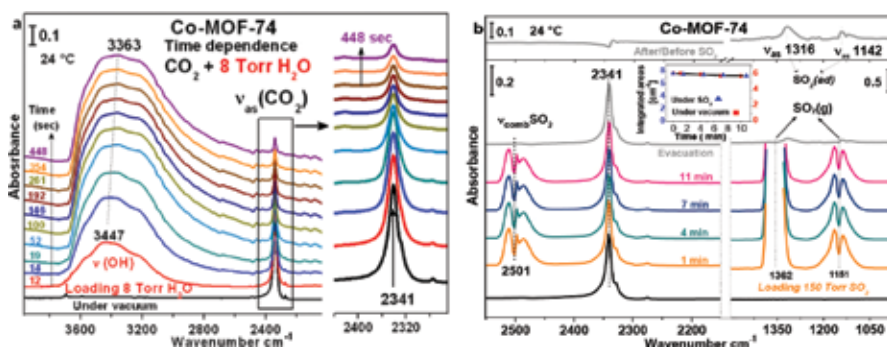


Figure 11. (Left, a) IR absorption spectra of 8 Torr H_2O (broad peak above $\sim 2600\text{ cm}^{-1}$) adsorbed into Co-MOF-74 with preloaded CO_2 (peak at 2341 cm^{-1}) as a function of time. All referenced to the activated MOF under vacuum ($<20\text{ mTorr}$). The black line in the bottom shows the absorption spectra of CO_2 before loading water. (Right, b) IR absorption spectra of activated and CO_2 -preloaded Co-MOF-74 exposed to $\sim 150\text{ Torr SO}_2$. The bottom spectrum shows the adsorbed CO_2 in Co-MOF-74 under vacuum ($<20\text{ mTorr}$). The middle part shows the time-dependent spectrum during SO_2 exposure and the spectrum after evacuation of gas phase SO_2 . The differential spectrum on the top right of (b) shows the spectrum recorded after loading SO_2 for 10 min and evacuation of gas phase, referenced to the spectrum before loading SO_2 as shown in the bottom black spectrum. Reprinted with permission from [31]. Copyright (2015) American Chemical Society.

were much faster than diffusion. It represents the amount of CO₂ displaced by water as it arrives at the CO₂ site. This simulated CO₂ concentration was specifically plotted to highlight that the measured CO₂ concentration (black curve in **Figure 12**) evolved more slowly (additional time is required for exchange since the barrier is not negligible). This simulated curve (based on the water intake) is then used to normalize the CO₂ absorption measurements, i.e., remove the transport part of the time evolution by subtracting the time due to transport (diffusion of water molecules to inner pores). The net result is shown in the inset of **Figure 12** that now represents only the exchange kinetics.

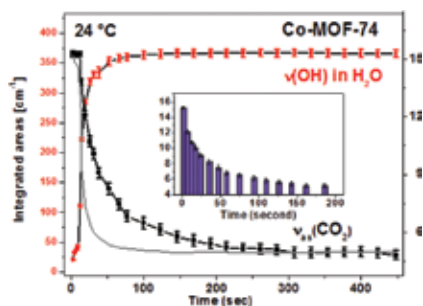


Figure 12. Evolution of integrated areas of the IR bands of water $\nu(\text{OH})$ (red) and CO₂ $\nu_{\text{as}}(\text{CO}_2)$ (black) in Co-MOF-74 at 24°C. The inset purple bar curve shows the $\nu_{\text{as}}(\text{CO}_2)$ band evolution corrected by removing the water transport time (taken from the gray curve) and hence provides the intensity evolution solely controlled by exchange kinetics. Reprinted with permission from [31]. Copyright (2015) American Chemical Society.

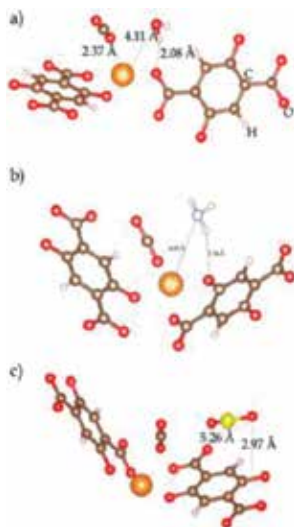


Figure 13. Adsorption configuration of the H₂O (top), NH₃ (middle), SO₂ (bottom) molecule on Mg-MOF-74 fully loaded with CO₂ molecules at the metal centers. Red, brown, gray, blue, and orange spheres denote O, C, H, N, and Mg atoms, respectively. Parts of the MOF have been removed for visualization purposes. Reprinted with permission from [31]. Copyright (2015) American Chemical Society.

Ab initio simulations were performed to calculate the exchange barrier (activation energy) and study the reaction pathway for the $\text{H}_2\text{O} \rightarrow \text{CO}_2$ and $\text{SO}_2 \rightarrow \text{CO}_2$ exchange processes at the primary adsorption site of the open metal center. It was found that hydrogen bonding of H_2O or NH_3 molecules with the nearby oxygen of the organic linker facilitates the positioning of the H_2O oxygen atom toward the metal center and displacing the preadsorbed CO_2 molecule as shown in **Figure 13**. However, SO_2 (and other molecules without H atoms) are not able to do so and remain bound at a distant site of carbon ring from metal center. In order to displace the CO_2 molecules at metal site, SO_2 needs to break away from the attractive force of the initial adsorption sites to move to the metal center and overcome a high energy barrier (~ 20 kJ/mol) than water molecules (~ 13 kJ/mol) to remove the preoccupied CO_2 molecules.

This important scientific finding revolutionized the understanding of MOF coadsorption by establishing that the displacement of one molecule by another within porous materials is a complex process that the energetics consideration alone cannot successfully predict. In other words, the binding energy at the most favorable adsorption site is not a sufficient indicator of the molecular stability in MOFs and kinetics of exchange process must be considered.

3. Conclusion

Vibrational spectroscopy has been proved to be the very informative technique to investigate the interaction of small gas molecules with metal organic frameworks. By examining subtle changes in the spectra of both adsorbate and adsorbent, insightful details regarding the adsorption mechanism are revealed. With the help of theoretical calculation, which provides direct access to many properties of the system, the experimental models are validated and a complete understanding of the adsorption behaviors can be derived.

For H_2 , although free molecule is IR inactive, the stretching mode is activated and becomes observable once the molecule is polarized by binding to the surface. A wealth of information for the interaction details, i.e., binding site and geometry, interaction potential can be extracted by analyzing the peak position, intensity, and width.

For CO_2 molecules, both the perturbation of stretching and bending mode convey important information for the nature of interaction. For physical adsorption with lower binding energy (< 50 – 60 kJ/mol), the stretching mode suffers a small shift (< 15 cm^{-1}) compare to gas phase value and the bending mode is split due to the loss of degeneracy. If the molecules are chemically adsorbed with a high adsorption heat over 60 – 70 kJ/mol, IR adsorption features of new species such as carbamate can be observed. The structural modifications for functional groups are reflected by tracking the spectroscopic signatures.

For the reactive molecules such as H_2O , O_2 , H_2S , SO , and NO adsorbing into MOFs, the crystalline structure is strongly modified and even become degraded. By examining the difference spectra before and after adsorption, the weak point of the complicated MOFs structure can be identified and reaction pathway can be also unveiled, which is crucial to design robust structure.

Finally, infrared spectroscopy provides an unique advantage to study the adsorption behaviors of mixture components since the vibrational modes of different molecules usually can be well distinguished in the infrared spectra. The occupation of actual adsorption sites for mixtures can be measured as a function of parameters such as time, temperature, and partial pressure. Recent works in measuring CO₂ competition with a variety of molecules, e.g., H₂O, NH₃, SO₂, NO, and NO₂ in MOF-74 show kinetics for exchange process is an important parameter which needs to be taken into account for coadsorption and separation process. It also underscores the need of combined studies, using spectroscopic methods and *ab initio* simulations to uncover the atomistic interactions of small molecules in MOFs that directly influence coadsorption.

Author details

Kui Tan* and Yves Jean Chabal

*Address all correspondence to: kuitannk@gmail.com

Department of Materials Science and Engineering, The University of Texas at Dallas,
Richardson, Texas, USA

References

- [1] Nijem N, Veyan JF, Kong L, Li K, Pramanik S, Zhao Y, Li J, Langreth DC, Chabal YJ. Interaction of molecular hydrogen with microporous metal organic framework materials at room temperature. *J Am Chem Soc.* 2010; 132(5): 1654–1664. DOI: 10.1021/ja908817n
- [2] Nijem N, Veyan JF, Kong L, Wu H, Zhao Y, Li J, Langreth DC, Chabal YJ. Molecular hydrogen “Pairing” interaction in a metal organic framework system with unsaturated metal centers (MOF-74). *J Am Chem Soc.* 2010; 132(42): 14834–14848. DOI:10.1021/ja104923f
- [3] Garrone E, Otero Arean C. Variable temperature infrared spectroscopy: a convenient tool for studying the thermodynamics of weak solid-gas interactions. *Chem Soc Rev.* 2005; 34(10): 846–857. DOI:10.1039/b407049f
- [4] Yao Y, Nijem N, Li J, Chabal YJ, Langreth DC, Thonhauser T. Analyzing the frequency shift of physisorbed CO₂ in metal organic framework materials. *Phys Rev B.* 2012; 85(6): 064302. DOI:10.1103/PhysRevB.85.064302
- [5] FitzGerald SA, Schloss JM, Pierce CJ, Thompson B, Rowsell JLC, Yu K, Schmidt JR. Insights into the anomalous vibrational frequency shifts of CO₂ adsorbed to metal sites

- in microporous frameworks. *J Phys Chem C*. 2015; 119(10): 5293–5300. DOI:10.1021/jp5104356
- [6] Vimont A, Travert A, Bazin P, Lavalley JC, Daturi M, Serre C, Férey G, Bourrelly S, Llewellyn PL. Evidence of CO₂ molecule acting as an electron acceptor on a nanoporous metal-organic-framework MIL-53 or Cr³⁺(OH)(O₂C—C₆H₄—CO₂). *Chem Commun*. 2007; (31): 3291–3293. DOI:10.1039/b703468g
- [7] Kazarian SG, Vincent MF, Bright FV, Liotta CL, Eckert CA. Specific intermolecular interaction of carbon dioxide with polymers. *J Am Chem Soc*. 1996; 118(7): 1729–1736. DOI:10.1021/ja950416q
- [8] Gascon J, Aktay U, Hernandez-Alonso MD, van Klink GPM, Kapteijn F. Amino-based metal-organic frameworks as stable, highly active basic catalysts. *J Catal*. 2009; 261(1): 75–87. DOI: j.jcat.2008.11.010
- [9] McDonald TM, D'Alessandro DM, Krishna R, Long JR. Enhanced carbon dioxide capture upon incorporation of N,N[prime or minute]-dimethylethylenediamine in the metal-organic framework CuBTtri. *Chem Sci*. 2011; 2(10): 2022–2028. DOI:10.1039/c1sc00354b
- [10] McDonald TM, Mason JA, Kong X, Bloch ED, Gygi D, Dani A, Crocella V, Giordanino F, Odoh SO, Drisdell WS, Vlasisavljevich B, Dzubak AL, Poloni R, Schnell SK, Planas N, Lee K, Pascal T, Wan LF, Prendergast D, Neaton JB, Smit B, Kortright JB, Gagliardi L, Bordiga S, Reimer JA, Long JR. Cooperative insertion of CO₂ in diamine-appended metal-organic frameworks. *Nature*. 2015, advance online publication. DOI: 10.1038/nature14327
- [11] Serre C, Bourrelly S, Vimont A, Ramsahye NA, Maurin G, Llewellyn PL, Daturi M, Filinchuk Y, Leynaud O, Barnes P, Férey G. An explanation for the very large breathing effect of a metal-organic framework during CO₂ adsorption. *Adv Mater*. 2007; 19(17): 2246–2251. DOI: 10.1002/adma.200602645
- [12] Nijem N, Thissen P, Yao Y, Longo RC, Roodenko K, Wu H, Zhao Y, Cho K, Li J, Langreth DC, Chabal YJ. Understanding the preferential adsorption of CO₂ over N₂ in a flexible metal-organic framework. *J Am Chem Soc*. 2011; 133(32): 12849–12857. DOI: 10.1021/ja2051149
- [13] Huang L, Wang H, Chen J, Wang Z, Sun J, Zhao D, Yan Y. Synthesis, morphology control and properties of porous metal-organic coordination polymers. *Microporous Mesoporous Mater*. 2003; 58(2): 105–114. DOI: 10.1016/S1387-1811(02)00609-1
- [14] Li Y, Yang RT. Gas adsorption and storage in metal-organic framework MOF-177. *Langmuir*. 2007; 23(26): 12937–12944. DOI: 10.1021/la702466d
- [15] DeCoste JB, Peterson GW, Schindler BJ, Killups KL, Browe MA, Mahle JJ. The effect of water adsorption on the structure of the carboxylate containing metal-organic frame-

- works Cu-BTC, Mg-MOF-74 and UiO-66. *J Mater Chem.* 2013; 1(38): 11922–11932. DOI: 10.1039/c3ta12497e
- [16] Kizzie AC, Wong-Foy AG, Matzger AJ. Effect of humidity on the performance of microporous coordination polymers as adsorbents for CO₂ capture. *Langmuir.* 2011; 27(10): 6368–6373. DOI: 10.1021/la200547k
- [17] Tan K, Nijem N, Canepa P, Gong Q, Li J, Thonhauser T, Chabal YJ. Stability and hydrolyzation of metal organic frameworks with paddle-wheel SBUs upon hydration. *Chem Mater.* 2012; 24(16): 3153–3167. DOI:10.1021/cm301427w
- [18] Tan K, Zuluaga S, Gong Q, Canepa P, Wang H, Li J, Thonhauser T, Chabal YJ. Water reaction mechanism in metal organic frameworks with coordinatively unsaturated metal ions: MOF-74. *Chem Mater.* 2014; 26(23): 6886–6895. DOI:10.1021/cm5038183
- [19] Bonino F, Chavan S, Vitillo JG, Groppo E, Agostini G, Lamberti C, Zecchina A, Solari PL, Kongshaug KO, Bordiga S. Local structure of CPO-27-Ni metallorganic framework upon dehydration and coordination of NO. *Chem Mater.* 2008; 20(15): 4957–4968. DOI: 10.1021/cm052191g
- [20] McKinlay AC, Xiao B, Wragg DS, Wheatley PS, Megson IL, Morris RE. Exceptional behavior over the whole adsorption–storage–delivery cycle for NO in porous metal organic frameworks. *J Am Chem Soc.* 2008; 130(31): 10440–10444. DOI:10.1021/ja801997r
- [21] Bloch ED, Hudson MR, Mason JA, Chavan S, Crocellà V, Howe JD, Lee L, Dzubak AL, Queen WL, Zadrozny JM, Geier SJ, Lin LC, Gagliardi L, Smit B, Neaton JB, Bordiga S, Brown CM, Long JR. Reversible CO binding enables tunable CO/H₂ and CO/N₂ separations in metal-organic frameworks with exposed divalent metal cations. *J Am Chem Soc.* 2014; 136(30): 10752–10761. DOI:10.1021/ja505318p
- [22] Bloch ED, Murray LJ, Queen WL, Chavan S, Maximoff SN, Bigi JP, Krishna R, Peterson VK, Grandjean F, Long GJ, Smit B, Bordiga S, Brown CM, Long JR. Selective binding of O₂ over N₂ in a redox-active metal-organic framework with open iron(II) coordination sites. *J Am Chem Soc.* 2011; 133(37): 14814–14822. DOI: 10.1021/ja205976v
- [23] Shimomura S, Higuchi M, Matsuda R, Yoneda K, Hijikata Y, Kubota Y, Mita Y, Kim J, Takata M, Kitagawa S. Selective sorption of oxygen and nitric oxide by an electron-donating flexible porous coordination polymer. *Nat Chem.* 2010; 2(8): 633–637. DOI: 10.1038/nchem.684
- [24] Britt D, Tranchemontagne D, Yaghi OM. Metal-organic frameworks with high capacity and selectivity for harmful gases. *Proc Natl Acad Sci.* 2008; 105(33): 11623–11627. DOI: 10.1073/pnas.0804900105
- [25] Tan K, Canepa P, Gong Q, Liu J, Johnson DH, Dyevoich A, Li J, Thonhauser T, Chabal YJ. Mechanism of preferential adsorption of SO₂ into two microporous paddle wheel

- frameworks $M(\text{bdc})(\text{ted})_{0.5}$. *Chem Mater.* 2013; 25(23): 4653–4662. DOI:10.1021/cm401270b
- [26] Fernandez CA, Thallapally PK, Motkuri RK, Nune SK, Sumrak JC, Tian J, J. Liu. Gas-induced expansion and contraction of a fluorinated metal–organic framework. *Cryst Growth Des.* 2010; 10(3): 1037–1039. DOI: 10.1021/cg9014948
- [27] Yang S, Sun J, Ramirez-Cuesta AJ, Callear SK, DavidWilliam IF, Anderson DP, Newby R, Blake AJ, Parker JE, Tang CC, Schröder M. Selectivity and direct visualization of carbon dioxide and sulfur dioxide in a decorated porous host. *Nat Chem.* 2012; 4(11): 887–894. DOI:10.1038/nchem.1457
- [28] Hamon L, Serre C, Devic T, Loiseau T, Millange F, Férey G, Weireld GD. Comparative study of hydrogen sulfide adsorption in the MIL-53(Al, Cr, Fe), MIL-47(V), MIL-100(Cr) and MIL-101(Cr) Metal–organic frameworks at room temperature. *J Am Chem Soc.* 2009; 131(25): 8775–8777. DOI: 10.1021/ja901587t
- [29] Petit C, Mendoza B, Bandoz TJ. Hydrogen sulfide adsorption on MOFs and MOF/graphite oxide composites. *Chem Phys Chem.* 2010; 11(17) 3678–3684. DOI: 10.1002/cphc.201000689
- [30] Chavan S, Bonino F, Valenzano L, Civalleri B, Lamberti C, Acerbi N, Cavka JH, Leistner M, Bordiga S. Fundamental aspects of H_2S adsorption on CPO-27-Ni. *J Phys Chem C.* 2013; 117(30): 15615–15622. DOI: 10.1021/jp402440u
- [31] Tan K, Zuluaga S, Gong Q, Gao Y, Nijem N, Li J, Thonhauser T, Chabal YJ. Competitive coadsorption of CO_2 with H_2O , NH_3 , SO_2 , NO , NO_2 , N_2 , O_2 and CH_4 in M-MOF-74 (M = Mg, Co, Ni): The role of hydrogen bonding. *Chem Mater.* 2015; 27(6): 2203–2217. DOI: 10.1021/acs.chemmater.5b00315

Looking into Metal-Organic Frameworks with Solid-State NMR Spectroscopy

Gregor Mali

Additional information is available at the end of the chapter

<http://dx.doi.org/10.5772/64134>

Abstract

Nuclear magnetic resonance (NMR) spectroscopy is a powerful tool for characterization of materials. It can detect local structure around selected atomic nuclei and provide information on the dynamics of these nuclei. In case of metal-organic frameworks, NMR spectroscopy can help elucidate the framework structure, locate the molecules adsorbed into the pores, and inspect and characterize the interactions of these molecules with the frameworks. The present chapter discusses selected recent examples of solid-state NMR studies that provide valuable insight into the structure and function of metal-organic frameworks.

Keywords: MAS NMR, organic linker, metal centre, molecules within pores, short-range order, disorder, mixed-linker MOFs

1. Introduction

Preparing the most efficient metal-organic framework materials (MOFs) for selected applications requires not only knowledge about the atomic-scale structures of these MOFs but also understanding of the atomic-scale processes during the action of MOFs in catalysis, gas separation and storage, drug delivery, etc. In order to gain this knowledge and this understanding, it is mandatory that MOFs are inspected by a set of complementary techniques that elucidate short- and long-range structural motifs, static and dynamic properties, interactions among the frameworks and the adsorbates. That is why, in addition to the very well established thermal, sorption and diffraction analyses, modeling and spectroscopic investigations are becoming more and more important in the studies of MOFs.

Among the spectroscopic techniques, solid-state nuclear magnetic resonance (NMR) is one of the most powerful characterization techniques, because it can provide element-specific atomic-resolution insight into materials. It can be used at many different stages of research connected to MOFs; from studies of their formation, their structure determination, to in-situ studies of their performance. As a local spectroscopic tool, solid-state NMR is complementary to diffraction techniques that rely on the existence of long-range order and that provide a picture of an average crystal structure. NMR experiments can prove or disprove the hypotheses proposed by modeling, predicting preferential adsorption sites and estimating strength of interactions between the adsorbed molecules and the MOF matrices. It can follow gradual adsorption or desorption of molecules into pores, locate and quantify these molecules, and thus complement the data obtained by the thermal and sorption analyses. Solid-state NMR is also extremely important for studying dynamics of the frameworks and of the adsorbed molecules. Therefore, employing NMR spectroscopy is crucial for deducing the structure-to-function relationships of MOFs.

The present chapter begins with a short introduction into solid-state NMR spectroscopy. Here, the basic characteristics of NMR and the most important techniques and recent methodological developments for studying the framework and the adsorbed molecules are briefly mentioned. NMR spectroscopy is particularly important for studying motifs in MOFs that do not exhibit long-range order. Such motifs can be found in the frameworks themselves, especially when one is dealing with mixed-linker or mixed-metal MOFs, and when the molecules within the pores do not occupy equal positions within each unit cell. The second section of the chapter presents some interesting and representative examples of NMR studies of frameworks of the metal-organic materials. For example, in case of mixed-linker MOFs two recent studies demonstrate that solid-state NMR is the only technique, which not only proves or disproves the incorporation of different linkers into the framework, but also provides an answer about the distribution of different linkers within the frameworks. The third, largest section of the chapter is devoted to the application of NMR spectroscopy for studying the molecules adsorbed into the pores of MOFs. These molecules can be solvent molecules, which remain trapped in MOFs after the synthesis and can play a stabilizing role in these materials, or can be molecules adsorbed during the application of MOFs in catalysis, in gas separation and storage, in energy storage, and in drug-delivery.

The chapter does not attempt to present a complete review of the solid-state NMR studies on MOFs, but focuses on prominent recent examples and discusses their impact on the understanding of the properties and functioning of MOFs. Some other, more extensive reviews on NMR spectroscopy of MOFs can be found in literature [1, 2].

2. Briefly about solid-state NMR spectroscopy

Atomic nuclei with nonzero magnetic dipole moment and atomic nuclei with nonzero electric quadrupole moment are extremely sensitive probes capable of detecting tiny differences in local magnetic and local electric fields. Local magnetic field at the position of an atomic nucleus

depends on the electric currents in the vicinity of this nucleus and on the number and geometrical arrangement of magnetic moments in its neighborhood. A strong external magnetic field, which is in a modern NMR spectrometer generated by a superconducting magnet, induces electric current in the cloud of electrons that is surrounding an atomic nucleus. This electric current gives rise to a local magnetic field that partially shields the external magnetic field. We are talking about chemical shielding and chemical shift, because the extent of shielding and the consequent shift of the spectral line in the NMR spectrum depend on the chemical environment of the atomic nucleus. With chemical environment we mean the nature and the number of neighbors in the first and second coordination shells, and the nature, strength and angles of the nearest chemical bonds. For example, chemical shielding and the resulting local magnetic fields are not equal at the positions of ^{13}C nuclei in CH_4 and in CH_3OH ; consequently, the ^{13}C NMR signals of CH_4 and CH_3OH resonate at different frequencies.

As mentioned above, the second important contribution to the local magnetic field at the position of an atomic nucleus is the contribution of the neighboring atomic nuclei with nonzero magnetic moments. Each atomic nucleus with a magnetic moment acts as a tiny source of magnetic field in a similar way as a bar magnet generates magnetic field in its surroundings. What is particularly important with such magnetic fields is that their strengths depend strictly on the distances between the atomic nuclei that generate the fields and the atomic nucleus that detects these fields. We say that a pair of proximal nuclei is coupled through the magnetic dipolar coupling. With the advanced NMR experiments we can exploit this dipolar coupling for obtaining qualitative or sometimes even quantitative information about the interatomic distance.

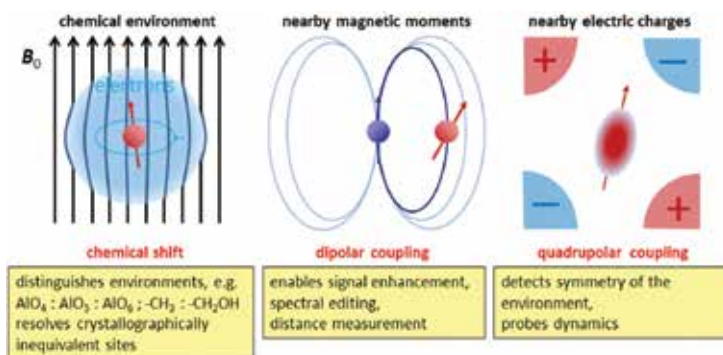


Figure 1. Summary of the most important interactions, detected by NMR, and of the available information.

Local electric field at the position of an atomic nucleus depends on the arrangement of electric charges in the neighborhood of the nucleus. In fact, NMR spectroscopy detects electric field gradients to which only the nonspherical atomic nuclei are sensitive. These nuclei are often called quadrupolar nuclei and they all have spin quantum number larger than $\frac{1}{2}$. The sensitivity of quadrupolar nuclei to the local electric field gradients can provide useful information on the symmetry of the environments around them. Measurement of the

magnitude of the electric field gradient (the strength of the electric quadrupolar interaction) can also yield an insight into the dynamics of the species in which the atomic nuclei are located, that is, for example, into the dynamics of a framework or a molecule. **Figure 1** schematically shows the most important sources of local fields detectable by solid-state NMR. The figure also briefly summarizes the information that is offered by chemical shifts, dipolar couplings, and electric quadrupolar interactions.

The magnitude and the direction of a local magnetic field do not depend only on the molecular or crystalline environment, but also on the orientation of the molecule or the crystal fragment with respect to the direction of the external magnetic field. For example, chemical shieldings in a phenyl ring that is perpendicular to the external magnetic field and in a phenyl ring that is parallel to the external magnetic field will differ from one another, because the induced electric currents in the rings will be different. When studying materials, we are very often dealing with powders in which the particles are oriented in many different directions. This means that, for example, atomic nuclei at equal crystallographic sites but in differently oriented crystallites will detect different local fields. In an NMR spectrum of such a powder, the corresponding NMR signal will reflect the distribution of the local fields and will appear as a broad distributed line, which is called a powder pattern. In this respect, NMR spectra of powders are very much different from the NMR spectra of solutions. In solutions, due to fast motion and reorientation of molecules, atomic nuclei detect orientationally averaged local fields and NMR spectra exhibit very sharp signals. We say that in solutions, NMR detects only the isotropic contributions to the local fields. The resolution of the obtained NMR spectra is excellent and the detection of tiny differences in chemical environments is easy. As opposed to that, the resolution in solid-state NMR spectra of powdered materials is very poor, because the broad powder patterns overlap extensively. In order to improve resolution and thus to gain more information about the inequivalent sites in materials, we try to mimic fast molecular reorientations by spinning powdered samples very quickly. Indeed, fast spinning about the axis that is inclined from the direction of the external magnetic field by 54.7° improves resolution of NMR spectra of powders drastically. The special angle mentioned above is called the magic angle and the method is named magic angle spinning (MAS) [3]. MAS is the basis of almost all modern solid-state NMR experiments.

Apart from attempts for improving spectral resolution, solid-state NMR faces two other major technical challenges. The first is how to increase the NMR signal, which is very weak compared to signals of other spectroscopies. One of routinely employed approaches to achieve that is the usage of cross polarization (CP) step [4]. With this step, the signal of the selected atomic nuclei is enhanced via the transfer of spin polarization from atomic nuclei with larger magnetic moments. For example, ^1H nuclei have four- and ten-times as large magnetic moment as ^{13}C and ^{15}N nuclei, respectively, thus the application of ^1H - ^{13}C and ^1H - ^{15}N CP approach can greatly enhance ^{13}C and ^{15}N NMR signals. The method is most efficient if both types of atomic nuclei have spin quantum number of $\frac{1}{2}$ and if the nuclei are coupled with strong dipolar coupling (i.e., if the nuclei of the two types are proximal one to another). The above listed nuclei ^1H , ^{13}C , and ^{15}N all have spin equal to $\frac{1}{2}$. Because they are the major constituents of the organic linkers

in MOFs and of many molecules that are adsorbed within MOFs (small organic molecules, drug molecules), CP-MAS-based experiments are regularly employed for studying MOFs.

NMR-active nuclei in the inorganic metal-oxo vertices in MOFs are typically quadrupolar nuclei, that is nuclei with spin larger than $1/2$. Among them, ^{27}Al , ^{45}Sc , and ^{51}V are abundant and have moderately large magnetic moments, therefore NMR spectroscopy of these nuclei is very sensitive. In majority of other cases, such as in case of ^{25}Mg , ^{67}Zn , or ^{91}Zr , we are dealing with low-abundance nuclei and/or with nuclei with small magnetic moments, with which NMR spectroscopy is very demanding. Increasing the NMR signal of these nuclei is often attempted through the acquisition of the Carr-Purcell-Meiboom-Gill (CPMG) train of echoes [5], and through the usage of strong external magnetic fields and large amounts of samples. Additionally, because spectral lines of quadrupolar nuclei can be very wide, broadbanded WURST (Wideband, Uniform Rate, and Smooth Truncation) or similar type of excitation is often needed [6].

Even WURST-CPMG and strong magnetic fields are usually not sufficient for a successful NMR spectroscopy of oxygen nuclei. Because the NMR-active isotope ^{17}O is a very rare isotope of oxygen, only 0.04% abundant in nature, practical ^{17}O NMR spectroscopy relies on isotopic enrichment of samples. Isotopic enrichment can be useful or even necessary also when measuring ^{13}C or ^{15}N NMR spectra of adsorbed molecules, especially if these molecules are present in small concentrations within MOFs and if CP via ^1H nuclei is not possible (either because the molecules do not contain hydrogen atoms, or because the dipolar coupling with ^1H nuclei is motionally averaged out). Typical examples of NMR studies of isotopically enriched molecules are studies of $^{13}\text{CO}_2$ molecules within the pores of MOFs. **Table 1** lists selected physical properties for atomic nuclei (isotopes) that are most often employed as probes in NMR spectroscopy of MOFs.

Isotope	Ground state spin	Natural abundance	NMR frequency at 14.10 T/MHz
^1H	1/2	~100%	600.00
^2H	1	0.015%	92.10
^{13}C	1/2	1.1%	150.87
^{15}N	1/2	0.37%	60.82
^{17}O	5/2	0.04%	81.34
^{25}Mg	5/2	10%	36.73
^{27}Al	5/2	100%	156.34
^{67}Zn	5/2	3.1%	37.54
^{91}Zr	5/2	11%	55.78

Table 1. Selected properties of nuclear isotopes, which are frequently encountered in MOFs.

The third technical challenge of solid-state NMR spectroscopy is how to extract the information about the selected internuclear distances. In case of MOFs, these could be the distances

among the atomic nuclei of the adsorbed molecules and the atomic nuclei within the frameworks. As mentioned above, the information on the distances is contained in the magnitude of the dipolar coupling between these nuclei. However, because dipolar coupling is an anisotropic interaction, it is very efficiently suppressed or entirely averaged out by MAS. To keep the enhanced resolution of NMR spectra obtainable by MAS, but still to be able to detect the magnitude of the dipolar coupling among the selected nuclei, several recoupling techniques were developed and were included into different types of homonuclear and heteronuclear correlation experiments. Homonuclear correlation experiments, like ^1H - ^1H correlation experiments, most often exploit spin diffusion enhanced by RFDR (Radio-Frequency-driven Dipolar Recoupling) [7], or recoupling of the dipolar interaction by BABA or POST-C7 pulse sequences [8, 9]. Heteronuclear dipolar couplings, like ^1H - ^{13}C couplings, can be probed qualitatively by various two-dimensional HETCOR (HETero-nuclear CORrelation) experiments [10, 11] or quantitatively by the REDOR-type pulse sequences [12].

In the above discussion of local magnetic fields, we have skipped a contribution that is often quite important in MOFs. It is the contribution of paramagnetic centers, such as Cr, Mn, Fe, Co, Ni, and Cu centers. Unpaired electrons of these centers have much larger magnetic moments than atomic nuclei and therefore drastically affect the NMR spectra of neighboring nuclei. In powders, the strong dipolar interaction with unpaired electrons leads to very fast nuclear spin-lattice relaxation and to huge line broadening of NMR signals. These effects depend on the geometrical arrangement of the unpaired electrons around an atomic nucleus and again offer some information on the distances between the paramagnetic centers and atomic nuclei. If electronic spin polarization is through bonds transferred to the position of an atomic nucleus, the so-called hyperfine electron-nucleus interaction has to be taken into account. This interaction can be very strong and can severely shift NMR lines. For example, for nuclei that are two bonds apart from the paramagnetic metal centre (e.g., for ^{13}C in the $-\text{C}-\text{O}-\text{Cu}$ motif), the shifts can be several hundred or even several thousand ppm. Because of the difficulties connected with the measurement of extremely broad, severely shifted NMR signals and because of very quick nuclear spin relaxation, NMR measurements in paramagnetic MOFs are relatively rare.

3. Framework structure

Metal organic frameworks can comprise several NMR active nuclei, for example, ^1H , ^{13}C , $^{14/15}\text{N}$, ^{17}O , ^{19}F , ^{35}Cl , or ^{79}Br in organic linkers and functional groups, and ^{17}O , ^{25}Mg , ^{27}Al , ^{43}Ca , ^{45}Sc , $^{47/49}\text{Ti}$, ^{51}V , ^{67}Zn , or ^{91}Zr in metal-oxo clusters. These nuclei, especially the abundant ones and/or the ones with large magnetic moments, can be readily exploited for inspection of the framework structure. Very straightforward measurements of ^{13}C and ^1H NMR spectra can quickly confirm the identity of the organic linkers and the presence of functional groups attached to linker molecules [13, 14]. An example of ^{13}C and ^1H spectra of UiO-66, bearing different functional groups, is presented in **Figure 2**. The ^{13}C spectra can clearly resolve the inequivalent aromatic and carboxyl carbon atoms. Tentative assignment of individual NMR signals to different carbon sites within the linkers, and thus the verification of the nature of the incor-

porated linker or functional groups, can often be done simply by using the 'empirical' chemical-shift-prediction programs like ChemDraw or ACD/Labs, or via the comparison of the solid-state NMR spectra with the solution NMR spectra of the corresponding linkers. Inspection of the line widths can be useful, because it provides information on the crystallinity of the materials and can alert about the presence of a local disorder in the solids. ^1H and ^{13}C NMR spectra also show if there are some unreacted linker molecules, water molecules and solvent molecules left in the samples.

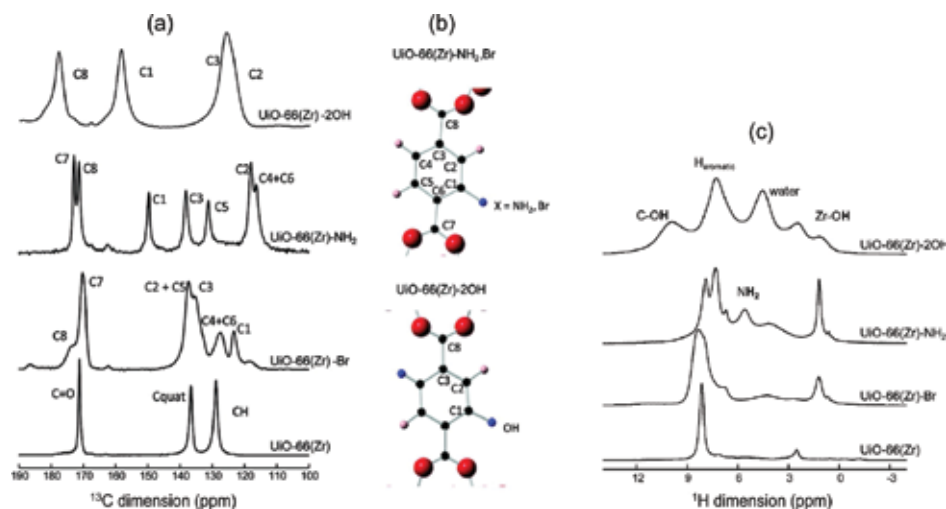


Figure 2. Inspection of organic linkers in differently functionalized UiO-66 materials. (a) ^1H - ^{13}C CP-MAS and (c) ^1H MAS NMR spectra. NMR signals were assigned based on DFT calculations. Labels for the individual carbon sites in the organic linkers of the NH₂- and Br- (top), and 2OH- (bottom) functionalized UiO-66 are presented in (b). Broad lines in the ^1H - ^{13}C CP-MAS spectrum of UiO-66-2OH indicate the presence of local disorder or of lower degree of crystallinity in this sample. Unlabeled ^1H MAS NMR signal at about 6.5 ppm corresponds to residual ligand. Figures were published by Devautour-Vinot et al. [13]. Copyright © 2012 American Chemical Society.

Solid-state NMR can provide valuable information on the dynamics of linkers. There have been several reports on the dynamics of linkers inspected by ^2H NMR spectroscopy of deuterated aromatic rings. In d_4 -MOF-5, for example, it was shown that at temperature of 298 K and lower, the 1,4-phenyldicarboxylate groups were stationary, whereas at temperature of 373 K and above the aromatic rings exhibited π -flips about their *para* axes [15]. The onset of π -flips was manifested through the change of the quadrupolar line-shape of the ^2H NMR signal. Similar were the findings in case of MIL-53 and MIL-47 [16]. The π -flips of the benzene rings were faster in the flexible MIL-53 than in the rigid MIL-47, but still not as fast as in MOF-5. It was concluded that in MIL materials with a 1D channel system, environment is considerably more constrained than in MOF-5 with a 3D system of channels. The detailed study of dynamics of benzene rings in UiO-66 showed that the temperature-dependent rotational motion affects the effective size of the windows between the pores and can thus influence the performance of the material in gas separation processes [17]. The dynamics of linkers and

functional groups can be effectively studied also by the measurements of ^1H and ^{13}C spin-lattice relaxation times, as was done, for example, in IRMOF-3, ZIF-4 and ZIF-8 [18, 19].

In the recent years, a substantial interest in the preparation and application of the so-called mixed-linker MOFs has arisen. Deng et al. prepared a series of MOF-5-type materials by mixing differently modified terephthalic acids in different relative amounts and combinations [20]. Altogether 18 mixed-linker MOFs with up to eight distinct functionalities in one phase were synthesized. Kong et al. employed NMR spectroscopy to obtain an insight into the distribution of different linkers [21]. They isotopically labeled various linkers used in the synthesis of MOF-5 with ^{15}N , and carried out ^{13}C - ^{15}N REDOR NMR measurements. The measurements provided information on the average distances among different linker molecules. By comparing the results of REDOR measurements with results of Monte Carlo simulations, Kong et al. were able to discriminate between cases where linkers of one type formed domains within crystals, where different linkers were alternating with one another, and where different linkers were distributed randomly throughout the crystalline framework. This valuable information helped them rationalize the observed differences in adsorption capacity and separation efficiency of mixed-linker MOFs characterized by different types of linker distributions. Another approach for studying the distribution of different linkers in mixed-linker MOFs was undertaken by Krajnc et al. [22]. They prepared Al-based metal-organic material DUT-5 with biphenyl and bipyridyl dicarboxylic molecules (bpdc and bpydc) as linkers. With two-dimensional ^1H - ^{13}C HETCOR spectroscopy and ab-initio chemical shift calculations they successfully assigned ^1H MAS NMR signals to different hydrogen atoms and showed that a peak belonging only to bpydc could be clearly resolved from a peak belonging only to bpdc. Afterward, they studied polarization transfer between these two types of hydrogen nuclei. They carried out variable-contact-time ^1H spin-diffusion MAS NMR experiments and modeled spin-diffusion curves for various types of distributions of bpydc and bpdc. Comparison between the experiment and modeling allowed them to show that in their particular material the distribution of the minority bpydc linker was very homogeneous throughout the crystals and that no single-linker domains or crystallites were formed (see **Figure 3**). Both studies, the one of Kong et al. [21] and the one of Krajnc et al. [22], demonstrated that solid-state NMR spectroscopy is indeed a unique tool, capable of providing information that is not attainable by any other technique.

Aluminum is the most studied metal centre of MOFs. ^{27}Al MAS NMR measurements can provide very interesting information about the framework, which is sometimes complementary to the information obtained by diffraction. Volkringer et al. employed microdiffraction and solid-state NMR to elucidate the structure of Al-MIL-100 [23]. From the X-ray diffraction (XRD) analysis, the Al-MIL-100 structure contains seven inequivalent Al crystallographic sites that belong to three distinct $\{\text{Al}_3\text{O}(\text{OH})(\text{H}_2\text{O})_2\}_4[\text{btc}]_4$ supertetrahedra. ^{27}Al MAS NMR spectrum of the as-synthesized Al-MIL-100 exhibited three overlapped signals in the chemical shift range between -20 ppm and 10 ppm, all belonging to 6-fold coordinated aluminum sites. The signals displayed very similar isotropic chemical shifts but different quadrupolar coupling constants varying from 1.3 to 5.6 MHz. The relative areas of the three signals of $2:10:5$ could be mapped onto the multiplicities of the XRD inequivalent Al sites of $2:(4:2:4):(2:1:2)$.

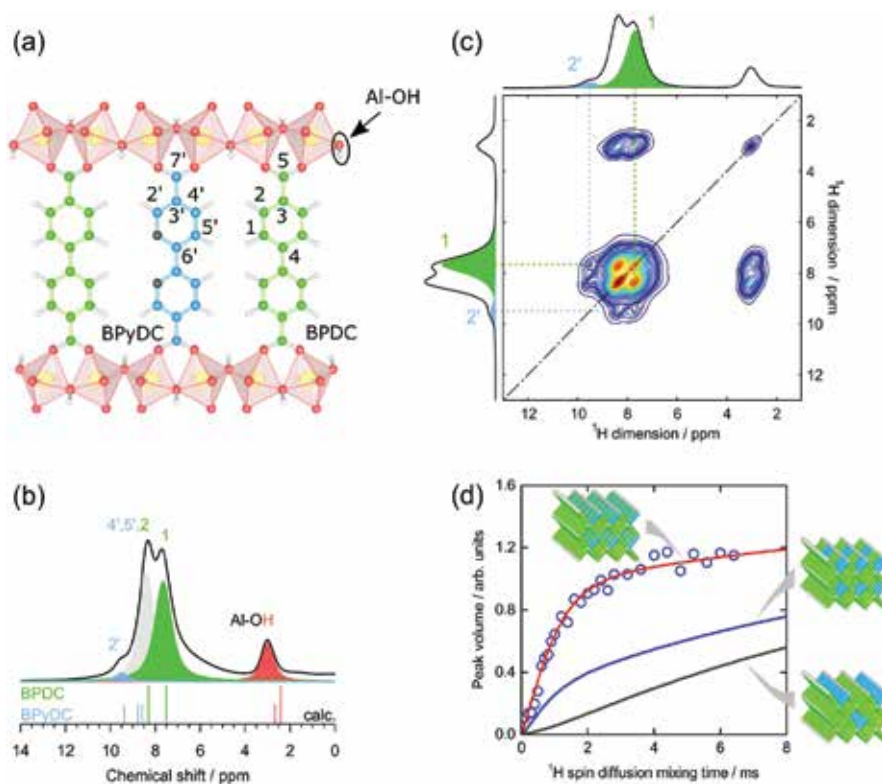


Figure 3. Analysis of the distribution of bpdc and bpydc linkers in the mixed-linker DUT-5 material. (a) Labeling of the framework carbon and hydrogen atoms. (b) ^1H MAS NMR spectrum, which revealed that the peak belonging to bpydc ($\text{H}2'$) can be resolved from the peak belonging to bpdc ($\text{H}1$). Assignment was based on DFT calculations and ^1H - ^{13}C HETCOR NMR measurement. (c) ^1H spin-diffusion homonuclear correlation NMR spectrum. Horizontal and vertical dotted lines mark the frequencies of the $\text{H}2'$ and $\text{H}1$ resonances, and their crossings mark the $\text{H}2'$ - $\text{H}1$ cross peaks. (d) Measured and calculated ^1H spin-diffusion curves for the $\text{H}2'$ - $\text{H}1$ cross peak. Results of calculations for three different models of mixed-linker DUT-5 are presented. The models are characterized by an equal bpdc/bpydc ratio but different spatial distributions of the two linkers. Only the model with a homogeneously distributed bpydc linker leads to good agreement with the experimental data. Figures were published by Krajnc et al. [22]. Copyright © 2015 Wiley-VCH.

The observed difference between NMR and XRD proportions suggested that the symmetry order was higher for NMR than for XRD. The origin of this higher symmetry was attributed to the motion of the framework protons, which led to averaging of some crystallographically distinct environments.

Very recently, first studies of ^{67}Zn and ^{25}Mg centers have also been described [24–29]. In these studies, ^{67}Zn and ^{25}Mg NMR spectroscopy mostly served as a tool for the verification of structural models of MOFs, which had been proposed by X-ray diffraction analyses. From the ^{25}Mg NMR spectrum one can determine the number of crystallographically inequivalent magnesium sites (**Figure 4**), as well as chemical shift and quadrupolar coupling constant for each of these sites. Based on the proposed structural model, the same NMR observables can be calculated ab initio, using the gauge-included projector-augmented wave approach

(GIPAW) within the frame of the density functional theory (DFT). By comparing the measured and the calculated chemical shifts and quadrupolar coupling constants one can judge about the quality of the proposed structural models. In a recent study, Mali et al. [28] have compared the calculated and the measured ^{13}C and ^{25}Mg chemical shifts and ^{25}Mg quadrupolar constants for a series of Mg-based MOFs. They have shown that the agreement between the calculation and the experiment was quite nice for the chemical shifts, but not for the quadrupolar coupling constants, for which the calculated values were typically substantially overestimated. The discrepancy in the calculation of electric field gradients was attributed to the dynamics of water molecules that were coordinated to the magnesium atoms. Motion of these water molecules could, namely, partially average out electric field gradients and could thus lead to apparently smaller quadrupolar couplings. Another study by Alvarez et al. showed that ^{27}Al quadrupolar coupling constants in aluminum fumarate MOF A520 crucially depended on the hydration state of the material [30]. These examples thus suggest that an important role of NMR spectroscopy of metal centers could be the inspection of the coordination state of the centers and the analysis of the dynamics of the metal-oxo clusters.

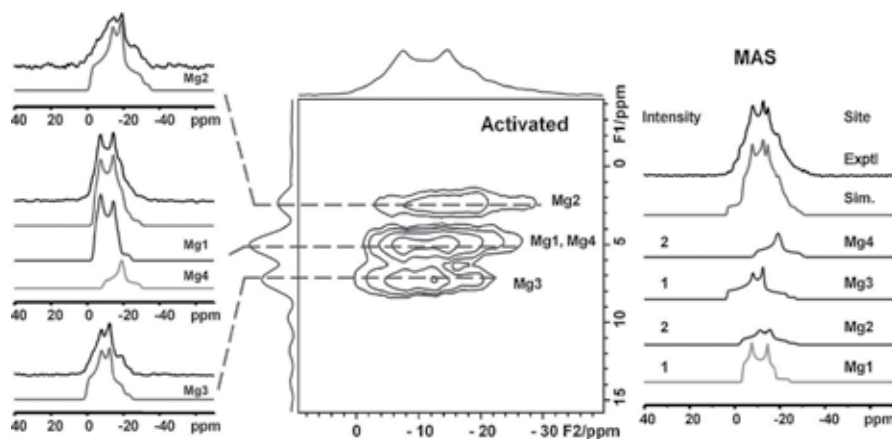


Figure 4. Inspection of metal centers of the activated microporous $\alpha\text{-Mg}_3(\text{HCOO})_6$ material. Advanced two-dimensional ^{25}Mg 3QMAS NMR spectroscopy was employed to resolve the signals of the four inequivalent Mg sites. After the slices of the 2D spectrum were simulated (shown on the left), the obtained chemical shifts and quadrupolar coupling constants for each of the four Mg sites enabled successful simulation of the ^{25}Mg MAS spectrum (shown on the right). Figures were published by Xu et al. [27]. Copyright © 2013 Wiley-VCH.

Many MOFs comprise metal centers that are paramagnetic. Such centers make NMR spectroscopy quite demanding. Even though the atomic nuclei within paramagnetic ions often do possess magnetic moments, their NMR spectra cannot be measured, because the hyperfine interactions of these nuclei with the unpaired electrons are too strong. In some cases, however, the presence of paramagnetic centers does not prevent the detection of well resolved spectra of ^1H and ^{13}C nuclei from linkers. One of the first examples of a detailed NMR study of paramagnetic MOFs was presented by Dawson et al. [31]. They showed ^{13}C MAS NMR spectra of Cu-containing HKUST-1 and STAM-1, in which the NMR signals exhibited substantial paramagnetic shifts of up to about 800 ppm. As can be seen in **Figure 5**, ^{13}C spin-lattice

relaxation times in HKUST-1 depend on the distances between the carbon atoms of the BTC linker and the copper centers, and thus enable reliable assignment of the three ^{13}C signals to the three carbon sites in the linkers. The sensitivity of NMR shifts to the proximity between the NMR-active atomic nuclei and paramagnetic centers could be well exploited in the studies of mixed-metal MOFs, especially if one of the metals was paramagnetic and the other was diamagnetic. Indeed, in the case of mixed Cu-Al fluorinated MOF, ^{19}F NMR detected a signal with an unusual shift of -456 ppm, with large line width of 12 kHz, and with a broad manifold of spinning sidebands [32]. The signal was assigned to fluorine atoms that formed bridges between the diamagnetic aluminum and the paramagnetic copper atoms. It should be noted, however, that most of the paramagnetic centers within MOFs will give rise to much stronger paramagnetic effects than the Cu(II) ions. Especially strong effects are, for example, expected in the case of Fe(III) centers.

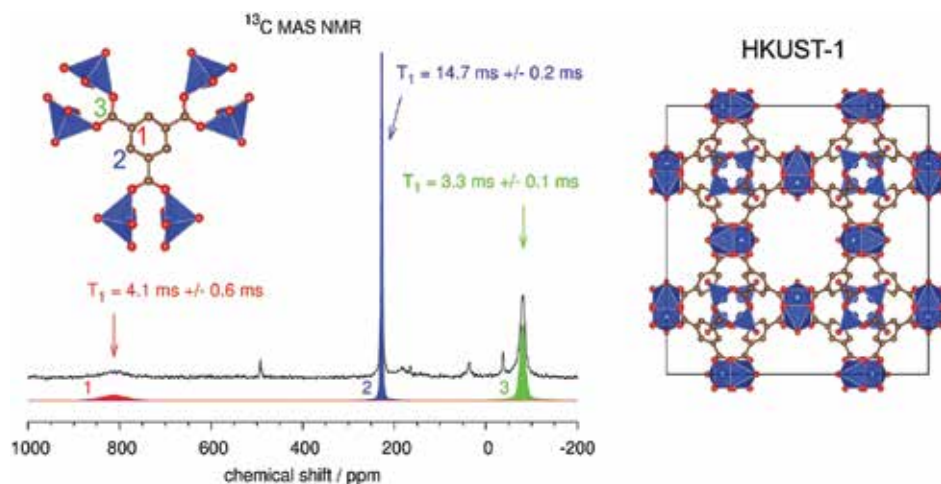


Figure 5. NMR analysis of the paramagnetic metal-organic framework HKUST-1. Because of the strong hyperfine interaction between the unpaired electrons and the ^{13}C nuclei of the organic BTC linkers, signals in the ^{13}C MAS NMR spectrum are severely shifted. Assignment of the shifted signals can be accomplished based on the corresponding ^{13}C spin-lattice relaxation times T_1 . The relaxation times depend on the distances between the paramagnetic centers and the ^{13}C nuclei. The structure and the organic linker of HKUST-1 are schematically presented.

4. Guest molecules and host-guest interactions

The role of solid-state NMR spectroscopy becomes extremely important when studying molecules within the pores of MOFs. The set of interesting species, adsorbed or incorporated into MOFs, is very large. Within this set, water is probably one of the most often studied species. Water has a strong impact on MOFs, and studying the water-framework interaction is crucial for the understanding of the MOF stability. NMR spectroscopy can be very helpful in such studies. In HKUST-1, ^1H and ^{13}C MAS NMR spectroscopy was employed for investigating gradual hydration of the material [33]. In spite of the fact that the copper metal centers

of HKUST-1 are paramagnetic, in the ^1H MAS spectra no significant shifts of NMR signals were detected, which suggested that the electron-nucleus hyperfine couplings for ^1H nuclei were rather weak. This further implied that the physico-chemical bonding of water molecules to the copper centers was weak or that adsorption and desorption of water molecules to the metal centers was very dynamic. Upon further hydration of HKUST-1, the material collapsed. The collapse of HKUST-1 due to its hydrothermal instability was evidenced by the broadening of the signals in the ^{13}C MAS NMR spectrum.

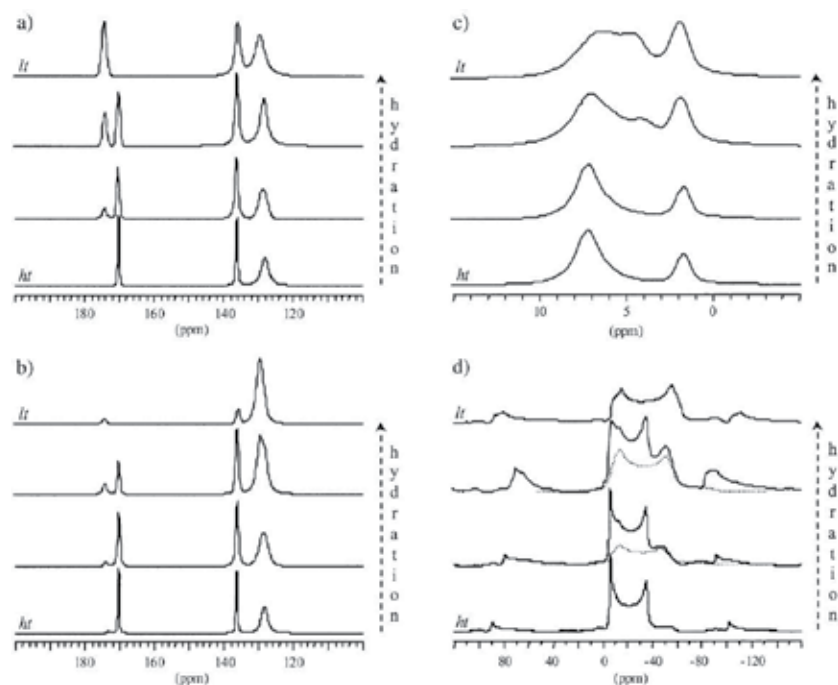


Figure 6. Studying hydration of Al-MIL-53. (a) ^{13}C MAS, (b) ^1H - ^{13}C CP-MAS, (c) ^1H MAS, and (d) ^{27}Al MAS NMR spectra of the as-prepared material (*ht* form = 'dry' material), 30% hydrated material, 50% hydrated material, and fully hydrated material (*lt* form = 'wet' material). In the ^{27}Al MAS NMR spectra of the partly hydrated materials the simulated components of the wet forms are shown with dotted lines. Figures were published by Loiseau et al. [34]. Copyright © 2004 Wiley-VCH.

Several MOFs are stable in humid atmosphere or in water. Among them, Al-MIL-53 with its flexible framework is a very interesting representative. Taulelle et al. used ^{27}Al , ^{13}C , and ^1H MAS NMR to thoroughly inspect breathing of the material as a consequence of the reversible hydration and dehydration [34]. They showed that hydrogen bonds among the water molecules in the channels and the carboxyl groups of the linkers are responsible for the contraction of the pores upon hydration. The NMR signals of the carboxyl groups in the ^{13}C MAS and ^1H - ^{13}C CP-MAS spectra were, namely, the most affected by the presence of the water molecules. Surprisingly, ^{27}Al MAS spectra showed that the bridging OH groups were practically intact during the hydration. Both, ^{13}C and ^{27}Al NMR spectra nicely distinguished

the contributions of the 'dry' and the 'wet' material (**Figure 6**), and allowed one to follow the gradual filling of the pores with water. Because NMR did not detect any polarization transfer between the dry and the wet material, the authors could conclude that individual crystallites in the powder were either dry or wet, but not composed of dry and wet domains. A very detailed NMR study was performed also on Al-MIL-100, which is another MOF capable of reversibly adsorbing and desorbing water [35]. The process of dehydration of Al-MIL-100 was investigated using a set of solid-state NMR techniques, including several two-dimensional homo- and heteronuclear correlation ones. The material showed a remarkable thermal stability up to 370°C. Up to 350°C, only one water molecule per aluminum-oxo trimer was found to leave the trimer, producing only one coordinatively unsaturated aluminum site among the three sites.

In the as-prepared Mg-MOF-74, the basic inorganic building units are MgO₆ octahedra. In each octahedron five out of six oxygen atoms belong to the carboxylate groups of the organic linkers, and one oxygen atom belongs to a water molecule. Xu et al. showed that during the dehydration, this water molecule can be expelled from the material [26]. Whereas the dehydration did not affect the ¹³C MAS NMR spectrum, the changes in the ²⁵Mg MAS NMR spectrum were quite pronounced. The ²⁵Mg signal with a well-defined quadrupolar line-shape and a small quadrupolar coupling constant changed into a broad and smeared signal with a large quadrupolar coupling constant. The increase in the quadrupolar interaction was due to the change of the coordination of Mg atoms from the rather symmetrical octahedral one to the distorted square pyramidal. The smearing of the spectral line in the dehydrated material indicated that on the short-range scale the Mg environment became quite disordered. On the long-range scale, the material still exhibited an ordered porous structure. Upon rehydration of the material, the Mg local environment reversibly changed into the ordered octahedral one. The described study is particularly interesting, because in MgMOF-74 adsorption of water can compete with the adsorption of carbon dioxide. MgMOF-74 is, namely, one of the most promising materials for CO₂ separation, and an interesting question of great practical importance is, how the material will perform as a sieve for carbon dioxide, if the gas mixture will contain non-negligible fraction of water.

Some hydrothermally stable MOFs can absorb very large amounts of water. Such representatives could become very interesting materials for water-adsorption based heat-storage applications. Desorption of water can be considered as an efficient energy-storage step. Upon a controlled rehydration of the dried material, large amounts of energy could be released. Again NMR spectroscopy can provide useful insight into such materials. In case of a hydrothermally stable Zn-trimesate, ¹H and ²H variable-temperature MAS NMR showed that water was expelled from the material in three distinct steps (**Figure 7**) [36]. In the first step, water was desorbed from the larger pores, in the second step hydrogen-bonded water molecules from the narrow pores were expelled, and in the third step the water molecules that were coordinated to zinc atoms were desorbed. The last step occurred at about 250°C. ²H NMR spectroscopy provided additional information on the dynamics of the water molecules within the pores. Mobility of water molecules within the larger pores increased quickly with the increased temperature; their NMR signal in the ²H spectrum narrowed so that no quadrupo-

lar line-shape could be detected for this signal. On the contrary, water molecules that were coordinated to zinc atoms exhibited a well-defined quadrupolar pattern of spinning sidebands well above 100°C, meaning that motion of these water molecules was still considerably hindered at that temperature. The ^{13}C spectrum recorded at 250°C was only slightly different from the spectrum of the fully hydrated material and confirmed that the framework was still well ordered at 250°C. Upon rehydration, the spectrum reversibly transformed to the initial one, showing that indeed the material was hydrothermally stable and that reversible dehydration and rehydration was possible. Recently, Cadiau et al. investigated MIL-160, which is an even more promising material for heat storage [37]. Its water uptake is as high as 320 g per 1 kg of the dry matrix. The researchers monitored gradual hydration of the dried material and detected two steps in water adsorption. Firstly, water molecules were attached to the framework hydroxyl groups on the inorganic aluminate chains, and secondly, water molecules entered into the centre of the channels. These latter water molecules did not interact appreciably with the framework.

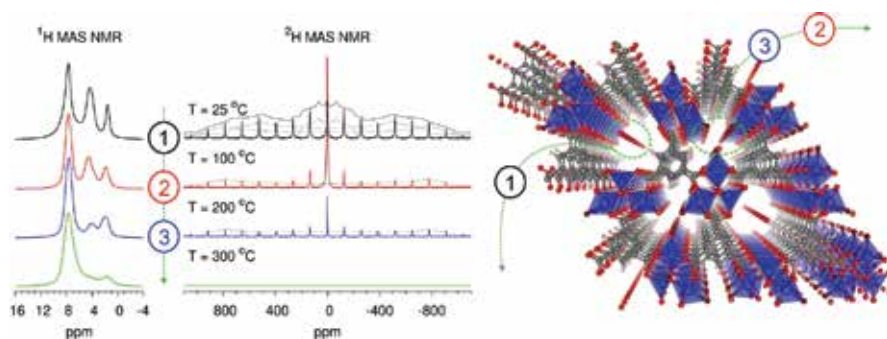


Figure 7. Variable-temperature ^1H and ^2H MAS NMR spectra of porous Zn-trimesate show that water is expelled from the material in three distinct steps. Step 1 corresponds to removal of water molecules from the larger channels, step 2 corresponds to the removal of hydrogen-bonded water molecules from the narrower channels, and step 3 corresponds to the removal of water molecules that were attached to Zn centers. In ^1H MAS NMR spectra, the contribution of water molecules resonates between 4 and 5 ppm; the signal at 8 ppm belongs to H atoms of the aromatic rings of the linkers and the signal at 1–2 ppm belongs to the H atoms of the framework OH groups. In ^2H MAS NMR spectra broad manifolds of spinning-sidebands correspond to rigid species, whereas high, narrow signals close to 0 ppm correspond to mobile species.

Next to water, carbon dioxide is the most interesting specie adsorbed within MOFs. Mg-MOF-74 (also termed $\text{Mg}_2(\text{dobdc})$ or CPO-27-Mg) has been one of the most investigated systems with NMR spectroscopy. In this material, the exposed Mg^{2+} cation sites give rise to exceptional CO_2 capture properties. NMR studies of Mg-MOF-74 managed to elucidate the dynamics of the adsorbed $^{13}\text{CO}_2$ molecules [38, 39]. Analysis of static ^{13}C NMR spectra quickly showed that $^{13}\text{CO}_2$ molecules indeed bond to the Mg^{2+} sites with end-on coordination, and that the line-shape of the ^{13}C signal cannot be merely a result of the spatial confinement of $^{13}\text{CO}_2$ in the pores of Mg-MOF-74. Lin et al. carried out Monte Carlo simulations to probe equilibrium configurations of CO_2 in this material [39]. Based on the calculations, they predicted that two kinds of motions of CO_2 molecules are possible in the material, fluctuations of the CO_2

molecule near the minimum-energy configuration and hops of the CO₂ molecule between different metal sites. Considering these two types of motions, they were able to very nicely explain the measured ¹³C NMR spectra at different temperatures between 100 K and 375 K (Figure 8). At the temperature of 100 K, the pronounced ¹³C chemical shift anisotropy could be assigned exclusively to localized motions (fluctuations) of the ¹³CO₂ molecules. At higher temperatures, in addition to these localized motions, also hopping of ¹³CO₂ molecules between different metal sites in the plane perpendicular to the direction of the channel started to take place. With a further increase in the temperature, motion of ¹³CO₂ molecules along the channel began. Lin et al. carried out equivalent ¹³C NMR measurement also on ¹³CO₂ adsorbed into Mg₂(dobpdc), a material that is analogous to Mg-MOF-74, but in which separation between the neighboring magnesium sites is by 30% larger than in Mg-MOF-74 [39]. As expected, hopping motion in this material started at notably higher temperature. The study of dynamics of CO₂ molecules within Mg-MOF-74 was complemented by Wang et al., who monitored variable temperature ¹⁷O NMR spectra of the adsorbed C¹⁷O₂ molecules [40]. ¹⁷O solid-state NMR line-shapes comprise contributions from quadrupolar and chemical shift interactions, and are thus very sensitive to motions. Indeed, in the above mentioned study, the researchers were for the first time able to quantify the fourth type of motion of CO₂ molecules, that is wobbling about the CO₂ minimum-energy configuration.

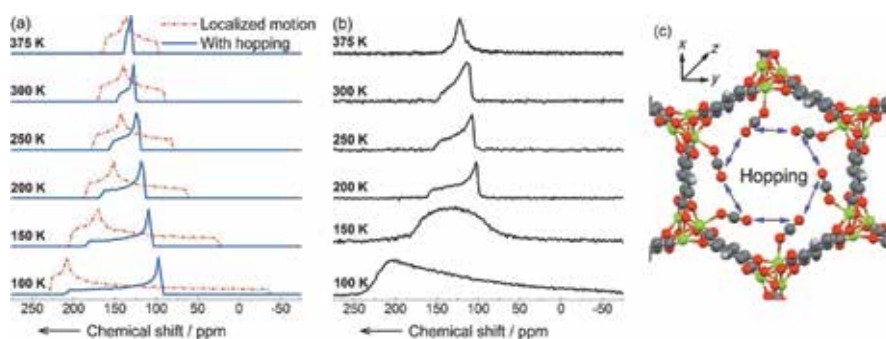


Figure 8. Studying dynamics of ¹³CO₂ molecules adsorbed into Mg-MOF-74. (a) and (b) The comparison between the simulated and the measured static ¹³C NMR spectra, which show lines broadened by chemical shift anisotropy. The comparison indicates that at about 100 K CO₂ molecules undergo localized motion around the minimum-energy positions, whereas at 200 K and above motion includes hopping of molecules between different metal sites, as indicated in (c). Figures were published by Lin et al. [39]. Copyright © 2013 Wiley-VCH.

In several MOFs, CO₂ can be reversibly chemically bonded to the framework. An example of such a MOF is CD-MOF-2, for which ¹H-¹³C CP-MAS NMR showed a signal at 158 ppm after the adsorption of carbon dioxide into the activated material [41]. This signal could be attributed to the carbonate that is formed upon adsorption. Other signals in the carbon spectrum, belonging to the linker molecules, were also affected by the incorporation of CO₂ and thus additionally confirmed that chemical reaction between the gaseous CO₂ and CD-MOF-2 took place. Let us note that the CP-MAS experiment is able to detect only rather rigid, not very mobile species, in which ¹H and ¹³C nuclei are not far apart. It cannot detect the gaseous CO₂. The latter could be detected with directly excited ¹³C MAS NMR spectroscopy at about 126

ppm. The above described study concluded that the chemisorption of CO_2 in CD-MOF-2 relied on free hydroxyl groups, which acted as reactive hotspots for formation of carbonic acid groups. Chemisorption of CO_2 , more precisely formation of carbamamic acid and carbamate ions, was detected also in some modified IRMOF-74 materials [42].

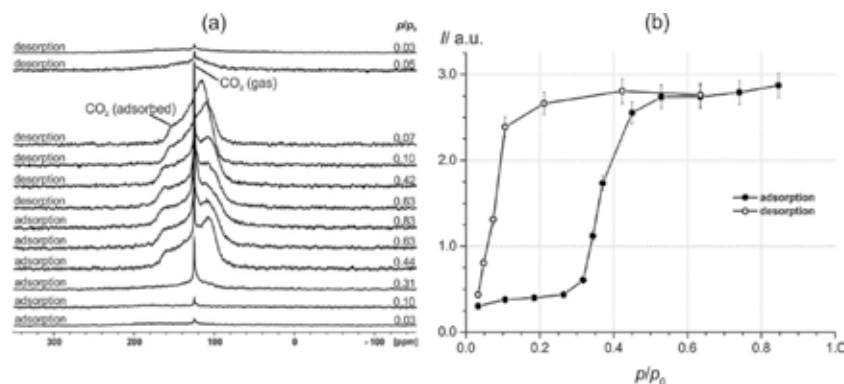


Figure 9. Adsorption and desorption of $^{13}\text{CO}_2$ in $[\text{Zn}_2(\text{BME-bdc})_2 \text{dabco}]_n$. ^{13}C NMR spectra (left) were recorded at $T = 232$ K and $p_0 = 9.6$ bar. Intensities of the adsorbed CO_2 , as extracted from the ^{13}C NMR spectra, are shown on the right. Figures were published by Bon et al. [43]. Copyright © 2015 Elsevier Inc.

Breathing of MIL-53 during hydration-dehydration is only one particular representation of porosity switching in this material. This more general phenomenon can be in flexible MOFs induced by changing the pressure of different gases, also of CO_2 . The increased pressure induces structural phase transition and increases the pores of flexible MOFs. The pressure, at which the phase transition takes place, is called the gate pressure. Bon et al. used ^{129}Xe and ^{13}C NMR spectroscopy to inspect the influence of nonpolar Xe atoms and polar CO_2 molecules on the porosity switching of a series of functionalized MOFs $[\text{Zn}_2(\text{BME-bdc})_x(\text{DB-bdc})_{2-x} \text{dabco}]_n$ ($x = 2, 1.5, 1, 0.5, 0$) [43]. Whereas ^{129}Xe chemical shift is very sensitive to the confinement/physisorption, the difference in the ^{13}C isotropic chemical shift of free CO_2 and of physisorbed CO_2 is only few ppm. However, as shown above, if motion of CO_2 molecules is spatially anisotropic or restricted, the corresponding ^{13}C signals can exhibit pronounced chemical shift anisotropy. In their study, Bon et al. followed ^{13}C NMR spectra while increasing the $^{13}\text{CO}_2$ pressure (Figure 9). At phase transition from the narrow-pore to the large-pore form, the signal of the adsorbed $^{13}\text{CO}_2$ narrowed and the sign of the chemical shift anisotropy changed. In different MOFs, the NMR study detected different gate pressures and different degrees of ordering of CO_2 molecules. Complemented by modeling, the study showed that in these MOFs without open metal sites, CO_2 molecules were preferentially found in the neighborhood of carboxylate carbon atoms of the linker molecules.

Water and carbon dioxide molecules are both small molecules, very important for the stability and applicability of MOFs in gas separation and storage and energy storage. Several MOFs comprise very large pores (mesopores) with the diameters of several nanometers. Into such pores also much larger molecules than H_2O and CO_2 can be incorporated. Particularly

interesting and important examples of larger molecules are drug molecules. Indeed, very quickly after the preparation of the first large-pore MOFs, studies on the possibilities of usage of MOFs as drug-delivery matrices had begun [44, 45]. In addition to the large pore volumes of MOFs and thus to their very high drug-loading capacities, one of the most important advantages of MOFs over other potential drug-delivery matrices is the great versatility of their structures and functionalities.

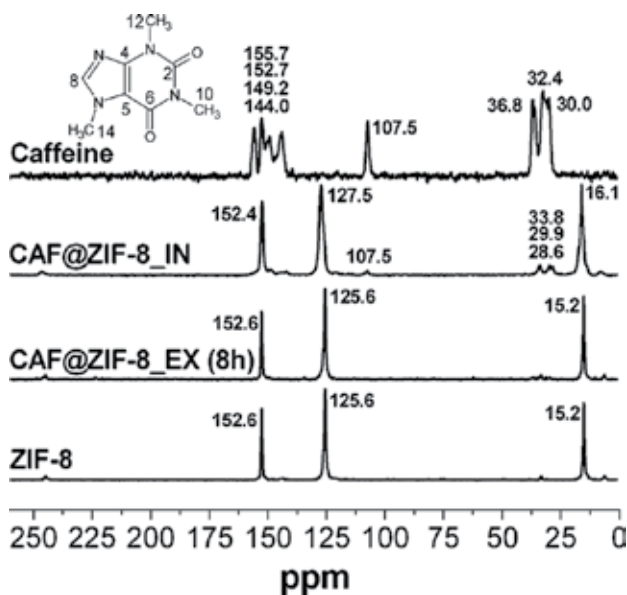


Figure 10. ^1H - ^{13}C CP-MAS NMR spectra of crystalline caffeine, empty ZIF-8, and of two differently prepared drug-delivery systems. CAF@ZIF-8_IN denotes the delivery system obtained with a one-step preparation. CAF@ZIF-8_EX was obtained by impregnating empty ZIF-8 with an aqueous solution of caffeine for 8 h and by subsequent drying at room temperature. The detected shifts of ^{13}C NMR signals of caffeine embedded into CAF@ZIF-8_EX suggest that caffeine molecules are interacting with the ZIF-8 framework. Figure was published by Liédana et al. [46]. Copyright © 2012 American Chemical Society.

NMR spectroscopy was quite often used as a tool for obtaining the information about the nature of the incorporated drug molecules within MOFs. Very often ^1H and ^{13}C MAS NMR spectra of the MOFs loaded with a drug were compared to the spectra of the pure crystalline drug and of the empty MOF. The detected changes in chemical shifts of individual NMR signals could indicate, which part of the drug molecule and which part of the framework interacted one with another. ^{13}C MAS NMR spectroscopy was employed for studying the incorporation of caffeine into ZIF-8 (Figure 10) [46]. Based on the shifts of the NMR signals of the caffeine's methyl group and of the 2-methylimidazole's CH group, the authors concluded that caffeine formed weak Van der Waals bonds and strong hydrogen bonds with the framework. Caffeine was incorporated also into pure UiO-66, and UiO-66 functionalized with NH_2 , Br, or OH groups [47]. Detailed NMR and DFT study showed that caffeine's ^{13}C chemical shift did not change after the incorporation of drug into the pores, suggesting that if there were

any interactions between caffeine molecules and the UiO frameworks, they were weak and they predominantly affected H atoms. ^1H spin-lattice relaxation times for the incorporated caffeine molecules were much shorter than for the molecules within the pure crystalline caffeine. This indicated that the caffeine molecules, even though confined, were still more mobile within the pores of UiO-66 than within the caffeine crystals. ^1H - ^1H homonuclear correlation spectra showed that only weak Van der Waals bonds between the caffeine's methyl groups and the framework's phenyl rings existed, whereas interactions with the amine and hydroxyl functional groups were not detected. The experimental findings were supported by the results of the DFT-based calculations, which proposed the energetically most favorable locations for the embedded caffeine molecules.

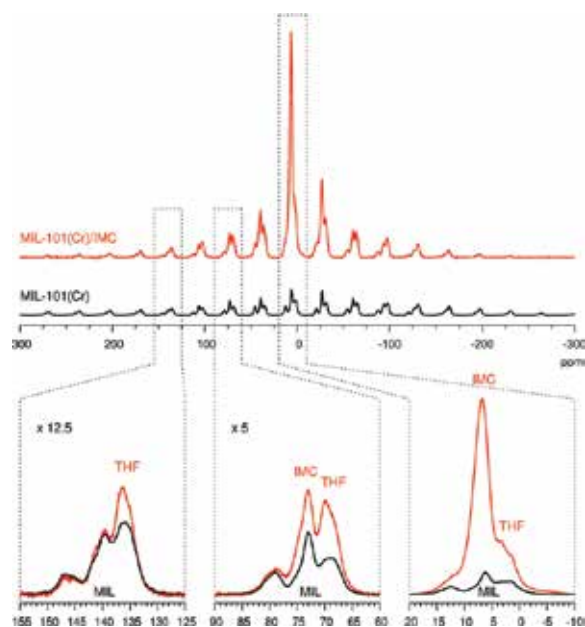


Figure 11. ^1H MAS NMR spectra of empty MIL-101(Cr) (black) and MIL-101(Cr) loaded with indomethacin (red). Enlarged segments show the centerband next to second and fourth spinning sidebands. Labels THF and IMC point to the non-negligible contributions of tetrahydrofuran (solvent) and indomethacin (drug) in the spectrum of the loaded MIL-101(Cr). Comparison of the two spectra indicates that tetrahydrofuran molecules are much more affected by the paramagnetic chromium centers than indomethacin molecules, suggesting that the former molecules are much closer to the framework metal centers than the latter molecules. Figure was published by Ćendak et al. [49].

The second, quite often studied model drug is ibuprofen. Ibuprofen was incorporated into MIL-53, MIL-100, and MIL-101 [44, 48]. The most informative were ^1H MAS NMR spectra, showing that in MIL-101, for example, ibuprofen was incorporated in the form of anions. Another model drug, indomethacin, was also incorporated into MIL-101. A detailed NMR study was carried out on Cr-MIL-101, Fe-MIL-101, Fe-MIL-101(NH_2), and Al-MIL-101(NH_2), into which large amounts of indomethacin were incorporated (ca. 1 g of indomethacin/1 g of an empty MIL-101 matrix) [49]. The loaded Al-MIL-101(NH_2) sample was the easiest to inspect by NMR, because its framework was diamagnetic. The measurement showed that indome-

thacin did not form strong bonds with the framework or its functional NH_2 groups. Interestingly, in spite of careful drying procedure, NMR spectroscopy still detected a substantial amount of solvent tetrahydrofuran molecules within the pores of Al-MIL-101(NH_2). ^1H - ^1H homonuclear correlation and ^1H - ^{13}C heteronuclear correlation experiments showed that the tetrahydrofuran molecules were attached to the hydroxyl groups on the metallic trimeric units via hydrogen bonds. Very similar conclusions were obtained also for Fe- and Cr-based drug-delivery systems. In case of the Cr-MIL-101 loaded with indomethacin (and tetrahydrofuran), ^1H MAS NMR spectrum clearly showed that tetrahydrofuran signals exhibited much broader pattern of spinning sidebands than indomethacin signals. This demonstrated that tetrahydrofuran was much closer to the paramagnetic chromium centers and was thus much more affected by the strong electron-nucleus dipolar coupling (**Figure 11**). It seems that strong bonding of tetrahydrofuran molecules to the metallic trimeric units and hindered transportation through the relatively narrow windows between the mesopores of MIL-101 were the reasons that drying in vacuum could not entirely remove the solvent from the pores of this potential drug-delivery matrix.

5. Conclusions

Selected examples of the application of solid-state NMR spectroscopy for studying MOFs showed that this spectroscopic technique can offer very valuable information about the structure and about the functioning of MOFs. Many times this information is unique and it crucially complements the information that is about MOFs obtained by other characterization tools. It is worth noting that for several of the above described studies the role of molecular modeling was particularly important. It is in fact a quite general observation that solid-state NMR spectroscopy gained a lot of power as a material's characterization tool since the introduction of modeling and accurate quantum-chemical calculations of NMR observables.

Author details

Gregor Mali

Address all correspondence to: gregor.mali@ki.si

National Institute of Chemistry, Ljubljana, Slovenia

References

- [1] Sutrisno A, Huang Y. Solid-state NMR: A powerful tool for characterization of metal-organic frameworks. *Solid State Nuclear Magnetic Resonance*. 2013 Feb;49–50:1–11.

- [2] Hoffmann HC, Debowski M, Müller P, Paasch S, Senkovska I, Kaskel S, et al. Solid-state NMR spectroscopy of metal-organic framework compounds (MOFs). *Materials*. 2012 Nov 28;5(12):2537–72.
- [3] Andrew ER, Bradbury A, Eades RG. Nuclear magnetic resonance spectra from a crystal rotated at high speed. *Nature*. 1958 Dec 13;182(4650):1659–1659.
- [4] Pines A, Gibby MG, Waugh JS. Proton-enhanced NMR of dilute spins in solids. *J. Chem. Phys.* 1973 Jul 15;59(2):569–590.
- [5] Carr HY, Purcell EM. Effects of diffusion on free precession in nuclear magnetic resonance experiments. *Phys Rev.* 1954 May 1;94(3):630–638.
- [6] O'Dell LA, Schurko RW. QCPMG using adiabatic pulses for faster acquisition of ultra-wideline NMR spectra. *Chem Phys Lett.* 2008 Oct 13;464(1–3):97–102.
- [7] Bennett AE, Griffin RG, Ok JH, Vega S. Chemical shift correlation spectroscopy in rotating solids: radio frequency-driven dipolar recoupling and longitudinal exchange. *J Chem Phys.* 1992 Jun 1;96(11):8624–8627.
- [8] Feike M, Demco DE, Graf R, Gottwald J, Hafner S, Spiess HW. Broadband multiple-quantum NMR spectroscopy. *J Magn Resonance, Ser A.* 1996 Oct;122(2):214–221.
- [9] Hohwy M, Jakobsen HJ, Edén M, Levitt MH, Nielsen NC. Broadband dipolar recoupling in the nuclear magnetic resonance of rotating solids: a compensated C7 pulse sequence. *J Chem Phys.* 1998 Feb 15;108(7):2686–2694.
- [10] van Rossum B-J, Förster H, de Groot HJM. High-field and high-speed CP-MAS¹³C NMR heteronuclear dipolar-correlation spectroscopy of solids with frequency-switched Lee–Goldburg homonuclear decoupling. *J Mag Resonance.* 1997 Feb;124(2):516–519.
- [11] Mao K, Pruski M. Directly and indirectly detected through-bond heteronuclear correlation solid-state NMR spectroscopy under fast MAS. *J Magn Resonance.* 2009 Dec;201(2):165–174.
- [12] Gullion T, Schaefer J. Rotational-echo double-resonance NMR. *J Magn Resonance* (1969). 1989 Jan 1;81(1):196–200.
- [13] Devautour-Vinot S, Maurin G, Serre C, Horcajada P, Paula da Cunha D, Guillerm V, et al. Structure and dynamics of the functionalized MOF type UiO-66(Zr): NMR and dielectric relaxation spectroscopies coupled with DFT calculations. *Chem Mater.* 2012 Jun 12;24(11):2168–2177.
- [14] Wittmann T, Siegel R, Reimer N, Milius W, Stock N, Senker J. Enhancing the water stability of Al-MIL-101-NH₂ via postsynthetic modification. *Chem Eur J.* 2015 Jan 2;21(1):314–323.

- [15] Gonzalez J, Nandini Devi R, Tunstall DP, Cox PA, Wright PA. Deuterium NMR studies of framework and guest mobility in the metal-organic framework compound MOF-5, $Zn_4O(O_2CC_6H_4CO_2)_3$. *Microporous Mesoporous Mater.* 2005 Sep 15;84(1–3):97–104.
- [16] Kolokolov DI, Jovic H, Stepanov AG, Guillerm V, Devic T, Serre C, et al. Dynamics of benzene rings in MIL-53(Cr) and MIL-47(V) frameworks studied by 2H NMR spectroscopy. *Angew Chem Int Ed.* 2010 Jun 28;49(28):4791–4794.
- [17] Kolokolov DI, Stepanov AG, Guillerm V, Serre C, Frick B, Jovic H. Probing the dynamics of the porous Zr terephthalate UiO-66 framework using 2H NMR and neutron scattering. *J Phys Chem C.* 2012 Jun 7;116(22):12131–12136.
- [18] Morris W, Taylor RE, Dybowski C, Yaghi OM, Garcia-Garibay MA. Framework mobility in the metal-organic framework crystal IRMOF-3: evidence for aromatic ring and amine rotation. *J Mol Struct.* 2011 Oct 12;1004(1–3):94–101.
- [19] Morris W, Stevens CJ, Taylor RE, Dybowski C, Yaghi OM, Garcia-Garibay MA. NMR and X-ray Study revealing the rigidity of zeolitic imidazolate frameworks. *J Phys Chem C.* 2012 Jun 21;116(24):13307–13312.
- [20] Deng H, Doonan CJ, Furukawa H, Ferreira RB, Towne J, Knobler CB, et al. Multiple functional groups of varying ratios in metal-organic frameworks. *Science.* 2010 Feb 12;327(5967):846–850.
- [21] Kong X, Deng H, Yan F, Kim J, Swisher JA, Smit B, et al. Mapping of functional groups in metal-organic frameworks. *Science.* 2013;341(6148):882–885.
- [22] Krajnc A, Kos T, Zabukovec Logar N, Mali G. A simple NMR-based method for studying the spatial distribution of linkers within mixed-linker metal-organic frameworks. *Angew Chem Int Ed.* 2015 Sep 1;54(36):10535–10538.
- [23] Volkringer C, Popov D, Loiseau T, Férey G, Burghammer M, Riekel C, et al. Synthesis, single-crystal X-ray microdiffraction, and NMR characterizations of the giant pore metal-organic framework aluminum trimesate MIL-100. *Chem Mater.* 2009 Dec 22;21(24):5695–5697.
- [24] Sutrisno A, Terskikh VV, Shi Q, Song Z, Dong J, Ding SY, et al. Characterization of Zn-containing metal-organic frameworks by solid-state ^{67}Zn NMR spectroscopy and computational modeling. *Chem Eur J.* 2012 Sep 24;18(39):12251–12259.
- [25] He P, Lucier BEG, Terskikh VV, Shi Q, Dong J, Chu Y, et al. Spies within metal-organic frameworks: investigating metal centers using solid-state NMR. *J Phys Chem C.* 2014 Oct 16;118(41):23728–23744.
- [26] Xu J, Terskikh VV, Huang Y. ^{25}Mg solid-state NMR: a sensitive probe of adsorbing guest molecules on a metal center in metal-organic framework CPO-27-Mg. *J Phys Chem Lett.* 2013 Jan 3;4(1):7–11.

- [27] Xu J, Terskikh VV, Huang Y. Resolving multiple non-equivalent metal sites in magnesium-containing metal-organic frameworks by natural abundance ^{25}Mg solid-state NMR spectroscopy. *Chem Eur J.* 2013 Apr 2;19(14):4432–4436.
- [28] Mali G, Trebosc J, Martineau C, Mazaj M. Structural study of Mg-based metal-organic frameworks by X-ray diffraction, ^1H , ^{13}C , and ^{25}Mg solid-state NMR spectroscopy, and first-principles calculations. *J Phys Chem C.* 2015 Apr 9;119(14):7831–7841.
- [29] Xu J, Lucier BEG, Sinelnikov R, Terskikh VV, Staroverov VN, Huang Y. Monitoring and understanding the paraelectric–ferroelectric phase transition in the metal-organic framework $[\text{NH}_4][\text{M}(\text{HCOO})_3]$ by solid-state NMR spectroscopy. *Chem Eur J.* 2015 Oct 5;21(41):14348–14361.
- [30] Alvarez E, Guillou N, Martineau C, Bueken B, Van de Voorde B, Le Guillouzer C, et al. The structure of the aluminum fumarate metal-organic framework A520. *Angew Chem Int Ed.* 2015 Mar 16;54(12):3664–3668.
- [31] Dawson DM, Jamieson LE, Mohideen MIH, McKinlay AC, Smellie IA, Cadou R, et al. High-resolution solid-state ^{13}C NMR spectroscopy of the paramagnetic metal-organic frameworks, STAM-1 and HKUST-1. *Phys Chem Chem Phys.* 2012 Dec 13;15(3):919–929.
- [32] Cadiou A, Auguste S, Taulelle F, Martineau C, Adil K. Hydrothermal synthesis, ab-initio structure determination and NMR study of the first mixed Cu–Al fluorinated MOF. *CrystEngComm.* 2013 Apr 2;15(17):3430–3435.
- [33] Gul-E-Noor F, Jee B, Pöppel A, Hartmann M, Himsl D, Bertmer M. Effects of varying water adsorption on a $\text{Cu}_3(\text{BTC})_2$ metal-organic framework (MOF) as studied by ^1H and ^{13}C solid-state NMR spectroscopy. *Phys Chem Chem Phys.* 2011 Apr 14;13(17):7783–7788.
- [34] Loiseau T, Serre C, Huguenard C, Fink G, Taulelle F, Henry M, et al. A rationale for the large breathing of the porous aluminum terephthalate (MIL-53) upon hydration. *Chem Eur J.* 2004 Mar 19;10(6):1373–1382.
- [35] Haouas M, Volkringer C, Loiseau T, Férey G, Taulelle F. Monitoring the activation process of the giant pore MIL-100(Al) by solid state NMR. *J Phys Chem C.* 2011 Sep 15;115(36):17934–1744.
- [36] Birsa Čelič T, Mazaj M, Guillou N, Elkaïm E, El Roz M, Thibault-Starzyk F, et al. Study of hydrothermal stability and water sorption characteristics of 3-dimensional Zn-based trimesate. *J Phys Chem C.* 2013 Jul 18;117(28):14608–14617.
- [37] Cadiou A, Lee JS, Damasceno Borges D, Fabry P, Devic T, Wharmby MT, et al. Design of hydrophilic metal organic framework water adsorbents for heat reallocation. *Adv Mater.* 2015 Aug 1;27(32):4775–4780.

- [38] Kong X, Scott E, Ding W, Mason JA, Long JR, Reimer JA. CO₂ dynamics in a metal-organic framework with open metal sites. *J Am Chem Soc.* 2012 Sep 5;134(35):14341–14344.
- [39] Lin L-C, Kim J, Kong X, Scott E, McDonald TM, Long JR, et al. Understanding CO₂ dynamics in metal-organic frameworks with open metal sites. *Angew Chem Int Ed.* 2013 Apr 15;52(16):4410–4413.
- [40] Wang WD, Lucier BEG, Terskikh VV, Wang W, Huang Y. Wobbling and hopping: studying dynamics of CO₂ adsorbed in metal-organic frameworks via 17O solid-state NMR. *J Phys Chem Lett.* 2014 Oct 2;5(19):3360–3365.
- [41] Gassensmith JJ, Furukawa H, Smaldone RA, Forgan RS, Botros YY, Yaghi OM, et al. Strong and reversible binding of carbon dioxide in a green metal-organic framework. *J Am Chem Soc.* 2011 Oct 5;133(39):15312–15315.
- [42] Sung Cho H, Deng H, Miyasaka K, Dong Z, Cho M, Neimark AV, et al. Extra adsorption and adsorbate superlattice formation in metal-organic frameworks. *Nature.* 2015 Nov 26;527(7579):503–507.
- [43] Bon V, Pallmann J, Eisbein E, Hoffmann HC, Senkovska I, Schwedler I, et al. Characteristics of flexibility in metal-organic framework solid solutions of composition [Zn₂(BME-bdc)_x(DB-bdc)_{2-x}dabco]_n: In situ powder X-ray diffraction, in situ NMR spectroscopy, and molecular dynamics simulations. *Microporous Mesoporous Mater.* 2015 Nov 1;216:64–74.
- [44] Horcajada P, Serre C, Maurin G, Ramsahye NA, Balas F, Vallet-Regí M, et al. Flexible porous metal-organic frameworks for a controlled drug delivery. *J Am Chem Soc.* 2008 May 1;130(21):6774–6780.
- [45] Horcajada P, Chalati T, Serre C, Gillet B, Sebrie C, Baati T, et al. Porous metal-organic-framework nanoscale carriers as a potential platform for drug delivery and imaging. *Nat Mater.* 2010 Feb;9(2):172–178.
- [46] Liédana N, Galve A, Rubio C, Téllez C, Coronas J. CAF@ZIF-8: one-step encapsulation of cCaffeine in MOF. *ACS Appl Mater Interfaces.* 2012 Sep 26;4(9):5016–5021.
- [47] Devautour-Vinot S, Martineau C, Diaby S, Ben-Yahia M, Miller S, Serre C, et al. Caffeine confinement into a series of functionalized porous zirconium MOFs: a joint experimental/modeling exploration. *J Phys Chem C.* 2013 Jun 6;117(22):11694–11704.
- [48] Horcajada P, Serre C, Vallet-Regí M, Sebban M, Taulelle F, Férey G. Metal-organic frameworks as efficient materials for drug delivery. *Angew Chem Int Ed.* 2006 Sep 11;45(36):5974–5978.
- [49] Čendak T, Žunkovič E, Godec TU, Mazaj M, Logar NZ, Mali G. Indomethacin embedded into MIL-101 frameworks: a solid-state NMR study. *J Phys Chem C.* 2014 Mar 27;118(12):6140–6150.

Molecular Simulations for Adsorption-Based CO₂ Separation Using Metal Organic Frameworks

Seda Keskin

Additional information is available at the end of the chapter

<http://dx.doi.org/10.5772/64226>

Abstract

Metal organic frameworks (MOFs) have received significant attention as a new family of nanoporous materials in the last decade. Variations in geometry, size, and chemical functionality of these materials have led to several thousands of different MOF structures. MOFs typically have high porosities, large surface areas, and reasonable thermal and mechanical stabilities. These properties make them ideal adsorbents for adsorption-based gas separations. It is not practically possible to test the adsorption-based gas separation potential of all available MOFs using purely experimental techniques. Molecular simulations can guide experimental studies by providing insights into the gas adsorption and separation mechanisms of MOFs. Several molecular simulation studies have examined adsorption-based CO₂ separation using MOFs due to the importance of CO₂ capture for clean energy applications. These simulations have been able to identify the MOF having the most promising CO₂ separation properties prior to extensive experimental efforts. The aim of this chapter is to address current opportunities and challenges of molecular simulations of MOFs for adsorption-based CO₂ separations and to provide an outlook for prospective simulation studies.

Keywords: MOF, molecular simulation, adsorption, separation

1. Introduction

We have witnessed the quick growth of a new group of nanoporous materials named as metal organic frameworks (MOFs) in the last decade. MOFs are crystalline nanoporous materials composed of metal complexes that are linked by organic ligands to create highly porous frameworks [1, 2]. MOFs become strong alternatives to more traditional nanoporous materials such as zeolites due to their fascinating physical and chemical properties. MOFs

typically have very large surface areas (500–6000 m²/g), high pore volumes (1–4 cm³/g), wide range of pore sizes from micro- to mesoscale (1–98 Å), and reasonable thermal and mechanical stabilities. The most important characteristic of MOFs is that their physical, chemical, and structural properties can be tuned during synthesis. This controllable synthesis leads to a large diversity of materials having different geometry, pore size, and chemical functionality [3, 4]. As a result, thousands of MOFs have been reported in the Cambridge Crystallographic Database [5]. The family of MOFs can be divided into subgroups such as isoreticular MOFs (IRMOFs), zeolitic imidazolate frameworks (ZIFs), zeolite-like MOFs (ZMOFs), and covalent organic frameworks (COFs).

MOFs have been examined for a variety of chemical applications including gas storage [6, 7], gas sensing [8], gas separating membranes [9], mixed matrix membranes [10], catalysis [11], and biomedical applications [12, 13]. Among these applications, gas separation has received a significant interest because the pore sizes of MOFs can be tuned to selectively separate gases at the molecular level. Gas separation using MOFs has been generally studied in two categories: equilibrium-based gas separations and kinetic-based gas separations [14]. In equilibrium-based gas separations, MOFs are used as adsorbents and in kinetic-based separations, MOFs are used as membranes. Adsorption-based gas separation is governed by the thermodynamic equilibrium. Gas components are reversibly adsorbed into the pores of the adsorbent. An ideal adsorbent material must have a good combination of adsorption selectivity and working capacity in addition to high stability, high void volume, and well-defined pore sizes. High porosities, large surface areas, different pore sizes and shapes, and reasonable stabilities of MOFs suggest that these materials can be ideal adsorbents in equilibrium-based gas separation applications. Several experimental studies have been carried out for adsorption-based gas separations using MOFs [15–17].

Two criteria are widely investigated to assess the potential of MOF adsorbents: adsorption selectivity and working capacity. Adsorption selectivity is determined by the adsorption affinity of the MOF for one gas species relative to another. High adsorption selectivity means a high-purity product and hence lower energy requirements. Working capacity is defined as the difference between the adsorbed amounts of gas at the adsorption and desorption pressures. High working capacity means easy regeneration of the adsorbent material. For an efficient and economic adsorption-based gas separation, both high selectivity and high working capacity are desired. Therefore, experimental studies on MOF adsorbents generally examine selectivity and working capacity of the materials [18].

Most of the experimental studies have focused on CO₂ separation. Because of the growing environmental concerns, removal of CO₂ from natural gas (CO₂/CH₄), flue gas (CO₂/N₂), and other gases (CO₂/H₂) becomes an important issue. Experimentally measured selectivity and gas uptake capacity of several MOFs for separation of CO₂ from CH₄ and N₂ have been summarized in the literature [19]. Currently available adsorbents such as activated carbons, carbon molecular sieves, and zeolites are not highly selective for CO₂ separation, especially for separation of CO₂ from flue gas [20]. A good comparison of CO₂ separation performances of different nanoporous materials such as MOFs, zeolites, and activated carbons is available in a recent review [21]. It is shown that CO₂/N₂ selectivity changes from low in zeolites to moderate

in carbon-based adsorbents and becomes high in MOFs. Therefore, research on adsorption-based gas separations has focused on identifying highly selective MOF adsorbents with high CO₂ capacities that can replace traditional adsorbents.

Considering the very large number of available MOFs, it is not possible to test thousands of different MOFs as adsorbents using purely experimental methods. Molecular simulations play an increasingly important role in understanding the potential of MOFs in adsorption-based gas separations. Among molecular simulation methods, grand canonical Monte Carlo (GCMC) simulations have been widely used to accurately predict adsorption isotherms of various gases in MOFs [22]. Gas selectivities calculated from simulated adsorption isotherms are generally found to be in good agreement with the experiments [23]. In most studies, single-component gas adsorption isotherms are computed using GCMC simulations; mixture adsorption isotherms are then predicted based on pure gas adsorption data using ideal adsorbed solution theory (IAST). IAST is a well-developed technique to describe adsorption equilibria for gas components in a mixture using only single-component adsorption data at the same temperature and on the same adsorbent [24]. GCMC simulations can be also performed to obtain mixture adsorption data directly. This data is then used to predict adsorption selectivity and working capacity of the MOF. Results of molecular simulations provide molecular-level insights which can be used to design new MOFs with better separation performances. In the early years of these studies, simulations examined only one or a few MOFs at a time. With the development of new computational approaches and with the quick increase in the number of synthesized MOFs, molecular simulations have started to screen a large numbers of materials. The results of large-scale MOF screening studies are highly useful to direct experimental efforts, resources, and time to the most promising MOF materials.

This chapter aims to address the importance of molecular simulations to evaluate the potential of MOFs in adsorption-based CO₂ separations. Section 2.1 introduces details of GCMC simulations to study CO₂ adsorption in MOFs. Section 2.2 describes evaluation criteria used to assess CO₂ separation potential of MOF adsorbents. Studies on large-scale computational screening of MOF adsorbents are discussed in Section 2.3. Structure-separation performance relations obtained from molecular simulations of MOFs are summarized in Section 2.4. Section 3 closes by addressing the opportunities of using molecular simulations for examining the potential of MOF adsorbents in CO₂ separations.

2. Molecular simulations for CO₂ separation using MOFs

2.1. GCMC simulations for CO₂ adsorption

GCMC is a well-known method to estimate the adsorption equilibria of gases in nanoporous materials. This simulation mainly mimics an adsorption experiment. In an experimental setup, the adsorbed gas is in equilibrium with the gas in the reservoir at fixed temperature, volume, and chemical potential [25]. GCMC simulations are run at an ensemble where the temperature, volume, and chemical potential are kept constant and the number of gas molecules is allowed to fluctuate during the simulation at the imposed temperature and chemical potential. The

output of a GCMC simulation is the number of adsorbed gas molecules per unit cell of the MOF structure at predetermined temperature and pressure. These simulations provide single-component adsorption isotherms, binary mixture adsorption isotherms, and isosteric heat of adsorptions which are directly comparable with the output of adsorption experiments. In GCMC simulations where only a single-component gas such as CO_2 is studied, four different types of moves are considered including translation, rotation, insertion, and deletion of a molecule. In mixture GCMC simulations where a binary gas mixture is considered such as CO_2/H_2 , CO_2/CH_4 , and CO_2/N_2 , another trial move, exchange of molecules is also performed in order to speed up the equilibrium. The adsorbed amounts of each gas component are calculated by specifying pressure, temperature, and composition of the bulk gas mixture in GCMC simulations.

In a typical GCMC simulation of CO_2 adsorption in an MOF, CO_2 is the adsorbate and MOF is the adsorbent. Adsorbate molecules interact with the MOF atoms and with other adsorbates through dispersive and electrostatic interactions. These interactions are defined using a force field. A force field is the functional form and parameter sets are used to calculate the potential energy of a system of atoms in molecular simulations [26]. There are several potentials such as Lennard-Jones (LJ) [27] and Morse [28] potentials. In almost all molecular simulations of gases in MOFs, Lennard-Jones (LJ) potential is used. Results of a GCMC simulation may vary depending on the force field choice. General-purpose force fields such as universal force field (UFF) [29] and DREIDING force field [30] have been widely employed for simulations of MOFs. At the early stages of the molecular simulation studies of MOFs, efforts have been made to develop new force fields specific to MOF-gas interactions using quantum-level calculations [31, 32]. Some studies refined the force field parameters to match the predictions of molecular simulations with the available experimental measurements of gas adsorption in MOFs [32–36]. However, considering the large number and variety of MOFs, it is challenging to develop a new force field or refine an existing one for every single MOF. Therefore, generic force fields such as UFF and DREIDING are mostly preferred in molecular simulations of CO_2 adsorption in MOFs, especially for large-scale computational screening of MOFs. The reliability of the molecular simulation studies, of course, hinges on the accuracy of the force fields used. Schmidt et al. [37] computed CO_2 adsorption isotherms in a very large number of MOFs using *ab initio* force fields to probe the accuracy of common force fields. They concluded that there are significant quantitative differences between gas uptakes predicted by generic force fields such as UFF and *ab initio* force fields, but the force fields predict similar ranking of the MOFs, supporting the further use of generic force fields in large-scale material screening studies.

The LJ potential parameters of CO_2 are generally taken from the force field developed by Potoff and Siepmann [38]. A rigid linear triatomic molecule with three charged LJ interaction sites located at each atom is used for CO_2 molecules. Partial point charges centered at each LJ site approximately represent the first-order electrostatic and second-order induction interactions. Charge-quadrupole interactions between MOF atoms and CO_2 molecules significantly contribute to the adsorption of CO_2 . It was shown that if these interactions are not taken into account, adsorption isotherms of CO_2 molecules in MOFs can be significantly underestimated [39]. In order to compute the electrostatic interactions between CO_2 molecules and MOF, partial

point charges must be assigned to the MOF atoms. Several different methods are available in the literature to assign partial charges such as density-derived electrostatic and chemical charge (DDEC) method [40], connectivity-based atom contribution (CBAC) method [41], extended charge equilibration (EQeq) method [42], and quantum mechanical methods based on the ChelpG [43] density functional theory (DFT) calculations. Charges obtained from different methods generally do not agree well with each other. This is acceptable because atomic charges are not experimentally observable and the methods used to derive them depend on the physical phenomenon the charges are intended to be reproduced [44]. A simulated CO₂ adsorption isotherm is generally compared with the experimentally measured one to tune the charges if necessary. After atomic models, force fields and charges are defined for CO₂ molecules and MOF atoms, GCMC simulations can be carried out to obtain the adsorbed gas amounts. Results of these simulations are directly used to calculate the adsorption-based gas separation potential of MOFs based on several criteria as discussed below.

2.2. Evaluation of MOF adsorbents for CO₂ separation

In adsorption-based gas separation processes such as pressure swing adsorption (PSA), selectivity and working capacity of the adsorbent are the two important parameters that define the efficiency of the process [45, 46]. Adsorption selectivity is described as the ratio of mole fractions of gases in the adsorbed phase normalized by the bulk composition of the gas mixture:

$$S_{\text{ads}(1/2)} = \frac{x_1/x_2}{y_1/y_2} \quad (1)$$

Here, x stands for the molar fraction of the adsorbed phase obtained from the GCMC simulations, while y represents the molar fraction of the bulk gas phase. Eq. (1) defines the adsorption selectivity of an MOF adsorbent with respect to component 1, meaning that if selectivity is greater than 1, then the adsorbent is selective for component 1 over 2. Selectivities for CO₂/CH₄, CO₂/H₂, and CO₂/N₂ mixtures are calculated using the results of binary mixture GCMC simulations where 1 is CO₂ and 2 is the other gas component in Eq. (1). The bulk gas compositions of CO₂/CH₄, CO₂/H₂, and CO₂/N₂ mixtures are generally set to 50/50, 15/85, and 15/85, respectively, in molecular simulations to represent industrial operating conditions.

Working capacity (ΔN) is described as the difference between the loading amounts of the strongly adsorbed gas at the corresponding adsorption (N^{ads}) and desorption (N^{des}) pressures [46]. It is defined in the unit of mol gas per kg of MOF adsorbent. GCMC simulations are performed at specific adsorption and desorption pressures to calculate the working capacity as shown in Eq. (2).

$$\Delta N_1 = N_1^{\text{ads}} - N_1^{\text{des}} \quad (2)$$

Bae and Snurr [45] recently suggested some other adsorbent evaluation criteria in addition to selectivity and working capacity. The CO₂ uptake of an MOF under adsorption conditions

(N^{des}), sorbent selection parameter (S_{sp}), and regenerability ($R\%$) are also considered as adsorbent evaluation criteria to assess the potentials of MOFs in CO_2 separation processes such as natural gas purification, landfill gas separation, and CO_2 capture from power-plant flue gas. The CO_2 uptake of an MOF under adsorption conditions (N^{ads}) is the direct output of GCMC simulations. Sorbent selection parameter (S_{sp}) is defined as the combination of adsorption selectivity and working capacity. It is used to compare performances of different nanoporous materials in adsorption-based separation processes and is defined as shown in Eq. (3). Here, subscripts 1 and 2 indicate the strongly adsorbed component and the weakly adsorbed component, respectively. In CO_2 -related mixtures, CO_2 is generally the strongly adsorbed component (1), whereas other gases such as CH_4 and N_2 are weakly adsorbed (2).

$$S_{\text{sp}} = \frac{(S_{\text{ads}(1/2)})^2}{S_{\text{des}(1/2)}} \times \frac{\Delta N_1}{\Delta N_2} \quad (3)$$

Regenerability ($R\%$) is defined as the ratio of working capacity to the amount of the adsorbed gas at the adsorption pressure and it is an important parameter to evaluate the practical usage of an adsorbent for cyclic PSA and vacuum swing adsorption (VSA) processes:

$$R(\%) = \frac{\Delta N_1}{N_1^{\text{ads}}} \times 100 \quad (4)$$

At that point, it is important to mention that none of these criteria are perfect but they are complementary with each other to assess adsorbent potential of MOFs under practical conditions. Bae and Snurr [45] calculated adsorption selectivity, working capacity, gas uptake capacity, sorbent selection parameter, and regenerability values of several MOFs for adsorption-based separation of CO_2/CH_4 :10/90, CO_2/CH_4 :50/50, and CO_2/N_2 :10/90 mixtures. Although mixtures are considered, they used the experimental single-component adsorption isotherm data from the literature and obtained mixture amounts under adsorption and desorption conditions at the partial pressure of the specific component. In order to investigate the effect of mixture data, Ozturk and Keskin [47] calculated the same separation properties of MOFs using both single-component and mixture GCMC data. They showed that selectivity calculated from single-component GCMC simulations can be enormously different than the selectivity calculated from mixture GCMC simulations due to strong competition effects between different gas species. Therefore, it is better to characterize adsorbent materials based on their performance for mixed-gas feeds to reflect the real operation conditions [48].

Llewellyn et al. [49] recently suggested a new criterion named as adsorbent performance indicator (API) as shown in Eq. (5) to initially highlight porous materials of potential interest for PSA processes. This indicator takes into account working capacity (represented as WC in Eq. (5)), adsorption energy ($\Delta H_{\text{ads},1}$) of the most adsorbed species, and selectivity (S_{ads}). It additionally uses weighting factors to reflect the specific requirements of a given process.

$$\text{API} = \frac{(S_{\text{ads}(1/2)} - 1)^A \times \text{WC}_1^B}{|\Delta H_{\text{ads},1}|^C} \quad (5)$$

They calculated APIs of seven MOFs for two different CO₂/CH₄ separation scenarios using the experimental gas adsorption data [49]. Results showed that API can be more versatile than previously discussed comparison criteria for an initial indication of potential adsorbent performance.

2.3. Performance of MOFs in CO₂ separations

It is beyond the scope of this chapter to give a complete account of all GCMC studies of MOFs for CO₂ separation. Several molecular simulation studies examined a single MOF or a few MOFs at a time [50–59]. Most of these studies focused on adsorption-based separation of CO₂ using the two most widely studied MOFs, MOF-5 and CuBTC [60–64]. This section will focus on molecular simulation studies that examine a family of MOFs for adsorption-based CO₂ separations and large-scale computational screening studies to provide a relation between structure and separation performance of MOFs.

2.3.1. IRMOFs

IRMOFs are isorecticular MOFs. The “IR” stands for isorecticular, which essentially means that the molecular system is “stitched together” into a netlike structure through strong chemical bonds. Molecular simulations were used to compare the separation of CO₂/N₂ mixtures in two different classes of nanoporous materials, traditional zeolites (MFI, LTA, and DDR) and MOFs (IRMOF-1, -11, -12, -13, -14, CuBTC, and MIL-47 (V)) [65]. Results showed that although MOFs perform much better for gas storage than zeolites, their CO₂ separation performance is comparable to zeolites with adsorption selectivities in the range of 5–35. Krishna and van Baten [46] used configurational-bias Monte Carlo (CBMC) simulations to examine zeolites and IRMOF-1, MOF-177, rho-ZMOF, CuBTC, ZnMOF-74, and MgMOF-74 for separation of CO₂/CH₄, CO₂/N₂, and CO₂/H₂ mixtures using PSA units. The best CO₂ capture performance was obtained with MgMOF-74 that offers strong electrostatic interactions of CO₂ molecules with the exposed metal cation sites. Selectivity of MgMOF-74 was reported as ~300, 50, and 10 for CO₂/H₂, CO₂/N₂, and CO₂/CH₄ separations, respectively. Traditional zeolite adsorbents such as NaX and NaY show higher adsorption selectivities for these gas separations but these two zeolites suffer from relatively low working capacities that are important in PSA units. For CO₂/N₂ and CO₂/H₂ separation in PSA units, MgMOF-74 was found to offer the best combination of high adsorption selectivity and high working capacity. Han et al. [66] used GCMC simulations with first-principles-based force fields to report the effects of interpenetration on the CO₂/H₂ separation of MOFs. Non-interpenetrating IRMOF-1, -7, -8, -10, -14, -16, MOF-177, and MOF-200 and interpenetrating IRMOF-9, -13, -62, and SUMOF-4 were considered for comparison. For example, IRMOF-9 and IRMOF-13 are interpenetrating versions of IRMOF-10 and -14, respectively. The interpenetration of MOFs at low pressure remarkably enhanced the selectivity of CO₂ over H₂ by creating new adsorption sites for CO₂. However, selectivity of

the interpenetrating and non-interpenetrating MOFs was reversed at higher pressures. Since interpenetration lowers the pore volume of MOFs, it significantly reduced CO_2 uptake at high pressures. The decrease in the H_2 uptake resulting from interpenetration was found to be marginal. Therefore, selectivity of the interpenetrating MOFs was reported to be lower than that of non-interpenetrating MOFs at high pressures.

2.3.2. ZIFs

Zeolitic imidazolate frameworks (ZIFs) are composed of tetrahedral networks that resemble those of zeolites with transition metals connected by imidazolate ligands. Zeolites are known with the $\text{Al}(\text{Si})\text{O}_2$ unit formula, whereas ZIFs are recognized by $\text{M}(\text{Im})_2$, where M is the transition metal and Im is the imidazolate-type linker. Battisti et al. [67] calculated CO_2/CH_4 , CO_2/H_2 , and CO_2/N_2 adsorption selectivity in the zero-pressure limit for nine ZIFs, ZIF-2, -3, -4, -5, -6, -7, -8, -9, and -10 using GCMC simulations. These ZIFs were characterized by pores

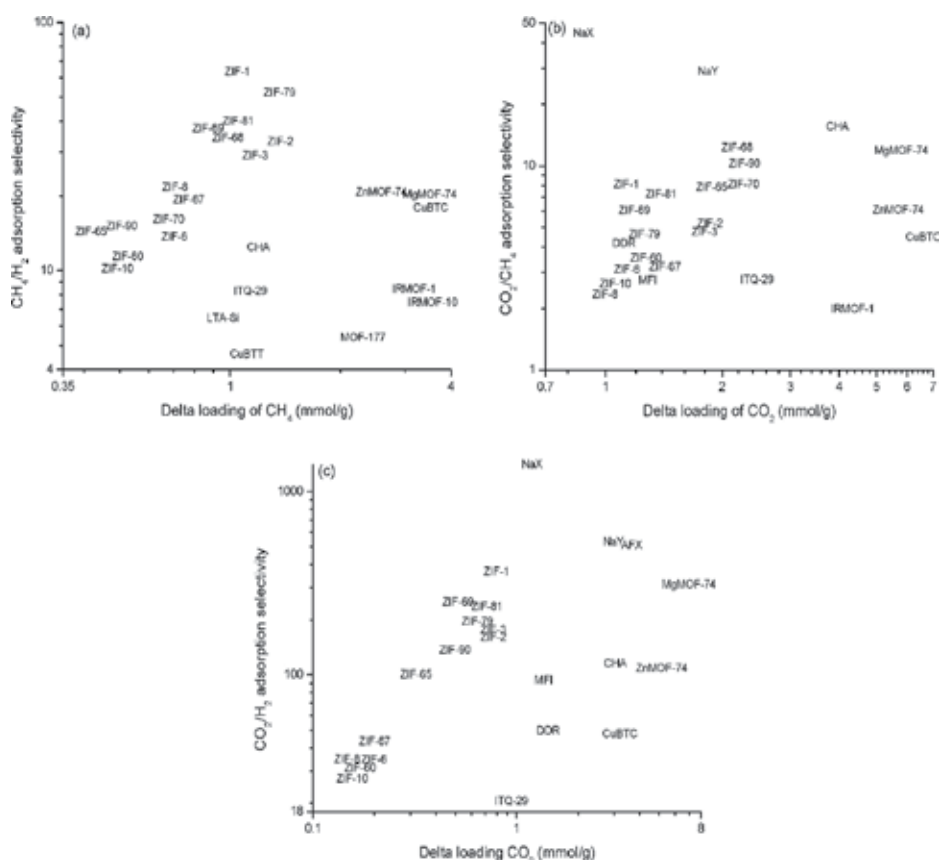


Figure 1. Adsorption-based separation performance of ZIFs for (a) CH_4/H_2 , (b) CO_2/CH_4 , and (c) CO_2/H_2 mixtures. The compositions of the bulk gas mixtures are (a) 10/90, (b) 10/90, and (c) 1/99 for ZIFs at 298 K and (a) 50/50, (b) 50/50, and (c) 15/85 for zeolites at 300 K. Reprinted with permission from Ref. [68]. Copyright (2012) American Chemical Society.

of medium to small size compared to other MOFs. Therefore, they were able to store at most half of the amount of gases than other MOFs. ZIF-7 and ZIF-9 were shown to be promising due to their high adsorption selectivities of 280 and 15 for CO₂/H₂ and CO₂/N₂ separations, respectively. Atci and Keskin [68] used GCMC simulations to predict the performance of 15 different ZIFs (ZIF-1, -2, -3, -6, -8, -10, -60, -65, -67, -68, -69, -70, -79, -81, and -90) in both adsorption-based and membrane-based separations of CH₄/H₂, CO₂/CH₄, and CO₂/H₂ mixtures. Adsorption selectivity, working capacity, membrane selectivity, and gas permeability of ZIFs were predicted using GCMC and molecular dynamics simulations. **Figure 1** compares adsorption selectivities and working capacities (shown as delta loadings) of ZIFs calculated at an adsorption pressure of 10 bar and desorption pressure of 1 bar with the data for zeolites and MOFs [68]. Several ZIFs were identified to outperform traditional zeolites and widely studied MOFs in CO₂/CH₄ and CO₂/H₂ separations. Keskin's group [69] also calculated adsorption of both single-component gases (CH₄, CO₂, H₂, and N₂) and binary gas mixtures (CO₂/CH₄, CO₂/N₂, and CO₂/H₂) using GCMC simulations and predicted the ideal and mixture adsorption selectivities of ZIFs. They showed that the adsorption selectivity calculated from mixture GCMC simulations can be significantly higher than the ideal adsorption selectivity calculated from single-component adsorption isotherms. This result highlighted the importance of using mixture selectivity to assess the performance of MOF adsorbents.

The calculated adsorption selectivity of ZIFs may vary significantly depending on the force field parameters used in molecular simulations [70]. Generic force fields generally tend to overestimate gas adsorption capacities; hence, adsorption selectivities of ZIF-68 and ZIF-69 compared to the tailored-force fields. However, the difference between predicted adsorption selectivities of different force fields is not high enough to change the assessment about the separation performance of the material. Both generic and tailored-force fields were able to identify the promising adsorbent materials that exhibit high adsorption selectivities. In other words, generic force fields can be safely used to screen large number of MOFs to differentiate between the promising and non-promising materials.

2.3.3. PCNs

MOFs are also referred as porous coordination networks (PCNs) in the literature and several synthesized materials have been named as PCNs [71]. Ozturk and Keskin [72] studied 20 different PCNs (PCN-6, 6', 9-Co, 9-Mn, 9-Fe, 10, 11, 13, 14, 16, 16', 18, 19, 20, 26, 39, 46, 80, 131', and 224-Ni) using molecular simulations to identify the most promising adsorbent and membrane candidates for CO₂/H₂, CO₂/CH₄, and CO₂/N₂ mixtures. PCN-9-Co, -9-Mn, -14, and -16 were found to be strong adsorbents for CO₂ capture, especially for CO₂/CH₄ separations because of their high working capacities. They also developed a simple model that can predict adsorption selectivities of PCNs for CO₂/H₂ mixtures without performing extensive molecular simulations. The model was based on the structural and chemical properties of the materials that can be simply measured or computed, such as pore volume, surface area, and the inverse of difference of heat of adsorption of components in the mixture. Predictions of the model for adsorbent selectivities were found to be in good agreement with the direct results of detailed molecular simulations.

2.3.4. COFs

Covalent organic frameworks (COFs) are not strictly MOFs but similar materials. They are formed by building units linked into a periodic framework but in contrast to MOFs, all components are organic in COFs. Zhong's group [73] examined a diverse set of 46 COFs to predict their separation performance for industrial gas mixtures, CO_2/H_2 and CO_2/CH_4 , using PSA process. Results show that COFs outperform most commonly used zeolites and widely studied MOFs in the separation of CH_4/H_2 while they have a comparable performance in separating CO_2/H_2 and CO_2/CH_4 . The same group then studied the performance of 151 MOFs with large chemical and topological diversity for CO_2/CH_4 separation for temperature swing adsorption (TSA) process [74]. The thermal regeneration energy was used as an evaluation criterion in addition to adsorption selectivity, working capacity, and regenerability. Cu-TDPAT and IRMOF-1-2Li MOFs were reported as the most promising candidates for CO_2/CH_4 separation in TSA processes based on the ranking of the materials according to the four evaluation criteria. Cu-TDPAT was identified as the best adsorbent candidate because of its high thermal stability and water-stable property.

2.3.5. Large-scale screening of MOFs

In 2012, Sholl's group [75] used GCMC simulations to calculate adsorption of CO_2 and N_2 in 500 different MOFs. This was the largest set of structures for which this information has been reported until 2012. Adsorption selectivities of MOFs were calculated using Henry's constant at infinite dilute loading. More detailed calculations such as quantum chemistry methods and binary mixture GCMC simulations were then carried out to assess adsorption selectivities of highly promising MOFs. Watanabe and Sholl [76] later on screened a larger number of MOFs for CO_2/N_2 separation. They first analyzed pore characteristics of 1163 MOFs using a simple steric model developed by Haldoupis et al. [77]. Adsorption selectivity of the selected 201 MOFs was calculated using single-component GCMC simulations at infinite dilute loading. Selectivities were plotted as a function of largest cavity diameter (LCD) of MOFs as shown in **Figure 2**. This figure demonstrates that MOFs are promising materials for CO_2/N_2 separations. There is a significant number of MOFs with high selectivities of 100–1000. A small number of materials have extremely high adsorption selectivities, greater than 1000. Selectivities of the top 10 promising MOFs were also computed considering CO_2/N_2 :15/85 mixture and results showed that CO_2/N_2 selectivities of MOFs remained high even for binary gas mixtures with the composition of dry flue gas.

Lin et al. [78] screened hundreds of thousands of hypothetical zeolite and ZIF structures for CO_2 capture from flue gas. They determined the optimal process conditions of each material by minimizing the electric load imposed on a power plant by a temperature-pressure swing capture process using that material followed by compression. This minimum load was called as parasitic energy and it was introduced as a metric to compare different materials. Results of that study showed that parasitic energy for ZIFs is higher than for zeolites. Wilmer et al. [79] drastically expanded the scope of previous MOF screening studies by examining over 130,000 hypothetical MOFs. They used molecular simulation to calculate adsorption selectivity, working capacity, regenerability, and sorbent selection parameter of MOFs for CO_2/CH_4 and

CO₂/N₂ separations. Single-component GCMC simulations to obtain the pure component CO₂, CH₄, and N₂ adsorption data are required to calculate the five adsorbent evaluation criteria. The resulting simulation data exhibited sharply defined structure-property relationships as we will discuss in Section 2.4. These type of relationships were not apparent when smaller collections of MOFs were studied in the previous works, indicating that screening large number of MOFs is important to understand the effect of structure on the gas separation performance of MOFs.

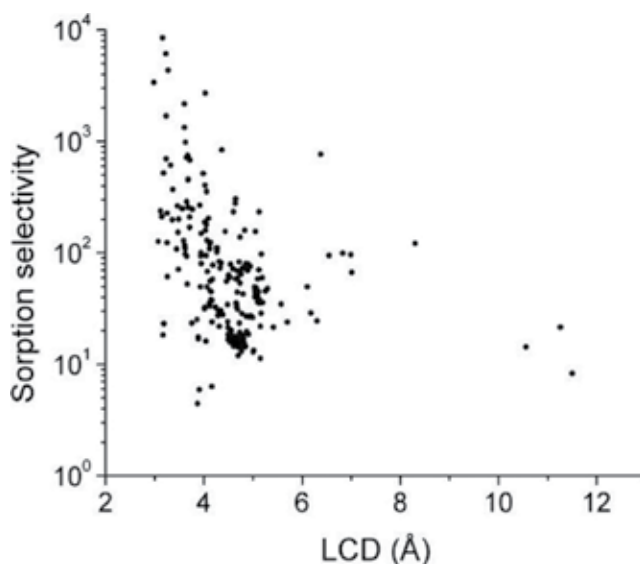


Figure 2. CO₂/N₂ sorption selectivity of the MOFs at 303 K. The data include only the materials with CO₂ diffusivity greater than 10⁻⁸ cm²/s. Reprinted with permission from Ref. [76]. Copyright (2012) American Chemical Society.

2.3.6. Breakthrough calculations

We so far discussed the molecular simulation studies in the literature that mimic a classical adsorption experiment. Other than isotherm experiments, breakthrough experiments are also carried out on nanoporous adsorbents in order to investigate the materials' kinetics. However, these experiments are labor-intensive and can present a range of technical challenges to achieve accurate results. Krishna and Long [80] suggested a new metric, breakthrough time (τ_{break}), that is based on the analysis of the transient response of an adsorber to a step input of a gaseous mixture. This metric determines the frequency of required regeneration of an adsorbent. High value of τ_{break} is desirable in practice because it reduces the frequency of required regeneration. Breakthrough calculations were done for separation of CO₂/H₂, CO₂/CH₄, and CO₂/CH₄/H₂ mixtures using five MOFs, MgMOF-74, CuBTTri, MOF-177, BeBTB, and Co(BDP) and results were compared with traditional zeolites. MgMOF-74 emerged as the best material from the viewpoints of both frequency of regeneration and productivity. The advantage of MgMOF-74 over traditionally used NaX zeolite was found to be evident at pressures exceeding 10 bar.

Krishna and van Baten [81] later studied breakthrough characteristics of an adsorber packed with a number of zeolites (MFI, JBW, AFX, and NaX) and MOFs (MgMOF-74, MOF-177, and CuBTri-mmen) for CO₂ capture from a CO₂/N₂ mixture. These calculations demonstrated that high capacities could have a dominant influence on the overall performance of PSA units. MgMOF-74 was again identified as a promising adsorbent with a CO₂ capture capacity more than twice that of other materials investigated. For separation of CO₂/H₂, CO₂/CH₄, and CH₄/H₂ mixtures, Jiang's group [82] recently studied seven different *rht*-MOFs namely Cu-TDPAT, PCN-61,-66,-68, NOTT-112, NU-111, and NU-110. These MOFs have the same *rht* topology with different ligands. The breakthrough profiles for CO₂-containing mixtures were predicted from the simulation results. Due to the presence of small ligands, unsaturated metals, and amine groups, Cu-TDPAT was found to exhibit the highest adsorption capacity and separation performance among the seven *rht*-MOFs. Upon substituting the phenyl rings in Cu-TDPAT by pyridine rings, Cu-TDPAT-N was designed and the breakthrough time for CO₂ in Cu-TDPAT-N was found to be extended by twofold. This result shows the importance of understanding structure-separation performance relations for MOFs as we discuss below.

2.4. Structure-performance relations

High-throughput computational screening is a very useful approach to identify promising MOF materials for gas separation applications and to uncover structure-property relations [83]. With the development of new computational methodologies, it is now easier to perform large-scale computational screening studies where the properties of thousands of MOF candidates can be evaluated and compared. When this type of large-scale MOF screening is performed, a large amount of data is produced and used to investigate correlations between MOFs' structural properties and their gas separation performances.

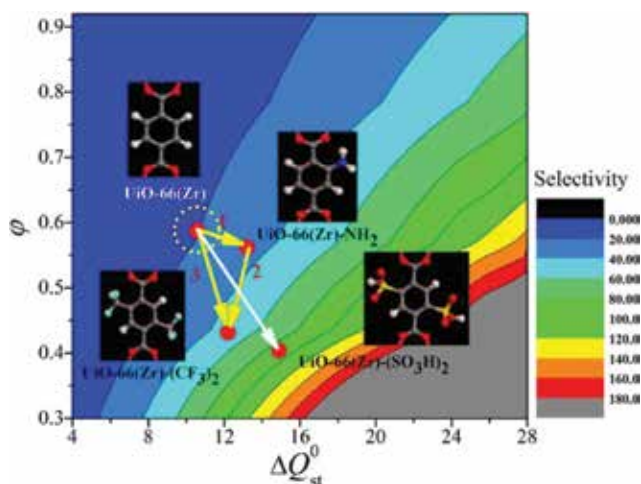


Figure 3. The interplay map of ϕ and ΔQ_{st}^0 on their impact on the selectivity at 1 bar for CO₂/N₂ mixture in MOFs, where the design strategy based on UiO-66(Zr) is also given. Reprinted with permission from Ref. [84]. Copyright (2012) American Chemical Society.

Maurin's group [84] used molecular simulations to examine separation performance of 105 MOFs with a large chemical and topological diversity for CO₂ capture from flue gas under industrial operating conditions. They developed a quantitative structure-property relationship (QSPR) model from this extended series of MOFs to rationalize the resulting CO₂/N₂ selectivity. The difference of isosteric heats of adsorption between CO₂ and N₂ at infinite dilution (ΔQ_{st}^0) and porosity (ϕ) were found to be the main features of the MOFs that strongly impact the CO₂/N₂ adsorption selectivity at 1 bar. **Figure 3** shows the interplay map of these two factors on the calculated CO₂/N₂ adsorption selectivity. Results of QSPR analysis suggested that increasing ΔQ_{st}^0 and simultaneously decreasing ϕ seems to be an appropriate route to enhance the CO₂/N₂ selectivity of MOFs. Motivated from this structure-performance relation, a new functionalized MOF, UiO-66(Zr)-(SO₃H)₂, was computationally designed and predicted to exhibit a high CO₂/N₂ selectivity as shown in **Figure 3**.

The CO₂ separation potential of a new class of porous aromatic frameworks (PAFs) with diamond-like structure was studied by molecular simulations [85]. It was discussed that selectivity might be only determined by the difference of the gas-material interactions of the mixtures at a pressure close to zero. The CO₂/H₂, CO₂/N₂, and CO₂/CH₄ selectivities and the difference of isosteric heats (ΔQ_{st}^0) were calculated at the pressure close to zero. The ΔQ_{st}^0 was found to be linear with the logarithm of the selectivity no matter what the gas mixtures and materials were. This result suggested that at zero pressure the selectivity is only dependent on the values of ΔQ_{st}^0 and is independent of the type of the gases and the materials. With the increase of ΔQ_{st}^0 , the selectivity increases correspondingly, which means that the ΔQ_{st}^0 can be used instead of the selectivity to screen out the promising nanoporous materials for gas separation. Finding a correlation between adsorption selectivity and ΔQ_{st}^0 is useful. However, it is difficult to design new MOF materials that have a priori chosen Q_{st} value. It is easier to design materials based on measurable structural properties such as porosity, pore size, or surface area. Wilmer et al. [79] studied a very large number of hypothetical MOFs and showed clear correlations between purely structural characteristics such as pore size, surface area, and pore volume as well as chemical characteristics such as functional groups with five adsorbent evaluation criteria listed in Section 2.2. For example, it was shown that adsorption selectivity correlates well with the maximum pore diameter for flue gas separation. Adsorption selectivity also correlates with the heat of adsorption of CO₂ for flue gas and natural gas separation. Certain chemical functional groups, particularly those with fluorine and chlorine atoms, were frequently found among the best performing MOF adsorbents. These type of structure-property relationships can be used as a guide for experimental MOF synthesis studies.

In a recent study, in silico screening of 4764 MOFs was performed for adsorption-based CO₂/CH₄ and CO₂/N₂ separations [86]. Quantitative relations between the metal type and adsorbent properties such as selectivity, working capacity, and regenerability were investigated for the first time in the literature. A wide variety of metals exists in MOFs such as alkalis, alkalines, lanthanides (Ln), and transition metals. **Figure 4** shows the probabilities of different metals in the selected MOFs based on their selectivity and working capacity for CO₂/CH₄ and CO₂/N₂ separations. For instance, the probability of K is about 0.8 for CO₂/N₂ separation, meaning that 80% of K-based MOFs show high selectivity and working capacity. Combining selectivity,

working capacity, and regenerability, however, alkali- and alkaline-MOFs possess the lowest performance for CO₂ separation. Among 4764 MOFs, about 1000 were found to contain Ln metals, 50% contain Ln as open metal sites. These open metal sites have high adsorption affinity for CO₂; therefore, MOFs with Ln metals have the highest CO₂ separation performance. The 30 best candidates identified for CO₂/CH₄ and CO₂/N₂ separations have Ln metals. These results can be used to synthesize MOFs having predetermined metal atoms to enhance the CO₂ separation performance of materials.

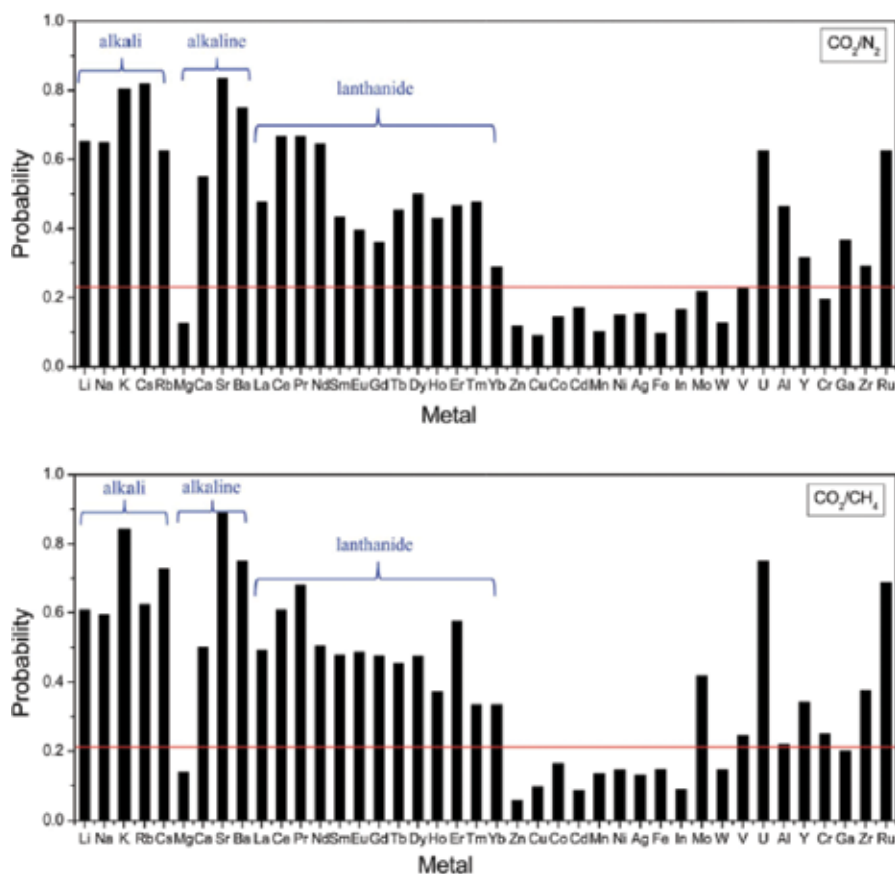


Figure 4. Probabilities of different metals in the selected MOFs (based on S and N_{CO_2}). The red lines indicate the percentages of the selected MOFs from the total. Reprinted with permission from Ref. [84]. Copyright (2015) The Royal Society of Chemistry.

As can be seen from this literature review, current studies have generally focused on establishing relations between adsorption selectivity and a single chemical or structural property such as difference of isosteric heat of adsorption of gases or metal type. However, separation performances of materials are determined by the interplay of various factors and cannot be easily correlated to only one or two properties. All physical and chemical properties of MOFs including pore size, shape, porosity, surface area, topology, metal and organic linker type must

be considered to better understand structure-performance relations. Deriving structure-performance relations for MOFs is a new and developing research area and more studies in this area will be valuable to synthesize new MOFs with useful physical and chemical properties to achieve targeted gas separations.

3. Conclusion and outlook

Molecular simulations are very useful to quickly evaluate the potential of new MOF materials in adsorption-based gas separation processes. The outcome of molecular simulations can be used as a guide to design and develop new materials with enhanced separation properties. There is a continuous growth in the number of molecular simulation studies of MOFs for adsorption-based CO₂ separations. However, there are still several open areas in which future studies will be valuable. Opportunities and challenges related with these open research areas are discussed below:

3.1. Computational design of new materials

Strategies to improve the ability of MOFs to selectively adsorb CO₂ are reviewed in detail in the literature [87]. Some of these strategies are control of pore size, using materials with open metal sites, introduction of alkali-metal cations into MOFs, interpenetration, and using materials with polar functional groups [45, 88]. Among these, rational design of functionalized materials is a feasible way to improve the CO₂ separation efficiency of MOFs. GCMC simulations were recently used to study the effect of amine functionalization on the CO₂/CH₄ separation performance of MIL-53 [89]. Results showed that CO₂/CH₄ separation factor of $-(\text{NH}_2)_4$ amine-functionalized MIL-53 is the best and predicted separation performance of $-\text{NH}_2$ and $-\text{NHCO}$ functionalized MIL-53 surpasses that of the original one. Future molecular simulation studies examining the effects of functionalization on the separation performance of MOFs will be very useful to establish guidelines for the experimental design and development of new materials.

3.2. Considering impurities in CO₂-related mixtures

As discussed in Section 2.3., most molecular simulation studies of MOFs focus on the separation of CO₂ from its binary mixtures such as CO₂/CH₄ and CO₂/N₂. However, in reality, these gas mixtures include some impurities. Water and the other minor components mostly H₂O, O₂, SO₂, and NO_x cannot be ignored in assessing the performance of MOFs especially for post-combustion CO₂ capture. However, the number of molecular simulation studies examining the effects of trace gases on the CO₂/N₂ and CO₂/CH₄ separation performance of MOFs is limited. Bahamon and Vega [90] recently used GCMC simulations to study 11 materials including zeolites and MOFs for separation of CO₂ from N₂, including water as an impurity. Sun et al. [91] studied 12 materials including MOFs, ZIFs, and zeolites for removal of SO₂ and NO_x from flue gas using GCMC simulations. The influences of water and SO₂ on CO₂ adsorption and separation in UiO-66(Zr) MOFs with different functional groups were

evaluated using a combination of GCMC and DFT simulations [92]. Babarao et al. [93] considered small amounts of O₂, H₂O, and SO₂ impurities typically found in flue gas and evaluated the CO₂/N₂ selectivity of four PCNs in the presence of these impurities. Zhong's group [94] used molecular simulations to investigate the effect of trace amount of water on CO₂ capture in natural gas upgrading process in a diverse collection of 25 MOFs. These studies concluded that the effect of H₂O impurities on the CO₂ selectivity is highly specific to the chemistry of the framework and needs to be evaluated on an individual case-by-case basis. The CO₂ selectivity of MOFs was generally reported to decrease in the presence of water. Future studies on GCMC simulations of MOFs considering impurities in CO₂-related mixtures must be conducted to evaluate the potential use of MOFs in industrial CO₂ capture processes.

3.3. Multi-scale modeling

While CO₂ separation using MOF adsorbents has been extensively investigated in different MOFs, their performance under practical process conditions is scarcely examined. A multi-scale modeling study was recently carried out to examine CO₂ capture from flue gas by vacuum swing adsorption (VSA) process using *rho*-ZMOFs as adsorbents [95]. The full adsorption process was simulated and optimized and results showed that the operating spaces of *rho*-ZMOFs are similar to that of traditional 13X zeolite. Further studies that employ multi-scale modeling approaches will be useful to design and develop MOF-based industrial CO₂ separation processes. A related point is to test the long-term stability of MOF adsorbents under industrial operating conditions. An ideal MOF adsorbent must have good thermal and mechanical stability. Several MOFs are sensitive to atmospheric moisture and lose their crystal structures when exposed to water. This may be a significant problem when MOFs are used as adsorbents in flue gas separations since flue gas contains water. Molecular simulation studies that can provide information about the long-term stability of MOF adsorbents will be useful to evaluate the real performance of MOFs.

Author details

Seda Keskin

Address all correspondence to: skeskin@ku.edu.tr

Koc University, Chemical and Biological Engineering Department, Istanbul, Turkey

References

- [1] Eddaoudi M, Li H, Yaghi O. Highly porous and stable metal-organic frameworks: structure design and sorption properties. *Journal of the American Chemical Society*. 2000;122:1391–1397. DOI: 10.1021/ja9933386

- [2] Rowsell JL, Yaghi OM. Metal-organic frameworks: a new class of porous materials. *Microporous and Mesoporous Materials*. 2004;73:3–14. DOI: 10.1016/j.micromeso.2004.03.034
- [3] Farha OK, Hupp JT. Rational design, synthesis, purification, and activation of metal-organic framework materials. *Accounts of Chemical Research*. 2010;43:1166–1175. DOI: 10.1021/ar1000617
- [4] Stock N, Biswas S. Synthesis of metal-organic frameworks (MOFs): routes to various MOF topologies, morphologies, and composites. *Chemical Reviews*. 2011;112:933–969. DOI: 10.1021/cr200304e
- [5] Allen FH. The Cambridge structural database: a quarter of a million crystal structures and rising. *Acta Crystallographica Section B: Structural Science*. 2002;58:380–388. DOI: 10.1107/S0108768102003890
- [6] Ren JW, Langmi HW, North BC, Mathe M. Review on processing of metal-organic framework (MOF) materials towards system integration for hydrogen storage. *International Journal of Energy Research*. 2015;39:607–620. DOI: 10.1002/er.3255
- [7] Duan X, Wu CD, Xiang SC, Zhou W, Yildirim T, Cui YJ, et al. Novel microporous metal-organic framework exhibiting high acetylene and methane storage capacities. *Inorganic Chemistry*. 2015;54:4377–4381. DOI: 10.1021/acs.inorgchem.5b00194
- [8] Li WJ, Gao SY, Liu TF, Han LW, Lin ZJ, Cao R. In situ growth of metal-organic framework thin films with gas sensing and molecule storage properties. *Langmuir*. 2013;29:8657–8664. DOI: 10.1021/la402012d
- [9] Qiu SL, Xue M, Zhu GS. Metal-organic framework membranes: from synthesis to separation application. *Chemical Society Reviews*. 2014;43:6116–6140. DOI: 10.1039/c4cs00159a
- [10] Zornoza B, Tellez C, Coronas J, Gascon J, Kapteijn F. Metal organic framework based mixed matrix membranes: an increasingly important field of research with a large application potential. *Microporous and Mesoporous Materials*. 2013;166:67–78. DOI: 10.1016/j.micromeso.2012.03.012
- [11] Gascon J, Corma A, Kapteijn F, Xamena FXLI. Metal organic framework catalysis: Quo vadis? *ACS Catalysis*. 2014;4:361–378. DOI: 10.1021/cs400959k
- [12] Della Rocca J, Liu DM, Lin WB. Nanoscale metal-organic frameworks for biomedical imaging and drug delivery. *Accounts of Chemical Research*. 2011;44:957–968. DOI: 10.1021/ar200028a
- [13] Keskin S, Kizilel S. Biomedical applications of metal organic frameworks. *Industrial & Engineering Chemistry Research*. 2011;50:1799–1812. DOI: 10.1021/ie101312k

- [14] Skoulidas AI, Sholl DS. Self-diffusion and transport diffusion of light gases in metal-organic framework materials assessed using molecular dynamics simulations. *The Journal of Physical Chemistry B*. 2005;109:15760–15768. DOI: 10.1021/jp051771y
- [15] Liu J, Thallapally PK, McGrail BP, Brown DR, Liu J. Progress in adsorption-based CO₂ capture by metal-organic frameworks. *Chemical Society Reviews*. 2012;41:2308–2322. DOI: 10.1039/C1CS15221A
- [16] Li J-R, Sculley J, Zhou H-C. Metal-organic frameworks for separations. *Chemical Reviews*. 2011;112:869–932. DOI: 10.1021/cr200190s
- [17] Keskin S, van Heest TM, Sholl DS. Can metal-organic framework materials play a useful role in large-scale carbon dioxide separations? *ChemSusChem*. 2010;3:879–891. DOI: 10.1002/cssc.201000114
- [18] Liu YY, Wang ZYU, Zhou HC. Recent advances in carbon dioxide capture with metal-organic frameworks. *Greenhouse Gases-Science and Technology*. 2012;2:239–259. DOI: 10.1002/ghg.1296
- [19] Li JR, Ma YG, McCarthy MC, Sculley J, Yu JM, Jeong HK, et al. Carbon dioxide capture-related gas adsorption and separation in metal-organic frameworks. *Coordination Chemistry Reviews*. 2011;255:1791–1823. DOI: 10.1016/j.ccr.2011.02.012
- [20] Aaron D, Tsouris C. Separation of CO₂ from flue gas: a review. *Separation Science and Technology*. 2005;40:321–348. DOI: 10.1081/Ss-200042244
- [21] Ben-Mansour R, Habib MA, Bamidele OE, Basha M, Qasem NAA, Peedikakkal A, Laoui T, Ali M. Carbon capture by physical adsorption: materials, experimental investigations and numerical modeling and simulations – a review. *Applied Energy*. 2016;161:225–255. DOI: 10.1016/j.apenergy.2015.10.011
- [22] Keskin S, Liu J, Rankin RB, Johnson JK, Sholl DS. Progress, opportunities, and challenges for applying atomically detailed modeling to molecular adsorption and transport in metal-organic framework materials. *Industrial & Engineering Chemistry Research*. 2009;48:2355–2371. DOI: 10.1021/Ie800666s
- [23] Düren T, Bae YS, Snurr RQ. Using molecular simulation to characterise metal-organic frameworks for adsorption applications. *Chemical Society Reviews*. 2009;38:1237–1247. DOI: 10.1039/B803498M
- [24] Myers AL, Prausnitz JM. Thermodynamics of mixed-gas adsorption. *AIChE Journal*. 1965;11:121–125. DOI: 10.1002/aic.690110125
- [25] Frenkel D, Smit B. *Understanding Molecular Simulation: From Algorithms to Applications*. 2nd ed. San Diego: Academic Press; 2002.
- [26] Getman RB, Bae YS, Wilmer CE, Snurr RQ. Review and analysis of molecular simulations of methane, hydrogen, and acetylene storage in metal-organic frameworks. *Chemical Reviews*. 2012;112:703–723. DOI: 10.1021/cr200217c

- [27] Lennard-Jones JE. Cohesion. *Proceedings of the Physical Society*. 1931;43:461–482. DOI: 10.1088/0959-5309/43/5/301
- [28] Morse PM. Diatomic molecules according to the wave mechanics. II. Vibrational levels. *Physical Review*. 1929;34:57–64. DOI: 10.1103/PhysRev.34.57
- [29] Rappe AK, Casewit CJ, Colwell KS, Goddard WA, Skiff WM. UFF, a full periodic table force field for molecular mechanics and molecular dynamics simulations. *Journal of the American Chemical Society*. 1992;114:10024. DOI: 10.1021/ja00051a040
- [30] Mayo SL, Olafson BD, Goddard WA. DREIDING: a generic force field for molecular simulations. *Journal of Physical Chemistry C*. 1990;94:8897–8909. DOI: 10.1021/j100389a010
- [31] Bordiga S, Vitillo JG, Ricchiardi G, Regli L, Cocina D, Zecchina A, et al. Interaction of hydrogen with MOF-5. *Journal of Physical Chemistry B*. 2005;109:18237–18242. DOI: 10.1021/jp052611p
- [32] Sagara T, Klassen J, Ganz E. Computational study of hydrogen binding by metal-organic framework-5. *Journal of Chemical Physics*. 2004;121:12543–12547. DOI: 10.1063/1.1809608
- [33] Sagara T, Ortony J, Ganz E. New isoreticular metal-organic framework materials for high hydrogen storage capacity. *Journal of Chemical Physics*. 2005;123:214707. DOI: 10.1063/1.2133734
- [34] Sagara T, Klassen J, Ortony J, Ganz E. Binding energies of hydrogen molecules to isoreticular metal-organic framework materials. *Journal of Chemical Physics*. 2005;123:014701. DOI: 10.1063/1.1944730
- [35] Yang Q, Zhong C. Molecular simulation of adsorption and diffusion of hydrogen in metal-organic frameworks. *Journal of Physical Chemistry B*. 2005;109:11862–11864. DOI: 10.1021/jp051903n
- [36] Yang Q, Zhong C. Understanding hydrogen adsorption in metal-organic frameworks with open metal sites: a computational study. *Journal of Physical Chemistry B*. 2006;110:655–658. DOI: 10.1021/jp055908w
- [37] McDaniel JG, Li S, Tylianakis E, Snurr RQ, Schmidt JR. Evaluation of force field performance for high-throughput screening of gas uptake in metal-organic frameworks. *Journal of Physical Chemistry C*. 2015;119:3143–3152. DOI: 10.1021/jp511674w
- [38] Potoff JJ, Siepmann JI. Vapor-liquid equilibria of mixtures containing alkanes, carbon dioxide, and nitrogen. *AIChE Journal*. 2001;47:1676–1682. DOI: 10.1002/aic.690470719
- [39] Rankin RB, Liu J, Kulkarni AD, Johnson JK. Adsorption and diffusion of light gases in ZIF-68 and ZIF-70: a simulation study. *Journal of Physical Chemistry C*. 2009;113:16906–16914. DOI: 10.1021/jp903735m

- [40] Manz TA, Sholl DS. Chemically meaningful atomic charges that reproduce the electrostatic potential in periodic and nonperiodic materials. *Journal of Chemical Theory and Computation*. 2010;6:2455–2468. DOI: 10.1021/ct100125x
- [41] Xu Q, Zhong C. A general approach for estimating framework charges in metal organic frameworks. *Journal of Physical Chemistry C*. 2010;114:5035–5042. DOI: 10.1021/jp910522h
- [42] Wilmer CE, Kim KC, Snurr RQ. An extended charge equilibration method. *Journal of Physical Chemistry Letters*. 2012;3:2506–2511. DOI: 10.1021/jz3008485
- [43] Francl MM, Carey C, Chirlian LE, Gange DM. Charges fit to electrostatic potentials. II. Can atomic charges be unambiguously fit to electrostatic potentials? *Journal of Computational Chemistry*. 1996;17:367–383. DOI: 10.1002/(SICI)1096-987X(199602)17:3<367::AID-JCC11>3.0.CO;2-H
- [44] Wilmer CE, Snurr RQ. Towards rapid computational screening of metal-organic frameworks for carbon dioxide capture: calculation of framework charges via charge equilibration. *Chemical Engineering Journal*. 2011;171:775–781. DOI: 10.1016/j.ccej.2010.10.035
- [45] Bae Y-S, Snurr RQ. Development and evaluation of porous materials for carbon dioxide separation and capture. *Angewandte Chemie International Edition*. 2011;50:11586–11596. DOI: 10.1002/anie.201101891
- [46] Krishna R, van Baten JM. In silico screening of metal-organic frameworks in separation applications. *Physical Chemistry Chemical Physics*. 2011;13:10593–10616. DOI: 10.1039/C1CP20282K
- [47] Ozturk TN, Keskin S. Predicting gas separation performances of porous coordination networks using atomistic simulations. *Industrial & Engineering Chemistry Research*. 2013;52:17627–17639. DOI: 10.1021/ie403159c
- [48] Keskin S, Sholl DS. Screening metal-organic framework materials for membrane-based methane/carbon dioxide separations. *Journal of Physical Chemistry C*. 2007;111:14055–14059. DOI: 10.1021/jp075290l
- [49] Wiersum AD, Chang JS, Serre C, Llewellyn PL. An adsorbent performance indicator as a first step evaluation of novel sorbents for gas separations: application to metal-organic frameworks. *Langmuir*. 2013;29:3301–3309. DOI: 10.1021/la3044329
- [50] Keskin S. Atomistic simulations for adsorption, diffusion, and separation of gas mixtures in zeolite imidazolate frameworks. *Journal of Physical Chemistry C*. 2011;115:800–807. DOI: 10.1021/jp109743e
- [51] Atci E, Erucar I, Keskin S. Adsorption and transport of CH₄, CO₂, H₂ mixtures in a bio-MOF material from molecular simulations. *The Journal of Physical Chemistry C*. 2011;115:6833–6840. DOI: 10.1021/jp200429x

- [52] Erucar I, Keskin S. Separation of CO₂ mixtures using Zn(bdc)(ted)_{0.5} membranes and composites: a molecular simulation study. *The Journal of Physical Chemistry C*. 2011;115:13637–13644. DOI: 10.1021/jp203522u
- [53] Erucar I, Keskin S. High CO₂ selectivity of an amine-functionalized metal organic framework in adsorption-based and membrane-based gas separations. *Industrial & Engineering Chemistry Research*. 2013;52:3462–3472. DOI: 10.1021/ie303343m
- [54] Keskin S. Gas adsorption and diffusion in a highly CO₂ selective metal-organic framework: molecular simulations. *Molecular Simulation*. 2013;39:14–24. DOI: 10.1080/08927022.2012.700485
- [55] Keskin S. High CO₂ selectivity of a microporous metal-imidazolate framework: a molecular simulation study. *Industrial & Engineering Chemistry Research*. 2011;50:8230–8236. DOI: 10.1021/Ie200540y
- [56] Babarao R, Jiang JW, Sandler SI. Molecular simulations for adsorptive separation of CO₂/CH₄ mixture in metal-exposed, catenated, and charged metal-organic frameworks. *Langmuir*. 2009;25:6590–6590. DOI: 10.1021/la803074g
- [57] Bae Y-S, Mulfort KL, Frost H, Ryan P, Punnathanam S, Broadbelt LJ, et al. Separation of CO₂ from CH₄ using mixed -ligand metal-organic frameworks. *Langmuir*. 2008;24:8592–8598. DOI: 10.1021/la800555x
- [58] Liu B, Smit B. Molecular simulation studies of separation of CO₂/N₂, CO₂/CH₄, and CH₄/N₂ by ZIFs. *Journal of Physical Chemistry C*. 2010;114:8515–8522. DOI: 10.1021/jp101531m
- [59] Chen YF, Nalaparaju A, Eddaoudi M, Jiang JW. CO₂ adsorption in mono-, di- and trivalent cation-exchanged metal-organic frameworks: a molecular simulation study. *Langmuir*. 2012;28:3903–3910. DOI: 10.1021/la205152f
- [60] Keskin S, Sholl DS. Assessment of a metal-organic framework membrane for gas separations using atomically detailed calculations: CO₂, CH₄, N₂, H₂ mixtures in MOF-5. *Industrial & Engineering Chemistry Research*. 2009;48:914–922. DOI: 10.1021/ie8010885
- [61] Keskin S, Sholl DS. Efficient methods for screening of metal organic framework membranes for gas separations using atomically detailed models. *Langmuir*. 2009;25:11786–11795. DOI: 10.1021/la901438x
- [62] Yang QY, Zhong CL. Molecular simulation of carbon dioxide/methane/hydrogen mixture adsorption in metal-organic frameworks. *Journal of Physical Chemistry B*. 2006;110:17776–17783. DOI: 10.1021/Jp062723w
- [63] Yang Q, Chunyu X, Zhong C, Chen J-F. Molecular simulation of separation of CO₂ from flue gases in Cu-BTC metal-organic framework. *AIChE Journal*. 2007; 53:2832–2840. DOI: 10.1002/aic.11298

- [64] Babarao R, Hu ZQ, Jiang JW, Chempath S, Sandler SI. Storage and separation of CO₂ and CH₄ in silicalite, C-168 schwarzite, and IRMOF-1: a comparative study from Monte Carlo simulation. *Langmuir*. 2007;23:659–666. DOI: 10.1021/La062289p
- [65] Liu B, Smit B. Comparative molecular simulation study of CO₂/N₂ and CH₄/N₂ separation in zeolites and metal-organic frameworks. *Langmuir*. 2009;25:5918–5926. DOI: 10.1021/la900823d
- [66] Han SS, Jung DH, Heo J. Interpenetration of metal organic frameworks for carbon dioxide capture and hydrogen purification: good or bad? *Journal of Physical Chemistry C*. 2013;117:71–77. DOI: 10.1021/jp308751x
- [67] Battisti A, Taioli S, Garberoglio G. Zeolitic imidazolate frameworks for separation of binary mixtures of CO₂, CH₄, N₂ and H₂: a computer simulation investigation. *Microporous and Mesoporous Materials*. 2011;143:46–53. DOI: 10.1016/j.micromeso.2011.01.029
- [68] Atci E, Keskin S. Understanding the potential of zeolite imidazolate framework membranes in gas separations using atomically detailed calculations. *Journal of Physical Chemistry C*. 2012;116:15525–15537. DOI: 10.1021/Jp305684d
- [69] Yilmaz G, Ozcan A, Keskin S. Computational screening of ZIFs for CO₂ separations. *Molecular Simulations*. 2014;41: 713–726. DOI: 10.1080/08927022.2014.923568
- [70] Ozcan A, Keskin S. Effects of molecular simulation parameters on predicting gas separation performance of ZIFs. *Journal of Chemical Technology and Biotechnology*. 2015;90:1707–1718. DOI: 10.1002/jctb.4482
- [71] Ma SQ, Zhou HC. Gas storage in porous metal-organic frameworks for clean energy applications. *Chemical Communications*. 2010;46:44–53. DOI: 10.1039/B916295j
- [72] Ozturk TN, Keskin S. Computational screening of porous coordination networks for adsorption and membrane-based gas separations. *Journal of Physical Chemistry C*. 2014;118:13988–13997. DOI: 10.1021/Jp5033977
- [73] Tong MM, Yang QY, Zhong CL. Computational screening of covalent organic frameworks for CH₄/H₂, CO₂/H₂ and CO₂/CH₄ separations. *Microporous and Mesoporous Materials*. 2015;210:142–148. DOI: 10.1016/j.micromeso.2015.02.034
- [74] Li ZJ, Xiao G, Yang QY, Xiao YL, Zhong CL. Computational exploration of metal-organic frameworks for CO₂/CH₄ separation via temperature swing adsorption. *Chemical Engineering Science*. 2014;120:59–66. DOI: 10.1016/j.ces.2014.08.003
- [75] Haldoupis E, Nair S, Sholl DS. Finding MOFs for highly selective CO₂/N₂ adsorption using materials screening based on efficient assignment of atomic point charges. *Journal of the American Chemical Society*. 2012;134:4313–4323. DOI: 10.1021/Ja2108239

- [76] Watanabe T, Sholl DS. Accelerating applications of metal-organic frameworks for gas adsorption and separation by computational screening of materials. *Langmuir*. 2012;28:14114–14128. DOI: 10.1021/la301915s
- [77] Haldoupis E, Nair S, Sholl DS. Efficient calculation of diffusion limitations in metal organic framework materials: a tool for identifying materials for kinetic separations. *Journal of the American Chemical Society*. 2010;132:7528–7539. DOI: 10.1021/ja1023699
- [78] Lin LC, Berger AH, Martin RL, Kim J, Swisher JA, Jariwala K, et al. In silico screening of carbon-capture materials. *Nature Materials*. 2012;11:633–641. DOI: 10.1038/NMAT3336
- [79] Wilmer CE, Farha OK, Bae YS, Hupp JT, Snurr RQ. Structure-property relationships of porous materials for carbon dioxide separation and capture. *Energy & Environmental Science*. 2012;5:9849–9856. DOI: 10.1039/c2ee23201d
- [80] Krishna R, Long JR. Screening metal-organic frameworks by analysis of transient breakthrough of gas mixtures in a fixed bed adsorber. *Journal of Physical Chemistry C*. 2011;115:12941–12950. DOI: 10.1021/jp202203c
- [81] Krishna R, van Baten JM. A comparison of the CO₂ capture characteristics of zeolites and metal-organic frameworks. *Separation and Purification Technology*. 2012;87:120–126. DOI: 10.1016/j.seppur.2011.11.031
- [82] Zhang K, Nalaparaju A, Jiang JW. CO₂ capture in rht metal-organic frameworks: multiscale modeling from molecular simulation to breakthrough prediction. *Journal of Materials Chemistry A*. 2015;3:16327–16336. DOI: 10.1039/c5ta01866h
- [83] Colon YJ, Snurr RQ. High-throughput computational screening of metal-organic frameworks. *Chemical Society Reviews*. 2014;43:5735–5749. DOI: 10.1039/C4cs00070f
- [84] Wu D, Yang QY, Zhong CL, Liu DH, Huang HL, Zhang WJ, et al. Revealing the structure-property relationships of metal-organic frameworks for CO₂ capture from flue gas. *Langmuir*. 2012;28:12094–12099. DOI: 10.1021/la302223m
- [85] Yang ZL, Peng X, Cao DP. Carbon dioxide capture by pafs and an efficient strategy to fast screen porous materials for gas separation. *Journal of Physical Chemistry C*. 2013;117:8353–8364. DOI: 10.1021/jp402488r
- [86] Qiao Z, Zhang K, Jiang J. In silico screening of 4764 computation-ready, experimental metal-organic frameworks for CO₂ separation. *Journal of Materials Chemistry A*. 2016;4:2105–2114. DOI: 10.1039/C5TA08984K
- [87] Lu XQ, Jin DL, Wei SX, Wang ZJ, An CH, Guo WY. Strategies to enhance CO₂ capture and separation based on engineering absorbent materials. *Journal of Materials Chemistry A*. 2015;3:12118–12132. DOI: 10.1039/c4ta06829g

- [88] D'Alessandro DM, Smit B, Long JR. Carbon dioxide capture: prospects for new materials. *Angewandte Chemie-International Edition*. 2010;49:6058–6082. DOI: 10.1002/anie.201000431
- [89] Qiao ZW, Zhou J, Lu XH. Designing new amine functionalized metal-organic frameworks for carbon dioxide/methane separation. *Fluid Phase Equilibria*. 2014;362:342–348. DOI: 10.1016/j.fluid.2013.10.050
- [90] Bahamon D, Vega LF. Systematic evaluation of materials for post-combustion CO₂ capture in a temperature swing adsorption process. *Chemical Engineering Journal*. 2016;284:438–447. DOI: 10.1016/j.cej.2015.08.098
- [91] Sun WZ, Lin LC, Peng X, Smit B. Computational screening of porous metal-organic frameworks and zeolites for the removal of SO₂ and NO_x from flue gases. *AIChE Journal*. 2014;60:2314–2323. DOI: 10.1002/aic.14467
- [92] Yu JM, Balbuena PB. How impurities affect CO₂ capture in metal-organic frameworks modified with different functional groups. *ACS Sustainable Chemistry & Engineering*. 2015;3:117–124. DOI: 10.1021/sc500607y
- [93] Babarao R, Jiang YQ, Medhekar NV. Postcombustion CO₂ capture in functionalized porous coordination networks. *Journal of Physical Chemistry C*. 2013;117:26976–26987. DOI: 10.1021/jp409361j
- [94] Huang HL, Zhang WJ, Liu DH, Zhong CL. Understanding the effect of trace amount of water on CO₂ capture in natural gas upgrading in metal-organic frameworks: a molecular simulation study. *Industrial & Engineering Chemistry Research*. 2012;51:10031–10038. DOI: 10.1021/ie202699r
- [95] Nalaparaju A, Khurana M, Farooq S, Karimi IA, Jiang JW. CO₂ capture in cation-exchanged metal-organic frameworks: Holistic modeling from molecular simulation to process optimization. *Chemical Engineering Science*. 2015;124:70–78. DOI: 10.1016/j.ces.2014.09.054

Classical Density Functional Theory for Fluids Adsorption in MOFs

Yu Liu and Honglai Liu

Additional information is available at the end of the chapter

<http://dx.doi.org/10.5772/64632>

Abstract

The designing of metal organic frameworks (MOFs) requires an efficient method to predict its adsorption properties. The conventional method to do this is molecular simulation, which is time consuming. In contrast, classical density functional theory (CDFT) is a much more efficient tool. Recently, CDFT has been successfully applied to MOF adsorptions. In this chapter, we will introduce the development and the different versions of CDFT and show how to apply CDFT to predict fluid adsorption in MOFs. We have reviewed the recent applications of CDFT in MOF adsorption and mainly focused on material screening. According to the recent developments, it seems CDFT is an efficient and robust tool for material screening; how to deal with more complicated fluids is the challenge of current CDFT.

Keywords: classical density functional theory, fluids, material-screening, MOFs, thermodynamics

1. Introduction

Adsorption is one of the essential properties of MOF materials, to give an efficient prediction of which is an important issue in the designing and application of MOFs. The traditional method to do this is molecular simulation, which is time consuming and may not be the best choice in real applications [1–3]. Take the high-throughput screenings for example, the number of MOFs in a typical screening database is more than 10^5 ; the typical computational time of MC simulation for each MOF is approximately 0.25 CPU hour; this means a screening time cost over 10^3 CPU days, which is a waste of resources. In this case, a more efficient method is needed, and the CDFT seems to be a promising alternative.

CDFT is a thermodynamic-statistical mechanics theory for inhomogeneous fluids. The concept of CDFT originates from quantum density functional theory and was formed in the 1970s [4, 5]. During the past 40 years, CDFT has been developed from simple fluids to polymers, from equilibrium to dynamic, from high symmetry modeling systems to real systems, and has revealed itself as an efficient and robust tool in various fields including adsorption, wetting, freezing, solvation, and so on [6–35].

The application of CDFT to MOF adsorption was first proposed by Siderius et al. [27] in 2009 and has been advanced by Liu et al. [26] subsequently. Siderius and Liu et al. have demonstrated that CDFT can be used to predict gas adsorption in MOFs. However, the numerical algorithm of these pioneered applications is too simple, which makes the computational cost of CDFT even higher than molecular simulations. Such disadvantage has been solved by Liu and Wu recently by applying the fast Fourier transform (FFT) and conjugate gradient (CG) descent method [31, 33, 35]. Now, the advanced CDFT is faster than conventional simulations by two orders of magnitude and has been successfully applied to high-throughput screening for material design [33–36].

In the rest of this chapter, we will introduce the classical density functional theory and show how to implement the theory to MOF adsorptions. The remainder of this chapter is organized as follows: Section 2 will introduce the theoretical framework of CDFT; Section 3 will show how to apply CDFT to MOF adsorption and review recent reports in this field; and finally, Section 4 will summarize and prospect the current and future applications of CDFT on MOF adsorption.

2. Classical density functional theory

2.1. Thermodynamic framework

The central idea of CDFT is to obtain the fluid's microscopic conformation (density profile) by minimizing the grand potential or free energy and obtain the macroscopic information (such as uptake, heat of adsorption, selectivity, etc.) from the density profile. The main task of this procedure is to represent the grand potential as a functional of density profile. According to the definition, grand potential can be written by:

$$\Omega[\rho(\mathbf{r})] = F[\rho(\mathbf{r})] - \mu \int \rho(\mathbf{r}) d\mathbf{r} \quad (1)$$

where Ω is the grand potential, F is the free energy, $\rho(\mathbf{r})$ is the density profile and μ is the chemical potential, which can be obtained from the equilibrium condition

$$\mu = \mu_b \quad (2)$$

where μ_b is the chemical potential of the bulk system which is in equilibrium with the inhomogeneous system. In statistical mechanics, the free energy, F , can be obtained from the Hamiltonian of the system. Generally, the Hamiltonian is given by:

$$H = \sum_{i=1}^N \frac{p_i^2}{2m} + V(\{\mathbf{r}_i\}) \quad (3)$$

where p_i is the momenta of molecule i , m is the mass of the molecule, N is the number of molecules, and V is the potential, which can be expanded mathematically:

$$V(\{\mathbf{r}_i\}) = u^{(0)} + \sum_{i=1}^N u_i^{(1)}(\mathbf{r}_i) + \sum_{1 \leq i < j \leq N} u_{ij}^{(2)}(\mathbf{r}_{ij}) + \dots \quad (4)$$

For fluid (guest) adsorption in a rigid MOF (host), the 0th order term $u^{(0)}$ represents the host-host interactions, which is a constant and can be eliminated by defining the zero potential point. The first order term $u^{(1)}$ is the one-body potential representing the host-guest interactions. The second order term represents the guest-guest interactions. By ignoring the high order terms in classical systems, there are three contributions in the Hamiltonian: the kinetic contribution, the host-guest interaction and the guest-guest interaction, corresponding to the three terms in the free energy, the ideal gas free energy F^{id} , the external free energy F^{ext} , and the excess free energy F^{ex} :

$$F[\rho(\mathbf{r})] = F^{id}[\rho(\mathbf{r})] + F^{ext}[\rho(\mathbf{r})] + F^{ex}[\rho(\mathbf{r})] \quad (5)$$

For simple fluids, the ideal term and the external term can be exactly derived from the statistical mechanics by:

$$F^{id}[\rho(\mathbf{r})] = k_b T \int \rho(\mathbf{r}) [\ln \rho(\mathbf{r}) \Lambda^3 - 1] d\mathbf{r} \quad (6)$$

$$F^{ext}[\rho(\mathbf{r})] = \int \rho(\mathbf{r}) V^{ext}(\mathbf{r}) d\mathbf{r} \quad (7)$$

where k_b is the Boltzmann constant, T is the temperature, Λ is the de Broglie wave length and $V^{ext}(\mathbf{r})$ is the external potential, which can be calculated from the direct interaction between host-guest interacting sites:

$$V^{ext}(\mathbf{r}) = \sum_{i \in \text{host}} u_{i, \text{guest}}(\mathbf{r} - \mathbf{r}_i) \quad (8)$$

where \mathbf{r} , is the coordinate of the host (MOF) atoms and the host-guest interacting potential $u_{i,\text{guest}}(\mathbf{r})$ can be formed by standard force field such as the universal force field (UFF) [37] and Dreiding force field [38].

In contrast, the exact form of the excess free energy functional $F^{\text{ex}}[\rho(\mathbf{r})]$ is unknown for most systems, and approximations are needed. The detailed expression and discussions of these approximations will be introduced in Section 2.2. Here, we just assume the expression of $F^{\text{ex}}[\rho(\mathbf{r})]$ has already been given, in this case, we can establish the grand potential functional from Eqs. (1), (5)–(7). According to the second law of thermodynamics, the grand potential of an open system should reach its minimum when in equilibrium, which can be mathematically written by:

$$\frac{\delta\Omega[\rho(\mathbf{r})]}{\delta\rho(\mathbf{r})} = 0 \quad (9)$$

Substituting Eqs. (1), (5)–(7) in (9), we have:

$$\rho(\mathbf{r}) = \frac{1}{\Lambda^3} \exp \left[\beta\mu - \beta V^{\text{ext}}(\mathbf{r}) - \frac{\delta\beta F^{\text{ex}}}{\delta\rho(\mathbf{r})} \right] \quad (10)$$

where $\beta = 1/(k_B T)$. In principle, the density profile $\rho(\mathbf{r})$ can be solved from Eq. (10), and the macroscopic properties can be calculated from $\rho(\mathbf{r})$. For example, the uptake N is given by:

$$N = \int \rho(\mathbf{r}) d\mathbf{r} \quad (11)$$

The simplest application of Eq. (10) is the ideal gas system, representing fluids at low density limit. For ideal gas, $F^{\text{ex}}=0$, Eq. (10) can be simplified as:

$$\rho(\mathbf{r}) = \frac{1}{\Lambda^3} \exp \left[\beta\mu - \beta V^{\text{ext}}(\mathbf{r}) \right] \quad (12)$$

Applying Eq. (12) to bulk system, where $V^{\text{ext}}(\mathbf{r})=0$, we have:

$$\rho_b = \frac{1}{\Lambda^3} \exp(\beta\mu_b) \quad (13)$$

where ρ_b is the corresponding bulk density. Substituting Eq. (2) and (13) in (12), we have:

$$\rho(\mathbf{r}) = \rho_b \exp[-\beta V^{\text{ext}}(\mathbf{r})] \quad (14)$$

Then, the adsorption isotherm is given by:

$$N = \rho_b \int \exp[-\beta V^{\text{ext}}(\mathbf{r})] d\mathbf{r} \quad (15)$$

As $V^{\text{ext}}(\mathbf{r})$ only depends on the host-guest interaction instead of the loading of the guest molecule, Eq. (15) leads to a linear adsorption isotherm, which is true at low density limit. Moreover, the slope of the isotherm is determined by $V^{\text{ext}}(\mathbf{r})$, which means the adsorption at low loadings is correlated with the host-guest interaction. This conclusion is also consistent with Snurr et al.'s findings in their high-throughput screening [1, 2].

2.2. Excess free energy functional

Ideal gas system is valid only for low loading systems. For more complicated systems, we need to consider the excess free energy functional. The excess free energy originates from the guest-guest correlations, which is much more complicated than the ideal free energy and external free energy. How to approximate the excess free energy is the center of concern in most CDFT. Up to now, various approximations have been proposed and applied, such as fundamental measure theory (FMT), weighted density approximation (WDA), and functional expansion theory.

2.2.1. Local density approximation (LDA)

LDA is the simplest approximation for excess free energy, which is given by an integration of homogeneous fluids:

$$F_{\text{LDA}}^{\text{ex}} = \int f_{\text{V}}^{\text{ex}}(\rho(\mathbf{r})) d\mathbf{r} \quad (16)$$

where $f_{\text{V}}^{\text{ex}}(\rho)$ is the excess free energy density (per volume) as a function of fluid density for homogeneous systems. The methodology of Eq. (16) comes from the thinking of calculus: the system is first separated into small units, $d\mathbf{r}$; the fluid in each $d\mathbf{r}$ is assumed to be homogeneous; the total excess free energy is represented as the summation of each local excess free energy. Due to its simplicity, LDA has been widely used for both classical and quantum systems when the scheme of DFT has been proposed [39–41]. However, there is an obvious disadvantage of LDA: the correlations between different $d\mathbf{r}$ are abandoned. The extensiveness of free energy is invalid for systems at molecular level. Representing the total excess free energy as the summation of each part is an approximation, which is valid only when the fluctuation of $\rho(\mathbf{r})$ is weak, such as vapor-liquid interface. However, for MOF adsorption, the fluctuation of $\rho(\mathbf{r})$ is very strong, as the guest molecules are usually highly localized at the favorable adsorption

sites, where $\rho(\mathbf{r})$ approaches the Dirac delta function $\delta(\mathbf{r}-\mathbf{r}_i)$. In this case, LDA is not a proper approximation.

2.2.2. Gradient approximation

Gradient approximation considers the inhomogeneity beyond LDA. One of the widely used forms of gradient approximation is the so-called square-gradient approximation (SGA), which is derived from Ginzburg-Landau theory or Landau expansion [4, 5]:

$$F_{\text{SGA}}^{\text{ex}}[\rho(\mathbf{r})] = \int d\mathbf{r} \left\{ f^{\text{ex}}(\rho(\mathbf{r})) + \frac{k_B T}{12} |\nabla \rho(\mathbf{r})|^2 \int r^2 c_0^{(2)}(r) d\mathbf{r} \right\} \quad (17)$$

where

$$c_0^{(2)}(|\mathbf{r}-\mathbf{r}'|) = - \left. \frac{\delta^2 \beta F^{\text{ex}}}{\delta \rho(\mathbf{r}) \delta \rho(\mathbf{r}')} \right|_{\rho(\mathbf{r})=\rho_b} \quad (18)$$

is the direct correlation function. Gradient approximation has been developed into the famous generalized gradient approximation (GGA) in quantum DFT but it is not so successful in CDFT. Although gradient approximation is more advanced than LDA, it is still invalid once the fluctuation of $\rho(\mathbf{r})$ is strong. Besides, Eq. (17) is mathematically more complicated than Eq. (16), which makes the usage of gradient approximation even less than LDA.

2.2.3. Weighted density approximation (WDA)

WDA considers the guest-guest correlations by replacing the local density $\rho(\mathbf{r})$ in Eq. (16) with a weighted density [42, 43]:

$$\bar{\rho}(\mathbf{r}) = \int \rho(\mathbf{r}') w(\mathbf{r}-\mathbf{r}') d\mathbf{r}' \quad (19)$$

where $w(\mathbf{r})$ is the so-called weighting function. By applying the weighted density, the excess free energy is written by:

$$F_{\text{WDA-V}}^{\text{ex}} = \int f_V^{\text{ex}}(\bar{\rho}(\mathbf{r})) d\mathbf{r} \quad (20)$$

or

$$F_{\text{WDA-N}}^{\text{ex}} = \int \rho(\mathbf{r}) f_N^{\text{ex}}(\bar{\rho}(\mathbf{r})) d\mathbf{r} \quad (21)$$

where $f_N^{\text{ex}}(\rho)$ is the excess free energy density (per molecule) as a function of fluid density for homogeneous systems, which can be obtained (along with $f_V^{\text{ex}}(\rho)$) by the corresponding equation of state (EOS). Compared to LDA and gradient approximation, WDA seems much more reliable according to its wide applications for both classical and quantum systems. The introduction of weighted density avoids the singular point of $f^{\text{ex}}(\rho(\mathbf{r}))$ when $\rho(\mathbf{r}) \rightarrow \infty$ and can be used for systems with strong inhomogeneity, such as in MOF adsorption.

In WDA, there are different choices of the weighting function, which correspond to different versions of WDA. The simplest version of $w(\mathbf{r})$ is the Heaviside step function [42]:

$$w(\mathbf{r}) = \frac{3}{4\pi\sigma^3} \Theta(r - \sigma) \tag{22}$$

where

$$\Theta(x) = \begin{cases} 0 & x > 0 \\ 1 & x < 0 \end{cases} \tag{23}$$

and σ is the molecular diameter. The advanced version is regarding the w as a function of density profile, $w(\mathbf{r}-\mathbf{r}'; \rho(\mathbf{r}))$, and solve $w(\mathbf{r}-\mathbf{r}'; \rho(\mathbf{r}))$ from relevant closures. Typical examples are Curtin-Ashcroft's WDA [44]:

$$-\tilde{c}_0^{(2)}(k, \rho) = 2 \frac{d\beta f_N^{\text{ex}}(\rho)}{d\rho} \tilde{w}(k, \rho) + \rho \frac{\partial}{\partial \rho} \left[\frac{d\beta f_N^{\text{ex}}(\rho)}{d\rho} \tilde{w}^2(k, \rho) \right] \tag{24}$$

where subscript “~” stands for the Fourier transform, Tarazona's WDA [45]:

$$w(r, \rho) = w_0(r) + w_1(r)\rho + w_1(r)\rho^2 + \dots \tag{25}$$

modified WDA (MWDA) [46]

$$w(r, \rho) = -\frac{d\rho}{2df_N^{\text{ex}}(\rho)} \left[k_B T c_0^{(2)}(r, \rho) + \frac{\rho}{V} \cdot \frac{d^2 f_N^{\text{ex}}(\rho)}{d\rho^2} \right] \tag{26}$$

Denton-Ashcroft's version [47]:

$$w(r, \rho) = c_0^{(2)}(r, \rho) \frac{d\rho}{dc_0^{(1)}(\rho)} \tag{27}$$

and hybrid WDA (HWDA) [48].

$$-\tilde{c}_0^{(2)}(k, \rho) = 2 \frac{d\beta f_N^{\text{ex}}(\rho)}{d\rho} \tilde{w}(k, \rho) + \rho \frac{d\beta f_N^{\text{ex}}(\rho)}{d\rho} \tilde{w}^2(k, \rho) \quad (28)$$

The sophisticated WDA gives more accurate predictions on one hand but increases the computational cost on the other hand. It seems there is a trade-off between accuracy and computational cost. For MOF adsorption, the computational cost is an important factor and a simple weighting function like Eq. (22) may be more preferred.

2.2.4. Mean field approximation (MFA)

According to statistical mechanics, the excess free energy can be exactly written by:

$$F^{\text{ex}} = \frac{1}{2} \iint \rho(\mathbf{r}) \rho(\mathbf{r}') g(\mathbf{r}, \mathbf{r}') u(|\mathbf{r} - \mathbf{r}'|) d\mathbf{r} d\mathbf{r}' \quad (29)$$

where $g(\mathbf{r}, \mathbf{r}')$ is the radial distribution function (RDF) for inhomogeneous fluids, and $u(\mathbf{r}, \mathbf{r}')$ is the two-body interacting potential. Different from that of homogeneous system, the RDF for inhomogeneous fluids is a 6-dimensional function, which is difficult to obtain. The simplest approximation is to let

$$g(\mathbf{r}, \mathbf{r}') = 1 \quad (30)$$

which leads to the so-called MFA:

$$F_{\text{MFA}}^{\text{ex}} = \frac{1}{2} \iint \rho(\mathbf{r}) \rho(\mathbf{r}') u(|\mathbf{r} - \mathbf{r}'|) d\mathbf{r} d\mathbf{r}' \quad (31)$$

Although Eq. (30) seems to be a coarse approximation, MFA is still successful in various real applications. Due to its efficiency, MFA seems to be a potential method for MOF adsorption [49–51].

2.2.5. Functional expansion

Functional expansion theory expands the excess free energy functional with respect to the bulk system as a Taylor series:

$$F^{\text{ex}} = F_b^{\text{ex}} + \mu_b^{\text{ex}} \int \Delta\rho(\mathbf{r}) d\mathbf{r} - \frac{k_B T}{2} \iint c_0^{(2)}(\mathbf{r} - \mathbf{r}') \Delta\rho(\mathbf{r}) \Delta\rho(\mathbf{r}') d\mathbf{r} d\mathbf{r}' + \dots \quad (32)$$

where F_b^{ex} and μ_b^{ex} are the excess free energy and excess chemical potential for the bulk system, respectively; $\Delta\rho(\mathbf{r}) = \rho(\mathbf{r}) - \rho_b$ is the deviation of density with respect to its bulk value. A common treatment of Eq. (32) is to truncate the series at the second order, which is the so-called square functional expansion (SFE). An intuitive understanding of SFE is that $\Delta\rho(\mathbf{r})$ should be small, otherwise the high-order terms should be considered. However, in real application, it seems the second-order truncation is valid even though $\Delta\rho(\mathbf{r})$ is so large [32, 52].

2.2.6. Fundamental measure theory (FMT)

Different from the universal theories introduced above, FMT is specific for hard sphere fluids, where the interacting potential is given by:

$$u_{\text{hs}}(r) = \begin{cases} \infty & r < \sigma \\ 0 & r > \sigma \end{cases} \quad (33)$$

where σ is the hard sphere diameter. According to the decomposing of Heaviside function, FMT represents the excess free energy by [9, 13]:

$$\beta F^{\text{ex}} = \int \Phi[n_\alpha(\mathbf{r})] d\mathbf{r} \quad (34)$$

and

$$\Phi = f_0(n_3)n_0 + f_{12}(n_3)n_1n_2 + f_{222}(n_3)n_2^3 + f_{12}^{\text{V}}(n_3)\mathbf{n}_{\text{V}1} \cdot \mathbf{n}_{\text{V}2} + f_{222}^{\text{V}}(n_3)n_2(\mathbf{n}_{\text{V}2} \cdot \mathbf{n}_{\text{V}2}) \quad (35)$$

where n_α are weighted density:

$$n_\alpha(\mathbf{r}) = \int \rho(\mathbf{r}') \omega^{(\alpha)}(\mathbf{r} - \mathbf{r}') d\mathbf{r}' \quad (36)$$

where

$$\left\{ \begin{array}{l} \omega^{(3)} = \theta(|\mathbf{r}| - \sigma / 2) \\ \omega^{(2)}(\mathbf{r}) = \delta(r - \sigma / 2) \\ \omega^{(1)}(\mathbf{r}) = \frac{1}{2\pi\sigma} \delta(r - \sigma / 2) \\ \omega^{(\text{V}2)}(\mathbf{r}) = \frac{\mathbf{r}}{r} \delta(|\mathbf{r}| - \sigma / 2) \\ \omega^{(\text{V}1)}(\mathbf{r}) = \frac{\mathbf{r}}{2\pi\sigma r} \delta(|\mathbf{r}| - \sigma / 2) \end{array} \right. \quad (37)$$

f_i is undetermined coefficient, which can be determined by the bulk limit of Eq. (35). Applying the Carnahan-Starling (CS) equation of state, one can obtain Rosenfeld's original FMT:

$$\left\{ \begin{array}{l} \Phi = \Phi_s + \Phi_v \\ \Phi_s = -n_0 \ln(1 - n_3) + \frac{n_1 n_2}{1 - n_3} + \frac{n_2^3}{24\pi(1 - n_3)^2} \\ \Phi_v = -\frac{\mathbf{n}_{v1} \cdot \mathbf{n}_{v2}}{1 - n_3} - \frac{n_2(\mathbf{n}_{v2} \cdot \mathbf{n}_{v2})}{8\pi(1 - n_3)^2} \end{array} \right. \quad (38)$$

Applying the Boublik-Mansoori-Carnahan-Starling-Leland (BMCSL) equation of state, one can obtain Yu et al.'s modified FMT (MFMT) [17].

$$\left\{ \begin{array}{l} \Phi = \Phi_s + \Phi_v \\ \Phi_s = -n_0 \ln(1 - n_3) + \frac{n_1 n_2}{1 - n_3} + \left[\frac{\ln(1 - n_3)}{36\pi n_3^2} + \frac{1}{36\pi n_3(1 - n_3)^2} \right] n_2^3 \\ \Phi_v = -\frac{\mathbf{n}_{v1} \cdot \mathbf{n}_{v2}}{1 - n_3} - \left[\frac{\ln(1 - n_3)}{12\pi n_3^2} + \frac{1}{12\pi n_3(1 - n_3)^2} \right] n_2(\mathbf{n}_{v2} \cdot \mathbf{n}_{v2}) \end{array} \right. \quad (39)$$

FMT excellently captures the properties for hard sphere system with low computational costs and is the most favorable theory for hard sphere fluids in CDFT [19, 28, 35, 53].

2.2.7. Hybrid method

In real application, it is more common to apply two or more approximations for one system. Generally, molecule-molecule interactions can be decoupled into different contributions such as repulsive interactions, attractive interactions, and electrostatic interactions, which have different effects on fluids' properties. In this case, to separate the excess free energy into different terms corresponding to the different interactions and applying different approximations for each term seems more efficient than a single approximation.

For spherical molecules such as CH_4 , H_2 , and N_2 , the excess free energy is usually separated into the hard sphere contribution F^{hs} , representing the repulsive interaction and the attractive contribution F^{attr} :

$$F^{\text{ex}} = F^{\text{hs}} + F^{\text{attr}} \quad (40)$$

By applying different approximations to F^{hs} and F^{attr} , respectively, one can formulate the complete expression of excess free energy. For example, see [25, 54], Yu et al. have employed

MFMT and WDA to approximate F^{hs} and F^{attr} , respectively, and predicted the gas adsorption and phase transition in MCM-41; Ritter et al. [55] have employed FMT and MFA to study the binary gas adsorption in heterogeneous BPL-activated carbon; Siderius et al. [27] have applied WDA and MFA to predict H_2 adsorption in MOF-5, which has then been improved by two versions of WDA in Liu et al.'s work [26]. Recently, Yu et al. [28] have introduced a correlation term F^{cor} to Eq. (40):

$$F^{\text{ex}} = F^{\text{hs}} + F^{\text{attr}} + F^{\text{cor}} \quad (41)$$

which has soon been applied to MOF adsorptions by Liu and Wu et al. [31, 33–35].

3. Applying CDFT to MOF adsorption

Although the framework of CDFT has been established for a long time, its application to MOF adsorption had not been reported until 2009. **Table 1** lists current reports of applying CDFT on MOF adsorption. There is an obvious transition of these reports from 2010 to 2013, where the time cost decreases from 10 days to less than 1 minute. As will be introduced later, this is the benefit of acceleration method. Later in this section, we will introduce the typical studies listed in this table.

Year	System		Method	Time cost per calculation	Ref.
	Adsorbate	Adsorbent			
2009	H_2	MOF-5	WDA + MFA		[27]
2009	H_2	MOF-5, ZIF-8	WDA + WDA	5 days	[26]
2010	CO_2/CH_4 , CO_2/N_2	ZIF-8, $\text{Zn}_2(\text{BDC})_2(\text{ted})$	WDA + WDA	10 days	[29]
2013	H_2 , He, Ne, Ar	MOF-5, MFI, CuBTC, ZIF-8	MFMT + MFA +WDA	<1 min.	[31]
2015	H_2	1200 MOFs	5 versions	20 s	[33]
2015	CH_4	1200 MOFs	4 versions	2 min.	[36]
2015	H_2	712 MOFs \times 21 temperatures \times 21 pressures	MFMT + MFA +WDA	18 s	[35]
2015	DBT	458 MOFs	MFMT + MFA +WDA	20 s	[34]

Table 1. Applications of CDFT on MOF adsorption.

3.1. Initial application

The first report of the application is done by Siderius et al. [27]. Siderius et al. have employed Tarazona's WDA and MFA to construct the hard sphere and attractive free energy functional, and applied the theory to H_2 adsorption in MOF-5 (**Figure 1(a)**). Siderius et al.'s CDFT predictions accord with simulations and experiments very well at room temperature, but lower the estimated uptake in low temperature region (**Figure 1**).

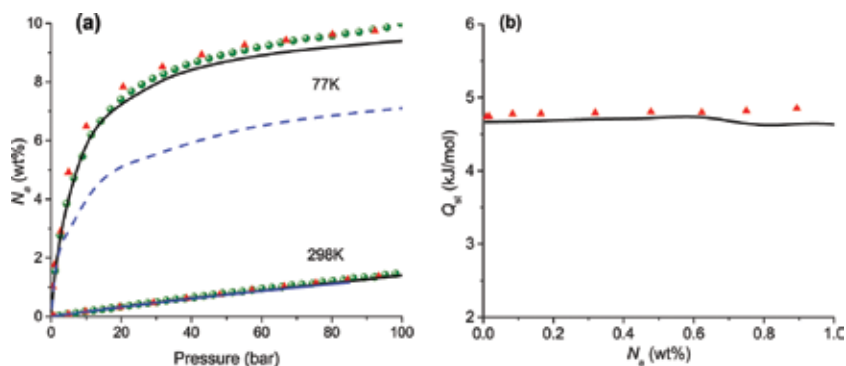


Figure 1. CDFT prediction of H_2 adsorption in MOF-5, (a) uptake, (b) isosteric heat. Solid line: Liu et al.'s CDFT; dashed line: Siderius et al.'s CDFT; triangle: MC simulation; sphere: experiments. Reprinted with permission from Ref. [26]. Copyright (2016) American Chemical Society.

Such shortcomings were soon solved by Liu et al. [26]. Liu et al. have employed two versions of WDA to approximate the hard sphere and attractive free energy, respectively. Liu et al.'s CDFT well predicted the adsorption isotherm and the isosteric heat for both high and low temperatures. Siderius et al. and Liu et al.'s CDFT have also revealed the microscopic conformation of the adsorbed gases. As shown in **Figure 2**, at low pressure, H_2 is mainly distributed at the favorable adsorption site, while at high pressure, H_2 is distributed at both the favorable adsorption sites and the surface of framework. These are consistent with other simulation findings.

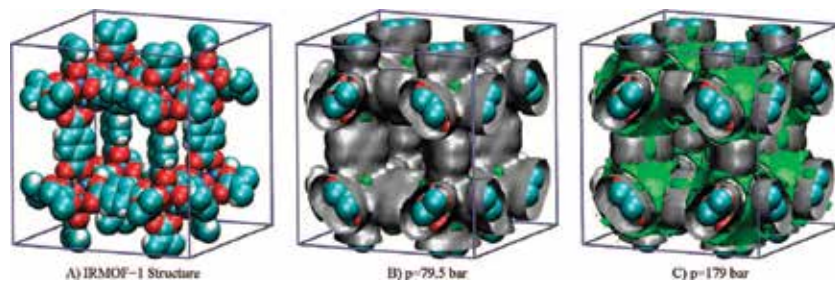
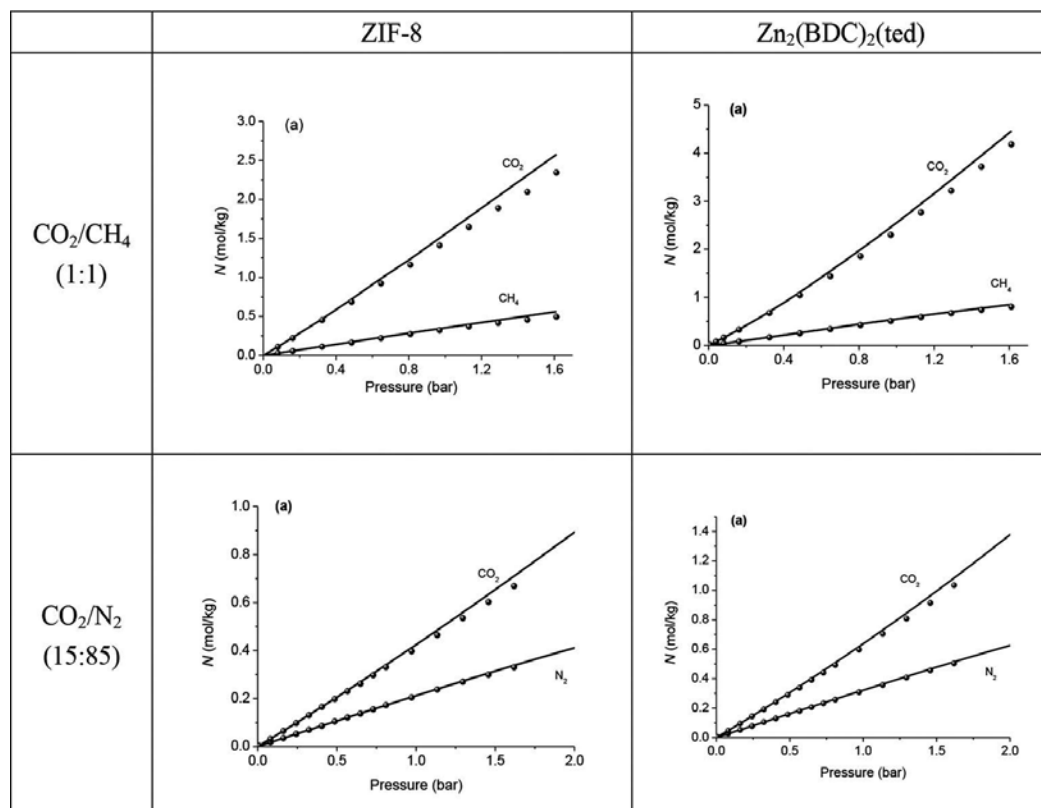


Figure 2. Molecular structure of MOF-5 (IRMOF-1) and density isosurface of H_2 in MOF-5 at 298 K. Color of the isosurface: gray, 1.33 mol/L; green, 19.9 mol/L. Color of the atoms: dark blue, Zn; light blue, C; red, O; white, H [27]. Reprinted with permission from Ref. [27]. Copyright (2016) American Chemical Society.

The theory has then been extended to mixtures by Liu et al. in 2010 [29]. Similar to that for pure component, two versions of WDA have been employed to construct the excess free energy functional, where the BMCSL and the modified Benedict-Webb-Rubin (MBWR) equation of state have been used to formulate the free energy density which is required in WDA. Liu et al. considered CO_2/CH_4 and CO_2/N_2 separation in two types of MOFs, respectively, where CDFT accords with simulations very well (Table 2).



*Line: CDFT prediction; dot: MC simulation.

Adapted with permission from Ref. [29]. Copyright (2016) American Chemical Society.

Table 2. Adsorption isotherm for CO_2/CH_4 and CO_2/N_2 in two MOFs*.

3.2. Acceleration method

Siderius et al. and Liu et al.'s work have demonstrated that CDFT can be used to predict gas adsorption in MOFs, however, there is a fatal flaw in these initial studies: the computational cost is too high. Before the application to MOF adsorption, CDFT mainly focuses on simple geometric systems such as slit pores and cylindrical pores, where the computation is very

efficient. However, when applying to 3-dimensional structured systems such as MOFs, the computational cost is unacceptable if an ordinary numerical treatment is employed. In principle, the accuracy of CDFT cannot exceed simulations; once the computational cost of CDFT is higher than simulation, CDFT will be useless in an application view.

Fortunately, CDFT can be accelerated. The most time consuming part of CDFT is the 3-dimensional integration such as Eqs. (19) and (36). These integrations can be simplified into 1-dimensional integration for slit and cylindrical pores but not for MOFs. However, as most of these integration are convolutions, which takes the form of:

$$A(\mathbf{r}) = \int B(\mathbf{r}')C(\mathbf{r} - \mathbf{r}')d\mathbf{r}' \quad (42)$$

By using the Fourier transform on both sides of Eq. (42), the convolution can be transformed into:

$$A = \mathcal{F}^{-1}[\mathcal{F}(B) \cdot \mathcal{F}(C)] \quad (43)$$

where \mathcal{F} and \mathcal{F}^{-1} stand for the forward and backward Fourier transform, respectively. By applying the fast Fourier transform (FFT) algorithm, the complexity of Eq. (43) is in order of $n \log_2 n$, where n is the number of the discrete sites of the system. In contrast, the complexity of Eq. (42) is in order of n^2 . For MOF adsorption, a typical value of n is $50^3 = 125,000$, which means applying Eq. (43) will accelerate the computation by more than 5 orders of magnitude. By applying FFT, the typical time cost for MOF adsorption is about 10–20 seconds, which is faster than state-of-the-art simulations by orders of magnitudes.

The introduction of FFT is a revolutionary advance in 3D-CDFT and makes 3D-CDFT much faster than simulations. With FFT, CDFT becomes a competitive method in predicting MOF adsorptions.

3.3. High-throughput calculation

One of the significant applications of the accelerated CDFT is material screening. Due to the various metal clusters, organic linkers, and 3-dimensional structures, there are billions of MOFs in principle. How to identify the best MOF in such a large database is an essential issue in material design. The traditional method to do this is the molecular simulation. Snurr et al. [1] have performed MC simulation of methane adsorption in 137,953 hypothetical MOFs and have screened out 300 MOFs which have higher methane capacity than any real MOFs. Based on the screening, Snurr et al. have synthesized a high-performance methane storage material, NOTT-107. Snurr et al.'s work has demonstrated the feasibility of high-throughput screening. However, Snurr et al.'s MC simulation is computationally expensive, which may not be the best method for high-throughput calculation. As mentioned above, as the accelerated CDFT is faster than MC simulation by two orders of magnitudes, CDFT seems to be a better choice.

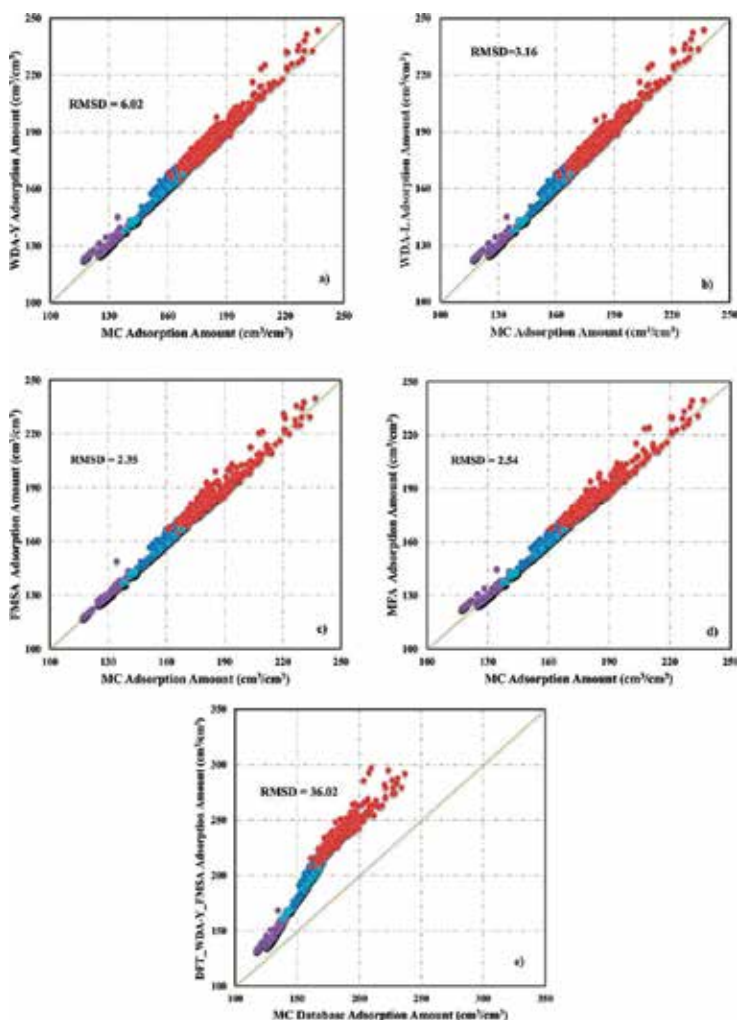


Figure 3. Uptake of H_2 in 1200 MOF at 243 K, 100 bar, comparison between five versions of CDFT and MC simulation. The versions for CDFT are (a) MFMT + WDA-V(MBWR) + MFA; (b) MFMT + WDA-N(MBWR) + MFA; (c) MFMT + SFE; (d) MFMT + MFA; (e) MFMT + WDA-V(FMSA) + MFA [33]. Reprinted with permission from Ref. [33]. Copyright (2016) American Chemical Society.

Applying CDFT to high-throughput screening has been reported very recently by Liu and Wu et al. [33–36]. First, Liu and Wu et al. [33] have predicted H_2 adsorption in 1200 MOFs by CDFT. As shown in **Figure 3**, five versions of CDFT have been tested. In **Figure 3(a),(b)**, and **(e)**, the excess free energy is given by Eq. (41), where F^{hs} , F^{attr} , and F^{cor} are approximated by MFMT, MFA, and WDA, respectively; the “MBWR” and “FMSA” in the brackets mean the correlation free energy density used in WDA that is calculated by MBWR EOS and FMSA (first-order mean sphere approximation) EOS [56], respectively. In **Figure 3(c)** and **(d)**, the excess free energy is represented by Eq. (40), where F^{hs} is approximated by MFMT for both, while F^{attr} is approximated by SFE and MFA, respectively. It seems the first four versions of CDFT accord

with simulations very well in contrast to the last one, where the correlation free energy density is approximated by FMSA. This reveals that the accuracy of EOS plays an important role in the accuracy of WDA, and the MBWR seems a good choice for MOF adsorption. To give a more comprehensive judgment of the other four versions of CDFT, Liu and Wu et al. have compared CDFT and simulation on different conditions. **Table 3** shows the root-mean-square deviation (RMSD) of the four CDFTs with respect to MC simulations. It seems MFMT + WDA-V + MFA and MFMT + WDA-N + MFA are the two most stable versions, while MFMT + SFE and MFMT + MFA are not so accurate at low temperatures. Besides, Liu and Wu et al.'s CDFT is processed in a single core (Intel E1230) with time cost around 10–20 seconds for each calculation, which is much faster than simulations (**Figure 4**).

	243 K 100 bar	77 K 1 bar	77 K 50 bar
MFMT + WDA-V + MFA	6.02	6.87	17.2
MFMT + WDA-N + MFA	3.16	8.38	16.9
MFMT + SFE	2.35	27	40.3
MFMT + MFA	2.54	11.3	39.3

Table 3. The RMSD of CDFT in different conditions (unit: cm^3 (STP) / cm^3).

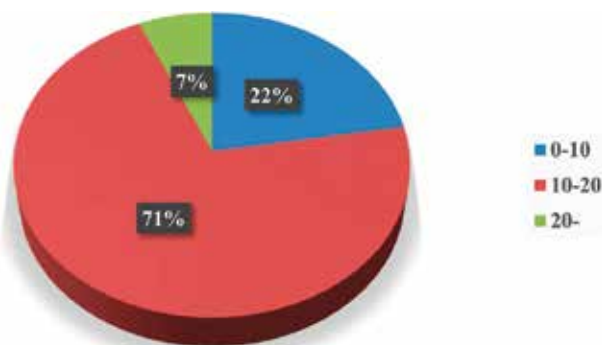


Figure 4. Time cost of the CDFT calculation for H_2 adsorption in 1200 MOFs (unit: second). Reprinted with permission from Ref. [33]. Copyright (2016) American Chemical Society.

CDFT has then been applied to screen out hydrogen storage materials for different conditions. By using CDFT, Liu et al. [35] have predicted H_2 adsorption in 712 MOFs under 441 different conditions. The whole computation ($712 \times 441 = 313,992$ cases in total) only takes approximately 1500 CPU hours.

As shown in **Figure 5**, Liu et al. have predicted the highest uptake of the 712 MOFs at temperature 77–373 K, pressure 0.01–100 atm. On one hand, the uptake of the MOFs at low temperature is striking: At 77 K 100 atm, the highest uptake is approximately 37 mol/L, exceeding the density of liquid hydrogen; even at low pressure, 77 K 0.01 atm, the highest uptake approaches 13 mol/L, which is higher than many real MOFs at high pressures. On the

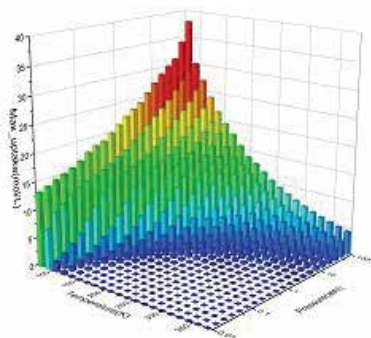


Figure 5. The highest uptakes of 712 types of MOF materials at different temperature and pressure [35]. Reprinted with permission from Ref. [35]. Copyright (2016) John Wiley & Sons, Inc.

other hand, the uptake at high temperature is not so satisfactory; most uptakes are lower than 5 mol/L. It appears that hydrogen storage at high temperature is still a big problem which is difficult to be solved by MOFs.

Based on Liu et al.'s screening, a set of promising MOFs have been identified. **Figure 6** shows the three promising MOFs and their adsorption isotherm for hydrogen storage at high, medium and low loadings, respectively. It seems narrower pore is more preferred for high temperatures in contrast to low temperatures.

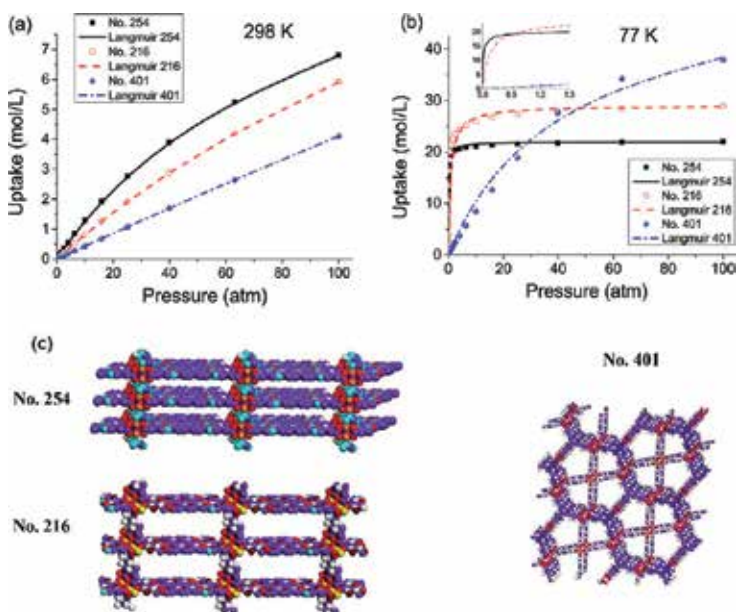


Figure 6. Adsorption isotherms for three MOF structures at (a) 298 K; (b) 77 K. (c) Structure of the three MOFs, color codes: C, purple; H, white; O, red; N, light blue; Zn, pink; Cu, orange; Br, wine; V, yellow [35]. Reprinted with permission from Ref. [35]. Copyright (2016) John Wiley & Sons, Inc.

Besides hydrogen storage, CDFT has also been extended to other screenings such as methane storage [36] and desulfurization [34]. Again, CDFT has revealed itself as a more efficient method than simulations in these high-throughput calculations.

3.4. Entropy scaling

Besides the density profile and uptake, CDFT could also predict other important properties of MOF adsorption, such as entropy and even self-diffusivity.

To generate entropy from CDFT is straightforward as the free energy functional is given explicitly in CDFT. Entropy can be obtained by a simple derivative:

$$S = - \left(\frac{\partial F}{\partial T} \right)_{\rho(\mathbf{r})} \quad (44)$$

One of the most important usage of entropy is the entropy scaling rule, which was proposed by Rosenfeld in 1977 [57] and explained by Dzугutov in 1996 [58]. The entropy scaling rule correlates excess entropy and self-diffusivity by a universal equation:

$$D^* = A \exp(Bs^{\text{ex}}) \quad (45)$$

where D^* is the dimensionless self-diffusivity, s^{ex} is the dimensionless excess entropy, A and B are universal constants that are independent of external conditions and molecular models. Eq. (45) had been first introduced for homogeneous fluids; however, Truskett et al. [59–61] have shown that the correlations between entropy and diffusivity also exist in inhomogeneous fluids. Recently, Liu et al. [31] have applied entropy scaling rule together with CDFT, MD simulation, and mean free volume theory to predict the self-diffusivity of MOFs:

$$\ln D_s = \left(1 - \frac{\alpha N \sigma^3}{V_{\text{free}}} \right) \ln D_K + \frac{\alpha N \sigma^3}{V_{\text{free}}} \ln D_E \quad (46)$$

where D_s is the self-diffusivity of fluids in MOFs, D_K is the Knudsen diffusivity, which can be calculated by one MD simulation, D_E is the diffusivity calculated from entropy scaling rule and CDFT, i.e., Eq. (45), V_{free} is the free volume and α is the mixing parameter, which can be determined from face center cubic (FCC) approximation or empirical method. Liu et al. have applied Eq. (46) to predict the self-diffusivity of fluids in MOFs. **Figure 7** shows the comparison between Eq. (46) and pure MD simulations. It seems combining CDFT and entropy scaling rule could capture the essentials of the diffusion curve, and Eq. (46) may accelerate the prediction of self-diffusivities.

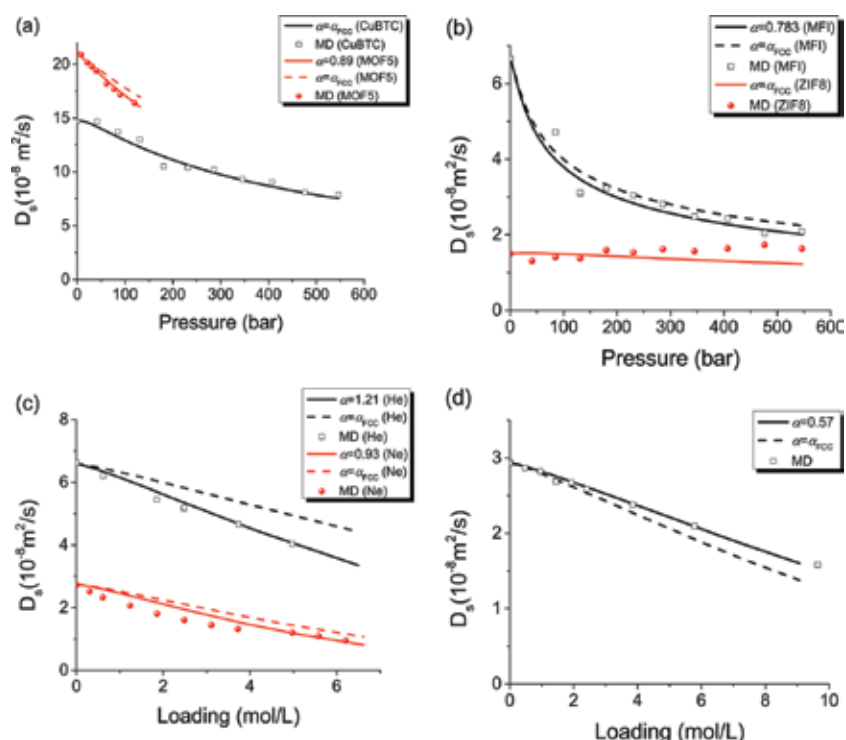


Figure 7. Self-diffusivity of (a) H₂ in CuBTC and MOF-5; (b) H₂ in MFI and ZIF-8; (c) He and Ne in MFI; (d) Ar in MOF-5. Comparison between CDFT-based entropy scaling rule and MD simulation [31]. Reprinted with permission from Ref. [31]. Copyright (2016) American Chemical Society.

4. Conclusion and prospect

We have introduced the theoretical framework of CDFT and reviewed the applications of using CDFT to predict fluid adsorption in MOFs. Although the framework of CDFT had been proposed 40 years ago, its application on real system such as MOF adsorption is still a new frontier. The applications of CDFT on MOF adsorption are reported in the past 6–7 years and mainly come from a few research groups. However, CDFT has been successfully applied to gas adsorption/diffusion in nanoporous materials and high-throughput screening of MOFs. In these applications, the FFT seems to be the key which makes CDFT more efficient than conventional simulations. One reason for the relatively fewer applications of CDFT is the lack of CDFT software in the current stage. Developing a usable CDFT software would extend the application of CDFT.

Besides the advantages, the challenge of current CDFT is how to deal with polar molecules which may not be coarse grained into a spherical model such as H₂O. It is well known that the hydrogen bonding network instead of spherical Van der Waals interaction is the dominating factor of such polar systems. For non-spherical molecule, the difficulty is how to construct an

accurate excess free energy functional which can be accelerated by numerical method such as Eq. (43). For example, in MFA, Eq. (31), the molecule-molecule interaction $u(\mathbf{R}_1, \mathbf{R}_2)$ is a multi-dimensional function which cannot be simplified into a one-dimensional function $u(r)$; in functional expansion theory, the high-order terms (so-called bridge functional) give an important contribution, which often cannot be accelerated by FFT. If such problems are solved, CDFT will be a perfect substitute for MC simulation.

Acknowledgements

This work is sponsored by the National Natural Science Foundation of China (No. 21506051, 91334203), the 111 Project of Ministry of Education of China (No. B08021), the Shanghai Pujiang Program (15PJ1401400), the Open Project of State Key Laboratory of Chemical Engineering (SKL-Che-15C05), and the Fundamental Research Funds for the Central Universities of China (222201414008).

Author details

Yu Liu* and Honglai Liu

*Address all correspondence to: hlliu@ecust.edu.cn

State Key Laboratory of Chemical Engineering, Department of Chemical Engineering, East China University of Science and Technology, Shanghai, China

References

- [1] Wilmer CE, Leaf M, Lee CY, et al. Large-scale screening of hypothetical metal-organic frameworks. *Nature Chemistry*. 2012;4(2):83–89. DOI: 10.1038/nchem.1192
- [2] Colon YJ, Snurr RQ. High-throughput computational screening of metal-organic frameworks. *Chemical Society Reviews*. 2014;43(16):5735–5749. DOI: 10.1039/c4cs00070f
- [3] Wu D, Wang C, Liu B, Liu D, Yang Q, Zhong C. Large-scale computational screening of metal-organic frameworks for CH₄/H₂ separation. *Aiche Journal*. 2012;58(7):2078–2084. DOI: 10.1002/aic.12744
- [4] Ebner C, Saam WF, Stroud D. Density-functional theory of simple classical fluids. I. Surfaces. *Physical Review A (General Physics)*. 1976;14(6):2264–2273. DOI: 10.1103/PhysRevA.14.2264

- [5] Ebner C, Punyanitya C. Density-functional theory of simple classical fluids. II. Localized excess electron states. *Physical Review A (General Physics)*. 1979;19(2):856–865. DOI: 10.1103/PhysRevA.19.856
- [6] Lado F, Foiles SM, Ashcroft NW. Solutions of the reference hypernetted-chain equation with minimized free-energy. *Physical Review A*. 1983;28(4):2374–2379. DOI: 10.1103/PhysRevA.28.2374
- [7] Chandler D, McCoy JD, Singer SJ. Density functional theory of nonuniform polyatomic systems. 1. General formulation. *Journal of Chemical Physics*. 1986;85(10):5971–5976. DOI: 10.1063/1.451510
- [8] Hansen JP, McDonald IR. *Theory of Simple Liquids*. 2nd Ed. London: Academic Press; 1986.
- [9] Rosenfeld Y. Free-energy model for the inhomogeneous hard-sphere fluid mixture and density-functional theory of freezing. *Physical Review Letters*. 1989;63(9):980–983. DOI: 10.1103/physrevlett.63.980
- [10] McMullen WE, Freed KF. A density functional theory of polymer phase transitions and interfaces. *The Journal of Chemical Physics*. 1990;92(2):1413–1426. DOI: 10.1063/1.458153
- [11] Kierlik E, Rosinberg ML. Density-functional theory for inhomogeneous fluids: adsorption of binary-mixtures. *Physical Review A*. 1991;44(8):5025–5037. DOI: 10.1103/PhysRevA.44.5025
- [12] Rosenfeld Y. Free-energy model for inhomogeneous fluid mixtures: Yukawa-charged hard-spheres, general interactions, and plasmas. *Journal of Chemical Physics*. 1993;98(10):8126–8148. DOI: 10.1063/1.464569
- [13] Rosenfeld Y. Phase separation of asymmetric binary hard-sphere fluids: self-consistent density functional theory. *Physical Review Letters*. 1994;72(24):3831–3834. DOI: 10.1103/PhysRevLett.72.3831
- [14] Perez-Jorda JM, Becke AD. A density-functional study of van der Waals forces: rare gas diatomics. *Chemical Physics Letters*. 1995;233(1–2):134–137. DOI: 10.1016/0009-2614(94)01402-h
- [15] Seok C, Oxtoby DW. Nucleation in n-alkanes: a density-functional approach. *Journal of Chemical Physics*. 1998;109(18):7982–7990. DOI: 10.1063/1.477445
- [16] Marconi UMB, Tarazona P. Dynamic density functional theory of fluids. *Journal of Chemical Physics*. 1999;110(16):8032–8044. DOI: 10.1063/1.478705
- [17] Yu YX, Wu JZ. Structures of hard-sphere fluids from a modified fundamental-measure theory. *Journal of Chemical Physics*. 2002;117(22):10156–10164. DOI: 10.1063/1.1520530
- [18] Yu YX, Wu JZ. A fundamental-measure theory for inhomogeneous associating fluids. *Journal of Chemical Physics*. 2002;116(16):7094–7103. DOI: 10.1063/1.1463435

- [19] Yu YX, Wu JZ. Density functional theory for inhomogeneous mixtures of polymeric fluids. *Journal of Chemical Physics*. 2002;117(5):2368–2376. DOI: 10.1063/1.1491240
- [20] Cao D, Wu J. Density functional theory for semiflexible and cyclic polyatomic fluids. *Journal of Chemical Physics*. 2004;121(9):4210–4220. DOI: 10.1063/1.1774983
- [21] Li Z, Wu J. Density-functional theory for the structures and thermodynamic properties of highly asymmetric electrolyte and neutral component mixtures. *Physical Review E*. 2004;70(3 Pt 1):031109.
- [22] Ye ZC, Cai J, Liu HL, Hu Y. Density and chain conformation profiles of square-well chains confined in a slit by density-functional theory. *Journal of Chemical Physics*. 2005;123(19):194902. DOI: 10.1063/1.2117009
- [23] Ye Z, Chen H, Cai J, Liu H, Hu Y. Density functional theory of homopolymer mixtures confined in a slit. *Journal of Chemical Physics*. 2006;125(12):124705. DOI: 10.1063/1.2354087
- [24] Yu YX, You FQ, Tang YP, Gao GH, Li YG. Structure and adsorption of a hard-core multi-Yukawa fluid confined in a slitlike pore: grand canonical Monte Carlo simulation and density functional study. *Journal of Physical Chemistry B*. 2006;110(1):334–341. DOI: 10.1021/jp055299s
- [25] Peng B, Yu Y-X. A density functional theory for Lennard-Jones fluids in cylindrical pores and its applications to adsorption of nitrogen on MCM-41 Materials. *Langmuir*. 2008;24(21):12431–12439. DOI: 10.1021/la8024099
- [26] Liu Y, Liu HL, Hu Y, Jiang JW. Development of a density functional theory in three-dimensional nanoconfined space: H₂ storage in metal organic frameworks. *Journal of Physical Chemistry B*. 2009;113(36):12326–12331. DOI: 10.1021/jp904872f
- [27] Siderius DW, Gelb LD. Predicting gas adsorption in complex microporous and mesoporous materials using a new density functional theory of finely discretized lattice fluids. *Langmuir*. 2009;25(3):1296–1299. DOI: 10.1021/la803666t
- [28] Yu YX. A novel weighted density functional theory for adsorption, fluid-solid interfacial tension, and disjoining properties of simple liquid films on planar solid surfaces. *Journal of Chemical Physics*. 2009;131(2): 024704. DOI: 10.1063/1.3174928
- [29] Liu Y, Liu HL, Hu Y, Jiang JW. Density functional theory for adsorption of gas mixtures in metal-organic frameworks. *Journal of Physical Chemistry B*. 2010;114(8):2820–2827. DOI: 10.1021/jp9104932
- [30] Zhao S, Ramirez R, Vuilleumier R, Borgis D. Molecular density functional theory of solvation: from polar solvents to water. *Journal of Chemical Physics*. 2011;134(19):194102. DOI: 10.1063/1.3589142
- [31] Liu Y, Fu J, Wu J. Excess-entropy scaling for gas diffusivity in nanoporous materials. *Langmuir*. 2013;29(42):12997–13002. DOI: 10.1021/la403082q

- [32] Liu Y, Zhao S, Wu J. A site density functional theory for water: application to solvation of amino acid side chains. *Journal of Chemical Theory and Computation*. 2013;9(4):1896–1908. DOI: 10.1021/ct3010936
- [33] Fu J, Liu Y, Tian Y, Wu J. Density functional methods for fast screening of metal-organic frameworks for hydrogen storage. *The Journal of Physical Chemistry C*. 2015;119:5374–5385. DOI: 10.1021/jp505963m
- [34] Liu Y, Guo F, Hu J, Zhao S, Liu H, Hu Y. Screening of desulfurization adsorbent in metal-organic frameworks: a classical density functional approach. *Chemical Engineering Science*. 2015;137:170–177. DOI: 10.1016/j.ces.2015.06.036
- [35] Liu Y, Zhao S, Liu H, Hu Y. High-throughput and comprehensive prediction of H₂ adsorption in metal-organic frameworks under various conditions. *AIChE Journal*. 2015;61:2951–2957. DOI: 10.1002/aic.14842
- [36] Fu J, Tian Y, Wu J. Classical density functional theory for methane adsorption in metal-organic framework materials. *Aiche Journal*. 2015;61(9):3012–3021. DOI: 10.1002/aic.14877
- [37] Rappe AK, Casewit CJ, Colwell KS, Goddard WA, Skiff WM. UFF, a full periodic table force field for molecular mechanics and molecular dynamics simulations. *Journal of the American Chemical Society*. 1992;114(25):10024–10035. DOI: 10.1021/ja00051a040
- [38] Mayo SL, Olafson BD, Goddard WA, III. DREIDING: a generic force field for molecular simulations. *Journal of Physical Chemistry*. 1990;94(26):8897–8909. DOI: 10.1021/j100389a010
- [39] Hohenberg P, Kohn W. Inhomogeneous electron gas. *Physical Review B*. 1964;136(3B):B864. DOI: 10.1103/PhysRev.136.B864
- [40] Kohn W, Sham LJ. Self-consistent equations including exchange and correlation effects. *Physical Review*. 1965;140(4A):A1133–A1138. DOI: 10.1103/physrev.140.a1133
- [41] Liu J, Herbert JM. Local excitation approximations to time-dependent density functional theory for excitation energies in solution. *Journal of Chemical Theory And Computation*. 2016;12(1):157–166. DOI: 10.1021/acs.jctc.5b00828
- [42] Johnson M, Nordholm S. Generalized van der Waals theory. VI. Application to adsorption. *Journal of Chemical Physics*. 1981;75(4):1953–1957. DOI: 10.1063/1.442220
- [43] Tarazona P, Evans R. A simple density functional theory for inhomogeneous liquids: wetting by gas at a solid-liquid interface. *Molecular Physics*. 1984;52(4):847–857. DOI: 10.1080/00268978400101601
- [44] Curtin WA, Ashcroft NW. Weighted-density-functional theory of inhomogeneous liquids and the freezing transition. *Physical Review A (General Physics)*. 1985;32(5):2909–2919. DOI: 10.1103/PhysRevA.32.2909

- [45] Tarazona P. Free energy density functional for hard spheres. *Physical Review A (General Physics)*. 1985;31(4):2672–2679. DOI: 10.1103/PhysRevA.31.2672
- [46] Denton AR, Ashcroft NW. Modified weighted-density-functional theory of nonuniform classical liquids. *Physical Review A (General Physics)*. 1989;39(9):4701–4708. DOI: 10.1103/PhysRevA.39.4701
- [47] Denton AR, Ashcroft NW. Density-functional approach to the structure of classical uniform fluids. *Physical Review A (Statistical Physics, Plasmas, Fluids, and Related Interdisciplinary Topics)*. 1991;44(2):1219–1227. DOI: 10.1103/PhysRevA.44.1219
- [48] Leidl R, Wagner H. Hybrid WDA: a weighted-density approximation for inhomogeneous fluids. *Journal of Chemical Physics*. 1993;98(5):4142–4148. DOI: 10.1063/1.465022
- [49] Ravikovitch PI, Vishnyakov A, Neimark AV. Density functional theories and molecular simulations of adsorption and phase transitions in nanopores. *Physical Review E*. 2001;64(1):011602. DOI: 10.1103/PhysRevE.64.011602
- [50] Zhidong L, Dapeng C, Jianzhong W. Density-functional theory and Monte Carlo simulation for the surface structure and correlation functions of freely jointed Lennard-Jones polymeric fluids. *Journal of Chemical Physics*. 2005;122(17):174708–174709. DOI: 10.1063/1.1886685
- [51] Libby B, Monson PA. Adsorption/desorption hysteresis in inkbottle pores: a density functional theory and Monte Carlo simulation study. *Langmuir*. 2004;20(10):4289–4294. DOI: 10.1021/la036100a
- [52] Tang YP, Wu JZ. Modeling inhomogeneous van der Waals fluids using an analytical direct correlation function. *Physical Review E*. 2004;70(1): 011201. DOI: 10.1103/PhysRevE.70.011201
- [53] Kong X, Gallegos A, Lu D, Liu Z, Wu J. A molecular theory for optimal blue energy extraction by electrical double layer expansion. *Physical Chemistry Chemical Physics*. 2015;17(37):23970–23976. DOI: 10.1039/c5cp03514g
- [54] Peng B, Yu Y-X. A Density functional theory with a mean-field weight function: applications to surface tension, adsorption, and phase transition of a Lennard-Jones Fluid in a slit-like pore. *Journal of Physical Chemistry B*. 2008;112(48):15407–15416. DOI: 10.1021/jp805697p
- [55] Ritter JA, Pan H, Balbuena PB. Adsorption of binary gas mixtures in heterogeneous carbon predicted by density functional theory: on the formation of adsorption azeotropes. *Langmuir*. 2010;26(17):13968–13975. DOI: 10.1021/la101865m
- [56] Tang Y, Lu BCY. Analytical description of the Lennard-Jones fluid and its application. *Aiche Journal*. 1997;43(9):2215–2226. DOI: 10.1002/aic.690430908
- [57] Rosenfeld Y. Relation between transport-coefficients and internal entropy of simple systems. *Physical Review A*. 1977;15(6):2545–2549. DOI: 10.1103/PhysRevA.15.2545

- [58] Dzugutov M. A universal scaling law for atomic diffusion in condensed matter. *Nature*. 1996;381(6578):137–139. DOI: 10.1038/381137a0
- [59] Mittal J, Errington JR, Truskett TM. Using available volume to predict fluid diffusivity in random media. *Physical Review E*. 2006;74(4): 040102. DOI: 10.1103/PhysRevE.74.040102
- [60] Mittal J, Errington JR, Truskett TM. Relationships between self-diffusivity, packing fraction, and excess entropy in simple bulk and confined fluids. *Journal of Physical Chemistry B*. 2007;111(34):10054–10063. DOI: 10.1021/jp071369e
- [61] Goel G, Krekelberg WP, Errington JR, Truskett TM. Tuning density profiles and mobility of inhomogeneous fluids. *Physical Review Letters*. 2008;100(10):106001. DOI: 10.1103/PhysRevLett.100.106001

Applications

Metal-Organic Frameworks and their Applications in Hydrogen and Oxygen Evolution Reactions

Fengxiang Yin, Xiao Zhang, Xiaobo He and
Hao Wang

Additional information is available at the end of the chapter

<http://dx.doi.org/10.5772/64657>

Abstract

The hydrogen evolution reaction (HER) and oxygen evolution reaction (OER) play a vital role in many energy storage and conversion systems, including water splitting, rechargeable metal-air batteries, and the unitized regenerative fuel cells. The noble-metal catalysts based on Pt, Ir, and Au are the best electrocatalysts for the HER/OER, but they suffer from high price and scarcity problems. Therefore, it is urgently necessary to develop efficient, low-cost, and environment-friendly non-noble metal electrocatalysts. Metal-organic frameworks (MOFs) are crystalline materials with porous network structure. MOFs possess various compositions, large specific surface area, tunable pore structures, and they are easily functionalized. MOFs have been widely studied and applied in many fields, such as gas adsorption/separation, drug delivery, catalysis, magnetism, and optoelectronics. Recently, MOFs-based electrocatalysts for HER/OER have been rapidly developed. These MOFs-based catalysts exhibit excellent catalytic performance for HER/OER, demonstrating a promising application prospect in HER/OER. In this chapter, the concept, structure, category, and synthesis of MOFs will be first introduced briefly. Then, the applications of the MOFs-based catalysts for HER/OER in recent years will be discussed in details. Specially, the synthesis, structure, and catalytic performance for HER/OER of the MOFs-based catalysts will be emphatically discussed.

Keywords: metal-organic frameworks, electrocatalytic water splitting, hydrogen evolution reaction, oxygen evolution reaction, electrocatalysts

1. Introduction

Electrocatalytic hydrogen evolution reaction (HER) and oxygen evolution reaction (OER) are the key reactions for many energy storage and conversion systems, including water splitting, rechargeable metal-air batteries, and the unitized regenerative fuel cells [1–3]. However, the two reactions are kinetically sluggish, which leads to large overpotentials in the electrodes, decreases the performance of these systems, and makes them difficult to meet the requirements for commercialization at present. It has been reported that suitable electrocatalysts can effectively accelerate the HER/OER and reduce their overpotentials in the electrodes. At present, noble metal catalysts show the best catalytic performance for HER and OER. For example, carbon-supported Pt catalysts exhibit the best catalytic performance for HER [4], while IrO₂ and RuO₂ are very effective for OER [5]. However, the reserves of these noble metals are extremely limited in nature resulting in a high price of these noble metal catalysts, which restricts their practical applications. Therefore, the development of highly efficient electrocatalysts with low cost for HER/OER is indispensable. In recent years, a large amount of non-noble metal catalysts have been synthesized for HER/OER. The non-noble metal catalysts for HER mainly include transition metal phosphides [6–8], such as CoP, NiP, transition metal sulfides [9–11], such as MoS₂, CoS, Ni-S, and their alloys [12, 13] such as Ni-Mo, Ni-Cu. As for OER, the non-noble metal catalysts mainly focus on metal oxides [14–16] such as Co₃O₄, MnO_x, Ni_xCo_{3-x}O₄, and metal sulfides [17, 18] such as Ni₃S₂, NiCo₂S₄. Although these non-noble metal catalysts have shown excellent catalytic performance for HER and/or OER, to date, there is no one catalyst that can fully meet the demands of the practical applications. It is necessary to develop more economically viable electrocatalysts with higher catalytic performance for HER and/or OER, and further accelerate the commercial applications of these energy storage and conversion systems.

Metal-organic frameworks (MOFs) are porous crystalline materials with topological structures. MOFs are formed by assembling metal nodes and organic ligands. The metal node precursors mainly come from metal nitrates or chlorides, while the organic ligands mainly include benzimidazolate, dicarboxylic acid, and others. MOFs can be synthesized by some simple methods under mild conditions such as solvothermal, diffusion, microwave, and ionothermal methods [19–22]. MOFs possess unique structural characterizations such as high porosity, ultrahigh specific surface area (~6240 m² g⁻¹) and tunable pore structure and easy functionalization [23], and they have been widely investigated and applied in gas adsorption/separation [24], magnetism [25], optoelectronics [26], and catalysis [27]. In recent years, MOFs have attracted great attention for use in energy conversion and storage systems such as water splitting, fuel cells, metal-air batteries, and supercapacitors. More recently, the applications of MOFs have been expanded to the HER and OER catalysis. To date, some novel MOF-based catalysts for HER and OER have been synthesized. On the one hand, the active species can be introduced into the structures of MOFs, directly acting as effective catalysts for HER and/or OER; on the other hand, MOFs also can be used as supports to disperse the active species for HER and/or OER due to their porosity. In addition, the highly porous MOFs can be transformed to the derived catalysts by self-sacrifice methods. These MOFs-derived catalysts usually possess improved electronic conductivity and remarkable HER and/or OER

catalytic performance. This chapter reviews recent progress of MOFs and MOFs-derived electrocatalysts for HER and/or OER. The MOFs are first introduced briefly. The applications of MOFs-based catalysts for HER and/or OER are the main contents and involve details. This work provides a helpful reference for researchers who are studying the MOFs-based electrocatalysts for HER and/or OER.

2. Overview of metal-organic frameworks

As a class of the coordination polymers, MOFs are crystalline porous materials. MOFs are formed through self-assembling using the inorganic metals as nodes and organic ligands as linkers [28, 29]. They possess unique structure properties, such as ultrahigh specific surface area and high porosity, tunable pore structure, and easy functionalization. The specific surface area of MOFs are much higher than that of other porous materials such as activated carbon and zeolites. For example, the synthesized MOF-201 possesses a high BET specific surface area of $\sim 6240 \text{ m}^2 \text{ g}^{-1}$ [30], while zeolites possess specific surface area less than $600 \text{ m}^2 \text{ g}^{-1}$. High porosity of MOFs also brings up a very low density ($\sim 0.13 \text{ g cm}^{-3}$) [23], which is important to the storage of fuels or the applications in energy conversion and storage. The pore structure of MOFs can be tuned by choosing different organic ligands or altering the length of organic ligands. It was reported that Deng et al. prepared a novel IRMOF (IRMOF-74 XI) with large apertures of $\sim 9.8 \text{ nm}$, by expanding the length of its organic linker to $\sim 5 \text{ nm}$ [31]. Apart from the tunable pore structure, MOFs can be easily functionalized by decorating the pores, surfaces, or introducing guests into MOFs, thus resulting in a large amount of MOFs with various physicochemical properties [32]. Due to these unique properties, MOFs have been widely developed and applied in gas adsorption/separation [24], magnetism [25], optoelectronics [26], and catalysis [27] in recent years.

According to topological structure features, MOFs can be generally divided into four categories: isorecticular metal-organic frameworks (IRMOFs), zeoliticimidazolate frameworks (ZIFs), materials of institute Lavoisier frameworks (MILs) and pocket-channel frameworks (PCNs) [33, 34].

IRMOFs are a large family of MOFs, which are built up by $[\text{Zn}_4\text{O}]^{6+}$ and organic hydroxyl acid as metal nodes and ligands, respectively. In the IRMOFs family, MOF-5 is the typical one which was prepared by Li et al. as early as in 1999 [35]. MOF-5 is highly porous, and the specific surface area and the density are about $2900 \text{ m}^2 \text{ g}^{-1}$ and 0.59 g cm^{-3} , respectively. Specially, the space access to guest substance reaches up to 55–61%.

The topological structures of pores of ZIFs are similar to aluminosilicate zeolite. Generally, imidazole or its derivatives and Zn or Co ions are used as ligands and metal nodes, respectively. The N atoms in imidazole and its derivatives can coordinate with Zn, Co, or other transitional metal ions. Compared with other kinds of MOFs, ZIFs show higher thermal and chemical stability. For example, as a typical ZIF material, ZIF-8 can sustain its structures in inorganic or organic solvents or even in boiling water for 1–7 days [36].

Generally, there are two categories of MILs. One is formed by using lanthanides or transition metals as metal nodes and dicarboxylic acids as organic ligands. The other is obtained using trivalent metals such as aluminum or vanadium as metal nodes, and terephthalic acids or trimesic acids as organic ligands. MILs are highly porous and possess ultrahigh specific surface area. MIL-100 and MIL-101 are typical MILs. In MIL-100, Cr^{3+} ions are metal nodes and BTC (1,3,5-benzenetricarboxylate) is used as organic ligands. It possesses a high specific surface area of $\sim 3100 \text{ m}^2/\text{g}$ and mesopores with the pore size of $\sim 2.9 \text{ nm}$ [37]. In addition, MIL-100 exhibits excellent thermal stability below 275°C [37].

During the synthesis of PCNs, Cu ions or oxo-clusters are generally used as metal nodes, and tricarboxylic acids, 4,4',4''-s-triazine-2,4,6-triyltribenzoate (H_3TATB) or s-heptazine tribenzoate (HTB) is usually used as an organic ligands. PCNs have pocket and three-dimensional orthogonal channels which are connected through small sized windows. As a typical PCN, Cu-BTC is formed by using $\text{Cu}_2(\text{COO})_4$ as metal nodes and BTC as organic ligands. Two typical channel structures can be observed in Cu-BTC. One is a small octahedron pocket, while the other is the three-dimensional orthogonal channels ($\sim 1 \text{ nm}$) [38].

To prepare MOFs, various synthetic methods have been proposed, such as solvothermal (hydrothermal) method, diffusion method, microwave-assisted method and ionothermal method. During the solvothermal (hydrothermal) process, water or organic solvents are usually used as reaction medium in an airtight reactor. High temperature and pressure condition can be achieved through heating the airtight reactor. Thus, some compounds with poor solubility at room temperature and atmospheric pressure can be dissolved and recrystallized to obtain the desirable MOFs. In addition, high crystallinity and controllable particle size for the resulting MOFs can be obtained through the solvothermal (hydrothermal) process. Therefore, the solvothermal (hydrothermal) method is effective to produce MOFs with good orientation and perfect crystals [19, 39].

The diffusion methods include vapor diffusion, liquid diffusion, and gel diffusion methods. The products are obtained in the two-phase interface through slow crystallization [20]. The diffusion methods have two advantages, including mild synthesis conditions and high quality crystal MOFs. However, the efficiency of this method is usually low, which requires a long synthesis time, up to 1 week. Furthermore, this method also requires precursors with good solubility.

In the microwave-assisted process, the charging particles are placed in electromagnetic fields. These charging particles collide with high speed, forming the final products. Due to the high frequency of microwave, the microwave-assisted method is considered as a high energy efficiency method [21]. It has many advantages, such as uniform heating, high reaction rate, selective heating, and no hysteresis effects.

For the ionothermal synthesis, ionic liquids and eutectic mixture are usually used as solvents [22]. Ionothermal synthesis can avoid the high-pressure reaction condition, and produce final MOFs in an open condition, because ionic liquids have almost no vapor pressure.

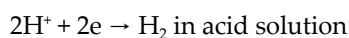
In MOFs, the organic ligands cannot only be used as linkers, but also adsorb gas molecules through Van der Waals force. This is the reason that MOFs materials can be used for gas

adsorption/separation [24]. Till date, most of the studies on MOFs still focus on gas adsorption/separation. Because some metals such as group VIII metals possess excellent magnetic properties, MOFs are also popular in magnetism field by using magnetic metal ions as nodes, and they possess paramagnetic or antiferromagnetic properties [25]. Similar regularity was observed of MOFs in the optoelectronics area. Luminescent lanthanide(III) ions which are utilized as nodes for MOFs are always designed as luminescent centers [26]. Due to the high specific surface area and tunable pore structure, MOFs have also been applied in electrocatalysis involving energy conversion and storage in recent years [32]. For instance, MOFs can be directly used as electrocatalysts in the applications for HER and/or OER. However, the electric conductivity of most MOFs is poor. The combination of MOFs and highly conductive substrates (such as graphene, carbon nanotubes, Ni foams and conductive glasses) is an efficient protocol to enhance the electrocatalytic performance of MOFs [27]. In addition, MOFs also can serve as precursors to form derived catalysts such as metal oxides, metal (oxides or carbides or sulfides or phosphides)/nanocarbon hybrids or porous nanocarbons, which is another effective way to take advantage of MOFs for HER and/or OER [40].

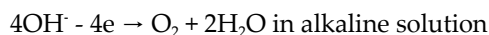
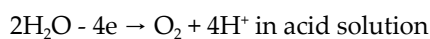
3. HER/OER

The growing concern of energy crisis and environment pollution promotes the development of highly effective clean energy storage and conversion systems, such as water splitting [1], metal-air batteries [2], and fuel cells [3]. In such systems, oxygen- and hydrogen-involving electrocatalytic processes, including oxygen reduction reaction (ORR), hydrogen oxidization reaction (HOR), hydrogen evolution reaction (HER), and oxygen evolution reaction (OER) are the most mentioned key components in determining the practical performance of these energy storage and conversion systems. The former two reactions consume oxygen and hydrogen to provide power, but the premise is that the available oxygen and hydrogen are generated from water splitting through OER and HER, respectively. The OER/HER involved in water splitting can be given in the following equations [9, 41]:

Hydrogen evolution reaction:



Oxygen evolution reaction:



Water splitting can produce pure hydrogen and oxygen which can be directly utilized as raw materials for fuel cells or for other industrial processes individually. Apart from water splitting, HER or OER can be associated with other electrochemical processes. For instance, OER is also a key reaction for rechargeable metal-air batteries [2] and regenerative fuel cells [3] when being charged. Rechargeable metal-air batteries and regenerative fuel cells

are seen as promising ways to produce electricity in the future and may effectively reduce our dependence on traditional fossil fuels and relieve environmental pollution.

Unlike HOR/ORR, HER/OER don't maintain a constant value at high overpotential. In other words, HER/OER are not limited by the mass transfer rate and they obey Butler-Volmer model even in high overpotential. Generally, the HER/OER catalytic mechanisms differ from each other. Even so, the descriptor (ΔG_{H^*} , hydrogen binding energy/adsorption free energy) is widely used to reflect HER activity for catalysts, while the descriptor ($\Delta G_{\text{O}^*} - \Delta G_{\text{OH}^*}$) is used to evaluate the OER activities [5]. HER involves the two-electron transfer processes, while OER includes more complex processes with the multistep charge-/proton-transfer. These complex processes result in the low efficiencies of HER/ORR and make it difficult for them to satisfy practical applications. Therefore, the development of efficient electrocatalysts for HER/OER to accelerate the kinetics and reduce the overpotentials is of great significance for the commercialization of HER/OER-related devices.

Currently, the HER/OER electrocatalysts mainly include precious metal catalysts and non-precious metal catalysts [5, 42]. The precious metal catalysts have been widely developed due to their extremely excellent catalytic performance. For instance, precious metal catalysts for HER are mainly dependent on Pt-based catalysts since they exhibit the best HER electrocatalytic performance in basic solution with a low onset overpotential. IrO_2 and RuO_2 have been demonstrated as the benchmark OER electrocatalysts (Pt-based catalysts barely show any OER catalytic activity), and even show remarkable stability in acid solution. However, although the precious metal catalysts possess excellent catalytic performance, their scarcity and high price hamper their large-scale applications. Thus, non-precious metal catalysts with low-cost and earth-abundance for HER/OER are urgently needed.

The non-precious metal catalysts for HER mainly include transition-metal sulfides, phosphides, alloys, etc. Through element selection, Co sulfides or phosphides are seen as the most promising HER catalysts, but they suffer from low stability. The alloys have been developed by integrating Ni with Mo or Cu [12, 13]. Diverse structures and composition are the advantages to those alloyed catalysts, but their restriction of activity limits their applications. The non-precious metal catalysts for the OER mainly contain transition metal oxides [14–16], sulfides [17, 18], hydroxides [43], and carbons [44], etc. Among them, metal oxides in single phase or in mixed phases are the most developed ones as efficient OER electrocatalysts due to their diverse compositions, superior stability, and remarkable OER performance. Thus, metal oxides are widely explored as promising OER catalysts, but the mechanism of OER is very sensitive to the compositions and structures of the catalysts, which requires further design, preparation, and optimization of OER catalysts. In spite of rapid development of the HER/OER electrocatalysts with relatively good performance, to date, no one catalyst can satisfy the practical demands. More researches for highly efficient HER and OER electrocatalysts are needed.

4. MOFs-based catalysts for HER

In recent years, MOFs have been widely explored to store hydrogen fuels due to high specific surface area, tunable pore structures, and various functions [45]. Meanwhile, they also have been developed as electrocatalysts for the HER through electrochemical splitting of water. Generally, MOFs can be directly used as catalysts or served as precursors for the derived catalysts for HER. Recently, Gong et al. synthesized $\text{Cu}_3(\text{Mo}_8\text{O}_{26})(\text{H}_2\text{O})_2(\text{OH})_2(\text{L1})_4$ ($\text{L1} = 4\text{H-4-amino-1,2,4-triazole}$) and $\text{Ag}_4(\text{Mo}_8\text{O}_{26})-(\text{L2})_{2.5}(\text{H}_2\text{O})$ ($\text{L2} = 3,5\text{-dimethyl-4-amino-4H-1,2,4-triazole}$) MOFs via a hydrothermal process [46]. The former had a chain-like structure, while the latter possessed a 3D structure. Both of them showed electrocatalytic activity for HER in 0.5 M H_2SO_4 with low overpotentials. $\text{Cu}_3(\text{Mo}_8\text{O}_{26})(\text{H}_2\text{O})_2(\text{OH})_2(\text{L1})_4$ had better HER activity than $\text{Ag}_4(\text{Mo}_8\text{O}_{26})-(\text{L2})_{2.5}(\text{H}_2\text{O})$. Their HER activities were related to the redox of $[\text{Mo}_8\text{O}_{26}]^{4-}$ polymolybdate anions. Qin et al. developed another polymolybdate (POM)-based MOF for HER [47]. This novel 3D open structure was formed by connecting POM fragments as nodes and H_3BTB ($\text{H}_3\text{BTB} = \text{benzene tribenzoate}$) or H_3BPT ($\text{H}_3\text{BPT} = [1,1'\text{-biphenyl]-3,4',5-tricarboxylic acid}$) as ligands. POM-based MOFs had excellent HER activity likely due to the combination of the redox of POM and the porosity of MOFs. Noticeably, the POM-based MOFs were stable not only in air but also in acid or basic solutions. Among these catalysts, NENU-500 ($[\text{TBA}]_3[\varepsilon\text{-PMo}^{\text{V}}_8\text{Mo}^{\text{VI}}_4\text{O}_{36}(\text{OH})_4\text{Zn}_4]$ [BTB] $_{4/3} \cdot 18\text{H}_2\text{O}$, $\text{TBA}^+ = \text{tetrabutylammonium ion}$) exhibited excellent HER activity with an onset overpotential of about 180 mV and Tafel slope of 96 mV dec^{-1} in 0.5 M H_2SO_4 . What's more, this catalyst could maintain its catalytic activity after 2000th cycles in 0.5 M H_2SO_4 solution.

Cobalt dithiolene species are highly efficient molecular catalysts for HER. Cloigh et al. integrated cobalt dithiolene into metal-organic surface (MOS, $[\text{Co}_3(\text{BHT})_2]^{3+}$ and $[\text{Co}_3(\text{THT})_2]^{3+}$ ($\text{BHT} = \text{benzenhexathiols}$, $\text{THT} = \text{triphenylene-2,3,6,7,10,11-hexathiols}$) materials to obtain effective catalysts for HER [48]. The prepared catalysts Co/MOS possessed a two-dimensional layer structure with high surface/volume ratio, resulting in high charge transfer efficiency and high surface active site concentration. The catalysts, especially $[\text{Co}_3(\text{BHT})_2]^{3+}$, showed not only remarkable stability in acidic solutions, but also excellent HER catalytic activity under wide pH conditions, and the current densities at 0.5 V (vs. Standard Hydrogen Electrode, RHE) increased with decreasing electrolyte pH. The mechanism of HER of the MOS involved $\text{Co}^{3+}/\text{Co}^{2+}$ redox reactions, following protonation of the S sites on the ligands.

Recently, MOFs also have been combined with 2D materials, such as graphene and metal dichalcogenide nanosheets, to form nanocomposites with unique properties and wide applications [49]. A Cu-MOF/graphene oxide (GO) nanocomposite catalyst for HER was successfully synthesized via a solvothermal process [27]. The Cu-MOF was prepared using $\text{Cu}(\text{NO}_3)_2$, 1,4-benzenedicarboxylic acid and triethylene-diamine as precursors. The integration of Cu-MOF with graphene oxide (GO) can effectively enhance the electron transfer, which further significantly improve HER activity. It was also found that the GO content affected the HER activity of the nanocomposite catalysts. The optimized GO content was about 8%. The HER current density of the (GO 8 wt%) Cu-MOF was high up to -30 mA cm^{-2} at an overpo-

tential of -0.2 V in N_2 -saturated 0.5 M H_2SO_4 , whereas the overpotential of 20 wt% Pt was -0.06 V at the current density of -30 mA cm^{-2} .

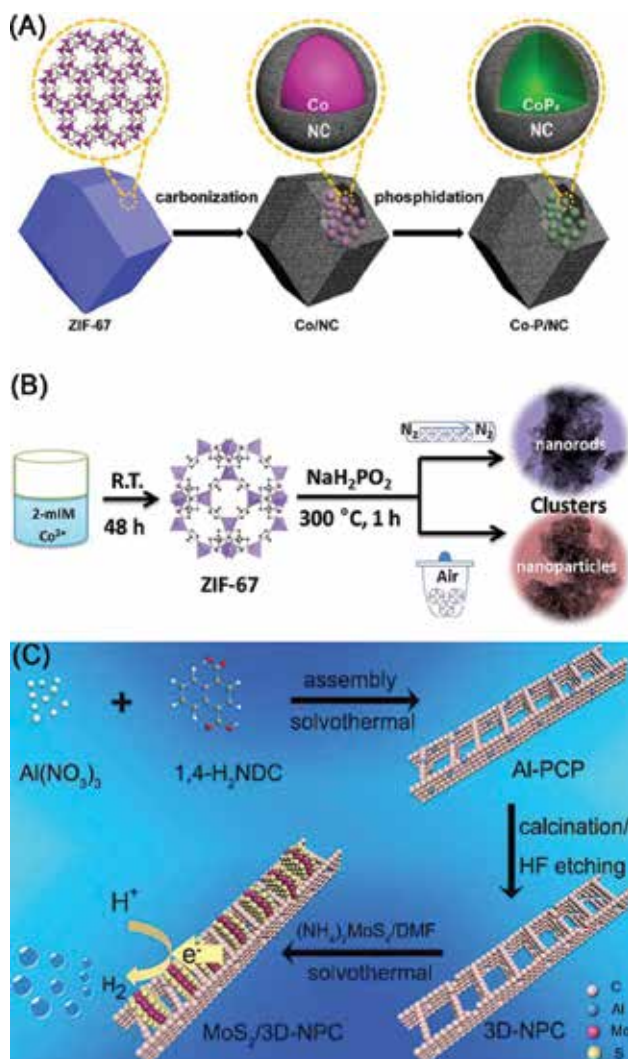


Figure 1. Schematic illustration of (A) synthesis of Co-P/NC [50]; (B) formation of CoP NPCs and CoP NRCs derived from ZIF-67-Co [51]; (C) the space-confined synthesis of MoS₂/3D-NPC composites and its application in HER [53].

Because MOFs possess structural diversity, high specific surface area, and large pore volume, MOFs are regarded as ideal precursors to prepare various inorganic nanomaterials as electrocatalysts, such as porous carbon, metal-oxide nanoparticles/porous carbon or metallic nanoparticles/carbon. It has been reported that cobalt species are active for HER. Among them, cobalt phosphides as HER electrocatalysts have been widely investigated in recent years. You et al. prepared a Co-P/NC catalyst by embedding CoP_x nanoparticles into N-doped carbon

through carbonizing Co-ZIF-67 and a subsequent phosphidation (**Figure 1A**) [50]. After carbonization, the obtained Co-ZIF-67 inherited the morphology of polyhedron-like ZIF-67, in which the metallic Co nanoparticles were wrapped by the porous N-doped carbon shells. Through the following phosphidation, the products also preserved the polyhedron-like morphology of ZIF-67, while the metallic Co nanoparticles were transformed into CoP_x nanoparticles. The optimal Co-P/NC catalyst afforded a high specific surface area of $183 \text{ m}^2 \text{ g}^{-1}$ and a high pore volume of $0.276 \text{ cm}^3 \text{ g}^{-1}$. The overpotentials of the catalyst at 10, 20, and 100 mA cm^{-2} were ~ 154 , 173, and 234 mV respectively in 1 M KOH solution, indicating an outstanding HER activity. Such high HER activity can be attributed to its unique structures, such as abundant HER active species (CoP_x and N-doped carbon), 3D interconnected mesopores, and the porous N-doped carbon shells. Jiang et al. synthesized several cobalt phosphides by directly phosphating Co-ZIF-67 under mild conditions [51]. The CoP nanorod assemblies (NRAs) were obtained by calcined precursor in N_2 atmosphere, while the CoP nanoparticle assemblies (NPAs) were obtained by thermally treated precursor air atmosphere (**Figure 1B**). The CoP NRAs showed better HER electrocatalytic performance than CoP NPAs. The CoP NRAs only needed overpotential of about 181 mV at 10 mA cm^{-2} in 0.5 M H_2SO_4 , whereas the overpotential for CoP NPAs was 393 mV at 10 mA cm^{-2} . After 1000th CV cycles, CoP NRAs and CoP NPAs both have slight loss of initial current density. The high efficiency of HER for CoP might be related to the charge transfer from Co to P, similar to the charge transfer process between hydride-acceptor and proton-acceptor of hydrogenase.

In addition to Co species, Ni species are also considered to be active for HER. Nickel phosphides (Ni_2P and Ni_{12}P_5) were prepared by phosphatizing Ni-MOF (Ni-BTC) in mild conditions [52]. During the preparation of Ni-BTC, nickel nitrates and BTC (benzene-1,3,5-tricarboxylic acid) were used as Ni sources and organic ligands, respectively. Then Ni_2P and Ni_{12}P_5 were obtained by phosphating from sodium hypophosphite at 275 and 325°C, respectively. The prepared Ni_{12}P_5 nanoparticles show similar morphology to the Ni_2P nanoparticles. However, the average diameter of the Ni_2P (25 nm) was smaller than that of the Ni_{12}P_5 (80 nm). The HER activity of the Ni_2P was better than that of the Ni_{12}P_5 nanoparticles in 0.5 M H_2SO_4 , due to the similar effects of CoP on the HER activity [51]. The durability of the Ni_2P nanoparticles was further evaluated by chronoamperometric durability test, and current density was reduced to 75% of the original value after 6 h test.

The two-step synthesis method was also utilized by Liu et al. to prepare MoS_2 -based HER catalyst with 3D hierarchical structure, in which MoS_2 nanosheets grew in the nanopores of MOFs-derived 3D carbons ($\text{MoS}_2/3\text{D-NPC}$) (**Figure 1C**) [53]. An Al-PCP was formed first by a solvothermal process, and a 3D-NPC was obtained through calcination. The 3D-NPC possessed randomly assembling nanopores, benefiting the intercalating of Mo precursors. After a solvothermal process, The $\text{MoS}_2/3\text{D-NPC}$ catalyst was finally obtained, where MoS_2 nanosheets were dispersed well in nanoporous 3D-NPC. This unique 3D hierarchical structure can provide exposed active site and enhanced conductivity, thus resulting in the high performance for HER. The $\text{MoS}_2/3\text{D-NPC}$ catalyst requires overpotentials of 180 and 210 mV to achieve current densities of 1 and 10 mA cm^{-2} in 0.5 M H_2SO_4 solution, respectively.

In addition to MoS₂, MoC_x has also been widely studied for HER. The porous MoC_x nano-octahedrons were prepared through an MOFs-derived strategy [54]. Cu-based MOF [HKUST-1; Cu₃(BTC)₂(H₂O)₃] was first used to hold the Mo-based Keggin-type POMs (H₃PMo₁₂O₄₀), forming an MOF, i.e., NENU-5 nano-octahedrons. The MoC_x-Cu intermediate was prepared by carbonizing NENU-5 in inert atmosphere, and the final MoC_x porous nanoparticles were obtained by removing Cu by Fe³⁺ etching. The obtained porous MoC_x catalysts were evaluated for HER in both acidic and basic aqueous solutions. The polarization curves showed that the overpotentials of this catalyst were only 142 and 151 mV to deliver a current density of 10 mA cm⁻² in acidic and alkaline solutions, respectively.

In summary, the highly porous MOFs containing redox sites have been developed as HER catalysts. However, their low conductivity limits their electrocatalytic performance for HER. Their combination with highly conductive substrates is an efficient way to enhance their HER activities. Furthermore, many researches have demonstrated that the MOFs-derived catalysts may exhibit greatly improved performance in HER. These MOFs-derived catalysts were obtained mainly through carbonization and a following phosphidation or sulfuration of MOFs containing active metal species (usually Co, Ni and Mo) at appropriate temperatures in inert or air atmosphere. Due to the active species, the novel porous structures, the enhanced conductivity and the protection from the heteroatom doped carbons, these MOF-derived catalysts usually exhibit higher activity and stability as compared to the pristine MOFs catalysts. Hence, because of these unique structures and properties, the MOF-derived materials benefit the development of HER catalysts with low costs and high performance.

5. MOFs-based catalysts for OER

MOFs possess high specific surface area and tunable pore structures, and they are easily functionalized by different metal centers and organic linkers, highlighting their great potentials in electrocatalysis. Similar to those utilized for HER, MOFs have already been developed for OER catalysis basically in two ways: direct and indirect ones. In the first case, MOFs will be received directly as electrocatalysts, and therefore element selection plays a key role to construct coordination modes which should facilitate oxygen-species adsorption/desorption and water dissociation. While in the second case, MOFs will be transformed into other composite materials in which metal, in the form of metallic-, oxide- or nitrite-phase, is associated with carbon. Despite having potential, MOFs-derived materials are at the expense of MOFs. For instance, the specific surface area decreased and the ordered porosities were destroyed. Therefore, structure modification is crucial to make the materials maintain higher specific surface area and hierarchical pore structures through pyrolysis in order to maximize the catalytic site density and provide accessible channels for mass transfer.

Regarding element selection, metal-O, metal-N, or mixed N-metal-O coordination modes have already been developed to construct OER catalysts. In MOFs, the metal ion redox typically involves in the electrochemical process, and the electron-accepting ability of the nitrogen and oxygen atoms in organic linkers may polarize the adjacent metal atoms to afford better catalytic performance.

Babu et al. [55] investigated the electrocatalytic activity of commercially available Fe(BTC) MOF (Basolite™ F300), with BTC=benzene-1,3,5-tricarboxylate. When studying the hydroxide on the voltammetric responses for Fe(BTC), a well-defined hydroxide oxidation response was clearly observed if NaOH was added to a 0.1 M KCl background electrolyte. Such an oxidation current was ascribed to OER current. However, such a current could be seen only by pre-scanning the Fe(BTC)-modified electrode lower than 0.5 V vs. saturated calomel electrode (SCE), a reduction potential zone where the hydrous iron oxide intermediates could be formed. Fe(III/II) played a key role in determining the electrochemical behavior of Fe(BTC).

Gong et al. [56] prepared two Co^{II} metal-organic frameworks, complex **1** (using 4,5-di(4'-carboxylphenyl) phthalic acid and 4,4'-bipyridine as co-ligands) and complex **2** (using 4,5-di(4'-carboxylphenyl)phthalic acid and azene as co-ligands) as electrocatalysts. The OER catalytic activity of these two complexes in an aqueous buffer solution (pH = 6.8) was investigated. The results showed that complex **1** possessed an oxidation peak of water at a more negative potential of 1.02 V vs. SCE accompanied by a much higher OER current than bare glassy-carbon (GC) electrode and ligand-modified glassy-carbon electrode. As confirmed by electrochemical impedance spectra, complex **1**-modified GC showed lower charge-transfer resistance than the bare GC, indicating that the framework promoted the charge-transfer, thus the OER catalytic activity. When applied complex **2**, the **2**-modified GC showed lower OER overpotential and higher OER current than complex **1**-modified GC. Such an enhancement could be ascribed to the better charge build-up of complex **2** than that of complex **1**, further due to the different co-linkers and frameworks in the two MOFs.

To verify the Co contributions for OER in MOFs, Yin's group [57] first synthesized an MOF(Fe) catalyst by hydrothermal process using Fe^{III} as metal precursor and 1,3,5-BTC as organic ligand. The synthesized MOF(Fe) afforded a specific surface area up to 1600 m² g⁻¹. MOF(Fe) afforded excellent OER activity with a delivered current density of 2.30 mA·cm⁻² at 0.90 V vs. Ag/AgCl in 0.1 M KOH, higher than the activated carbon (Super P). Further, they prepared an MOF(Fe/Co) as ORR/OER catalyst by a hydrothermal process using Fe and Co as mixed metal precursors, and the same organic ligand [58]. Surprisingly, MOF(Fe/Co) exhibited an improved OER activity with a delivered current density of 2.97 mA·cm⁻² at 0.90 V vs. Ag/AgCl than the aforementioned MOF(Fe). Although MOF(Fe/Co) possessed lower specific surface area (~1070.1 m²·g⁻¹) than MOF(Fe), MOF(Fe/Co) exhibited better OER activity than MOF(Fe) in 0.1 M KOH electrolyte, primarily due to the aid of Co species.

Wang et al. [59] synthesized a cobalt-based ZIF (Co-ZIF-9) by assembling Co ions with benzimidazolate ligands for water oxidation. Co-ZIF-9 had open-framework structure, in which Co ions were coordinated by N atoms in benzimidazolate linkers. It had been found that this catalyst was thermodynamically feasible for catalytically oxidizing water molecule by density functional theory (DFT) calculation because Co ions had redox function and could bond -OH resulting in low activation barriers. In addition, the nearby benzimidazolate also promoted the OER reaction by accepting the eliminated -H atoms. Thus, Co-ZIF-9 showed obvious OER activity in wide pH basic solutions. Besides, the activity stability of Co-ZIF-9 was also investigated and there was no obvious deactivation in current density after 25 h test in potassium phosphate buffer.

Tan et al. [60] synthesized an MOF-74 to study the water dissociation mechanism on open metal sites in MOFs through *in situ* IR spectroscopy and first-principles calculations (**Figure 2**). The *in situ* IR spectroscopy provided a direct evidence of water reaction occurred on the metal centers. The water dissociation mechanism in MOF-74 primarily depended on two aspects: (1) the covalent bond between water and metal center and (2) the hydrogen bonding between the O atoms of the linker and the H atoms of the water molecule. This work was of significance to demonstrate the coordinatively unsaturated metal centers as active sites for water dissociation.

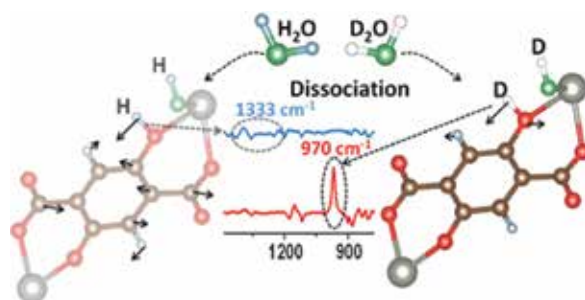


Figure 2. Schematic illustration of the OER catalytic mechanism on MOF-74 [60].

Based on the above results, it has been theoretically or experimentally demonstrated that bare MOFs can be designed by element selection to show excellent OER catalytic activity. However, compared with the noble metal-based and transition metal oxide-based electrocatalysts, MOFs are still insufficient to catalyze OER with higher current probably due to their intrinsic poor electronic conductivity. Therefore, Loh et al. [27] prepared a Cu-centered MOF from copper nitrate trihydrate, 1,4-benzenedicarboxylic acid and triethylene-diamine in the presence of GO. An optimal composition (GO 8 wt%) Cu-MOF afforded an OER onset potential of 1.19 V vs. RHE in acid electrolytes, a ~ 200 mV positive shift than that of pure Cu-MOF. The 8 wt% GO-incorporated Cu-MOF also showed fast OER kinetics with a smaller Tafel slope of $65 \text{ mV}\cdot\text{dec}^{-1}$ than pure Cu-MOF ($89 \text{ mV}\cdot\text{dec}^{-1}$). The results demonstrated that the enhanced electrocatalytic properties and stability in acid of the GO-MOF composite was due to the unique porous scaffold structure, improved charge transport, and synergistic interactions between the GO and MOF.

Because of the high specific surface area and the well-defined porosities, MOFs are excellent catalyst support materials. Therefore, doping MOFs with other active species in the forms of oxides, ions, and complexes can open up a new route for MOFs in OER electrocatalysis.

Yin et al. [61] prepared $\alpha\text{-MnO}_2/\text{MIL-101}(\text{Cr})$ catalyst through a hydrothermal process. In this catalyst, $\alpha\text{-MnO}_2$ particles were embedded in MIL-101(Cr) matrix, resulting in strong interactions between $\alpha\text{-MnO}_2$ and MIL-101(Cr). The OER catalytic activity of the composite was tested using a carbon paper containing this catalyst as working electrode. The results revealed that $\alpha\text{-MnO}_2/\text{MIL-101}(\text{Cr})$ composite afforded an excellent OER catalytic activity with a delivered current density of 23.67 mA cm^{-2} at 0.9 V in 0.1 M KOH solution which was about two times higher than that of pure $\alpha\text{-MnO}_2$ under the same conditions. The high specific surface

area of MIL-101(Cr) and abundant micropores of MIL-101(Cr) were advantageous for the diffusion of electrolyte and the high dispersion of α -MnO₂ particles made it easy to contact the electrolyte, resulting in enhanced OER catalytic activity.

Subsequently, Yin's group [62] decorated MIL-101(Cr) with Co ions with various oxidation states through impregnation followed by post-treatment under oxidant or reducing reagents. The Co species were highly dispersed on the MOF surface and showed various Co^{III}/Co^{II} ratios. Primary results demonstrated that the OER activity is related to the Co^{III} contents since the catalyst showed better OER catalytic activity as the surface Co^{III} content increased. The reason might be the Co^{III} species could promote the OH⁻ adsorbed onto the electrocatalyst surface. In addition, the porous and open structures of MIL-101(Cr) support were in favor of the contact between oxygen species and the active Co sites.

Wang et al. [19] decorated a Zr-MOF, namely UiO-67, with 1-3 Ir-containing complexes to form MOF 1-3, respectively. Many MOFs lack stability in water, but UiO-67 is one of the exceptions. The OER performance of the samples was investigated in a pH = 1 solution with Ce⁴⁺ as an oxidant. The Ce⁴⁺ was reduced to Ce³⁺, while water was oxidized to form oxygen. The results showed that after the incorporation of Ir-containing complexes in UiO-67, MOF 1-3 were the effective water oxidation catalysts with turnover frequencies of up to 4.8 h⁻¹. The parent UiO-67 showed negligible OER catalytic activity, demonstrating the significance of the Ir-containing dopants as active centers.

The OER current density at 10 mA·cm⁻² is a criterion used to judge an OER catalyst since such a current density is an important metric for practical solar fuel production. Unfortunately, most of the aforementioned MOF-based OER catalysts fail to reach such a current density even at high overpotentials. Apart from directly being the OER catalysts, MOFs can be converted into other forms of materials through pyrolysis. Through pyrolysis, the organic linkers can be transformed into carbon materials, and the well-dispersed metal centers in the MOFs' frameworks can be transformed into phosphate- or oxide-phase but still maintain excellent dispersion in carbons. Such a strategy is helpful to obtain materials with excellent charge-transfer properties.

You et al. [50] prepared a CoP_x/NC catalyst derived from ZIF-67 and its polyhedron-like morphology survived from the pyrolysis. The specific surface area of CoP_x/NC was up to 183 m²·g⁻¹, and the pore volume is 0.276 m³·g⁻¹. In OER activity test, the overpotential of CoP_x/NC was about 354 mV at a current density of 10 mA cm⁻², while IrO₂ is about 368 mV at the same current density. Moreover, after 1000th continuous CV cycles, the overpotential of CoP_x/NC at 10 mA cm⁻² showed only slight difference, demonstrating the excellent OER activity durability of the catalyst.

Apart from CoP_x, Co₃O₄ also has been reported to be active for OER, and can significantly improve the conductivity and stability properties of the catalysts when combined with carbon materials. The porous Co₃O₄-based hybrids were typically obtained through a one-step carbonization of Co-MOFs. Li et al. [63] introduced MWCNT to MOFs and obtained the Co₃O₄@MWCNTs by carbonization and subsequent oxidation process. The thermal oxidation led to Co₃O₄-N-C active sites uniformly dispersed on MWCNTs (20–50 nm). And the

introduction of MWCNT and the *in-situ* N-doped carbon carbonized from ligands could significantly improve the electronic conductivity of the catalysts. Thus, better OER activity was observed with an onset potential of only 1.5 V (vs. RHE). Ma et al. [64] synthesized MOF-derived Co_3O_4 -carbon porous nanowire arrays. The Co_3O_4 -carbon were directly prepared on Cu foil as a working electrode. Since this electrode is binder-free and carbon is formed *in situ*, the charge conductivity performance is greatly improved, resulting in excellent OER catalytic activity in 0.1 M KOH solution. It shows a sharp onset potential of 1.47 V (vs. RHE), very close to that of IrO_2/C (1.45 V vs. RHE). The durability is also an important criterion for OER catalysts. The chronopotentiometric response at a current density of $10 \text{ mA}\cdot\text{cm}^{-2}$ was also recorded, and only 6.5% attenuation was observed within 30 h on Co_3O_4 -carbon, while that of IrO_2/C is 4.7 times larger under the same condition.

The above results demonstrate that MOFs-derived catalysts show much enhanced OER catalytic performance than pristine MOFs. There are likely several reasons for that. On one hand, carbon materials formed *in situ* or *ex situ* in catalysts can promote electronic conductivity and accelerate charge transfer. On the other hand, the OER active species can be well-dispersed on carbon materials, resulting in improved OER activity. In addition, the strong interactions between OER active species and carbon materials stabilize the OER active site structures, thus leading to enhanced OER activity durability.

6. Conclusions

MOFs-based electrocatalysts for HER and/or OER are rapidly developed in recent years due to unique structures of MOFs. These catalysts mainly include MOFs catalysts, MOFs supports for catalysts, and MOFs-derived catalysts. Due to the fact that the pore structures and functions are tunable and devisable, it is convenient to directly design and construct the active sites for HER and/or OER in MOFs during the synthesis process. However, the vast majority of the synthesized MOFs suffer from poor electronic conductivity, leading to low electron transfer efficiency, which restricts catalytic performance. MOFs are highly porous materials and have ultrahigh specific surface area, thus they are regarded as the most promising support materials for catalysts. The active species for HER or OER can be well dispersed at the surfaces of MOFs or embedded in MOFs matrix, resulting in improved catalytic performance for HER or OER. However, MOFs are microporous materials with small aperture size (<2 nm). On one hand, the active species are difficult to be introduced in their pore channels. Hence, one cannot obtain the catalysts with high activity and stability for HER or OER. On the other hand, the accommodation of electrolyte in the pore channels is very limited. Thus, the active centers in MOFs cannot access the electrolytes with high efficiency. In addition, the poor electronic conductivity of MOFs is another drawback of these catalysts. Some post-treatment methods can greatly improve the electrical conductivity of MOFs-derived catalysts. However, the collapse of the pore structures of MOFs usually occurs during the preparation of the MOFs-derived catalysts leading to a decreased specific surface area of the catalysts, which is adverse to the development of MOFs-derived catalysts with high catalytic performance for HER or OER.

Although many MOFs-based catalysts with high catalytic performance for HER and/or OER have been developed in recent years, there are still a lot of scientific and technical problems to solve before the developed MOFs-based electrocatalysts can meet the requirements for commercialization. The problems mainly involve how to improve the electronic conductivity of MOFs, enlarge pore channels of MOFs to accommodate more electrolytes, limit the collapse of pore structure of MOFs, and maintain high specific surface area during pyrolysis. In addition, the reaction mechanisms of HER and OER, the transfer and diffusion properties of reactants and products, and the effects of electrolyte on the catalytic performance of MOFs-based catalysts need to be clarified.

Acknowledgements

This work is supported by the National Natural Science Foundation of China (Project No. 21276018), the Natural Science Foundation of Jiangsu Province of China (Project No. BK20140268), the Fundamental Research Funds for the Central Universities (Project No. buctrc201526), and the Changzhou Sci&Tech Program (Project No. CJ20159006).

Author details

Fengxiang Yin^{1,2*}, Xiao Zhang¹, Xiaobo He² and Hao Wang¹

*Address all correspondence to: yinfx@mail.buct.edu.cn

1 State Key Laboratory of Organic-Inorganic Composites, Beijing University of Chemical Technology, Beijing, PR China

2 Changzhou Institute of Advanced Materials, Beijing University of Chemical Technology, Changzhou, PR China

References

- [1] Ursúa A, Gandia LM, Sanchis P. Hydrogen production from water electrolysis: Current status and future trends. *Proceedings of the IEEE*. 2012;100:410-426. DOI: 10.1109/JPROC.2011.2156750
- [2] Suntivich J, Gasteiger HA, Yabuuchi N. Design principles for oxygen-reduction activity on perovskite oxide catalysts for fuel cells and metal-air batteries. *Nature Chemistry*. 2011;3:546-550. DOI: 10.1038/nchem.1069

- [3] Bashyam R, Zelenay P. A class of non-precious metal composite catalysts for fuel cells. *Nature*. 2006;443:63-66. DOI: 10.1038/nature05118
- [4] Grigoriev SA, Millet P, Fateev VN. Evaluation of carbon-supported Pt and Pd nanoparticles for the hydrogen evolution reaction in PEM water electrolyzers. *Journal of Power Sources*. 2008;177:281-285. DOI: 10.1016/j.jpowsour.2007.11.072
- [5] Jiao Y, Zheng Y, Jaroniec M. Design of electrocatalysts for oxygen- and hydrogen-involving energy conversion reactions. *Chemical Society Reviews*. 2015;44:2060-2086. DOI: 10.1039/C4CS00470A
- [6] Pu Z, Liu Q, Jiang P. CoP nanosheet arrays supported on a Ti plate: An efficient cathode for electrochemical hydrogen evolution. *Chemistry of Materials*. 2014;26:4326-4329. DOI: 10.1021/cm501273s
- [7] Zhang Z, Lu B, Hao J. FeP nanoparticles grown on graphene sheets as highly active non-precious-metal electrocatalysts for hydrogen evolution reaction. *Chemical Communications*. 2014;50:11554-11557. DOI: 10.1039/C4CC05285D
- [8] Gu S, Du H, Asiri AM. Three-dimensional interconnected network of nanoporous CoP nanowires as an efficient hydrogen evolution cathode. *Physical Chemistry Chemical Physics*. 2014;16:16909-16913. DOI: 10.1039/C4CP02613F
- [9] Xie J, Zhang J, Li S, Grote F. Controllable disorder engineering in oxygen-incorporated MoS₂ ultrathin nanosheets for efficient hydrogen evolution. *Journal of the American Chemical Society*. 2013;135:17881-17888. DOI: 10.1021/ja408329q
- [10] Chen Z, Cummins D, Reinecke BN. Core-shell MoO₃-MoS₂ nanowires for hydrogen evolution: A functional design for electrocatalytic materials. *Nano Letters*. 2011;11:4168-4175. DOI: 10.1021/nl2020476
- [11] Faber MS, Lukowski MA, Ding Q. Earth-abundant metal pyrites (FeS₂, CoS₂, NiS₂, and their alloys) for highly efficient hydrogen evolution and polysulfide reduction electrocatalysis. *The Journal of Physical Chemistry C*. 2014;118:21347-21356. DOI: 10.1021/jp506288w
- [12] McKone JR, Sadtler BF, Werlang CA. Ni-Mo nanopowders for efficient electrochemical hydrogen evolution. *ACS Catalysis*. 2013;3:166-169. DOI: 10.1021/cs300691m
- [13] Yin Z, Chen F. A facile electrochemical fabrication of hierarchically structured nickel-copper composite electrodes on nickel foam for hydrogen evolution reaction. *Journal of Power Sources*. 2014;265:273-281. DOI: 10.1016/j.jpowsour.2014.04.123
- [14] Wang D, Chen X, Evans DG. Well-dispersed Co₃O₄/Co₂MnO₄ nanocomposites as a synergistic bifunctional catalyst for oxygen reduction and oxygen evolution reactions. *Nanoscale*. 2013;5:5312-5315. DOI: 10.1039/c3nr00444a

- [15] Gong M, Zhou W, Tsai MC. Nanoscale nickel oxide/nickel heterostructures for active hydrogen evolution electrocatalysis. *Nature Communications*. 2014;5:1-6. DOI: 10.1038/ncomms5695
- [16] Li Y, Hasin P, Wu Y. Ni_xCo_{3-x}O₄ nanowire arrays for electrocatalytic oxygen evolution. *Advanced Materials*. 2010;22:1926-1929. DOI: 10.1002/adma.200903896
- [17] Feng LL, Yu G, Wu Y. High-index faceted Ni₃S₂ nanosheet arrays as highly active and ultrastable electrocatalysts for water splitting. *Journal of the American Chemical Society*. 2015;137:14023-14026. DOI: 10.1021/jacs.5b08186
- [18] Liu Q, Jin J, Zhang J. NiCo₂S₄@ graphene as a bifunctional electrocatalyst for oxygen reduction and evolution reactions. *ACS Applied Materials and Interfaces*. 2013;5:5002-5008. DOI: 10.1021/am4007897
- [19] Wang C, Xie Z, deKrafft KE. Doping metal-organic frameworks for water oxidation, carbon dioxide reduction, and organic photocatalysis. *Journal of the American Chemical Society*. 2011;133:13445-13454. DOI: 10.1021/ja203564w
- [20] Chen X Y, Zhao B, Shi W. Microporous metal-organic frameworks built on a Ln₃ cluster as a six-connecting node. *Chemistry of Materials*. 2005;17:2866-2874. DOI: 10.1021/cm050526o
- [21] Polshettiwar V, Varma RS. Aqueous microwave chemistry: a clean and green synthetic tool for rapid drug discovery. *Chemical Society Reviews*. 2008;37:1546-1557. DOI: 10.1039/B716534J
- [22] Jin K, Huang X, Pang L. [Cu(i)(bpp)] BF₄: The first extended coordination network prepared solvothermally in an ionic liquid solvent. *Chemical Communications*. 2002;2872-2873. DOI: 10.1039/B209937N
- [23] Furukawa H, Cordova KE, O'Keeffe M. The chemistry and applications of metal-organic frameworks. *Science*. 2013;341:1230444. DOI: 10.1126/science.1230444
- [24] Rosi N L, Eckert J, Eddaoudi M. Hydrogen storage in microporous metal-organic frameworks. *Science*. 2003;300:1127-1129. DOI: 10.1126/science.1083440
- [25] Zhang WX, Yang YY, Zai SB. Syntheses, structures and magnetic properties of dinuclear copper (II)-lanthanide (III) complexes bridged by 2-hydroxymethyl-1-methylimidazole. *European Journal of Inorganic Chemistry*. 2008;2008:679-685. DOI: 10.1002/ejic.200701041
- [26] Moore EG, Samuel APS, Raymond KN. From antenna to assay: Lessons learned in lanthanide luminescence. *Accounts of Chemical Research*. 2009;42:542-552. DOI: 10.1021/ar800211j

- [27] Jahan M, Liu Z, Loh KP. A Graphene oxide and copper-centered metal organic framework composite as a tri-functional catalyst for HER, OER, and ORR. *Advanced Functional Materials*. 2013;23:5363-5372. DOI: 10.1002/adfm.201300510
- [28] Kitagawa S. Metal-organic frameworks (MOFs). *Chemical Society Reviews*. 2014;43:5415-5418. DOI: 10.1039/C4CS90059F
- [29] Yaghi OM, Li H. Hydrothermal synthesis of a metal-organic framework containing large rectangular channels. *Journal of the American Chemical Society*. 1995;117:10401-10402. DOI: 10.1021/ja00146a033
- [30] Furukawa H, Ko N, Go YB. Ultrahigh porosity in metal-organic frameworks. *Science*. 2010;329:424-428. DOI: 10.1126/science.1192160
- [31] Deng H, Grunder S, Cordova KE. Large-pore apertures in a series of metal-organic frameworks. *Science*. 2012;336:1018-1023. DOI: 10.1126/science.1220131
- [32] Xia W, Mahmood A, Zou R. Metal-organic frameworks and their derived nanostructures for electrochemical energy storage and conversion. *Energy and Environmental Science*. 2015;8:1837-1866. DOI: 10.1039/C5EE00762C
- [33] Fang QR, Makal TA, Young MD. Recent advances in the study of mesoporous metal-organic frameworks. *Comments on Inorganic Chemistry*. 2010;31:165-195. DOI: 10.1080/02603594.2010.520254
- [34] Sun D, Ma S, Ke Y. An interweaving MOF with high hydrogen uptake. *Journal of the American Chemical Society*. 2006;128:3896-3897. DOI: 10.1021/ja0587771
- [35] Li H, Eddaoudi M, O'Keeffe M. Design and synthesis of an exceptionally stable and highly porous metal-organic framework. *Nature*. 1999;402:276-279. DOI: 10.1038/46248
- [36] Park KS, Ni Z, Côté AP. Exceptional chemical and thermal stability of zeoliticimidazolate frameworks. *Proceedings of the National Academy of Science of the United States of America*. 2006;103:10186-10191. DOI: 10.1073/pnas.0602439103
- [37] Mellot-Draznieks C, Girard S, Férey G. Novel inorganic frameworks constructed from double-four-ring (D4R) units: Computational design, structures, and lattice energies of silicate, aluminophosphate, and gallophosphate candidates. *Journal of the American Chemical Society*. 2002;124:15326-15335. DOI: 10.1021/ja0209991
- [38] Chui SSY, Lo SMF, Charmant JPH. A chemically functionalizable nanoporous material $[\text{Cu}_3(\text{TMA})_2(\text{H}_2\text{O})_3]_n$. *Science*. 1999;283:1148-1150. DOI: 10.1126/science.283.5405.1148
- [39] Qi Y, Luo F, Che Y. Hydrothermal synthesis of metal-organic frameworks based on aromatic polycarboxylate and flexible bis (imidazole) ligands. *Crystal Growth and Design*. 2007;8:606-611. DOI: 10.1021/cg700758c

- [40] Sun J K, Xu Q. Functional materials derived from open framework templates/precursors: synthesis and applications. *Energy and Environmental Science*. 2014 ;7:2071-210. DOI: 10.1039/C4EE00517A
- [41] Huang SY, Ganesan P, Popov BN. Electrocatalytic activity and stability of Titania-supported platinum-palladium electrocatalysts for polymer electrolyte membrane fuel cell. *ACS Catalysis*. 2012;2:825-831. DOI: 10.1021/cs300088n
- [42] Zou X, Zhang Y. Noble metal-free hydrogen evolution catalysts for water splitting. *Chemical Society Reviews*. 2015;44:5148-5180. DOI: 10.1039/C4CS00448E
- [43] Gong M, Dai H. A mini review of NiFe-based materials as highly active oxygen evolution reaction electrocatalysts. *Nano Research*. 2015;8:23-39. DOI: 10.1007/s12274-014-0591-z
- [44] Zhang J, Zhao Z, Xia Z. A metal-free bifunctional electrocatalyst for oxygen reduction and oxygen evolution reactions. *Nature Nanotechnology*. 2015;10:444-452. DOI: 10.1038/nnano.2015.48
- [45] Silva P, Vilela SMF, Tome JPC. Multifunctional metal-organic frameworks: From academia to industrial applications. *Chemical Society Reviews*. 2015;44:6774-6803. DOI: 10.1039/C5CS00307E
- [46] Gong Y, Wu T, Jiang PG. Octamolybdate-based metal-organic framework with unsaturated coordinated metal center as electrocatalyst for generating hydrogen from water. *Inorganic Chemistry*. 2012;52:777-784. DOI: 10.1021/ic3018858
- [47] Qin J S, Du DY, Guan W. Ultrastable polymolybdate-based metal-organic frameworks as highly active electrocatalysts for hydrogen generation from water. *Journal of the American Chemical Society*. 2015;137:7169-7177. DOI: 10.1021/jacs.5b02688
- [48] Clough AJ, Yoo JW, Mecklenburg MH. Two-dimensional metal-organic surfaces for efficient hydrogen evolution from water. *Journal of the American Chemical Society*. 2014;137:118-121. DOI: 10.1021/ja5116937
- [49] Li S, Yang K, Tan C. Preparation and applications of novel composites composed of metal-organic frameworks and two-dimensional materials. *Chemical Communications*. 2016;52:1555-1562. DOI: 10.1039/c5cc09127f
- [50] You B, Jiang N, Sheng M. High-performance overall water splitting electrocatalysts derived from cobalt-based metal-organic frameworks. *Chemistry of Materials*. 2015;27:7636-7642. DOI: 10.1021/acs.chemmater.5b02877
- [51] Li L, Li X, Ai L. MOF-derived nanostructured cobalt phosphide assemblies for efficient hydrogen evolution reaction. *RSC Advances*. 2015;5:90265-90271. DOI: 10.1039/C5RA17427A

- [52] Tian T, Ai L, Jiang J. Metal-organic framework-derived nickel phosphides as efficient electrocatalysts toward sustainable hydrogen generation from water splitting. *RSC Advances*. 2015;5:10290-10295. DOI: 10.1039/C4RA15680C
- [53] Liu Y, Zhou X, Ding T. 3D architecture constructed via the confined growth of MoS₂ nanosheets in nanoporous carbon derived from metal-organic frameworks for efficient hydrogen production. *Nanoscale*. 2015;7:18004-18009. DOI: 10.1039/C5NR03810C
- [54] Wu HB, Xia BY, Yu L. Porous molybdenum carbide nano-octahedrons synthesized via confined carburization in metal-organic frameworks for efficient hydrogen production. *Nature Communications*. 2015;6:6512. DOI: 10.1038/ncomms7512
- [55] Babu KF, Kulandainathan MA, Katsounaros I. Electrocatalytic activity of Basolite™ F300 metal-organic-framework structures. *Electrochemistry Communications*. 2010;12:632-635. DOI: 10.1016/j.elecom.2010.02.017
- [56] Gong Y, Hao Z, Meng J. Two Co^{II} metal-organic frameworks based on a multicarboxylate ligand as electrocatalysts for water splitting. *ChemPlusChem*. 2014;79:266-277. DOI: 10.1002/cplu.201300334
- [57] Song G, Wang Z, Wang L. Preparation of MOF (Fe) and its catalytic activity for oxygen reduction reaction in an alkaline electrolyte. *Chinese Journal of Catalysis*. 2014;35:185-195. DOI: 10.1016/S1872-2067(12)60729-3
- [58] Wang H, Yin F, Li G. Preparation, characterization and bifunctional catalytic properties of MOF (Fe/Co) catalyst for oxygen reduction/evolution reactions in alkaline electrolyte. *International Journal of Hydrogen Energy*. 2014;39:16179-16186. DOI: 10.1016/j.ijhydene.2013.12.120
- [59] Wang S, Hou Y, Lin S. Water oxidation electrocatalysis by a zeolitic imidazolate framework. *Nanoscale*. 2014;6:9930-9934. DOI: 10.1039/C4NR02399D
- [60] Tan K, Zuluaga S, Gong Q. Water reaction mechanism in metal organic frameworks with coordinatively unsaturated metal ions: MOF-74. *Chemistry of Materials*. 2014;26:6886-6895. DOI: 10.1021/cm5038183
- [61] Yin F, Li G, Wang H. Hydrothermal synthesis of α -MnO₂/MIL-101 (Cr) composite and its bifunctional electrocatalytic activity for oxygen reduction/evolution reactions. *Catalysis Communications*. 2014;54:17-21. DOI: 10.1016/j.catcom.2014.05.006
- [62] He X, Yin F, Li G. A Co/metal-organic-framework bifunctional electrocatalyst: The effect of the surface cobalt oxidation state on oxygen evolution/reduction reactions in an alkaline electrolyte. *International Journal of Hydrogen Energy*. 2015;40:9713-9722. DOI: 10.1016/j.ijhydene.2015.06.027
- [63] Li X, Fang Y, Lin X. MOF derived Co₃O₄ nanoparticles embedded in N-doped mesoporous carbon layer/MWCNT hybrids: extraordinary bi-functional electrocatalysts for

OER and ORR. *Journal of Materials Chemistry A*. 2015;3:17392-17402. DOI: 10.1039/C5TA03900B

- [64] Ma TY, Dai S, Jaroniec M. Metal-organic framework derived hybrid Co_3O_4 -carbon porous nanowire arrays as reversible oxygen evolution electrodes. *Journal of the American Chemical Society*. 2014;136:13925-13931. DOI: 10.1021/ja5082553

Bio-Inspired Metal-Organic Frameworks in the Pharmaceutical World: A Brief Review

Vânia André and Sílvia Quaresma

Additional information is available at the end of the chapter

<http://dx.doi.org/10.5772/64027>

Abstract

One of the great challenges in the pharmaceutical industry is the search for more efficient and cost-effective ways to store and deliver existing drugs. Bio-inspired metal-organic frameworks (BioMOFs) are groundbreaking materials that have recently been explored for drug storage, delivery and controlled release as well as for applications in imaging and sensing for therapeutic and diagnostic. This review presents a brief overview on these materials, and by alluding to a few reported examples, it intends to clearly show the extremely important role that BioMOFs have been playing in the pharmaceutical field.

Keywords: BioMOFs, drugs, ZIFs, smart drug delivery

1. Introduction

The development of new solid forms of pharmaceuticals is of utmost importance in modern science as they present a single opportunity to modify the properties of active pharmaceutical ingredients (API) without interfering with its biological role. The influence of the crystal forms is very wide and diverse, changing not only the solid-state characteristics (density, habit, shape, colour, stability, melting point) but also properties that might affect their function (dissolution rate, solubility, stability to temperature and humidity, thermal properties, moisture uptake, bioavailability, pharmacokinetics) and even some industrial aspects of formulation (flowability, mixability, stress stability, granulation, encapsulation, tableting). The combination of crystal engineering and supramolecular chemistry principles allows the design and synthesis of smartly designed drugs with tailor-made properties, keeping their pharmacological properties, and thus presenting major advantages, including reduced time for introduction in the market [1–6].

Consequently, the synthesis of new crystal forms evolved tremendously in the last decade, and the interest of pharmaceutical companies in the appearance/disappearance of new solid forms of APIs has vastly increased. Polymorphs, hydrates and salts of drugs are long-known forms with recognized impact in their properties. Cocrystals represent a more recent class of crystal forms that own particular scientific and regulatory advantages (FDA guidance is already available and cocrystals are now being commercialized as drugs in some countries). Many examples show their relevance in the pharmaceutical industry, most of them by enhancing stability, solubility and/or bioavailability of known drugs [7–20].

Likewise, nanoporous materials recently became of pertinent use in the medicinal and pharmacological fields for drug storage, delivery and controlled release in addition to applications in imaging and sensing for therapeutic and diagnostic [21–34]. Particularly, metal organic frameworks (MOFs) have generated large interest owing to their versatile architectures [35] and their promising applications not only in ion exchange, adsorption and gas storage [36–41], separation processes [42], heterogeneous catalysis [43, 44], polymerization reactions [45, 46], luminescence [47], non-linear optics [48] and magnetism [49], but also as drug carriers, systems for drug delivery [22, 23, 50, 51], contrast agents for magnetic resonance imaging (MRI) [21] and systems with potential use in other biomedical applications [23].

Up to now, drug delivery from porous solids has been achieved by encapsulation in mesoporous silicas or zeolites, methods that are strongly dependent on the pore size and on the host-guest interactions. Both hypotheses suffer from important drawbacks: low drug-storage capacity, too rapid delivery and solid degradation that brings toxicity concerns [23, 25, 26, 28, 29, 52]. Extended metal-ligand networks with metal nodes and bridging organic ligands such as coordination networks, porous coordination networks (PCNs), porous coordination polymers (PCPs) and MOFs have attracted great attention in the last years [24, 25, 28, 53, 54]. Particularly, MOFs with biological-friendly composition emerged as new drug carriers capable of tackling these problems [21, 23, 25, 26, 28, 29, 55, 56].

In fact, MOFs are among the most exciting architectures in nanotechnology and are defined as hybrid self-assemblies of metal ions or metal clusters (coordination centres) and organic fragments (linkers). They exhibit some of the highest porosities known, turning them into ideal materials for capture, storage and/or delivery applications [21, 24–26, 29, 54, 57]. Compared to other nanocarriers, MOFs are candidates to extensive applications since they combine high pore volume with a regular porosity, and the presence of tuneable organic groups allows an easy modulation of the framework as well as of the pore size [22, 24–26].

The first families of MOFs considered as potential drug delivery systems were the coordination polymers from Oslo (CPO), such as CPO-27(Mg) [58] built up from magnesium coordination polymers, and the materials of Institute Lavoisier (MIL) [22]. Horcajada et al. [22, 23] prepared MIL-100 (with trimesic acid) and MIL-101 (with terephthalic acid) applied for the delivery of ibuprofen in the gastrointestinal tract, exhibiting high drug-storage capacity and a complete drug-controlled release under physiological conditions [22, 23]. Less toxic systems, using iron and more flexible MILs, are under study [25], and the first biodegradable therapeutic MOF, BioMIL-1, was reported by Miller et al. in 2010 [27]. The large breathing effect that MOFs can

attain is another particularly interesting feature for potential applications in drug delivery [54, 59, 52].

Zeolite-like MOFs (ZMOFs) are a unique subset of MOFs with exceptional characteristics arising from the periodic pore systems and distinctive cage-like cavities, in conjunction with modular intra- and/or extra-framework components [60–62]. Zeolitic imidazolate frameworks (ZIFs) are a special class of ZMOFs comprising imidazolate linkers and metal ions. ZIFs simultaneously have the following characteristics of MOFs and zeolites, combining the advantages of both: ultrahigh surface areas, unimodal micropores, high crystallinity, various functionalities and exceptional thermal and chemical stabilities, making them very promising for biomedical applications [63, 64]. Several studies describe the successful incorporation of anticancer drugs into ZIF-8 with positive results for the controlled pH-sensitive drug release and fluorescence imaging [65–69]. Also caffeine was already encapsulated into ZIF-8 showing a controlled release [70, 71].

The scope of this brief review focuses on presenting some aspects on the BioMOFs preparation, and a few examples of promising bioapplications of MOFs, including ZIFs.

2. Building bio-inspired MOFs

2.1. Design

The use of porous solids for biomedical applications requires a biological friendly composition, making compulsory the use of metals and linkers with acceptable toxicity [28].

When designing BioMOFs, the decision to exclude one linker and/or metal depends on several parameters: application, balance between risk and benefit, degradation kinetics, biodistribution, accumulation in tissues and organs as well as body excretion [21, 23, 25, 26, 28, 55, 56]. Both exogenous (not intervening in the body cycles) and endogenous (constitutive part of body composition) linkers have been used in MOF synthesis for drug delivery, with the first group having a higher prevalence [21, 25–29, 57]. It is also worth noting that if the therapeutic molecule is directly used as a linker, no large pores are required and the release of the drug molecule is achieved directly through the degradation of the solid, without any side effects arising from the release of a non-active ligand [26, 52].

Different methods have been explored to design BioMOFs, including ZMOFs, from which we highlight the molecular building block (MBB), supermolecular building block (SBB) and supermolecular building layer (SBL) approaches. Also, a brief allusion to the influence that computational simulations may have in building and studying BioMOFs is made.

2.1.1. Molecular building block (MBB), supermolecular building block (SBB) and supermolecular building layer (SBL) approaches

To construct a MOF, it is necessary to make a pre-selection of building blocks that would give the desired structural and geometrical information for a given underlying network—molec-

ular building block approach (MBB) [72]. The prerequisites for the successful implementation of this approach are (a) selection of an ideal blueprint net exclusive for the assembly of its corresponding basic building units and (b) isolation of the reaction conditions that allow the formation of the desired MOF. Simple MBBs based on simple organic ligands or polynuclear clusters are often limited in terms of connectivity [72]. To overcome this issue, two conceptual approaches were recently implemented to facilitate the design and deliberate construction of MOFs: supermolecular building block (SBB) and supermolecular building layer (SBL). These approaches allow the rational design of made-to-order MOFs [73].

The SBB approach consists of using metal-organic polyhedral (MOPs) as SBBs in building an MOF, presenting great potential to control the targeted framework. To obtain the desired topology, the MOP must have the correct geometrical information and peripheral points of extension (connectivity). The prerequisites for this approach are (a) a blueprint net with minimal edge transitivity, preferably singular, exclusive for the assembly of given building units, and not susceptible to self-interpenetration upon net expansion and/or decoration and (b) reaction conditions that allow the formation of the SBB in situ.

The SBL is based on the use of 2-periodic MOF layers (SBLs) as building blocks for the desired functional 3-periodic porous MOFs. This implies the chemical cross-linking of layers via accessible bridging sites on the layers, such as open metal sites or functionalized positions on the organic linker, whose judicious selection is mandatory. This approach, in principle, allows to predict MOFs with tuneable cavities, the endless expansion of confined space (as cavities and pores), and its modularity further permits an easy functionalization and introduction of additional functionalities [74] to aim specific applications. The prerequisites for this approach are (a) a blueprint net with minimal edge transitivity, rather singular, exclusive for the particular pillaring of the given building units and (b) the reaction conditions to allow the consistent formation of the SBL in situ.

2.1.2. Screening using simulations

Systematic studies relating MOF structures with their performance in drug delivery is crucial for the identification of promising structures. Molecular simulations are a mean that can be explored to seek for the optimal structure for a given application. The grand canonical Monte Carlo (GCMC) simulation is the preferred method for simulating adsorption in porous materials and for explaining and predicting new results. However, the simulation in the case of large guest molecules is difficult and that justifies the limited number of studies on drug-porous solid systems [75].

Fatouros et al. reported the use of molecular dynamics to study the diffusion properties of salbutamol and theophylline in the zeolite BEA, an indication that this method can be used for screening purposes on zeolite-drug systems [76].

Regarding MOFs, very few computational studies are reported and those are focused on one or more structures simultaneously, limiting the possibility of correlating drug delivery performance with structural features. A combined experimental and computational study of three MOFs for the drug delivery of 5-fluorouracil was recently presented, in which GCMC

simulations were used to investigate the interactions between the drug and the porous cage [77]. Density functional theory (DFT) calculations have been applied to identify the most favourable conformations and adsorption sites of ibuprofen and busulfan on MIL-53(Fe) [78]. Quantitative structure-activity relationship (QSAR) models were used to rationalize the experimental uptake of caffeine as model in a series of MIL-88B(Fe) materials with different functional moieties [79]. The energetics and dynamics of ibuprofen in MIL-101 were also studied recurring to simulated annealing followed by DFT of one single ibuprofen molecule to study the preferential adsorption sites [56].

Also worth mentioning an extensive study on GCMC simulations to screen a series of bio-compatible MOFs as carriers of ibuprofen has been reported. Simulations include microporous, mesoporous and nanoporous MOFs and have shown to be a successful pathway to predict the drug adsorption properties of porous adsorbents. Furthermore, this work proposes new tools that allow the study of new porous materials as potential drug carriers prior to experiment [75].

2.2. Synthesis

MOFs are still widely synthesized using solvo/hydrothermal techniques, the most common methods to obtain coordination networks [21, 25, 28, 29]. Nevertheless microemulsion synthesis [80] is also a typical method and interesting alternatives are being used based on environmental-friendly synthetic routes: ionothermal [81], microwave, ultrasound-assisted, and sonochemical synthesis [21, 25, 28], as well as mechanochemistry [82, 83]. The synthesis of this type of compounds has been reviewed several times [63, 84, 85] and therefore only brief details on each technique are presented herein.

The solvo/hydrothermal synthesis involves polar solvents under moderate to high pressures and temperatures. This method often requires toxic solvents such as DMF, and its use is limited by safety and time-consuming reasons. Alternative techniques allow higher efficiencies, have lower energy costs and have less impact in the environment [86].

Microemulsion synthesis is based on thermodynamically stable dispersions of two immiscible liquids in the presence of an emulsifier or surfactant (i.e., microemulsions). This technique confines the synthesis of MOFs to the nanoscale and offers the possibility of tuning the size. The disadvantages of the microemulsion approach include poor yields, reproducibility issues, usage of highly toxic surfactants and solvents that strongly limit biomedical applications and the possible decrease of the sorption capacity due to the combination of surfactants with highly porous structures [80, 86].

Ionothermal synthesis requires the use of green solvents such as ionic liquids and eutectic mixtures (a special type of ionic liquid) to obtain MOFs and it can be performed in open air. These solvents act both as solvents and templates to avoid the competition interactions between the solvent framework and the template framework that are present in the solvo-thermal methods [63, 81].

Microwave and ultrasound-assisted syntheses usually lead to the fast crystallization of MOFs and are considered green methods. In the case of microwaves, the heating involved in the

process favours a rapid and uniform nucleation process, which results into a more homogeneous particle size distribution. Regarding ultrasounds, it has shown to be a highly efficient method [86].

Sonochemical synthesis or sonocrystallization method not only promotes the nucleation process but also stimulates the homogeneity of the nucleation, what represents an advantage over the traditional solvothermal methods. This approach is prone for industrial applications due to its easy scale-up [63].

Mechanochemistry is a green, solvent-free and efficient strategy to build MOFs. It is based on the direct grinding of the linkers and the metal salts either in a mortar or in a ball mill, without recurring to solvent (neat grinding, NG) or recurring only to catalytic amounts of solvent to activate the process (liquid-assisted grinding, LAG). Alternatively, also catalytic amounts of ionic salts can be used to trigger the process (ion- and liquid-assisted grinding, ILAG). This is a simple method and the absence of solvent makes it very appealing to biomedical applications [63, 82, 83, 86].

2.3. Loading of drugs and other biomedically relevant compounds into MOFs

The loading of relevant molecules, such as imaging and therapeutic agents, into MOFs can be done directly during the MOF synthesis or in the postsynthesis.

The direct incorporation implies using those molecules directly to assemble the framework. This strategy also encloses the networks in which paramagnetic metal ions, such as Gd^{3+} , Fe^{3+} and Mn^{2+} , do not act only as the metal sites to connect the ligand but act also as magnetic resonance imaging contrast agents. High loadings of the relevant compounds can be achieved by this strategy; however, it is necessary to tune the morphology and physicochemical properties of these MOFs for each case and it is important to guarantee that there is no degradation of the compound during the synthesis [21].

The postsynthesis strategy requires high porosity and the active compound is incorporated within the MOF by noncovalent or covalent interactions. In the case of noncovalent loading, the process is reversible and therefore the drug release can be premature. On the other hand, the covalent loading creates a prodrug in which the drug release happens at the same time as the MOF degradation and thus it may be considered a more robust approach [87].

2.4. Surface modifications

The improved biomedical properties of MOFs also depend on the rational design of the surface. However, the task of changing the outer surface of the MOF without changing its characteristics is still very difficult. Ideally, MOFs should have a coating shell to confer stability to the material under the different physiological media, but it must be non-toxic and must not interfere with the pores [86]. There are two approaches to achieve the surface modifications: covalent and noncovalent attachments. The choice of the best method relies on the parameters and nature of the MOF, as well as on the nature of the molecule to be grafted [88]. To date only a few successful examples have been reported of which we highlight the following three.

A simple, fast and biofriendly method was reported for the use of heparin for the external functionalization of MIL-100(Fe), preserving all the properties of the MOF. The coating obtained by this method led to improved biological properties, such as reduced cell recognition, lack of complement activation and reactive oxygen species production [89].

The coating of MIL-101(Fe) with a thin film of silica resulted in the prevention of the rapid degradation of the MOF [87].

Another example of successful coating of MOFs concerns the use of phosphate-modified biocompatible cyclodextrins. This method was applied to MIL-100(Fe) and resulted in improved stability in body fluids without interfering with the MOFs properties [90].

3. Applications of BioMOFs: selected examples

The first biomedical applications of nanoscale MOFs were as delivery vehicles for imaging contrast agents and molecular therapeutics. However, the large amount of paramagnetic metal ions in these systems further allows their exploration for magnetic resonance imaging (MRI) [21]. Furthermore, BioMOFs are also being studied as materials for drug storage as well as controlled drug delivery and release. A few examples of such applications are briefly discussed and the details of the mentioned BioMOFs are presented in **Table 1**. For a matter of clarification, examples of different bio-inspired applications of ZIFs are given in the next section.

3.1. Exploring synergetic effects between metal and drug within a BioMOF

As previously mentioned, one of the best approaches to construct BioMOFs is the direct incorporation of therapeutically active molecules containing multiple complexing groups with biocompatible metal cations (Ca^{2+} , Ag^{2+} , Zn^{2+} , $\text{Fe}^{2/3+}$), and thus the delivery of the active compounds is accomplished via framework degradation [25, 91, 94–97]. Tamames-Tabar et al. recently discussed the possibility of directly introducing azelaic acid as linker and an endogenous low-toxicity transition metal cation (Zn^{2+}) [98]. Both linker and metal exhibit interesting antibacterial and dermatological properties for the dermatological treatment of several skin disorders and their combination results into a novel biocompatible and bioactive MOF, named BioMIL-5. It was synthesized by hydrothermal methods and its stability was assessed through tests in water and in bacteria broth at 37°C; also antibacterial activity studies against two Gram-positive bacteria *Staphylococcus aureus* and *Staphylococcus epidermidis* were conducted [91].

In the antibacterial activity studies, the MIC/MBC (MIC = minimal inhibitory concentration; MBC = minimal bactericidal concentration) values in *S. aureus* and *S. epidermidis* demonstrate that the antimicrobial activity of azelaic acid and Zn^{2+} is maintained after the synthesis [91]. Regarding the stability tests, BioMIL-5 has shown to be stable in water and in bacterial culture medium, but especially in water, leading to the progressive release of both Zn^{2+} and azelaic acid. Indeed, this progressive and slow release of the active Zn^{2+} and azelaic acid in both media led to interesting and time-maintained antibacterial properties when used for 7 days against *S. epidermidis* [91]. The high stability demonstrated and the maintenance of its antibacterial

properties (**Figure 1**) turn BioMIL-5 into a promising candidate for future applications in the treatment of several skin disorders and in the cosmetic industry [91].

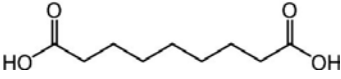
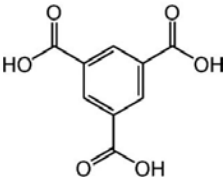
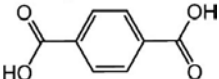
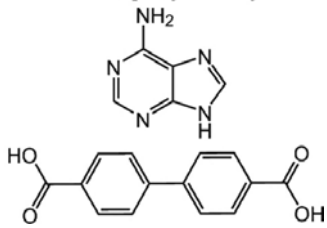
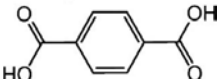
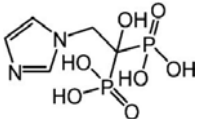
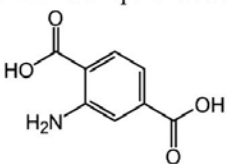
BioMOF	Metal	Ligand	Application	Ref
BioMIL-5	Zn ²⁺	Azelaic acid 	Treatment of skin disorders	[93]
MIL-100	Fe ³⁺	Trimesic acid 	Drug delivery of ibuprofen	[22, 23]
MIL-101	Fe ³⁺	Terephthalic acid 	Drug delivery of ibuprofen	[22, 23]
Bio-MOF-1	Zn ²⁺	Adenine and biphenyldicarboxylic acid 	Drug delivery of procainamide HCl	[30]
MIL-53	Fe ³⁺	Terephthalic acid 	Drug delivery of ibuprofen – “breathing effects”	[22]
CaZol nMOF	Ca ²⁺	Zoledronic acid 	Drug delivery of Zol – targeted anticancer agent	[94]
IRMOF-3	Zn ²⁺	2-Aminoterephthalic acid 	Drug delivery of Paclitaxel – targeted anticancer agent and MRI applications	[95]

Table 1. Details on the presented BioMOFs.

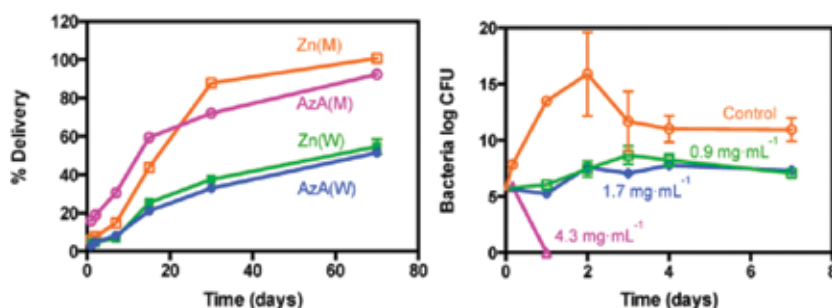


Figure 1. (Left) Delivery profile of azelaic acid (AzA) and zinc (Zn) in Mueller Hinton cation adjusted broth or MHCA (M) and in water (W): AzA(M) (pink), AzA(W) (blue), Zn(M) (orange) and Zn(W) (green); (right) Bacterial growth curves comparing the control group (orange) with BioMIL-5 at different concentrations (mg mL^{-1}): 0.9 (green), 1.7 (blue), and 4.3 mg mL^{-1} (pink) after 1 week in *S. epidermidis* (image from Tamames-Tabar et al. [91]—Copyright © 2014, Royal Society of Chemistry).

3.2. BioMOFs for the controlled drug delivery of ibuprofen

Bearing in mind that BioMOFs are envisaged as new tools for the controlled drug delivery [22, 19–23, 25, 26], Horcajada et al. prepared the first examples of MOFs for the delivery of ibuprofen in the gastrointestinal tract: MIL-100 (with trimesic acid) and MIL-101 (with terephthalic acid) [22, 56]. Ibuprofen was chosen as a model drug because it is a worldwide used pharmaceutical compound with analgesic and antipyretic features [56]. Both MOFs have large pores: MIL-100 contains pore diameters of 25–29 Å with pentagonal window openings of 4.8 Å, and hexagonal windows of 8.6 Å; MIL-101 contains 29–34 Å pore diameter with a large window opening of 12 Å for the pentagonal and 16 Å for the hexagonal windows. They exhibit a very high drug storage capacity: up to 0.35 g of ibuprofen per gram of porous solid for MIL-100 and 1.4 g of ibuprofen per gram of porous solid for MIL-101 [22, 23, 25, 56]. MIL-101 displays a higher loading capacity due to the fact that ibuprofen can fit in both pentagonal and hexagonal windows of MIL-101, but not into the smaller pentagonal window of MIL-100 [22, 23, 25]. This demonstrates the real importance of material's pore size in drug loading [25, 50]. The kinetics of ibuprofen delivery to stimulated body fluid at 37°C was also studied, revealing a complete drug controlled release from 3 to 6 days [22, 23, 25].

3.3. Cation-triggered release of procainamide HCl from BioMOF-1

Another example of a BioMOF constructed by the direct incorporation of simple biomolecules and biocompatible metal cations in their structures is Bio-MOF-1 proposed by An et al. [30] Bio-MOF-1 is based on (i) adenine, a purine nucleobase, as a biomolecular ligand, (ii) a second ligand, biphenyldicarboxylic acid, which was used to promote the formation of larger accessible pores, and (iii) Zn^{2+} as a biocompatible metal cation [30]. Bio-MOF-1 has shown to be stable and maintains its crystallinity for several weeks in biological buffers. Due to the intrinsic anionic nature of Bio-MOF-1, An et al. explored its potential use as a system for the storage and release of cationic drug molecules [30], more specifically the storage and release of procainamide HCl, an effective antiarrhythmic agent used to treat a variety of atrial and

ventricular dysrhythmias with a short half-life *in vivo* making necessary its administration every 3–4 h [29, 30, 99]. Procainamide HCl was successfully encapsulated into the pores of Bio-MOF-1 through a cation exchange process and the complete loading (0.22 g/g material) was achieved after 15 days corresponding to approximately 2.5 procainamide molecules per formula unit residing in the pores and 1 procainamide molecule at the exterior surface [29, 30]. Due to the ionic interaction between procainamide and Bio-MOF-1, cationic drugs are triggered by cations and then released from the framework. Steady procainamide release was observed within 20 h and a complete release was observed after 72 h (**Figure 2**) [30].

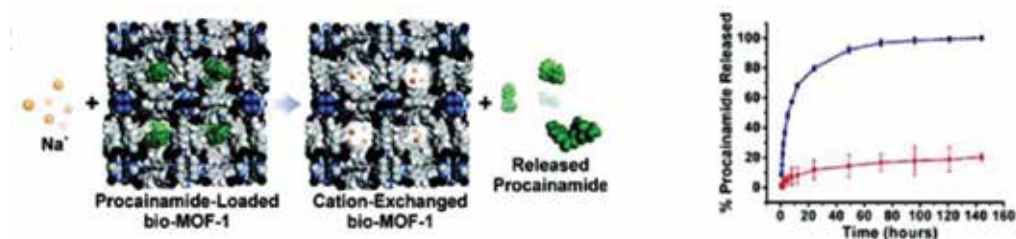


Figure 2. (Left) Scheme depicting cation-triggered procainamide release from Bio-MOF-1; (right) procainamide release profiles from Bio-MOF-1 (blue—PBS buffer; red—deionised nanopure water) (image from An et al. [30]—Copyright © 2009, American Chemical Society).

3.4. Exploring the potentialities of the breathing effects on BioMOFs

Some MOFs can present structural flexibility or “breathing effects,” which allows them to modulate their pore size upon adsorption of organic molecules into the pores, while their crystallinity is maintained [22, 50, 54, 59]. One example of BioMOFs presenting a “breathing effect” is MIL-53 [22, 54, 100]. The structure of MIL-53 consists on terephthalate anions and trans-chains of metal (III) octahedra sharing OH groups and thus creating a 3D framework with one-dimensional pore channel systems [22, 100]. The capacity to expand its structure upon heating explains the “breathing effect” observed in MIL-53 (**Figure 3**) [22]. In this study, Horcajada et al. also observed that aluminium and chromium MIL-53lt (It is low temperature) present a reversible pore opening involving atomic displacements by 5.2 Å upon dehydration, whereas the iron analogue only open its pores during the adsorption molecules [101, 102]. This can be explained by the formation of hydrogen bonds between the water molecules and the inorganic hydrophilic parts of the pore. After approximately 3 weeks, a complete release of ibuprofen is observed, where 20 wt% of ibuprofen loading was achieved at high temperature (**Figure 3**) [22].

3.5. pH-responsive BioMOFs

An interesting example that shows the potential use of BioMOFs in biomedical applications is the recently disclosed work of Au et al. which is based on the reformulation of zoledronate (Zol) exploring nanotechnology to develop a new nanoscale MOF (nMOFs) formulation of Zol, turning a bone antiresorptive agent into an anticancer agent [92].

Zol is a third-generation nitrogen heterocycle containing bisphosphonate that is widely used as an antiresorptive agent for bone cancer metastasis. In the preclinical data, it was observed that bisphosphonates such as Zol have direct cytotoxic effects on cancer cells. However, such effect has not been firmly established in the clinical settings, what led Au et al. to develop a new bioresorbable sub-100 nm diameter pH-responsive calcium zoledronate (CaZol) nMOF as a potential cytotoxic anticancer agent. Folate receptor (FR) is known to be overexpressed in tumours, and therefore folate (Fol) was incorporated as a target ligand into the CaZol nMOFs to facilitate tumour uptake. This study successfully demonstrated that the active-targeted CaZol nMOF possesses excellent chemical and colloidal stability on physiological conditions, encapsulating more Zol than other existing drug delivery systems. It further shows higher efficiency than small molecule Zol in inhibiting cell proliferation and inducing apoptosis in FR-overexpressing H460 non-small cell lung and PC3 prostate cancer cells *in vitro*. Au et al. also validated these results *in vivo* and observed that Fol-targeted CaZol nMOF proved to be an effective anticancer agent, increasing the direct antitumour activity of Zol by 80–85% [92].

3.6. Magnetic nanoscale MOF as potential anticancer drug delivery system, and imaging and MRI contrast agent

The combination of both imaging and therapeutic agents in the same MOF greatly facilitates the efficacy studies of theranostic nanoparticles. Having this in mind, Chowdhuri et al. developed a new magnetic nanoscale MOF (IRMOF-3) consisting of a MOF with encapsulated

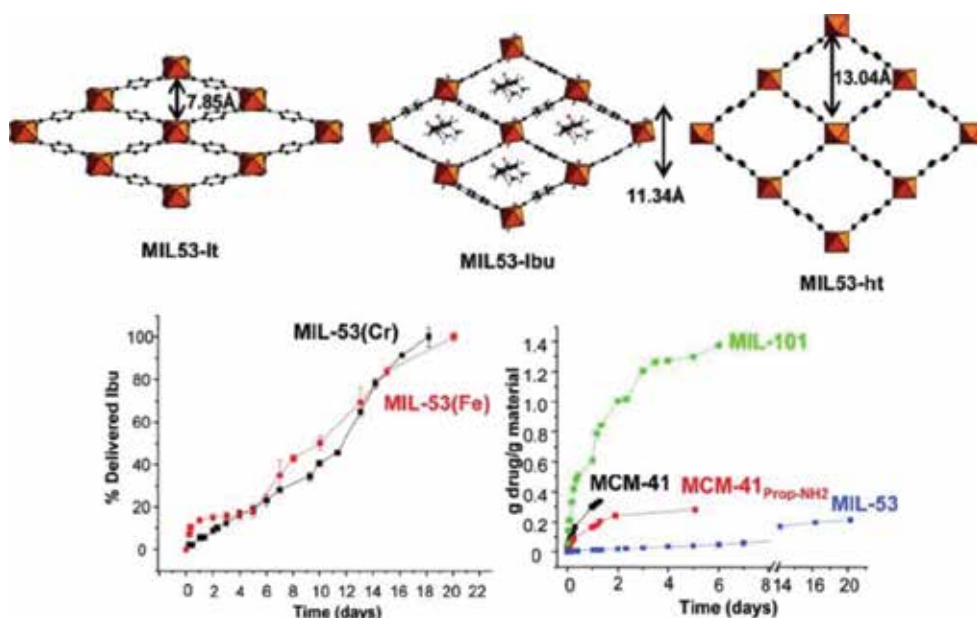


Figure 3. (Top) Schematic 3D representation of the breathing effect of MIL-53(Cr) hybrid solid upon dehydration-hydration; (bottom) ibuprofen delivery (left) from MIL-53(Cr) and MIL-53(Fe) materials and (right) from MIL-53 in comparison with MIL-101, MCM-41 and MCM-4 (images from Horcajada et al. [22])—Copyright © 2008, American Chemical Society).

Fe_3O_4 nanoparticles for targeted anticancer drug delivery with cell imaging and magnetic resonance imaging (MRI). More specifically, authors conjugated the magnetic nanoscale MOF with folic acid and labelled it with the fluorescent molecule rhodamine B isothiocyanate due to its fluorescent properties. These systems were then successfully loaded with the hydrophobic anticancer drug paclitaxel. The efficiency of this nMOF towards targeted drug delivery was evaluated using an *in vitro* cytotoxicity 5-diphenyltetrazolium bromide (MTT) assay and fluorescence microscopy, revealing that the loaded nMOF targeted and killed the cancer cells in a highly effective manner. Furthermore, they had also tested the effectiveness of MRI of this nMOF *in vitro* and observed a stronger T2-weighted MRI contrast towards the cancer cells, which proved the possible use of this system in imaging (**Figure 4**) [93].

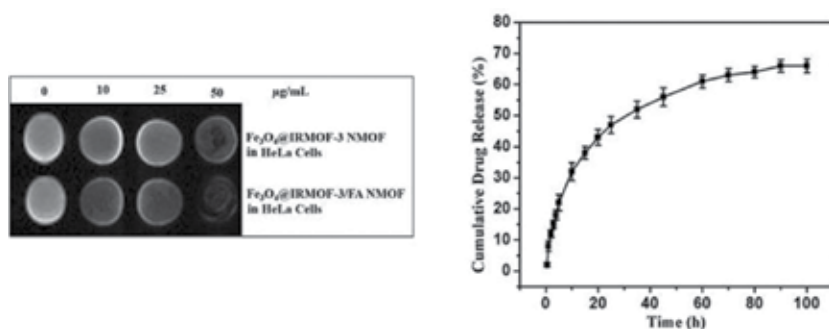


Figure 4. (Left) *In vitro* T2-weighted spin-echo MR phantom images of magnetic nanoscale Fe_3O_4 @IRMOF-3 and magnetic nanoscale Fe_3O_4 @IRMOF-3/FA at different concentrations incubated in HeLa cells; (right) *in vitro* paclitaxel release from magnetic nanoscale Fe_3O_4 @IRMOF-3/FA at different time intervals (images from Chowdhuri et al. [93]—Copyright © 2015, Royal Society of Chemistry).

4. Bio-inspired applications of ZIFs: selected examples

There are many applications for ZIFs, specifically ZIF-8 (**Figure 5**). However, this type of materials has largely been explored as a way to deliver anticancer drugs and other chemotherapeutics. Only a few relevant examples are mentioned herein.

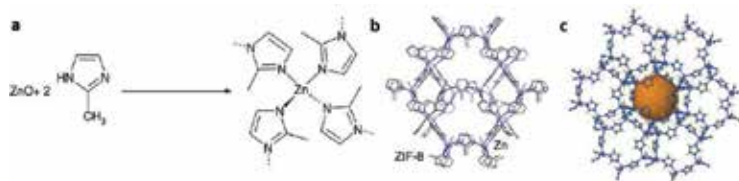


Figure 5. (a) Synthesis of ZIF-8; (b) fragment of the crystal structure of ZIF-8 (images adapted from Katsenis et al. [103]—Copyright © 2015, Rights Managed by Nature Publishing Group); and (c) image generated for ZIF-8 in <http://www.chemtube3d.com> (University of Liverpool).

4.1. Slow release of the anti-cancer drug doxorubicin from ZIF-8

Zheng et al. successfully developed a simple one-pot synthesis of ZIFs that contain encapsulated organic molecules. One-pot synthesis is a new approach that combines MOF synthesis and molecule encapsulation in a one-pot process and that has been extremely used to overcome the drawbacks observed when using the two processes separately [104].

In this study, the doxorubicin: ZIF-8 complex, which aims to treat mucoepidermoid carcinoma of human lung, human colorectal adenocarcinoma (HT-29) and human promyelocytic leukaemia (HL-60) cell lines, exhibits lower toxicity than pure doxorubicin, probably due to the slow release of the drug that is achieved with this complex (**Figure 6**) [69, 104]. Furthermore, ZIF-8 crystals loaded with doxorubicin proved to be efficient pH-responsive drug delivery systems, in which the drug is released in a controlled manner at low pH (5.0–6.5). With this work, Zheng et al. opened a new opportunity to develop multifunctional materials for biomedical applications using this simple, scalable, and environment-friendly one-pot synthesis [104].

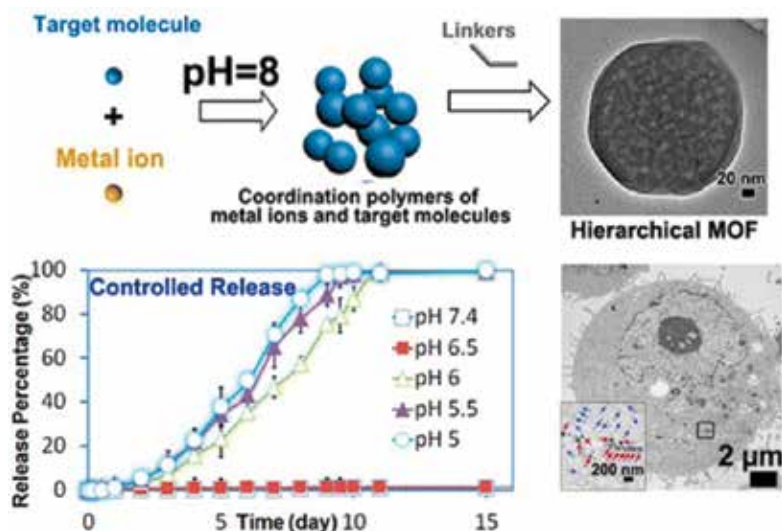


Figure 6. (Top) Schematic representation of the pH-induced one-pot synthesis of MOFs with encapsulated target molecules; (bottom left) The pH-responsive release of doxorubicin from doxorubicin@ZIF-8 particles determined by UV-vis spectrophotometry; (bottom right) TEM image of an MDA-MB-468 cell; and the inset is an enlarged image of the area marked by the square showing individual ZIF-8 particles (blue arrows) and their aggregates (red arrows) (image from Zheng et al. [104]—Copyright © 2016, American Chemical Society).

4.2. ZIF-8 as efficient pH-sensitive drug delivery

“Smart” drug delivery of anticancer drugs is being explored making use of pH-sensitive systems [65–68]. The interest in the use of a pH-responsive drug vehicle is due to the fact that they can reduce undesired drug release during transportation in blood circulation and improve the effective release of the drug in the tumour tissue or within tumour cells [105, 106].

Sun et al. evaluated the possibility to use ZIF-8 as a pH-responsive drug vehicle and they have demonstrated that ZIF-8 exhibits a remarkable loading capacity for the anticancer drug 5-fluorouracil (around 600 mg of 5-FU g^{-1} of desolvated ZIF-8) (**Figure 7**) [66]. Ren et al. further developed polyacrylic acid@ZIF-8 (PAA@ZIF-8) nanoparticles that exhibit ultrahigh doxorubicin loading capability (1.9 g doxorubicin/g nanoparticles) and that thus can be used as pH-dependent drug delivery vehicles [65].

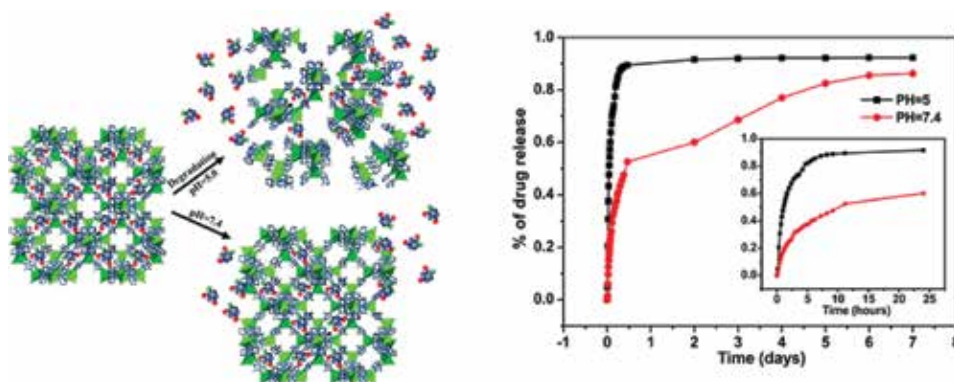


Figure 7. (Left) Schematic illustration showing two approaches of the encapsulated 5-FU released from ZIF-8 (C = grey, N = blue, O = red, F = light blue, Zn = green); (right) 5-FU delivery (% 5-FU vs. t) from ZIF-8; the inset shows the release process from 0 to 24 h (images from Sun et al. [66]—Copyright © 2012, Royal Society of Chemistry).



Figure 8. Schematic representation of the synthetic route of the C-dots@ZIF-8 for simultaneous anticancer drug delivery and fluorescence imaging of cancer cell (image from He et al. [67]—Copyright © 2014, Royal Society of Chemistry).

Zhuang et al. successfully encapsulated small molecules, such as fluorescein and the anticancer drug camptothecin, in ZIF-8 nanospheres for drug delivery. In this study, the evaluation of fluorescein-encapsulated ZIF-8 in the MCF-7 breast cancer line demonstrated cell internalization and a minimal cytotoxicity. Furthermore, the pH-responsive dissociation of the ZIF-8

framework likely results in endosomal release of the small-molecule cargo proved that ZIF-8 can be an ideal drug delivery vehicle [68].

Another example of a pH-responsive drug vehicle using ZIF-8 is the work of Liu et al., who fabricate green fluorescent carbon nanodots@ZIF-8 (c-dots@ZIF-8 NPs). In this work, the authors observed that the nanoparticles synthesized exhibit green fluorescence and microporosity, characteristics that unveil its ability as potential platforms for simultaneous pH-responsive anticancer drug vehicle and fluorescence imaging in cancer cells (**Figure 8**). Moreover, the fluorescence intensity and size of c-dots@ZIF-8 NPs can be tuned by varying the amount of C-dots and the concentration of the precursors [67].

4.3. ZIFs as potential carriers to brain capillary endothelial cells

One extraordinary example of the biomedical applications of ZIFs is the recent work from Chiacchia et al. who synthesized and characterized nanospheres of biodegradable zinc-imidazolate polymers (ZIPs) as a delivery system into human brain endothelial cells, the main component of the blood-brain barrier (BBB) [107].

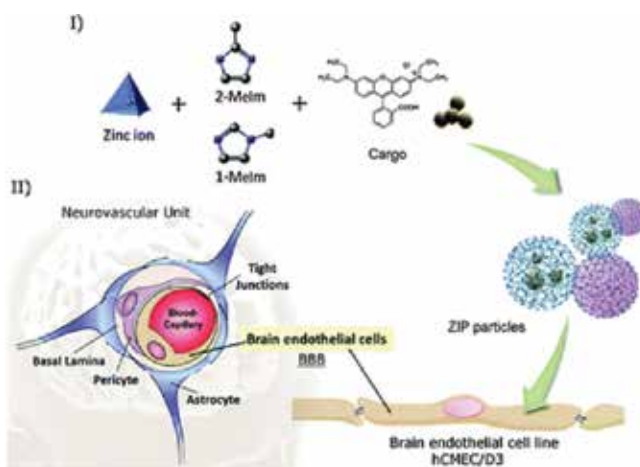


Figure 9. Synthesis and assembly of loaded ZIP particles and their uptake into human brain endothelial cells: (I) encapsulation process of cargo species into the ZIP matrices at the point of synthesis; (II) cross-section of the human cerebral microvasculature and cell-uptake of loaded ZIP particles by the isolated and immortalized human brain endothelial cell line (image from Chiacchia et al. [107]—Published by The Royal Society of Chemistry).

In this work, both biodegradable particles synthesized, RhB@ZIP and AuNP@ZIP, have shown to be able to encapsulate fluorophores and inorganic nanoparticles at the point of synthesis with extremely high loading efficiencies. Furthermore, these ZIP particles are non-cytotoxic, stable in cell culture medium and able to penetrate the hCMEC/D3 human cerebral microvascular endothelial cell line. This cell line is a well-established *in vitro* functional model for the human BBB, which expresses the same levels of transporters, cell-specific receptors and tight junction proteins found in healthy human brain microvessels [108, 109], to release their cargos within the cell cytoplasm (**Figure 9**) [107].

Nevertheless this work needs more studies related to the exact cellular uptake mechanism, clearance rate and blood-stream stability of the ZIPs, but this is a promising result in the use of ZIPs as a novel platform for brain-targeting treatments [107].

5. Final remarks

Bio-inspired metal-organic frameworks have already proven to have promising biomedical applications not only as drug delivery systems but also in magnetic resonance imaging (MRI), optical imaging and X-ray computed tomography (CT) imaging.

Acknowledgements

Authors acknowledge Fundação para a Ciência e Tecnologia for funding (RECI/QEQ-QIN70189/2012, SFRH/BPD/78854/2011, SFRH/BD/100029/2014, UID/QUI/00100/2013). Authors would also like to acknowledge Professor Maria Teresa Duarte for her support.

Author details

Vânia André^{1,2*} and Sílvia Quaresma¹

*Address all correspondence to: vaniandre@tecnico.ulisboa.pt

1 Centro de Química Estrutural, Instituto Superior Técnico, Universidade de Lisboa, Lisboa, Portugal

2 CICECO, Universidade de Aveiro, Aveiro, Portugal

References

- [1] N. Blagden, S. J. Coles and D. J. Berry, *CrystEngComm*, 2014, 16, 5753–5761.
- [2] M. D. Allendorf and V. Stavila, *Crystengcomm*, 2015, 17, 229–246.
- [3] A. Mukherjee, *Crystal Growth & Design*, 2015, 15, 3076–3085.
- [4] S. Satapathi, *Inorganic Chemistry Communications*, 2015, 56, 22–34.
- [5] A. Delori, T. Friscic and W. Jones, *Crystengcomm*, 2012, 14, 2350–2362.
- [6] K. Biradha, C.-Y. Su and J. J. Vittal, *Crystal Growth & Design*, 2011, 11, 875–886.

- [7] S. Aitipamula, P. S. Chow and R. B. H. Tan, *Crystal Growth & Design*, 2014, 14, 6557–6569.
- [8] N. K. Duggirala, A. J. Smith, L. Wojtas, R. D. Shytle and M. J. Zaworotko, *Crystal Growth & Design*, 2014, 14, 6135–6142.
- [9] D. Maddileti, B. Swapna and A. Nangia, *Crystal Growth & Design*, 2014, 14, 2557–2570.
- [10] D. P. Elder, R. Holm and H. L. de Diego, *International Journal of Pharmaceutics*, 2013, 453, 88–100.
- [11] I. Tomaszewska, S. Karki, J. Shur, R. Price and N. Fotaki, *International Journal of Pharmaceutics*, 2013, 453, 380–388.
- [12] C. Maheshwari, V. Andre, S. Reddy, L. Roy, T. Duarte and N. Rodrigez-Hornedo, *Crystengcomm*, 2012, 14, 4801–4811.
- [13] V. Andre, A. Fernandes, P. P. Santos and M. T. Duarte, *Crystal Growth & Design*, 2011, 11, 2325–2334.
- [14] V. Andre, D. Braga, F. Grepioni and M. T. Duarte, *Crystal Growth & Design*, 2009, 9, 5108–5116.
- [15] V. Andre, L. Cunha-Silva, M. Teresa Duarte and P. P. Santos, *Crystal Growth & Design*, 2011, 11, 3703–3706.
- [16] V. Andre, M. T. Duarte, D. Braga and F. Grepioni, *Crystal Growth & Design*, 2012, 12, 3082–3090.
- [17] V. Andre, M. F. M. da Piedade and M. Teresa Duarte, *Crystengcomm*, 2012, 14, 5005–5014.
- [18] V. Andre and M. T. Duarte, *Journal of Molecular Structure*, 2014, 1076, 238–243.
- [19] K. J. Ardila-Fierro, V. Andre, D. Tan, M. T. Duarte, R. W. Lancaster, P. G. Karamertzanis and T. Friscic, *Crystal Growth & Design*, 2015, 15, 1492–1501.
- [20] D. Braga, F. Grepioni, L. Maini, K. Rubini, M. Polito, R. Brescello, L. Cotarca, M. T. Duarte, V. Andre and M. F. M. Piedade, *New Journal of Chemistry*, 2008, 32, 1788–1795.
- [21] J. Della Rocca, D. Liu and W. Lin, *Accounts of Chemical Research*, 2011, 44, 957–968.
- [22] P. Horcajada, C. Serre, G. Maurin, N. A. Ramsahye, F. Balas, M. Vallet-Regi, M. Sebban, F. Taulelle and G. Ferey, *Journal of the American Chemical Society*, 2008, 130, 6774–6780.
- [23] P. Horcajada, C. Serre, M. Vallet-Regi, M. Sebban, F. Taulelle and G. Ferey, *Angewandte Chemie-International Edition*, 2006, 45, 5974–5978.
- [24] C. Janiak and J. K. Vieth, *New Journal of Chemistry*, 2010, 34, 2366–2388.
- [25] S. Keskin and S. Kizilel, *Industrial & Engineering Chemistry Research*, 2011, 50, 1799–1812.

- [26] A. C. McKinlay, R. E. Morris, P. Horcajada, G. Ferey, R. Gref, P. Couvreur and C. Serre, *Angewandte Chemie-International Edition*, 2010, 49, 6260–6266.
- [27] S. R. Miller, D. Heurtaux, T. Baati, P. Horcajada, J.-M. Greneche and C. Serre, *Chemical Communications*, 2010, 46, 4526–4528.
- [28] P. Horcajada, R. Gref, T. Baati, P. K. Allan, G. Maurin, P. Couvreur, G. Ferey, R. E. Morris and C. Serre, *Chemical Reviews*, 2012, 112, 1232–1268.
- [29] C.-Y. Sun, C. Qin, X.-L. Wang and Z.-M. Su, *Expert Opinion on Drug Delivery*, 2013, 10, 89–101.
- [30] J. Y. An, S. J. Geib and N. L. Rosi, *Journal of the American Chemical Society*, 2009, 131, 8376.
- [31] Q.-L. Li, J.-P. Wang, W.-C. Liu, X.-Y. Zhuang, J.-Q. Liu, G.-L. Fan, B.-H. Li, W.-N. Lin and J.-H. Man, *Inorganic Chemistry Communications*, 2015, 55, 8–10.
- [32] S. Li and F. Huo, *Nanoscale*, 2015, 7, 7482–7501.
- [33] N. Motakef-Kazemi, S. A. Shojaosadati and A. Morsali, *Microporous and Mesoporous Materials*, 2014, 186, 73–79.
- [34] M. R. Ryder and J. C. Tan, *Materials Science and Technology*, 2014, 30, 1598–1612.
- [35] M. O’Keeffe, *Chemical Society Reviews*, 2009, 38, 1215–1217.
- [36] B. Xiao, P. S. Wheatley, X. Zhao, A. J. Fletcher, S. Fox, A. G. Rossi, I. L. Megson, S. Bordiga, L. Regli, K. M. Thomas and R. E. Morris, *Journal of the American Chemical Society*, 2007, 129, 1203–1209.
- [37] J. Graetz, *Chemical Society Reviews*, 2009, 38, 73–82.
- [38] M. Mueller, X. Zhang, Y. Wang and R. A. Fischer, *Chemical Communications*, 2009, 119–121.
- [39] M. P. Suh, Y. E. Cheon and E. Y. Lee, *Coordination Chemistry Reviews*, 2008, 252, 1007–1026.
- [40] S. S. Han, J. L. Mendoza-Cortes and W. A. Goddard, III, *Chemical Society Reviews*, 2009, 38, 1460–1476.
- [41] T. Dueren, Y.-S. Bae and R. Q. Snurr, *Chemical Society Reviews*, 2009, 38, 1237–1247.
- [42] S. Ma, D. Sun, M. Ambrogio, J. A. Fillinger, S. Parkin and H.-C. Zhou, *Journal of the American Chemical Society*, 2007, 129, 1858.
- [43] D. Farrusseng, S. Aguado and C. Pinel, *Angewandte Chemie-International Edition*, 2009, 48, 7502–7513.
- [44] J. Lee, O. K. Farha, J. Roberts, K. A. Scheidt, S. T. Nguyen and J. T. Hupp, *Chemical Society Reviews*, 2009, 38, 1450–1459.
- [45] T. Uemura, N. Yanai and S. Kitagawa, *Chemical Society Reviews*, 2009, 38, 1228–1236.

- [46] T. Uemura, Y. Ono, K. Kitagawa and S. Kitagawa, *Macromolecules*, 2008, 41, 87–94.
- [47] M. D. Allendorf, C. A. Bauer, R. K. Bhakta and R. J. T. Houk, *Chemical Society Reviews*, 2009, 38, 1330–1352.
- [48] O. R. Evans and W. B. Lin, *Accounts of Chemical Research*, 2002, 35, 511–522.
- [49] M. Kurmoo, *Chemical Society Reviews*, 2009, 38, 1353–1379.
- [50] G. Ferey, *Chemical Society Reviews*, 2008, 37, 191–214.
- [51] F. Millange, N. Guillou, R. I. Walton, J.-M. Greneche, I. Margiolaki and G. Ferey, *Chemical Communications*, 2008, 39, 4732–4734.
- [52] R. Kuroda, T. Sato and Y. Imai, *Crystengcomm*, 2008, 10, 1881–1890.
- [53] B. Notash, N. Safari and H. R. Khavasi, *Crystengcomm*, 2012, 14, 6788–6796.
- [54] G. Ferey and C. Serre, *Chemical Society Reviews*, 2009, 38, 1380–1399.
- [55] J. An, S. J. Geib and N. L. Rosi, *Journal of the American Chemical Society*, 2009, 131, 8376.
- [56] R. Babarao and J. Jiang, *Journal of Physical Chemistry C*, 2009, 113, 18287–18291.
- [57] I. Imaz, M. Rubio-Martinez, J. An, I. Sole-Font, N. L. Rosi and D. MasPOCH, *Chemical Communications*, 2011, 47, 7287–7302.
- [58] P. D. C. Dietzel, R. Blom and H. Fjellvag, *European Journal of Inorganic Chemistry*, 2008, 23 3624–3632.
- [59] P. L. Llewellyn, G. Maurin, T. Devic, S. Loera-Serna, N. Rosenbach, C. Serre, S. Bourrelly, P. Horcajada, Y. Filinchuk and G. Ferey, *Journal of the American Chemical Society*, 2008, 130, 12808–12814.
- [60] M. Eddaoudi, D. F. Sava, J. F. Eubank, K. Adil and V. Guillerm, *Chemical Society reviews*, 2015, 44, 228–249.
- [61] T. D. Bennett, J. Sotelo, J.-C. Tan and S. A. Moggach, *Crystengcomm*, 2015, 17, 286–289.
- [62] H. Su, F. Sun, J. Jia, H. He, A. Wang and G. Zhu, *Chemical Communications*, 2015, 51, 5774–5777.
- [63] B. Chen, Z. Yang, Y. Zhu and Y. Xia, *Journal of Materials Chemistry A*, 2014, 2, 16811–16831.
- [64] R. Li, X. Ren, J. Zhao, X. Feng, X. Jiang, X. Fan, Z. Lin, X. Li, C. Hu and B. Wang, *Journal of Materials Chemistry A*, 2014, 2, 2168–2173.
- [65] H. Ren, L. Zhang, J. An, T. Wang, L. Li, X. Si, L. He, X. Wu, C. Wang and Z. Su, *Chemical Communications*, 2014, 50, 1000–1002.
- [66] C.-Y. Sun, C. Qin, X.-L. Wang, G.-S. Yang, K.-Z. Shao, Y.-Q. Lan, Z.-M. Su, P. Huang, C.-G. Wang and E.-B. Wang, *Dalton Transactions*, 2012, 41, 6906–6909.

- [67] L. He, T. Wang, J. An, X. Li, L. Zhang, L. Li, G. Li, X. Wu, Z. Su and C. Wang, *Crystengcomm*, 2014, 16, 3259–3263.
- [68] J. Zhuang, C.-H. Kuo, L.-Y. Chou, D.-Y. Liu, E. Weerapana and C.-K. Tsung, *ACS Nano*, 2014, 8, 2812–2819.
- [69] I. B. Vasconcelos, T. G. da Silva, G. C. G. Militao, T. A. Soares, N. M. Rodrigues, M. O. Rodrigues, N. B. da Costa, Jr., R. O. Freire and S. A. Junior, *RSC Advances*, 2012, 2, 9437–9442.
- [70] L. Pasetta, G. Potier, S. Abbott and J. Coronas, *Organic & Biomolecular Chemistry*, 2015, 13, 1724–1731.
- [71] N. Liedana, A. Galve, C. Rubio, C. Tellez and J. Coronas, *ACS Applied Materials & Interfaces*, 2012, 4, 5016–5021.
- [72] M. Eddaoudi, D. B. Moler, H. L. Li, B. L. Chen, T. M. Reineke, M. O’Keeffe and O. M. Yaghi, *Accounts of Chemical Research*, 2001, 34, 319–330.
- [73] V. Guillermin, D. Kim, J. F. Eubank, R. Luebke, X. Liu, K. Adil, M. S. Lah and M. Eddaoudi, *Chemical Society Reviews*, 2014, 43, 6141–6172.
- [74] J. F. Eubank, L. Wojtas, M. R. Hight, T. Bousquet, V. C. Kravtsov and M. Eddaoudi, *Journal of the American Chemical Society*, 2011, 133, 17532–17535.
- [75] M. C. Bernini, D. Fairen-Jimenez, M. Pasinetti, A. J. Ramirez-Pastor and R. Q. Snurr, *Journal of Materials Chemistry B*, 2014, 2, 766–774.
- [76] D. G. Fatouros, D. Douroumis, V. Nikolakis, S. Ntais, A. M. Moschovi, V. Trivedi, B. Khima, M. Roldo, H. Nazar and P. A. Cox, *Journal of Materials Chemistry*, 2011, 21, 7789–7794.
- [77] J.-Q. Liu, X.-F. Li, C.-Y. Gu, J. C. S. da Silva, A. L. Barros, S. Alves-Jr, B.-H. Li, F. Ren, S. R. Batten and T. A. Soares, *Dalton Transactions (Cambridge, England: 2003)*, 2015, 44, 19370–19382.
- [78] T. Chalati, P. Horcajada, P. Couvreur, C. Serre, M. Ben Yahia, G. Maurin and R. Gref, *Nanomedicine*, 2011, 6, 1683–1695.
- [79] C. Gaudin, D. Cunha, E. Ivanoff, P. Horcajada, G. Cheve, A. Yasri, O. Loget, C. Serre and G. Maurin, *Microporous and Mesoporous Materials*, 2012, 157, 124–130.
- [80] S. Vaucher, M. Li and S. Mann, *Angewandte Chemie-International Edition*, 2000, 39, 1793.
- [81] E. R. Parnham and R. E. Morris, *Accounts of Chemical Research*, 2007, 40, 1005–1013.
- [82] A. Pichon, A. Lazuen-Garay and S. L. James, *Crystengcomm*, 2006, 8, 211–214.
- [83] J. A. Perman, K. Dubois, F. Nouar, S. Zoccali, L. Wojtas, M. Eddaoudi, R. W. Larsen and M. J. Zaworotko, *Crystal Growth & Design*, 2009, 9, 5021–5023.

- [84] W. Lin, W. J. Rieter and K. M. L. Taylor, *Angewandte Chemie-International Edition*, 2009, 48, 650–658.
- [85] A. M. Spokoiny, D. Kim, A. Sumrein and C. A. Mirkin, *Chemical Society Reviews*, 2009, 38, 1218–1227.
- [86] M. Gimenez-Marques, T. Hidalgo, C. Serre and P. Horcajada, *Coordination Chemistry Reviews*, 2016, 307, 342–360.
- [87] K. M. L. Taylor-Pashow, J. Della Rocca, Z. Xie, S. Tran and W. Lin, *Journal of the American Chemical Society*, 2009, 131(40), 14261–14263.
- [88] K. E. Sapsford, W. R. Algar, L. Berti, K. B. Gemmill, B. J. Casey, E. Oh, M. H. Stewart and I. L. Medintz, *Chemical Reviews*, 2013, 113, 1904–2074.
- [89] E. Bellido, T. Hidalgo, M. V. Lozano, M. Guillevic, R. Simon-Vazquez, M. J. Santander-Ortega, A. Gonzalez-Fernandez, C. Serre, M. J. Alonso and P. Horcajada, *Advanced Healthcare Materials*, 2015, 4, 1246–1257.
- [90] T. Loftsson and D. Duchene, *International Journal of Pharmaceutics*, 2007, 329, 1–11.
- [91] C. Tamames-Tabar, E. Imbuluzqueta, N. Guillou, C. Serre, S. R. Miller, E. Elkaim, P. Horcajada and M. J. Blanco-Prieto, *Crystengcomm*, 2015, 17, 456–462.
- [92] K. M. Au, A. Satterlee, Y. Z. Min, X. Tian, Y. S. Kim, J. M. Caster, L. Z. Zhang, T. Zhang, L. Huang and A. Z. Wang, *Biomaterials*, 2016, 82, 178–193.
- [93] A. Ray Chowdhuri, D. Bhattacharya and S. K. Sahu, *Dalton Transactions*, 2016, 45, 2963–2973.
- [94] T. V. Slenters, J. L. Sague, P. S. Brunetto, S. Zuber, A. Fleury, L. Mirolo, A. Y. Robin, M. Meuwly, O. Gordon, R. Landmann, A. U. Daniels and K. M. Fromm, *Materials*, 2010, 3, 3407–3429.
- [95] S. R. Miller, E. Alvarez, L. Fradcourt, T. Devic, S. Wuttke, P. S. Wheatley, N. Steunou, C. Bonhomme, C. Gervais, D. Laurencin, R. E. Morris, A. Vimont, M. Daturi, P. Horcajada and C. Serre, *Chemical Communications*, 2013, 49, 7773–7775.
- [96] E. Alvarez, A. G. Marquez, T. Devic, N. Steunou, C. Serre, C. Bonhomme, C. Gervais, I. Izquierdo-Barba, M. Vallet-Regi, D. Laurencin, F. Mauri and P. Horcajada, *Crystengcomm*, 2013, 15, 9899–9905.
- [97] J. Della Rocca, D. Liu and W. Lin, *Nanomedicine*, 2012, 7, 303–305.
- [98] L. M. Plum, L. Rink and H. Haase, *International Journal of Environmental Research and Public Health*, 2010, 7, 1342–1365.
- [99] B. B. Yang, R. B. Abel, A. C. G. Uprichard, J. A. Smithers and S. T. Fogue, *Journal of Clinical Pharmacology*, 1996, 36, 623–633.

- [100] C. Serre, F. Millange, C. Thouvenot, M. Nogues, G. Marsolier, D. Louer and G. Ferey, *Journal of the American Chemical Society*, 2002, 124, 13519–13526.
- [101] T. R. Whitfield, X. Q. Wang, L. M. Liu and A. J. Jacobson, *Solid State Sciences*, 2005, 7, 1096–1103.
- [102] T. Loiseau, C. Serre, C. Huguenard, G. Fink, F. Taulelle, M. Henry, T. Bataille and G. Ferey, *Chemistry—A European Journal*, 2004, 10, 1373–1382.
- [103] A. D. Katsenis, A. Puskaric, V. Strukil, C. Mottillo, P. A. Julien, K. Uzarevic, P. Minh-Hao, D. Trong-On, S. A. J. Kimber, P. Lazic, O. Magdysyuk, R. E. Dinnebier, I. Halasz and T. Friscic, *Nature Communications*, 2015, 6, 6662.
- [104] H. Zheng, Y. Zhang, L. Liu, W. Wan, P. Guo, A. M. Nystrom and X. Zou, *Journal of the American Chemical Society*, 2016, 138, 962–968.
- [105] K. Engin, D. B. Leeper, J. R. Cater, A. J. Thistlethwaite, L. Tupchong and J. D. McFarlane, *International Journal of Hyperthermia*, 1995, 11, 211–216.
- [106] M. Stubbs, P. M. J. McSheehy, J. R. Griffiths and C. L. Bashford, *Molecular Medicine Today*, 2000, 6, 15–19.
- [107] M. Chiacchia, C. Cerutti, R. Gromnicova, K. Rietdorf, I. A. Romero and D. Bradshaw, *Journal of Materials Chemistry B*, 2015, 3, 9053–9059.
- [108] B. B. Weksler, E. A. Subileau, N. Perriere, P. Charneau, K. Holloway, M. Leveque, H. Tricoire-Leignel, A. Nicotra, S. Bourdoulous, P. Turowski, D. K. Male, F. Roux, J. Greenwood, I. A. Romero and P. O. Couraud, *FASEB Journal*, 2005, 19, 1872.
- [109] B. Weksler, I. A. Romero and P.-O. Couraud, *Fluids and Barriers of the CNS*, 2013, 10, 16.



Edited by Fahmina Zafar and Eram Sharmin

The emerging and interesting field of MOF encouraged us to bring forth the book titled “Metal Organic Frameworks”. The book is divided into three sections. Section A consists of introduction, Section B comprises the synthesis and characterization techniques, and Section C is dedicated to the applications of MOFs. The book would be useful for scientists and researchers interested in the field of MOFs.

Photo by Rost-9D / iStock

IntechOpen

